広島大学学位請求論文

Facies model, Geochronology and Sequence analysis of the Singhora Group of rocks: implications to age and basinal forcings in early history of the Chhattisgarh basin, central India

(Singhora 層群の堆積相モデル、地質年代およびシーケンス解析、特に、中央インド Chhattisgarh 堆積盆形成初期における年代論と堆積盆強制力について)

２014 年
広島大学大学院理学研究科
地球惑星システム学専攻
Das Priyabrata
（Balasore Alloys Limited, Orissa, India）

目　次

１．主論文

Facies model, Geochronology and Sequence analysis of the Singhora Group of rocks: implications to age and basinal forcings in early history of the Chhattisgarh basin, central India

（Singhora 層群の堆積相モデル、地質年代およびシーケンス解析、特に、中央インド Chhattisgarh 堆積盆形成初期における年代論と堆積盆強制力について）

Das Priyabrata

２．公表論文

1. Alluvial fan to storm-dominated shelf transition in the Mesoproterozoic Singhora Group, Chattisgarh Supergroup, Central India. Partha Pratim Chakraborty, Ashish Sarkar, Kaushik Das, Priyabrata Das. 2009. Precambrian Research, 170 (1-2) (2009) 88-106.

2. 1420 Ma diabasic intrusives from the Mesoproterozoic Singhora Group, Chhattisgarh Supergroup, India: Implications towards non-plume intrusive activity. Priyabrata Das, Kaushik Das, Partha Pratim Chakraborty, S. Balakrishnan. Journal of Earth System Sciences, 120 (2) (2011) 223-236.

3. Regressive depositional architecture on a Mesoproterozoic siliciclastic ramp: sequence stratigraphic and Nd isotopic evidences from Bhalukona Formation, Singhora Group, Chhattisgarh Supergroup, central India. Partha Pratim Chakraborty, Priyabrata Das, Kaushik Das, Subhojit Saha, S. Balakrishnan. Precambrian Research. 200-203 (2012) 129-149.

4. Microbial mat related structures (MRS) from Mesoproterozoic Chhattisgarh and Khariar basins, Central India and their bearing on shallow marine sedimentation. Partha Pratim Chakraborty, Priyabrata Das, Subhojit Saha, Kaushik Das, Shruti Ranjan Mishra and Pritam Paul. Episodes, 35 (4) (2012) 513-523.

5. Geology of Mesoproterozoic Chhattisgarh basin, central India: current status and future goals. Precambrian Basins of India: Stratigraphic and Tectonic Context. Partha Pratim Chakraborty, Subhojit Saha, and Priyabrata Das. 2014. Journal of Geological Society of London. Manuscript Accepted. 24.01.14.

３．参考論文

1. Tectono-magmatic evolution of Meosproterozoic Singhora basin, central India: Evidences for compressional tectonics from structural data, AMS study and geochemistry of basic rocks. Subhojit Saha, Kaushik Das, Partha Pratim Chakraborty, Priyabrata Das, Subrata Karmakar, Manish A. Mamtani. Precambrian Reseach, 227 (2013) 276-294 .

2. Reply to the discussion of Deb (2013) on the paper of Saha et al.(2013) entitled 'Tectono-magmatic evolution of the Mesoproterozoic Singhora basin, central India: Evidence for compressional tectonics from structural data, AMS study and geochemistry of basic rocks. Partha Pratim Chakraborty, Kaushik Das, Subhojit Saha, Priyabrata Das, Subrata Karmakar, Manish A. Mamtani. Precambrian Research, 236 (2013) 297-302.

学位論文要旨

Facies model, Geochronology and Sequence analysis of the Singhora Group of rocks: implications to age and basinal forcings in early history of the Chhattisgarh basin, central India（Singhora 層群の堆積相モデル、地質年代およびシーケンス解析、特に、中央インド Chhattisgarh 堆積盆形成初期における年代論と堆積盆強制力について）

Abstract

Study of fossil-less Precambrian sedimentary successions remains a challenge in absence of (a) geophysical back-up, (b) poor chronological constraint, (c) continuous and well-preserved outcrop, and finally (d) dominance of intra and/or epicratonic basin setting for which there is no available present day analogue. Multidisciplinary approach involving (i) systematic process-based facies and paleoenvironmental study supported by high-resolution litholog measurement, identification of key surfaces and tracking of surfaces in space, (ii) bulk geochemistry and/or isotope geochemical study, (iii) geochronology of concordant/discordant lithodemic units has shown potential in overcoming the hindrance to a large extent. The present thesis dwells with such multidisciplinary study on three contiguous Formations i.e., Rehtikhol, Saraipalli and Bhalukona Formations from the Mesoproterozoic Singhora Group of Chhattisgarh Supergroup, central India. The study unravels (i) time of opening of the Chhattisgarh basin; (ii) processes (terrestrial, transitional or marine) operative in the early depositional history of the basin; (iii) variability in depositional milieu in space and time, and (iv) allokinetic and autokinetic forcings, which triggered such variations. A sequence stratigraphic appraisal allowed understanding of relative sea level stands under which different stratigraphic intervals were deposited, which despite being Proterozoic in age is reasonably well constrained in time through geochronological backup.

Facies associations within the Rehtikhol and Saraipalli Formations represent products ranging between continental alluvial fan and distal marine shelf beyond storm wave base stacked in a transgressive motif. Sandstones of Bhalukona Formation overlie the Saraipalli Formation with an unconformity and constituted of products belonging to continental fluvial to wave-influenced delta through wave-dominated shallow marine set up. Application of sequence stratigraphic rationale allowed subdivision of studied interval into two depositional sequences *viz.* Depositional sequence-1 (DS-1) that includes sediments of Rehatikhol and Saraipalli Formations and Depositional sequence-2 (DS-2) constituted of Bhalukona and Chuipalli Formation sediments. Bounded between non-conformity at its base and Type-I intraformational unconformity at the top, the DS-1, made up of Rehatikhol alluvial fan, braid-plain and

delta products followed successively upward by volcanoclastic tuff and storm-influenced shelf sediments of the Saraipalli Formation, preserve record of early transgression in the Singhora Sea. Estimation of paleohydraulic parameters from the Rehatikhol braid-plain revealed a higher gradient (0.015 to 0.024m/m) character for Mesoproterozoic fluvial systems as compared to their modern analogues. The west-northwestward paleocurrent in the Rehatikhol fluvial system suggests source area in the east-southeast. A northeast-southwest shoreline trajectory is interpreted for the early Singhora Sea from crest line trends of swash-generated bedforms. High velocity storm return flow was operative on the Saraipalli shelf that incised deep narrow scours on the proximal shelf and made it a 'zone of bypass'. Deposition under storm action was restricted only within then distal part of the shelf.

With forced regression and formation of Type-I unconformity, Bhalukona fluvial system encroached the Saraipalli shelf. From reversal in paleocurrent direction (from WNW to ESW) and abrupt shift in 'Nd' isotope value across the unconformity, a tectonically triggered basin-reversal is inferred. The low-gradient Bhalukona ramp experienced a long distance (~ 15 km) regression. The onset of slow, steady rise in sea level established wave-dominated Bhalukona coast line. Wave reworking of fluvial sediments in the lowstand shoreline resulted development of pebbly ravinement deposit (within the wave base), which correlates with unconformity in landward part. With aggradational stacking the beach-foreshore, upper- and lower-shoreface sediments record lowstand deposition. A basin-scale transgression formed Transgressive Surface of Erosion at the top of the Bhalukona succession and established the Chuipalli shelf.

Two phases of tectono-thermal activities recorded from the studied stratigraphic interval. A 2 to 5 m thick bedded tuff demarcating boundary between the Rehatikhol and Saraipalli Formations represents the older phase and a discordant diabase intrusive within the Saraipalli Formation represents the younger one. The rhyolitic to dacitic tuff akin to volcanic arc granite yields an age ca. 1500Ma. This ~1500 Ma tectono-thermal event is also identified as the forcing behind basin subsidence and transgression of Saraipalli marine shelf on to the Rehatikhol braid-plain. On the other hand, the diabase intrusive is compositionally basalt to andesitic basalt with subalkaline basalt affinity and possibly resulted from crustal assimilation/sediment mixing. ε^{t}Nd values (+0.3-+2.3) indicate depleted isotopic character and calculated T_{DM} age is 1.7-1.9 Ga. The calculated Sm-Nd mineral-whole rock isochron age of 1420 Ma is suggestive of its age of emplacement. It is surmised that the tectonic destabilization that triggered the emplacement of diabase intrusive, is also responsible for the forced regression and generation of Type-I unconformity marked by incursion of Bhalukona fluvial system on the Saraipalli shelf.

CONTENTS

CHAPTER-I:

INTRODUCTION

The Proterozoic era (2500 Ma–543 Ma) represents nearly one-third the Earth history and records dramatic changes in the Earth evolution that includes accretion and dispersal of continental blocks in a cyclic manner. In the process, it witnessed repeated amalgamation and break-up of the 'Supercontinent's (*Dalziel,* 1997), dramatic changes of oceanic and atmospheric composition (*Hoffman et al.,* 1998), biological evolution leading up to the advent of multicellular life (*Knoll,* 1994), growing importance of Phanerozoic-style plate tectonics and major changes in upper crustal composition (*Taylor and McLennan,* 1997). Reconstruction of these processes related to the formation and dispersal of the 'Supercontinent' in Proterozoic time is a major challenge for Precambrian geologists and demands i) identification of crustal-scale processes those underpinned microcontinent docking leading to the stabilization of crust control evolution of inter-cratonic mobile belts and force depositional history of craton-margin extensional or compressional orogeny and ii) understanding of timings for such crustal-scale processes. The recent articles on crustal dynamics vis-à-vis evolution of sedimentary basin highlighted that the approach should be framed with four major causal factors, *viz.* plate-tectonics, magmatism, eustasy and palaeoclimate (*e.g. Miall,* 1990; *Allen and Allen,* 1990; *Eriksson,* 2001; *Leeder,* 2011). Hence, multi-proxy analyses involving different geodynamic units viz. sedimentary basin-fills, hosting cratons, magmatic suits hosted within the craton/s or transecting the basin fill/s and adjoining mobile belts, if any, is considered as the coveted pathway towards understanding relationships between lithospheric changes, crustal dynamics and concomitant biosphere-atmosphere interaction through space and time. In fact, for carrying out regional study of any sedimentary basin involving identification of forcings behind its origin and filling motif in space and time framework and providing some sort of global correlation for the delimited events, it is important to find out exact ages of the sedimentary strata and to understand the coeval crust-mantle interactions. This leads us to unravel the overall tectonic parlance of a terrain at a given period of time. It has increasingly been realized that the study of physical sedimentation should be collated with the geochemical and geochronological proxies registered in finer grained clastics that may become helpful not only for better constrain on the physico-chemical aspects of basin development, but also for tracking the provenance and the processes operative in the provenance.

Worldwide, supracratonic continental to shallow marine basins with large dimensions (often exceeding several thousands of square km. in aerial extent) and deposits with layer-cake stratigraphy represent the Proterozoic Eon. For example, the McArthur and Amadeus basins, Australia, lower

Transvaal basin, South Africa, Athabasca basin, Canada and Belt basin, USA and basins on the Russian platform are some of the classic examples of sedimentary basins belonging to the Proterozoic time. Examination of most widely accepted treatises on sedimentary geology, however, shows limited attention devoted to Precambrian sedimentation *per se*, and a preponderance of papers published in the leading journals dealing with the Phanerozoic sedimentary record. Apart from wide spread exposures and easy accessibility, the other significant reason behind such partitioned attention towards Phanerozoic record is the lack of interest shown by hydrocarbon industry in studying the Precambrian archives. Going beyond this barrier, the present work thrives towards investigation of sedimentary packages and igneous bodies hosted within three basal stratigraphic subdivisions of 'Formation' rank from a Mesoproterozoic basin of central India namely the Singhora basin, a proto-basin for the Chhattisgarh basin, using multi-proxy analyses.

1.7. Brief highlights on Precambrian sedimentary basins and clastic sedimentary processes:

Predominant warm climate in the Archean and most parts of the Proterozoic (*Eriksson et al.* 1998) and enhanced levels of greenhouse gasses promoted aggressive weathering (*Donaldson and de Kemp,* 1998); however, both the rates of weathering and absolute levels of atmospheric CO_2 remain uncertain (*Hessler and Lowe,* 2006). If the weathering products were not dissolved, or removed by the wind, a greater availability of fines should have promoted mass flow and hyperconcentrated-flow processes, at least in the alluvial fan and river systems. The lack of sediment binding, baffling, and trapping by plant roots, which would have promoted a tendency for flashy surface runoff, lower bank stability, and faster rates of channel migration than in post-Devonian river systems (*Schumm,* 1968; *Cotter,* 1978; *Long,* 1978, 2004; *Fuller*, 1985; *Els*, 1990, 1998). Also, the long and complex history of early plate tectonics followed by a modern style of plate interactions in the ca. < 2.0 Ga period and the subsequent Neoproterozoic and Phanerozoic regime of Wilson cycles as Supercontinents formed and dispersed, resulted in marine deposits at the margin of the two adjacent Precambrian cratons. Essentially, thus Precambrian marine deposits comprise a record of epeiric seas rather than the remnants of open ocean margins, shelves and deep sea settings (*Eriksson et al.,* 2004; *Bose et al.,* 2011). The Precambrian marine record must therefore be treated with caution due to this preservational bias towards epicontinental sea deposits. It is also necessary to discriminate

between epeiric seaways (with shelf-like portions, shelf-breaks and even deeper distal parts; strongly directional currents) and epeiric embayments (lacking shelf-breaks and ocean-type currents). The reduced shelf gradients of many epeiric seas would have tilted the balance in favour of tides instead of storms (and thus also waves) in shallow marine platforms. The development of the large scale, tide-dominated Precambrian epeiric embayments, with gentle gradients towards open oceans was commonly associated with large braided fluvial systems draining craton interiors and which flowed directly into these shallow seas (*Eriksson et al.,* 2008). However, the available knowledge base also recognises that the processes and products within glacial, desert, delta, and possibly lake settings show strong resemblance with their Phanerozoic counterparts. Hence, it is conceivable that many distinctions between Precambrian and Phanerozoic sedimentation patterns are subtle and remain masked by the overall similitude at the facies to basinal scale. It may not be irrational to reiterate the dictum of *Donaldson et al.* (2002) that it is really rates and intensities of processes rather than the nature of the processes that distinguishes the Precambrian record.

Apart from the issues related to rate, intensity and variability of exogenetic processes operational in the early earth, one more challenging issue is the understanding and characterization of tectono-magmatic processes operative at the initiation and evolution stages of a basin. Formation and evolution of sedimentary basins is considered as the products of long-lived isostatic compensation due to (i) tectono-thermal processes operating at the lithosphere scale and (ii) water- and sediment-load effective at the basinal scale (*Allen and Allen,* 1990; *Eriksson et al.,* 2001; *Slingerland et al.,* 1994). For Precambrian sedimentary basins such understanding is fraught with several problems that include precise age bracketing, reconstruction of changes in relative sea-level, role of climate on rate and nature of mass wasting processes, and above all, the tectono-magmatic processes operative at shallow to deep crustal levels that underpin the initiation and evolution of the basins. In the backdrop of Precambrian supercontinent assembly *viz.* Ur (3.0 Ga), Kenorland (2.7−2.5 Ga), Columbia (1.9−1.8 Ga), Rodinia (1.1 Ga) the understanding of tectono-magmatic processes that govern sedimentary basin evolution has become important. It is believed that the large-scale mantle down-welling and upwelling in course of 'Supercontinent' assembly and breakup affect the Earth's dynamo; which leads to the large-scale subsidence of the crust causing initiation of sedimentary basins hosted within it (*Santosh and Zhao,* 2009; *Yakubchuk,* 2010; *Santosh,* 2010). Fundamental controls on uplift, sediment supply and creation of accommodation although remained uniform through the geological time, the variability in the rates of crustal growth, plate movement and heat

flux forced the variations in rates of these parameters as well. Although consensus is yet to be achived on the time of initiation (*Miall,* 1990), a strong school believes in operation of plate tectonic processes and consequent development of Supercontinents since the late Archean-early Proterozoic time (*Brandl and De Wit,* 1997; *Martins-Neto et al.,* 2001; *Mueller and Corcoran,* 1998, 2001; *Windley,* 1995). Despite the understanding, studies remained compartmentalized; rarely attempts have been made for characterization of igneous inputs (concordant or discordant) within any sedimentary basin to appraise shallow to deeper level crustal processes operative in course of initiation and evolution of the basin. Examples are limited in global and particularly in Indian context. Such exercise also demands a proper constraint on chronology of events related to the development of basin, which is often ill constrained in the Precambrian fossil-poor systems (cf. *Das et al.,* 2009; *Bickford et al.,* 2011c).

1.8. A general overview on Precambrian crustal subdivisions of central India:

The central Indian Baster craton hosts a number of Mesoproterozoic sedimentary successions (Chhattisgarh, Khariar, Ampani, Indravati and Sukma), mostly on its eastern boundary (Fig.1.1). The entire area has been delimited by two regional crustal discontinuities *viz.* Pranhita– Godavari Rift on south–southwest and Mahanadi Rift on north– northeast, and the NNE–SSW trending Eastern Ghats Mobile belt (EGMB) on east–southeast. The boundary between the EGMB and the Bastar craton is demarcated by the presence of a narrow but regional terrain boundary shear zone (*Biswal,* 2000; *Bhadra et al.,* 2004; *Gupta et al.,* 2000). The different subdivisions have been studied independently by previous researchers focusing the possible age of cratonization, geochemical affinity of the rock suites, tectonothermal evolution of the orogenic belt and depositional history of the sediments (*Karmakar et al.,* 2009; *Srivastava and Gautam,* 2009; *Chakraborty et al.,* 2010; *Dasgupta et al.,* 2013). Evidences of mafic and felsic magmatism are reported from the Eastern Ghats granulite belt (1455±80 Ma and 1464±63 Ma; *Shaw et al.,* 1997), and emplacement of alkaline complexes is noted at the western boundary (~1.4 to 1.5 Ga, *Upadhyay et al.,* 2009) of the mobile belt. *Biswal et al.* (2003) documented development of terrain boundary shear zone on the east of Khariar basin and *Ratre et al.* (2010) recorded magmatic intrusions in Bastar craton in and around the shear zone. Recent discovery of ca. 1.33 Ga U–Pb zircon age data in the Kanigiri ophiolite mélange, close to the boundary of EGMB and Cuddapha basin, is significant as it implies an arc-continent collision at the craton–mobile belt contact (*Dharma Rao et al.,* 2011). The idea, however, fall short of getting support from other lines of study. Working on the tholeiite and boninite–norite

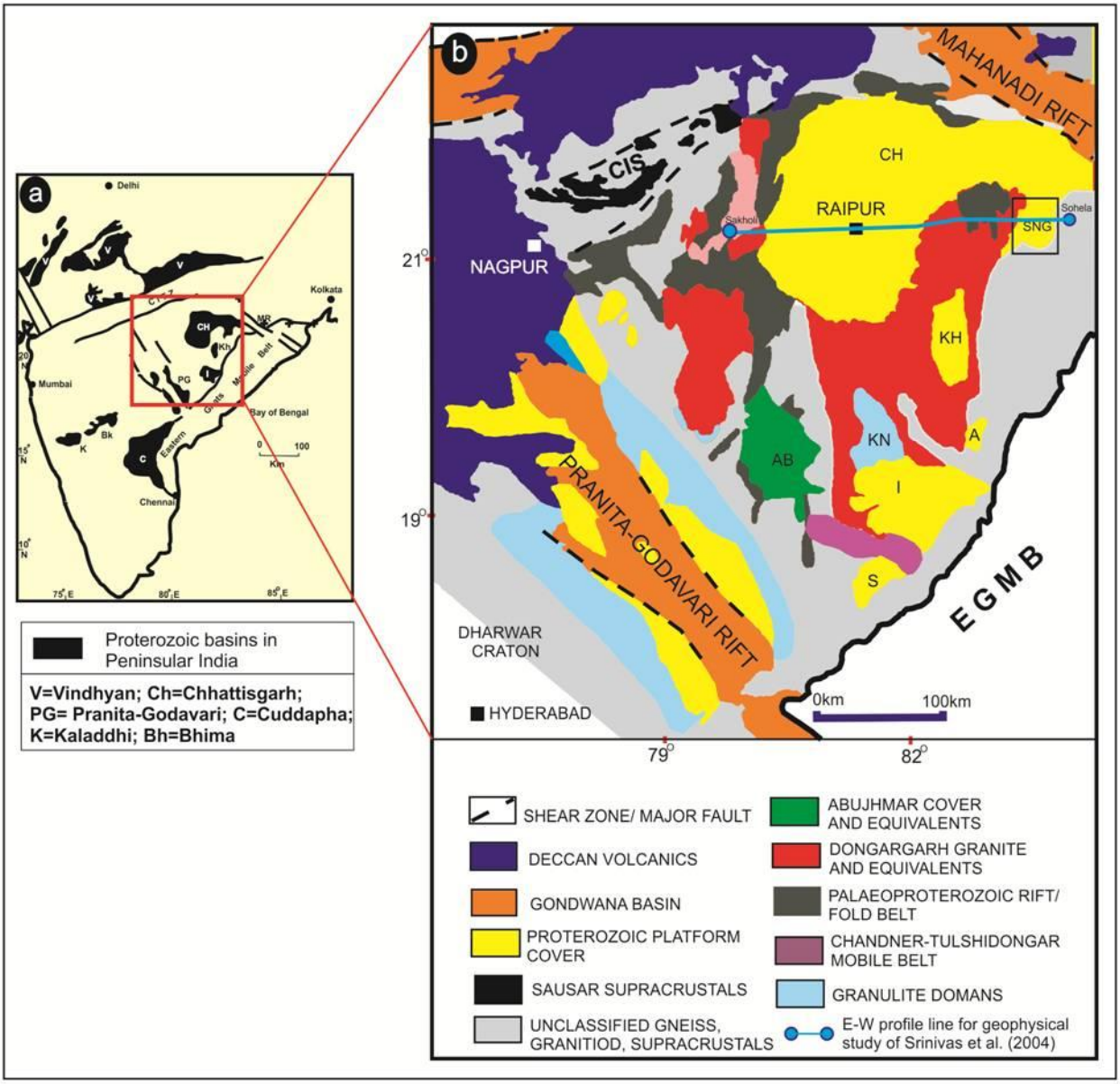

Fig.1.1. (a) Distribution of Proterozoic platformal basins in the Indian Shield. (b) Crustal subdivisions and tectonic elements associated with Bastar craton modified after *Santosh et al.* 2004. Note, a number of Mesoproterozoic sedimentary successions [Chhattisgarh (CH), Singhora (SNG) (marked in back box), Khariar (KH), Ampani (A), Indravati (I) and Sukma (S)] located mostly on the eastern boundary of Bastar craton fringing the Eastern Ghat Mobile Belt (EGMB).

rocks exposed in different parts of Bastar craton in the form of volcanics and dykes; *Srivastava and Singh* (2004), *Srivastava* (2006) and *Srivastava and Gautam* (2009) proposed rifting in the Mesoproterozoic time. *Roy et al.,* (2006) related the rifting in the southern Bastar craton with basic magmatism within the southern granulites of Sausar mobile belt. From structural fabric in the western part of the central EGGB and adjoining Ampani basin a co-deformed character is suggested

(*Gupta et al.,* 2004) and interpreted as an effect of westward thrusting of EGMB on Bastar craton during its final cratonization event in late Neoproterozoic to Paleozoic time (*Biswal, et al.,* 2007). The aligned alkaline complexes at the boundary of EGMB and Bastar craton, represented by deformed alkaline rocks, tholeiites and carbonatites, are interpreted as products of Mesoproterozoic rifting (1480±17 Ma; *Upadhyay et al.,* 2006) related to continental break-up and got subsequently deformed during the collisional event associated with the westward thrusting of the Eastern Ghats Province granulites over the cratonic foreland (*Gupta,* 2012). Although signatures of extensional tectonics cannot be denied in presence of alkaline and related igneous rock suites; it is also undeniable that an overall compressional tectonics was operative in the Mesoproterozoic time around the central Indian Bastar craton. A consensus view is, however, yet to be reached that can accommodate all lines of evidences.

The Chhattisgarh basin (33,000 km^2 in area) at the crustal boundary between the craton and the Proterozoic mobile belt (EGMB) represents the third largest 'Purana' succession in Indian Proterozoic stratigraphy (*Chaudhuri et al.,* 2002; *Paranabis-Deb and Chaudhuri,* 2007, 2008; *Bickford et al.,* 2011a, b; *Das et al.,* 2009; *Chakraborty et al.,* 2009; *Biswal et al.,* 2002; *Ratre et al.,* 2010, *Gupta,* 2012 and references there in). Although major exposures of the Chhattisgarh basin can be traced westward away from the margin of the craton, available depositional models envisage opening of the basin at the south-eastern part of the exposure area close to the cratonic fringe zone. The basin, despite occupying a crucial geotectonic position has drawn only cursory attention, principally centred on describing the lithology and establishing an acceptable basin-scale stratigraphy (*Dutt,* 1964; *Murthy,* 1987; *Moitra,* 1995; *Datta,* 1998). That there are signatures of cyclic sedimentation in the Chhattisgarh history, though pronounced as early as in 1969 by *Schnitzer*, no attempt has been made to document the scales of cyclicity, their controls (allogenetic or autogenetic) and spatio-temporal variability. Documentation of depositional processes, their variability in continental, transitional and marine settings through the history of basin filling also remained undocumented. Igneous inputs, although reported from different stratigraphic levels within the basin fill in the form of dykes and sills, their characterisation through the Chhattisgarh sedimentation history also remained unattended. Only the last decade has witnessed some attention on Chhattisgarh geology, albeit limited to specific stratigraphic intervals, to understand the history of basin-fill in space-time domain. Again, these studies were confined to the upper part of the basin fill package (*Chakraborty and Paul,* 2005; *Paul and Chakraborty,* 2003; *Partanabis-Deb and Chaudhuri,* 2007; *Chaudhuri et al.,* 1999); the operative

depositional processes; their variability in space and time remained for the early history of the basin evolution.

1.9. General geology of the Chhattisgarh Supergroup:

The Chhattisgarh Supergroup (~2300 m thick) is a succession of mixed siliciclastic-carbonate lithology and lies unconformably over the granites and gneisses of unclassified Archean or Paleoproterozoic gneiss of Bastar craton (*Santosh et al.,* 2004; *Conrad et al.* 2011). On the basis of basin-scale geological mapping (Fig.1.2), *Das et al.* (1992) collated the local-scale stratigraphy proposed by earlier workers in last four decades (*Dutt,* 1964; *Murti,* 1987; *Moitra,* 1990; *Schnitzer,* 1969) and proposed a three-tier classification for Chhattisgarh Supergroup *viz.*, Singhora Group, Chandarpur Group and Raipur Group, in order of superposition (table.1.1), exposed in two sub-basins *i.e.* Hirri and Baradwar and marked the 'Singhora Group' as the lowermost amongst them with a separate status as 'Proto-basin' (*Das et al.* 1992, 2003). While the Singhora and Chandarpur Groups are essentially siliciclastic, represented by conglomerates, sandstones of different size range and shale, the Raipur Group is dominated by stromatolites and lithographic limestones.

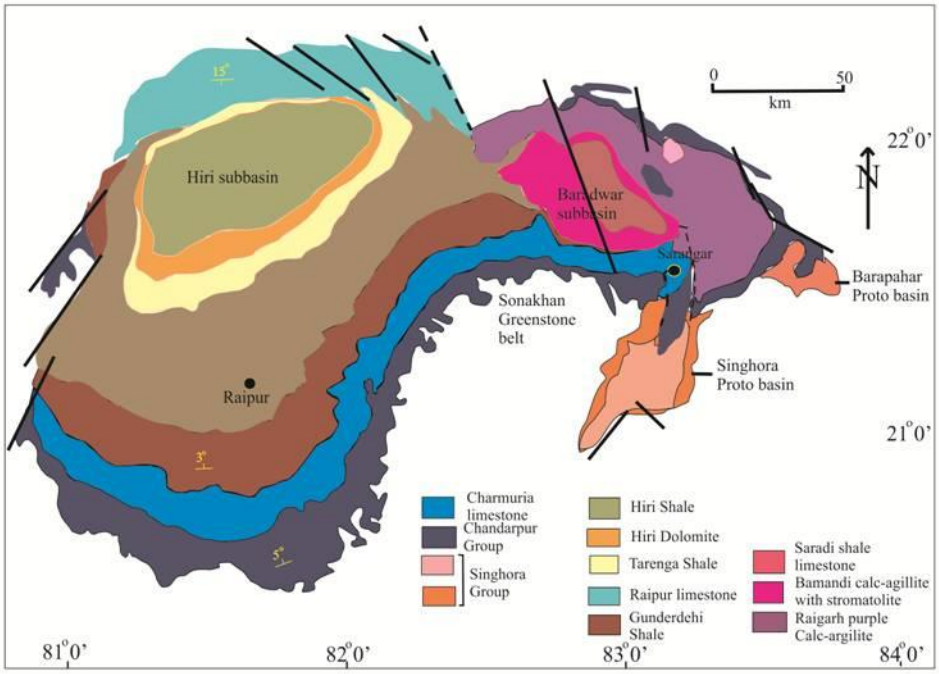

Fig.1.2. Generalized geological map of the Chhattisgarh basin, after *Das et al.* (1992) and *Moitra* (1996).

Table.1.1. Stratigraphic succession of Chhattisgarh Supergroup, as proposed by different workers.

		Dutta (1964)	Schnitzer (1969)	Murti (1987) (south central part)	Moitra (1990)	Das et al. (1992)
Chhattisgarh Supergroup	Raipur Group	Raipur Shale-limetone (450m) Khariagarah sandstone (variable tnickness) Gunderdehi Shale (180m) Charmuria Limestone (300m)	Maniari Shale(100m) Hiri-dolomite (50-100m) Belha Limestone (80m) Patharia-Umaria Shale (50m) Nandini Limestone (80-100m) Bhatapara Limestone and dolomite (50m) Lilagarh Shale (50m) Akaltara Dolomitic Limestone and arenite (40m)	 Tarenga Formation (+180m) Chandi Formation (670m) Gunderdehi Formation (430m) Charmuria Formation (490m)	 Tarenga Shale (180m) Khariagarh (Deodengar) sandstone(variable thickness) Raipur limestone Gunderdehi shale (430m) Charmuria limestone (490m)	Maniari Formation (70m) Hiri Formation (+70m) Tarenga Formation (180m) Chandi Formation (670m) Gunderdehi Formation Charmuria Limestone Formation
		~ Unconformity ~	~ Unconformity ~	~ Unconformity ~	????	~ Unconformity ~
	Chandarpur Group	Chandarpur Sandstone (300m)	 Karuid Shale (100-150m) Karuid Limestone (50m) Seorinarayan shale (100m) Saramgarh bituminous and silicious limestone (30-50m) Chandarpur quartzite (200m)	Kansapathar Formation (+125m) Chaporadhi Formation Lohardih Formation (240m)	 Chandarpur Sandstone	Kansapathar Formation (20-200m) Chaporadih Formation (20-200m) Lohardih Formation (20m)
						~ Unconformity ~
	Singhora Group					Chuipalli Formation Bhalukona Formation Sarapali Formation Rehatikhol Formation
		~ Unconformity ~	~ Unconformity ~	~ Unconformity ~	~ Unconformity ~	~ Unconformity ~
	Archean	Granite, Diorite	Crystalline complex	Sonakhan granite-greenstone and gneissic basement	Precambrian Granite	Precambrian basement

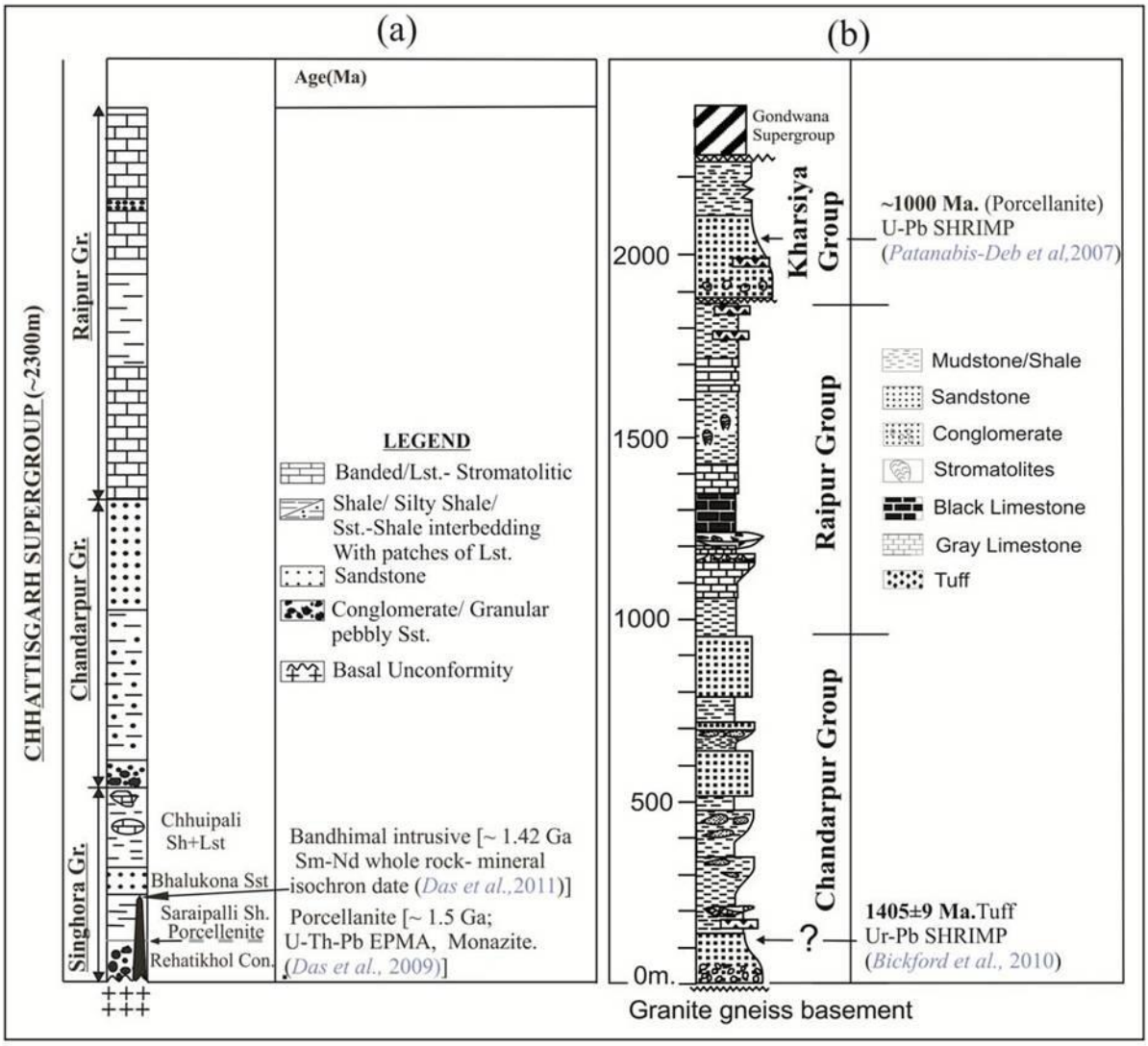

Fig.1.3. The two contrasting stratigraphic columns as available in published literature (i) modified after *Das et al.* (1992) and (ii*) Patranabis-Deb and Chaudhuri* (2008), followed by *Bickford et al.* (2011a,b,c). Note the later has no independent status for Singhora Group of rocks.

1.9.1. The ongoing debate on basin stratigraphy:

In recent time the three-tier classification of Chhattisgarh basin, as proposed by *Das et al.* (1992) and followed by *Das et al.* (2003) (Fig.1.3a) has become a topic of debate as one school of thought (*Patranabis-Deb and Chaudhuri,* 2008) considered Singhora and Chandarpur Group of rocks as one and the same. *Patranabis-Deb and Chaudhuri* (2008) (their fig. 1), working on the eastern half of the basin, subdivided the Chhattisgarh succession into two sequences viz. Sequence I and II. Without any reference to the Singhora Group, these authors described the Sequence I as

unconformably overlying the granitic/gneissic basement of the Bastar craton and internally constituted of siliciclastic formations belonging to the Chandarpur Group and carbonate-shale formations of the Raipur Group and identified the newly introduced Kharsiya Group as Sequence II that overlies the rocks of the Raipur Group with unconformable relationship (Fig.1.3b).

This idea was subsequently adopted by *Bickford et al.* (2011a) (their fig. 3) while putting forward an age bracket for Chhattisgarh deposition on the basis of U–Pb SHRIMP geochronology. This two-tier classification for Chhattisgarh succession, without any reference to the basal Singhora Group, is argued strongly by *Chakraborty et al.* (2009, 2011) by advocating the presence of an angular unconformity between the deformed Singhora Group and its overlying near horizontal strata of the Chandarpur Group. The recent work by *Saha et al.* (2013) has convincingly documented the deformed character of Singhora rocks and in the process established an angular unconformable relationship between north–south striking Singhora Group and its overlying east–west striking Chandarpur Group.

1.3.2 Age:

Table.1.2. summarizes the age constraints available for the Chhattisgarh Basin. Until 2007 there were few geochronologic data available in literature on geochronology of this basin. The basin was considered as of latest Neoproterozoic or older in age on the basis of K-Ar dating of Glauconite, paleomagnetic study of shale and stromatolite biochronology (*Naqvi,* 2005). From K-Ar dating of authigenic glauconite minerals from the sandstones of Chandarpur Group, *Kreuzer et al.* (1977) suggested an age of 700-750Ma. This age was regarded as the minimum age of sedimentation in the basin. From paleomagnetic studies, *Murti* (1987) had suggested that the age of Gundredehi Shale of Raipur Group is close to 1250-1300 Ma. The study of stromatolite in Chandi Formation of Raipur Group suggested middle to upper Riphean age (*Chatterjee et al.,* 1990). *Moitra* (1990) through his study of stromatolites in Raipur Group suggested a late Riphean to Vendian age for the upper part and middle Riphean to the lower part of the Raipur limestone. *Chakraborty et al.,* (2002) through their comparative stable isotope (C and O) study of Raipur Limestone with $\delta^{13}C$ secular curve for late Proterozoic time (*Kaufman et al.,* 1992) also suggested Upper Riphean age for Raipur Limestone in accordance to the possibility soughed by *Banerjee and Majumder* (1999) that the Chhattisgarh

Table.1.2. Age constraints available from three different Groups of Chhattisgarh Supergroup.

	Dated rocks	Methods	Raipur Group	Chandarpur Group	Singhora Group
Bikford *et al.*, 2011	Porcellanite	U-Pb, SHRIMP.	993±8Ma.		1405±9 Ma
Sinha *et al.*, 2011	Doleritic Sill	Rb-Sr, whole rock isochron			1121±742 Ma
Das *et al.*, 2011.	Diabasic intrusive	Sm-Nd, Mineral-whole rock isochron			1421±23Ma.
Das *et al.*, 2009.	Porcellanite	U-Th-Pb, EPMA			~1500 Ma.
Patranabis-Deb *et al.*, 2007.	Porcellanite	U-Pb, SHRIMP	~1000 Ma.		
Chakraborty *et al.*,2002.	Limestone	$\delta^{13}C$ secular curve	Up. Riphean age and transgressed the Pc-c boundary up the section		
Moitra, 1990.	Stromatolic limestone	Stromatolite	Mid.Riphean-Vendian age		
Chatterjee *et al.*, 1990.	Stromatolic limestone	Stromatolite	Mid.Riphean-Vendian age		
Murti, 1987.	Intrusive (Gunderdih Shale)	Paleomagnetic studies	1250-1300 Ma.		
Kreuzar *et al.*, 1977.	Authigenic glauconite from sandstones	K-Ar method		700-750 Ma.	

history might had transgressed the Precambrian-Cambrian (Pc/C) boundary up the section.

A trend shift is witnessed since 2007 with application of robust geochronology (U-Pb SHRIMP, U-Pb-Th EPMA) on zircon and monazite grains recovered from bedding parallel tuff and ignimbrite layers present at different stratigraphic levels within the Chhattisgarh sediment package. *Patranabis-Deb et al.* (2007) obtained U–Pb SHRIMP dates (1007 Ma) from zircon grains within ignimbrite and tuffaceous units in the upper apart of Chhattisgarh succession (Sukhda tuff and Sapos tuff) and proposed ~500 Ma tracking back for sedimentation history Chhattisgarh basin by assigning Mesoproterozoic time frame for the succession. The idea got support from the work of *Das et al.* (2009) (part of present study) in which U-Th-Pb monazite and zircon geochronology of the tuffaceous unit present within the Singhora basin along with its overlying and underlying

stratigraphic units allowed a narrowing of the Singhora tuff at ~1500 Ma. Subsequent U-Pb SHRIMP study on zircon grains from the same tuff layer within the Singhora basin (*Bickford et al.*, 2011a) has assigned the age of the tuff as at the most 1405 ± 9 Ma. *Bickford et al.* (2011b) also obtained a concordia upper intercept age of 993 ± 8 Ma from magmatic zircon grains from the Dhamda tuff within the Tarenga Formation (coeval with the Sukda tuff) in the uppermost part of the Chhattisgarh succession. It is now generally agreed upon by most of workers that most of the Chhattisgarh sediments were deposited between 1500 and 1000 Ma *i.e.* in the Mesoproterozoic time frame.

1.3.3. Previous sedimentological understanding:

Sedimentological studies within the Chhattisgarh basin are centred on the Chandarpur Group and in a limited way for the Raipur Group of sediments. An overview of literature shows that the products of continental [alluvial fan (*Patranabis-Deb and Chaudhuri,* 2007; *Chakraborty et al.,* 2009); and braid-plain (*Chakraborty and Paul,* 2005)], transitional [shoreface, foreshore and beach, tidal estuary and delta (*Patranabis-Deb and Chaudhuri,* 2002; *Chakraborty and Paul,* 2008)]; shallow marine [storm-dominated, intertidal and subtidal, occasionally lagoonal (*Datta et al.*, 1999; *Murti,* 1987; *Das et al.,* 1992, 2001; *Moitra,* 1995; *Patranabis-Deb and Chaudhuri,* 2002)] and deep marine [below strom wave base (*Chakraborty and Paul,* 2008)] are recorded from different stratigraphic levels of Chandarpur and Raipur sediments. Working on the upper Chandarpur succession, *Patranabis-Deb and Chaudhuri* (2002) proposed presence of depositional cycles (of alternating sandstone and mudstone dominated units) in different orders ranging in thickness between meter to several tens of meters and assigned 'punctuated aggradational cycle' (PAC) status to them. From a study across the transition from the Chaporadih to the Kansapathar Formation of Chandarpur Group, *Chakraborty and Paul* (2008) reported products related to lowstand, transgressive and highstand systems tracts and could delineate downstepping regressive (shoreface) wedges related to progressive lowering of wave base related to the formation of intra-formational unconformity. A broad marine subtidal to intertidal paleogeography has been invoked for the dominant stromatolitic succession of the Raipur Limestone (*Moitra,* 1995). Development of a sabkha condition towards the terminal part of the Chhattisgarh sedimentation history is presumed (*Das et al.,* 1990) from the occurrence of gypsum beds within the Kodwa and Dotu Formations of the Raipur Group. *Chakraborty et al.* (2002)

observed enriched $^{13}C/^{12}C$ ratio (2.27–3.89‰) from carbonates of Raipur Group and interpreted the signal in terms of higher oceanic productivity.

1.3.4 Evidences of Life:

Detailed report on form and species variant of stromatolites in Chhattisgarh sequence can be obtained from the works of *Ghosh and Shah* (1965), *Murti* (1978), *Schnitzer* (1977), *Jairam and Banerjee* (1980) *Moitra* (1990, 1995). For description of microfossils the works of *Srivastava* (1977), *Moitra* (1984, 1990) deserves mentioning. Sporadic occurrence of microbiota has also been reported but lack of any systematic study does not allow building up their significance in terms of genetic stratigraphy. The reports of microbiota including filamentous algae mainly came from different parts of Charmuria and Raipur Limestone (*Srivastava,* 1977; *Moitra and Pal,* 1984; *Moitra,* 1986, 1990, 1995, 1999). The varieties of microbiota community recorded in the Charmuria and Raipur Limestone are prokaryotic cyanobacteria; mostly filamentous and rarely coccoids, unidentified algal remains and acritarches (*Moitra,* 1999). Gunflintia and Eomycetopsis dominate the Charmuria Limestone, while the Raipur limestone revealed abundant occurrence of Siphonophyeus and Oscillatoriopsis. A rich fossil assemblage of tapic carbonaceous metaphytes referable to eukaryotic algae, preserved on the bedding surface of grey carbonaceous shales belonging to Saraipalli Formation of Singhora Group, Chhattisgarh Supergroup, is recorded in and around Tushgaon village, Mahasamund District, Chhattisgarh state (*Babu and Singh,* 2011). The enigmatic fossil assemblage includes 12 taxa belonging to *Tuanshanzia fasciaria*, *Tuanshanzia lanceolata*, *Tuanshanzia platyphylla*, *Changchengia stipitata*, *Phascolites imparilis*, *Eopalmaria prinstina, Proterotaenia montana*, *Aggregatosphaera* sp. *Tyrasotaenia podolica* and along with cf. *Chuaria circularis*, *Tawuia dalensis* and broad tubular empty sheath cf. *Siphonophycus solidum* belonging to Cyanophyta, Chlorophyta, Rhodophyta and Phaeophyta algae.

1.3.5 Geophysical studies, basement configuration and available tectonic models:

In the absence of detailed geophysical data, interpretations differ on the basement configuration and tectonic setting of the Chattisgarh Basin, in general, and of the Singhora Basin in particular. *Srinivas et al.,* (2000) undertook a gravity survey and *Srinivas et al.,* (2004) carried out magnetic survey of the basin on an east-west transect viz. Sakholi to Sohela (marked in Fig.1.1) covering some part of the basement, Sakoli Greenstone belt on the western flank and Sonakhan

Greenstone belt in between the Hirri sub-basin and Singhora protobasin in the east (Fig.1.4). Rajnandgaon-Tumgaon-magnetic profile over the Hirri sub-basin of *Srinivas et al.* (2004) shows long wave length regional high anomaly with superimposed highs and lows (varies from –210 to 200 nT). Since the sediment pile is non-magnetic the anomaly pattern is considered to be reflection of undulatory basement topography and/or heterogeneous nature of the basement. Large contrast in susceptibility values (300 to 800 x 10^{-5} C.G.S units) can be attributed to basic and acidic intrusives into the basement. The magnetic value across the Tumgaon-Basna section shows a rengs between -620 and -160 nT where the cental part of the section is showing comparatively low magmetic anomaly; magnatic 'highs' are interpreted as schistose rocks of Sonakhan greenstone belt (*Srinivas et al.,* 2004). The continuous profile along Basna to Sohela, across the Singhora basin and

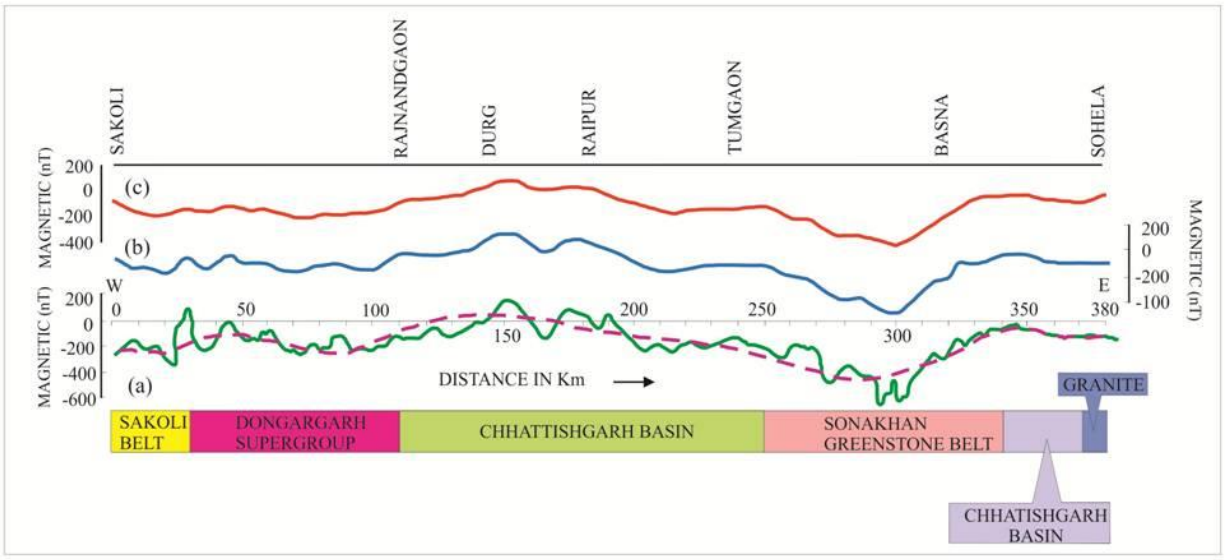

Fig.1.4. Magnetic profile, regional (b and c) upward continuous field of 3 and 6 km, surface geology along east-west profile. The dashed line indicate the assumed regional. Broad magnetic high id recovered over Chhattisgarh basin in comparition to Sakholi and Dongargarh Supergroup and Sonakhan Greenstone belt (after *Srinivas et al.* 2004).

part of Archaean/Proterozoic granitic basement shows broad magnetic high value range from -160 nT to 20 nT. The calculated sediment thickness i.e. 400-600 m for susceptibility of 200 X 10-5c.G.S.units (*Srinivas et al.,* 2004) matched with field –based thickness estimation (~400 m) of *Das et al.* (1992) and a sudden high value of 600 X 10-5 C.G.S. units at the depth of 8.6 km interpreted as presence of volcanic unit below the basement granite. Based on aeromagnetic anomalies, the basin is divided into the northern low anomaly zone and the southern high anomaly zone (*Ram et al.,* 2007). The northern portion has been further divided into two sub-basins viz. Hirri sub-basin (HRSB) in

the west and Baradwar sub-basin (BRSB) in the east by NW-SE trending Sonakhan greenstone belt with maximum negative amplitude.

Maximum thickness of Chhattisgarh sediments are estimated at 3500 m and 2400 m in the Hirri and Baradwar sub-basins, respectively. Incidentally, the sediment column thickness provided by different workers (Fig.1.2) on the basis of outcrop-based geological studies (1250 to 2200m) are also comparable with the thickness computed from the geophysical anomaly profiles. Overall, the basin shows a broad gravity high that is attributed to thin upper crust of the order of 13 to14 km except towards west of Raipur where thickness is slightly higher. The long wavelength gravity high observed over the basin is interpreted by the workers as the result of about 2 km Moho upwarp. The south-north magnetic profile (Dhamtari to Bilaspur) over Hirri sub-basin shows variation of values from –360 to + 90 nT. Modeling from the observed data reveals a few hundreds of meter thick sediment cover over Abhanpur to Raipur in the Chhattisgarh Basin, while an average thickness of 2000 m is interpreted towards the south of Abhanpur and 3000m to the north of Raipur. The apparent thickening of sediment on either side of Abhanpur and Raipur and thinning of sediment in between probably reflects a major structural feature (ridge like structure) associated with the evolution of Chattisgarh basin.

Besides geophysical data, attempts have also been made to propose tectonic model for the basin from other lines of evidences. Considering the depositional settings, *Chaudhuri et al.* (2002) and *Patranabis-Deb and Chaudhuri* (2007) proposed an intracratonic rift model, without citing any field-based supporting evidence, and claimed a late-stage basin inversion whereby normal faults rejuvenated as regional thrusts. Considering the lithological disposition and the map patterns, *Das et al.* (1992) suggested intracratonic sag setting, similar to the 'Desiccated Basin' model of *Allen and Allen* (1990). Based on the sedimentological modeling of the Chandarpur Group and the westward-wedging character of the basin-fill package away from the Eastern Ghat Mobile Belt (EGMB), *Paul* (2006), *Chakraborty and Paul* (2008) proposed a foreland model, in tune with the proposal of *Bishwal et al.* (2003) from their studies on the deformation pattern of the Bastar craton.

1.10. General overview of Singhora basin:

Unconformably overlying the Bastar granite gneiss complex, the ~ 400m thick sediment package, spreaded over 1000 sq. km. area, represents the Singhora Group and demarcates the lowermost Group in Chhattisgarh stratigraphy preserving early basin history for the Chhattisgarh basin (*Das et al.,* 2003). Singhora Group records basin-scale deformation and shows non-plane non-cylindrical fold geometry. Although, the non-planarity can be visualised in the regional scale, while non-cylindricity is more prominent on the outcrop-scale (*Saha et al.,* 2013). *Saha et al.* (2013) has explained the overall deformation pattern by two major compression directions, *i.e.* N-S and E-W, which was resulted by the overall compression direction of NW-SE. Also, these workers have reported a narrow shear zone (E-W) at the southern boundary of the Singhora basin and considered that the age of the deformation event should as younger than ~1420 Ma. However, the upper age bracket is still open and considered as pre-Chandarpur as the overlying Chandarpur Group has no report of deformation, so far. An alternate view on the deformation pattern is expressed by *Deb (2013)* in which the deformation within the Singhora cover sediment conserved as result of reactivation of basement fault.

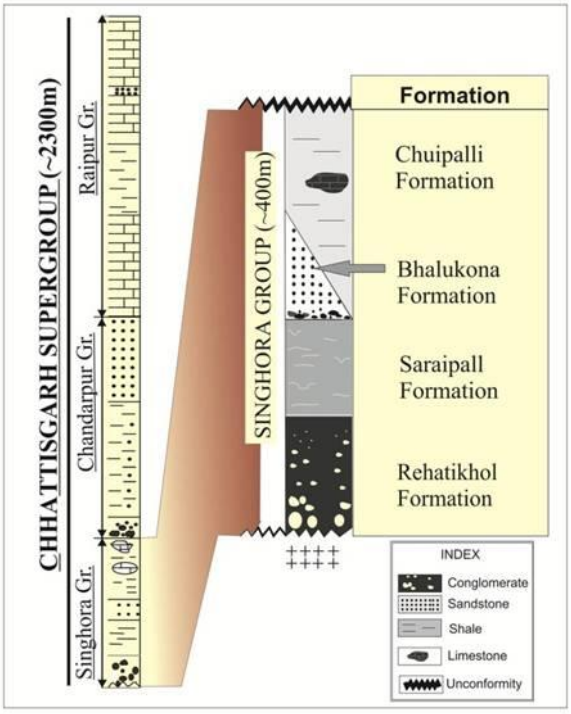

Fig.1.5. Stratigraphic framework of Chhattisgarh Supergroup (after das et al. 1992). Divisioning of Singhora Group in Formation level is shown on the right

The fossil-poor Singhora package is represented by arenite–argillite–carbonate sequence and comprised of four Formations, namely Rehtikhol, Saraipalli, Bhalukona and Chuipalli (Fig.1.5). As such, Singhora Group had escaped specialised sedimentological attention except for broad descriptions of different lithosomes (*Das et al.,* 1992 and *Das et al.* 2003). Rocks of this Group are punctuated by magmatic inputs at different stratigraphic levels either as concordant (volcanoclastics tuff) or discordant (dyke) bodies (*Chakraborti,* 1997; *Das et al.,* 2011) but no attempt has been made so far to use them as geochronological tools. Indeed, such dateable material helps in understanding the age of initiation of the basin and more precisely the age of litho-units in high resolution, though such studies merely uncommon in Precambrian sedimentary basins.

1.5. Necessity and scope of multi-proxy study in Singhora basin:

The salient reasons behind choosing the Chhattisgarh Supergroup, in general, and the Singhora Group, in particular, for the present study are:

1. Absence of any process-based sedimentological analysis and reconstruction of filling model for the basin in space-time framework using sequence stratigraphic rationale. Though exposure quality of the Singhora Group of rocks is not very good, the spatial variability in depositional motif in each of the constituent formations of this Group allowed application of epicontinental basin sequence model that understandably differ from passive margin in regard to physiography and hydrodynamic regime (*Hallam,* 1997; *Posamentier and Vail,* 1988).
2. Occurrence of sediments belonging to continental, transitional and marine set-up, the potential of these sediments of wide ranging environmental settings to offer important understanding on Mesoproterozoic sedimentation pattern, when land was devoid of vegetation and marine systems were unlike the modern ones.
3. Produce geochronologic data to put age bracket on the initiation of the basin using concordant and discordant lithodemic units present within the basin.
4. Characterizing the magmatic bodies and understanding the mutual interaction between the endogenetic as well as the exogenic processes in course of initiation of Chhattisgarh basin.
5. The Singhora succession is unmetamorphosed but, they are affected by post-depositional deformations. Yet, the sedimentary features are hermitically preserved.
6. Even though absence of fossils is disadvantageous, lack of bioturbation and spectacular preservation of primary as well as penecontemporaneous features help enormously determining depositional dynamics, identification of depositional agents and site of operation of these agents. Paleogeographic shifts traced over time and space provided clues for identifying the major forcings those guided the basin evolution.
7. Scope for exercising 'Nd' isotope mapping to cast idea on sediment provenance in the basin and its temporal shift, if any.
8. The unique geotectonic setting for the basin *i.e.*, presence of rift systems on its north and south and mobile belt in its east, which has prompted workers to propose widely varying tectonic model for the basin ranging between rift, intracratonic sag and foreland.

1.6. Outline of present work:

The present work aimed at gaining comprehensive geological knowledge on initial history of the Chhattisgarh sedimentation preserved in the Singhora basin with the help of field-based physical sedimentology and laboratory-based chemical appreciation of the studied sediment column. From mapping, high resolution litholog measurements, delineation of key stratigraphic surfaces, and tracking of those surfaces in space, the field based study allowed understanding of basin filling motif in space-time framework. Geochemical attributes provide corroborative evidences in order to substantiate field based inferences. One of the major objectives of present study is to provide time connotation two different events that forced the early Singhora sedimentation, which is addressed by geochronology of volcanic/volcano-sedimentary units present within the succession. Overall the present study aimed at multi-proxy analyses in the Mesoproterozoic Singhora Group to understand different intra-basinal and extra-basinal forcing/s operative in causes of evolution of the basin. Point wise the present work can be outlined as

- Process based facies analysis and palaeoenvironmental modeling of Rehatikhol, Saraipalli and Bhalukona Formation.
- Documentation of facies stacking pattern, facies sequence evolution motif and evaluation of the studied succession in terms of sequence stratigraphic rationale.
- Tracing geochemical proxy (Neodymium isotope signal) to corroborate inter-basinal unconformity and source reversal.
- Geochemistry and geochronology of concordant volcano-clastics and discordant volcanic units to constrain the age of events.
- Basin evolution model in spaceo-temporal framework involving all the available data gathered to multi-proxy study.

CHAPTER-II:

METHODOLOGY

Methodology includes field study; sampling; petrographic study under polarized microscope and Scanning Electron Microscope (SEM); major and trace element geochemistry using X-ray Fluorescence (XRF); Rare Earth Element analysis using ICP-MS; mineral chemistry and geochronology using Electron Probe Microanalysis (EPMA) and isotopic geochronological study using Thermal Ionizations Mass Spectrometer (TIMS).

2.1. Field methods:

The mainstay of the thesis is field study. The present work took into its purview three formations of the Singhora Group viz. Rehtikhol, Saraipalli and Bhalukona. Absence of any fossil data and common patchy outcrop forced making correlation between the detached outcrops relying principally on the process-based characterization (facies analysis) of the rock units. Based on the demand of the study, a basin-scale geological map was prepared (Fig.2.1) by taking several traverses along and across the general strike of the beds by using Survey of India toposheets (toposheet nos. 64 K/15, 64 K/16, 64 O/3, 64 O/4 and 64 O/7) in 1: 50,000 scale. However, the western boundary of the basin is drawn following *Das et al.* (2003) and *Basu and Singh* (2011). Using techniques conventionally employed for characterizing products of different sedimentary environments, process-based facies and paleo-environmental analyses were carried out on the rocks of all the three formations. Following facies and facies association analyses, a facies association map is prepared for the Bhalukona Formation. Lithologs were measured at several locations spread across the basin to document the stacking pattern. Facies-specific paleocurrents were measured and photomosaics were reconstructed to understand the mutual relationships between different genetic units. The depositional systems thus interpreted form the building blocks of systems tracts, the latter representing an essential concept for stratigraphic correlation and the genetic interpretation of the Singhora basin fill between the Rehtikhol and Bhalukona time. Isochronous and diachronous surfaces, *viz.* unconformity, flooding surface, ravinement surface etc. are identified and traced in basin scale to provide a sequence stratigraphic framework for the studied lithostratigraphic interval. Moreover, unweathered/relatively less weathered chunk samples were collected from different stratigraphical intervals of the sedimentary section for their petrographic study and 'Nd' isotope analysis; and a large number of unweathered samples (with individual sample weighing >5kg) from volcanic and volcano-sedimentary rocks were collected for geochemical and geochronological analyses.

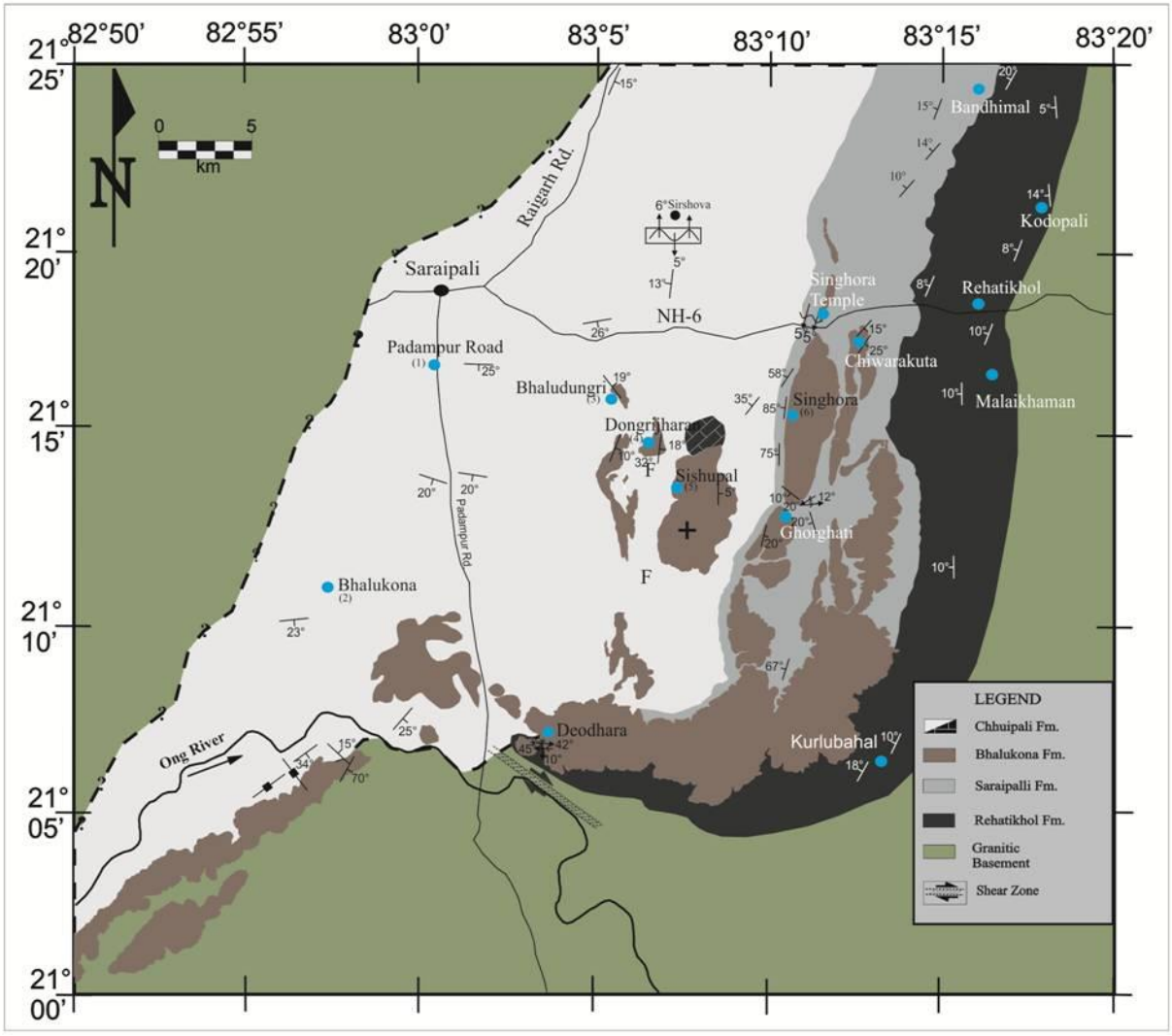

Fig.2.1. Generalized geological map of Singhora basin. The western boundary for the Singhora basin is drawn following *Das et al.* (2003) and *Babu and Singh* (2011). General attitudes of beds are depicted with locations of studied sections.

2.2. Laboratory Methods:

2.2.1. Instruments used:

- Polarized microscope for thin section study and reflected light binocular microscope for mineral separation by hand picking.
- Micrometer scale for grain size measurement.
- Electronic point-counter for modal analysis.
- Frantz® Isodynamic Magnetic Separator (Model LB-1). The instrument was used for mineral separation.
- Cameca SX 100 Electron Probe Micro Analyzer (EPMA) at the Wadia Institute of Himalayan Geology (WIHG) Dehradun, India for mineral chemistry.
- For the Bulk chemistry (major and trace elements), samples was analyzed by using XRF fused bead in Panalytical MagixPro machine at Hokkaido University, Japan.
- Rare earth elements (REE) were measured with ICP-MS (Perkin-Elmer) at WIHG.
- For determination of Rb–Sr and Sm–Nd isotope, Thermal Ionization Mass Spectrometer (Triton, Thermo-Finnigan) and clean lab facility were used at National Facility for Isotope Geosciences, Department of Earth Sciences, Pondicherry University. India.
- Softwares e. g. GCD-kit, Georient, Corel draw, photoshop, Microsoft office and isoplot were used extensively for representation.

2.2.2. Analytical methods followed:

i) Petrography and petrology:

Fresh samples were cut, polished, mounted on thin section and observed under polarizing microscope for i) petrographic study, grain size and modal analysis of sandstones, inferred as products of different depositional environments from outcrop-based studies, and ii) petrology and EPMA analysis for deciphering mineral chemistry and geochronology of the volcanic and volcano-sedimentary rocks. From the sedimentaries samples were collected from different facies associations and about 50- 75 thin sections were prepared from individual facies association for modal analysis. Following the Gazzi-Dickinson's QFL method (*Gazzi,* 1966; *Dickinson,* 1970), sandstone

petrography, i.e., estimation of quartz (Q), feldspar (F; also identified by acid-staining), and lithic fragments (L) of selected samples, was studied by a standard point-counting method wherein ~300 points were counted for each sample. The results are projected against the measured lithologs, wherever felt necessary. Grain size measurements were carried out on thin sections by using a transmitted light petrographic microscope fitted with an ocular micrometer (LEICA 0.01 mm). The value of statistical parameters determined from grain size measurement data, *viz.* median grain size (Mdφ), grain size sorting (inclusive graphic standard deviation, σ_1) are cited following *Folk* (1974).

ii) Scanning electron microscopy (SEM):

The fine-grained rocks of the Singhora basin were been studied using SEM attached with energy dispersive system (EDS), which proved to be particularly useful for the study of the fine-grained samples. Thin sections are polished up to 1μm diamond paste however; the tuff samples are polished up to ¼ μm diamond paste for SEM study. Images were taken using both secondary electron (SEI) and back-scattered electron (BSI). The monazite and zircon grains were searched using the BSI mode. The SEM images were taken at the Paleontology Division of Geological Survey of India, Kolkata using accelerating voltage of 15 kV. Some of the images were also taken by using Electron Probe Microanalyzer (JEOL JXA 8800) at National Science Museum of Tokyo using 15 kV of accelerating voltage. With same operating conditions, some samples were also studied using JEOL JSM-6390A equipped with JED-2300 energy dispersive system at the Hiroshima University, Japan.

iii) Electron Probe Microanalysis (EPMA):

Mineral chemical analyses were carried out using EPMA at two centres. The mineral chemistry of diabasic intrusive was analyzed at Wadia Institute of Himalayan Geology, Dehradun, India using Cameca SX 100 Electron Probe Micro Analyzer (EPMA). The EPMA was operated at 15 KV acceleration-voltage using 15 nA of specimen current. 1-2 μm probe diameter for the spot size was used for point analyses. Natural standards were used and raw data were corrected by PAP program.

In addition, monazite and zircon grains of the tuff samples were analyzed by EPMA to do U-Th-Pb chemical age dating. The EPMA dating technique followed in this study and the equations for age computations are described in detail by *Suzuki and Adachi* (1991, 1992), *Montel et al.* (1996), and *Santosh et al.* (2006). As number of grains on thin sections checked in SEM-BSI is very low, an amount of fresh rock chips was crushed into fine fractions in a stainless-steel stamp mill. Before powdering the broken chips were cleaned using reverse osmosis (RO) water. The powdered samples (<100 μm mesh size) were further cleaned using ultra-pure (Milli-Q) water, and then dried in an oven. The magnetic minerals were then removed using a hand magnet. Heavy fractions were separated by methylene iodide. Such fractions were then mounted on glass slides using epoxy resin, and diamond polished till ¼ μm size. Polished grain mounts were used for the study of grain characteristics and EPMA analyses. Chemical analyses were performed using an electron microprobe (JEOL JXA-8800) at the National Science Museum, Tokyo, with a 15 kV accelerating voltage, 0.5 μA probe current (0.2 μA for monazite), 2 μm probe diameter, and 200–300s of counting time for U, Th, and Pb. PRZ corrections (modified ZAF) were applied for the analyses. U, Th, and Pb standards were synthetic UO_2, ThO_2, and natural crocoite ($PbCrO_4$), respectively. Natural and synthetic minerals were used as standards for other elements. UM_α, ThM_α, and PbM_α lines were considered in the U, Th, and Pb analyses, respectively, and the spectral interferences of the ThM_ζ, YL_χ, and ZrL_γ lines with the PbM_α line and the ThM_β line with the UM_α line were corrected (Pyle *et al.* 2002). Accuracy of chemical ages were checked using monazite and zircon grains from Archean to Quaternary samples. A 994 ± 5 Ma zircon from Antarctica (K. Shiraishi, unpub. data), analyzed by SHRIMP, was used as an internal age working standard. This internal age standard was analyzed before and after the analyses of unknown samples to assess the daily drift of the analytical conditions, with the daily drift being less than 1% fluctuation. Details of the problems of chemical U-Th-Pb dating using the electron microprobe are summarized by *Montel et al.* (1996) and *Hokada et al.* (2004).

iv) X-ray Fluorescence analysis:

For major and trace element compositions of the studied rocks XRF technique was employed. The chips of porcellanitic tuff were powdered to 200 μm mesh size using a tungsten carbide mortar. Major and trace elements were analyzed by a wavelength-dispersive x-ray fluorescence spectrometry system (Siemens SRS 3000) at the Wadia Institute of Himalayan Geology

(WIHG), Dehradun. Analysis was carried out using pressed pellets glued with polyvinyl alcohol. The analytical procedure followed that of *Lucas-Tooth and Pyne* (1964). In addition, powdered samples of mafic intrusive samples were analyzed by XRF (major and trace elements) using fused bead in Panalytical MagixPro machine at Hokkaido University, Japan. For both tuff and diabasic intrusives, powdered samples were kept in oven at 100° C overnight. These dried samples were then measured in porcelain crucible before heated to 900° C for 5 hours. The loss-of-ignition (LOI) values were then calculated by the difference in weight before and after heating. Carbon content is measured by CHNS detector. The dried diabasic samples were mixed with flux mixture of $Li_2B_4O_7$ and $LiBO_2$ (4:1) and $LiNO_3$ oxidant in the ratio of flux:sample:oxidant= 4:2:0.6. This mixture is then heated to melt so as to make a fused bead to analyze in XRF.

v) Rare Earth Element analysis:

Rare earth elements (REE) were measured by ICP-MS (Perkin-Elmer) at Wadia Institute of Himalayan Geology, Dehradun, India with 0.04 gm of the sample subjected to standard acid digestion with HF-HNO_3. The standard acid treatment was repeated until a clear solution was obtained. The clear solution was then treated with 1N HNO_3, and a 100 ml solution was taken for analysis. The accuracy and precision were ±1%–3% for major oxides and ±5%–10% for trace elements and REEs.

vi) Rb-Sr and Sm-Nd Isotope analysis:

Flow chart of clean lab procedure for mineral separation and whole rock isotope geochemical analysis has been given in fig.2.2.

vi.a. Mineral separation:

Sm-Nd mineral whole rock isotope analysis of fine grain mafic intrusives requires pure minerals such as plagioclase, pyroxene, biotite and powdered whole-rock samples. The conventional mineral separation technique (*Mursky,* 1987) was followed during the analysis.

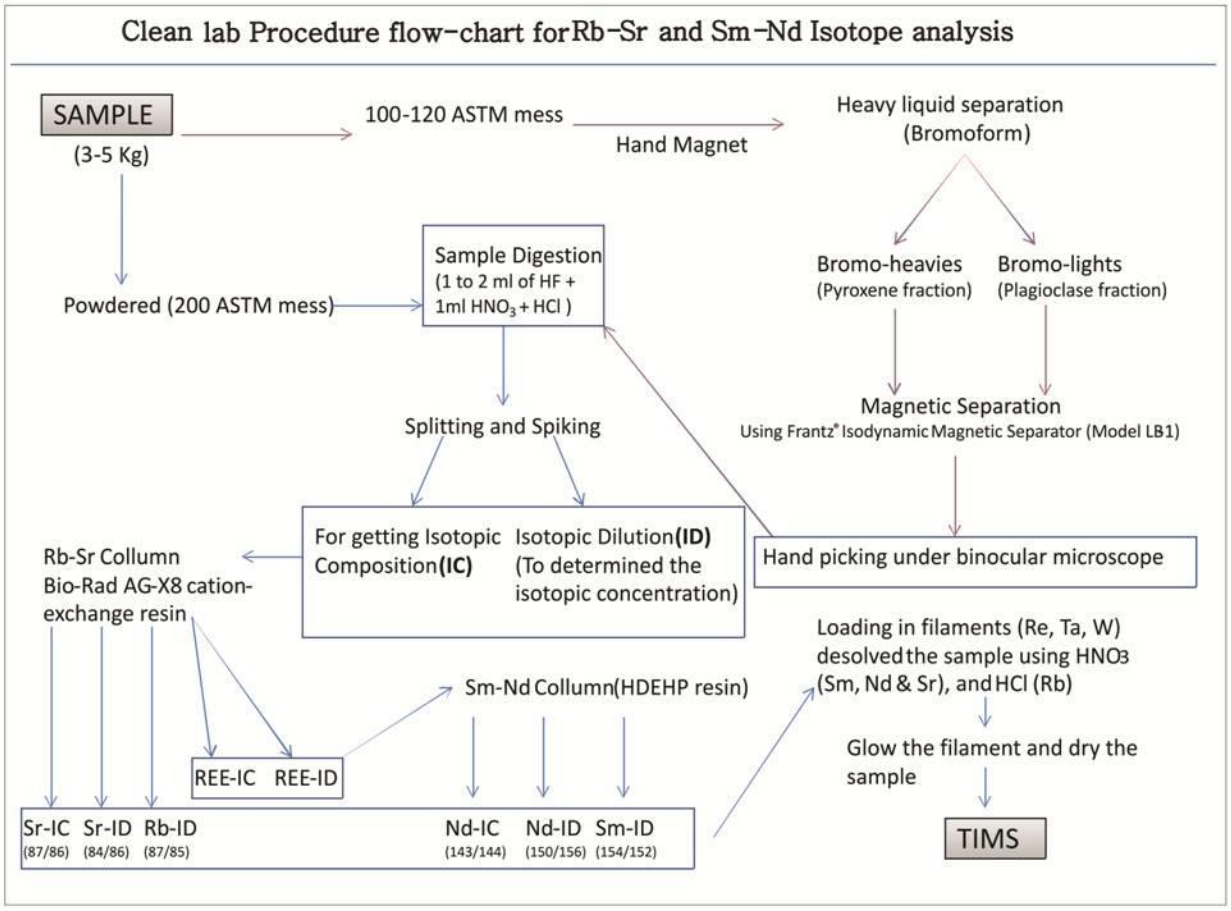

Fig.2.2. Flow chart illustrating clean lab procedure for mineral separation (red arrows) and whole rock isotope geochemical analysis.

Petrographically and geochemically well-studied fresh samples were chosen for mineral separation. The procedure started with the crushing and powdering of the samples. About 3-5 kg of the whole rock samples were cleaned, the weathered portions (if any) were removed and crushed using steel and agate mortar, respectively. The finer fractions were removed by continuous washing with Milli-Q water following which the samples were kept in a hot-air oven (temperature at 60°-70°C) for drying. The size fraction was set at about 100-120 ASTM mesh (i.e., 149-125 μm) for mineral separation. The common magnetic minerals were partially separated by hand magnet and rest of the minerals was concentrated by panning followed by heavy liquid (Bromoform $CHBr_3$) separation. Bromoform, with specific gravity of 2.89 at 20°C, is used as a heavy liquid. About 500ml of bromoform was taken in a separating funnel. About 150g of sample was poured and mixed with liquid using the glass rod and the mixture was given 5 minutes time to settle the heavier factions (specific gravity >2.89). Two fractions were collected separately in glass beakers. In bromoform

separated samples the heavier faction (bromo-heavies) was dominantly represented by concentrates of pyroxene, biotite, ilmenite and magnetite, and the lighter fraction (bromo-lights) was dominated by grains of plagioclase feldspar and quartz.

The individual (almost pure) mineral was then separated based on their magnetic susceptibility, at different current using Frantz® Isodynamic Magnetic Separator (Model LB-1). Magnetic field is produced by inducing current to the electromagnet and mineral fraction is then passed through a vibratory separatory channel/chute. Normally, it is recommendedable to keep the small inclination of the chute (few degrees) as variations of the magnetic field strength have strong influence on the separation characteristic. Systematically increasing current has been applied for separation of individual minerals. The minerals that are more magnetic are separated from less magnetic and collected in separate buckets. In present study almost pure pyroxene and feldspar grains has been separated from bromo-heavies and bromo-lights fraction, respectively. Finally under reflected light binocular microscope pure mineral grains were hand-picked for further chemical analysis.

vi.b. Chemical procedure of elemental separation (clean lab procedure) for isotopic study:

Approximately 100 mg of sample (mineral or whole rock) was taken for chemical digestion for Rb-Sr and Sm-Nd isotope analyses. Sample was precisely weighed (up to 4^{th} decimal) in a electronic balance and poured into pre-weighed 7ml Savillex® container. Then it is added with 1-2ml of HF, 1ml HNO_3 and few drops of HCl in and left on the hot plate overnight at 120°C for digestion. HNO_3 was added several times and the solution was dried to remove the fluorides present. At the final stage of digestion 2N HCl had been added to dissolve the sample to prepare a fluoride-free clear solution before moving to the next step, i.e. splitting and spiking. At this stage sample was split into two halves and added with isotope tracer (also known as spike, i.e. an element with one of its isotope enriched relative to its natural abundance) in one half. An isotope tracer solution was required for isotope dilution (ID) method of analysis for determination of highly precise elemental concentration. Remaining half of the solution was used for measuring the isotopic composition (IC) in the sample. The weight of the solutions and added spike had been measured accurately during this process. In next stage, the IC and ID fractions were passed through Bio-Red AG-X8 cation-exchange resin filled with HCl calibrated columns. Rb (ID) and Sr (ID and IC) ware collected with

2N HCl and REE fractions were collected with 6N HCl. The collected solutions were dried. The REE fractions of ID and IC were again diluted with 0.18N HCl and passed through the calibrated di(2-ethylhexyl) orthophosphoric acid (HDEHP resin) column for Sm and Nd separation. Nd (ID and IC) and Sm (ID) were collected with 0.3N HCl and 0.4N HCl, respectively. Few drops of 0.5M H_3PO_4 were added to the collected solutions and let them dry on the hot plate at a temperature of 120°C. H_3PO_4 ensure the visibility of samples within the beakers while picking up for loading on filament. If the collected sample (Rb or Sr) was found bulky then it was again passed through the cleanup column for further purification. Now, the dry sample was again converted into solution by adding 1µl HCl for Rb and 1 µl HNO_3 for Sr, Sm and Nd, and loaded into degassed filaments. Single filaments of Re were used for analysis of Sr, for Sm and Nd doubble Re filament and Ta single filament were used for Rb analysis. Ta filament was oxidized by TaO solution and followed the standard sandwich method of loading for Rb, in particular. After loading the sample at 1.5A current and allowing a stand-up time for it's drying so as to remove moisture it is kept in a safe box for final loading in Thermal Ionizations Mass Spectrometer (TIMS). The isotope ratios ($^{143/144}$Nd, $^{150/146}$Nd, $^{154/152}$Sm, $^{87/86}$Sr, $^{87/85}$Sr, $^{84/86}$Rb) were determined on Finnigan® TIMS. The laboratory work was carried out at National facility for Isotope geosciences, Department of Earth Sciences, Pondicherry University. AMES Nd standard analyzed nine times during the course of this study yielded mean $^{143Nd/144}$Nd ratio of 0.511968±2, and SRM-987 yielded a mean ^{87}Sr/^{86}Sr ratio of 0.710272±4. As the mean ^{87}Sr/^{86}Sr ratio on SRM is 30ppm higher than the reported value, the data on samples are corrected by this value.

CHAPTER-III:

FACIES ANALYSIS AND PALEOENVIRONMENTAL STUDY

In last four decades 'Sedimentology' as a discipline has evolved from understanding the operative processes in a grain scale (its roundness, sphericity, interaction with turbulent or laminar fluid etc.) to identification of basin-scale forcings (autokinetic and allokinetic) behind different kinds of stacking and sediment filling motif. Undoubtedly, concepts of 'Sequence stratigraphy' stands out as the most practiced modern paradigm that revolutionized the thinking process for understanding the evolution of a sedimentary basin fill in three-dimensional perspective, whether it is in outcrop-based studies or studies based on subsurface data. The backbone of such studies, however, remains in understanding products of different depositional agents and mutual association of such products in various terrestrial, transitional or marine settings, which is carried out by process-based facies and paleo-environmental studies. Importance of such process-based studies for sedimentary successions is well felt in seventies and eighties in the last century and significant advancements were achieved in making distinction between products of different depositional processes. In India, such practice within the Proterozoic basin fills remained confined within the Vindhyan and Pranhita-Godavari (P-G) basins; several other Proterozoic successions still await specialized sedimentological attention. The Singhora basin is one such basin that received little attention in terms of process-based studies. The present study thus aimed at process-based facies and paleo-environmental analysis within three basal 'Formation's of the Singhora Group and document spatio-temporal variability in depositional condition in basin scale through time.

Although the term 'facies' is old, the concept of facies modelling is much younger. Since the time of Paul Potter (*Potter,* 1959) the facies model evolved from a static model (*Walker,* 1979, 1984) based on consideration of modern environments to models in the light of responses to sea level change. In last three decades, there has been a large amount of new work on modern depositional environments. Consequently, with increase in size and diversity of data base and the appropriateness of using models in increasingly complex World, emphasis is shifted onto the individual depositional elements within environments, and the study of how these elements fit together laterally and vertically. The best models embody large amounts of information from as many examples as possible, modern and ancient. In generalizing this information, the resulting models can serve as reference points for interpretations of new situations and examples, and as a basis for making predictions from limited amounts of data in new situations. Although facies can be defined in many ways, the present study followed 'facies' definition on the basis of sedimentary features observed in the field, including variations in grain size and rock type (clastic or volcanoclastic), texture (matrix-

supported versus clast-supported), grading types (inverse, normal and ungraded), sedimentary structures and bed thickness.

Application of process-based study using facies analysis methodology revealed that the sediments of Rehtikhol and Saraipalli Formations represent a depositional continuum with paleoenvironmental settings ranging between continental alluvial fan and distal marine shelf. Also, application of sequence stratigraphic rationale (*described in Chapter-IV*) allowed interpretation of a prominent depositional discontinuity i.e 'Unconformity' that ceased the Saraipalli sedimentation and was followed by the deposition of Bhalukona Formation. Taking this into consideration the facies types and their paleoenvironment connotation of Rehtikhol and Saraipalli Formations are discussed together and the Bhalukona Formation is tackled separately for its facies and paleoenvironmental set-up.

SUB-CHAPTER- IIIA

FACIES AND PALEOENVIRONMENTAL STUDY OF REHATIKHOL AND SARAIPALLI FORMATIONS

Unconformably overlying the granites/gneisses of Bastar craton, ~60m thick coarse arenacous sediment package successively overlain upward by ~22m thick volcanoclastic and ~100m thick sandstone-shale heterolithic/ argillaceous sediment succession represent the Rehtikhol and Saraipalli Formation. Conglomerate, sandstone, and mudstone with subordinate tuff and coarser volcanoclastic constitute the lithology for this stratigraphic interval. Facies associations and their mutual interrelations has been carried out from studies in seven best exposed outcrops spread over the basin viz. Kodopalli, Rehatikhol, Malaikhaman, Kurlubahal, Murmuri, Chiwarakuta and Singhora temple (Fig.3.1). The Rehatikhol sandstones are coarse grained/granular, arkosic and constituted of quartz (polycrystalline), feldspar (K-feldspar, plagioclase and microcline) as framework grains set within sandy matix (Fig.3.2). Detailed logs are constructed in the four key sections to study the spatio-temporal relationships between different facies associations (Fig.3.3). The sections are: (i) on the southeastern flank of Malaikhaman hill, (ii) on the northern flank of the hillock at Kodopali village, (iii) towards the north of Rehtikhol village and (iii) Kurlubahal section at the south (Fig.3.1). Fifteen sedimentary facies types have been identified on the basis of lithological and geometrical criteria and the lateral relationships with other facies types. Table.3.1 illustrates the salient characters of these facies units. Following the facies definition, large-scale lithofacies associations are grouped according to dominant lithotype. Lithofacies associations (FAs) have been grouped into conglomerate-, sandstone- and shale-dominated. Within the broad lithologic subdivisions, discrete facies associations have been defined according to the abundance, stacking arrangement and geometry of facies and facies sequences. Considering the complexity of dealing with facies types on a basinal scale for a wide range of depositional settings, the overall facies trends are grouped into subaerial (alluvial fan and braid-plain), transitional (braid-delta) and marine (shelf) subdivisions. These are followed by a description of facies and subfacies associations and paleo-environmental interpretations. Contacts between the facies associations are traceable for kilometres within and between the outcrops. Architectural elements for the fluvial parts have been designated following the definitions of *Miall* (1983, 1985, 1988a). Construction of photomosaics of the outcrops, and

physical tracing of beds helped in defining the overall lateral variability and sand body geometry. The recognition of architectural elements, their characteristics, and their relationship allowed us to develop environmental interpretation and suggest the processes that influenced the fluvial system.

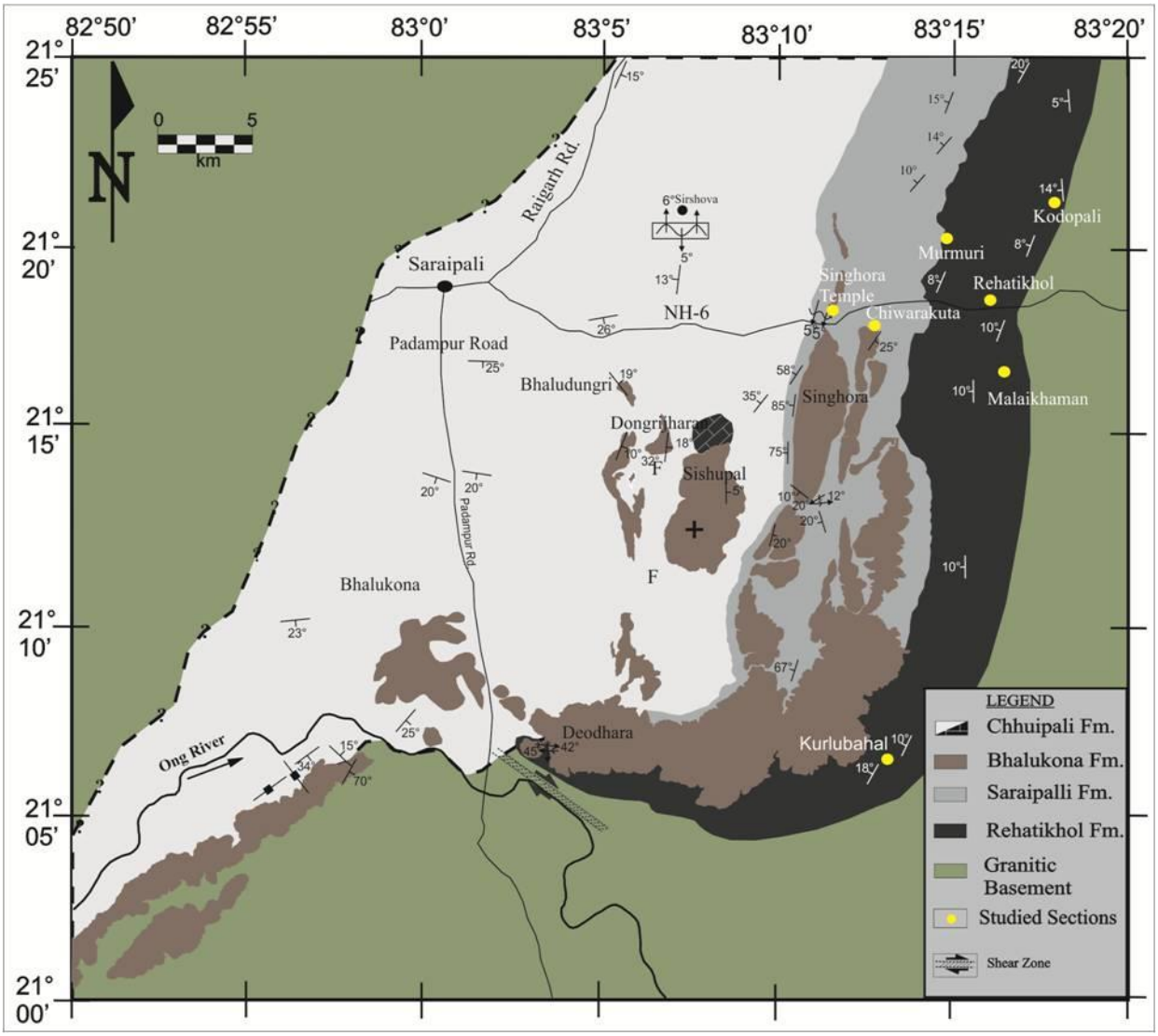

Fig.3.1. Geological map of Singhora basin showing spatial distribution of Rehtikhol and Saraipalli Formations. Locations of studied sections are shown on the map.

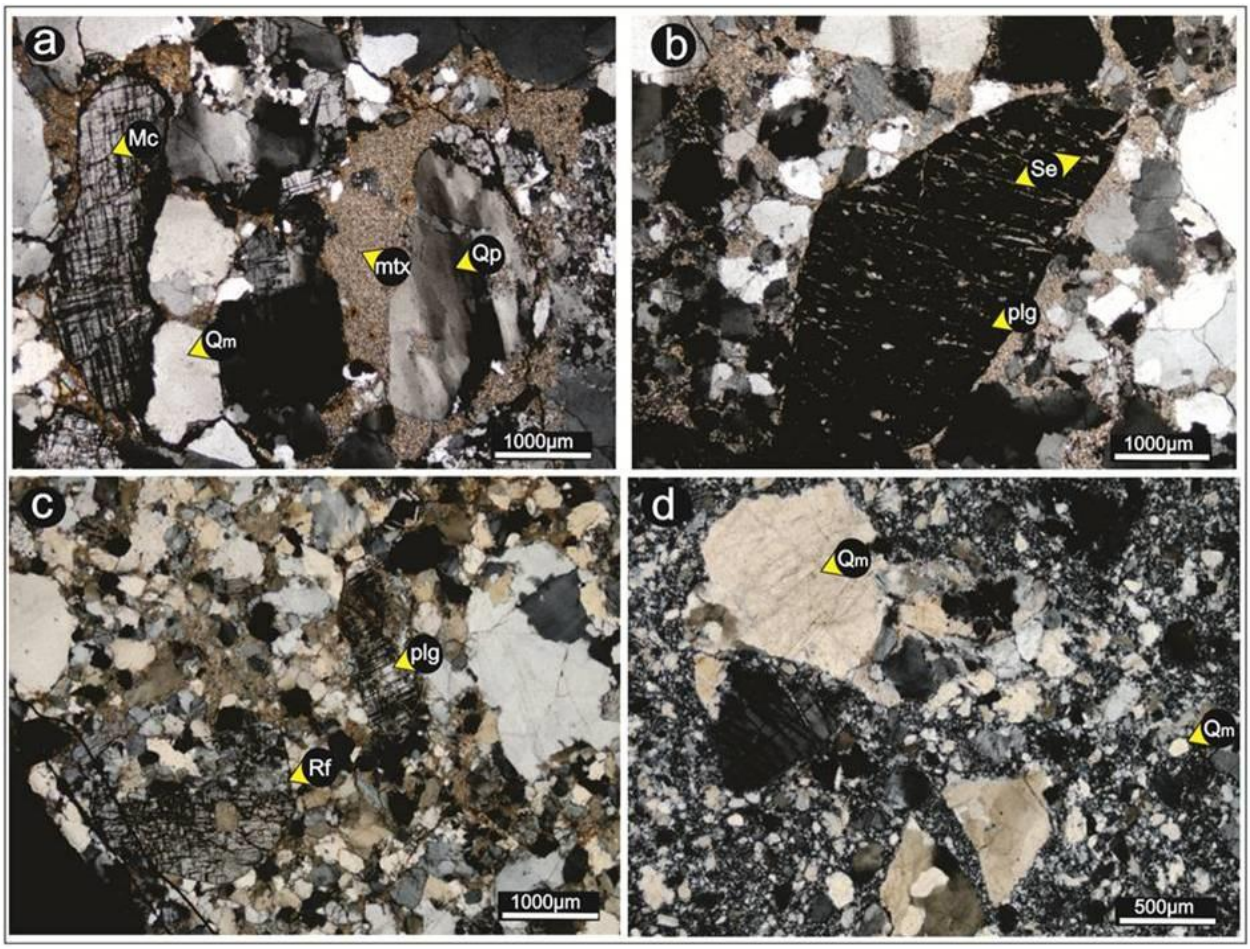

Fig.3.2. Microphotographs illustrating petrographic characters of Rehtikhol sandstones a) Potash feldspar (microcline; M_c) grains with cross-hatched twinning suggesting the arkosic character for sandstones, b) Sericitite (Se) formation from K-feldspar and occurrence of plagioclase feldspar (plg) as well along with mono (Q_m)- and polycrystalline quartz (Q_p), c) Presence of rock fragment, decomposition of K-feldspar and generation of pseudo-matrix, and d) poorly sorted character for the sandstone.

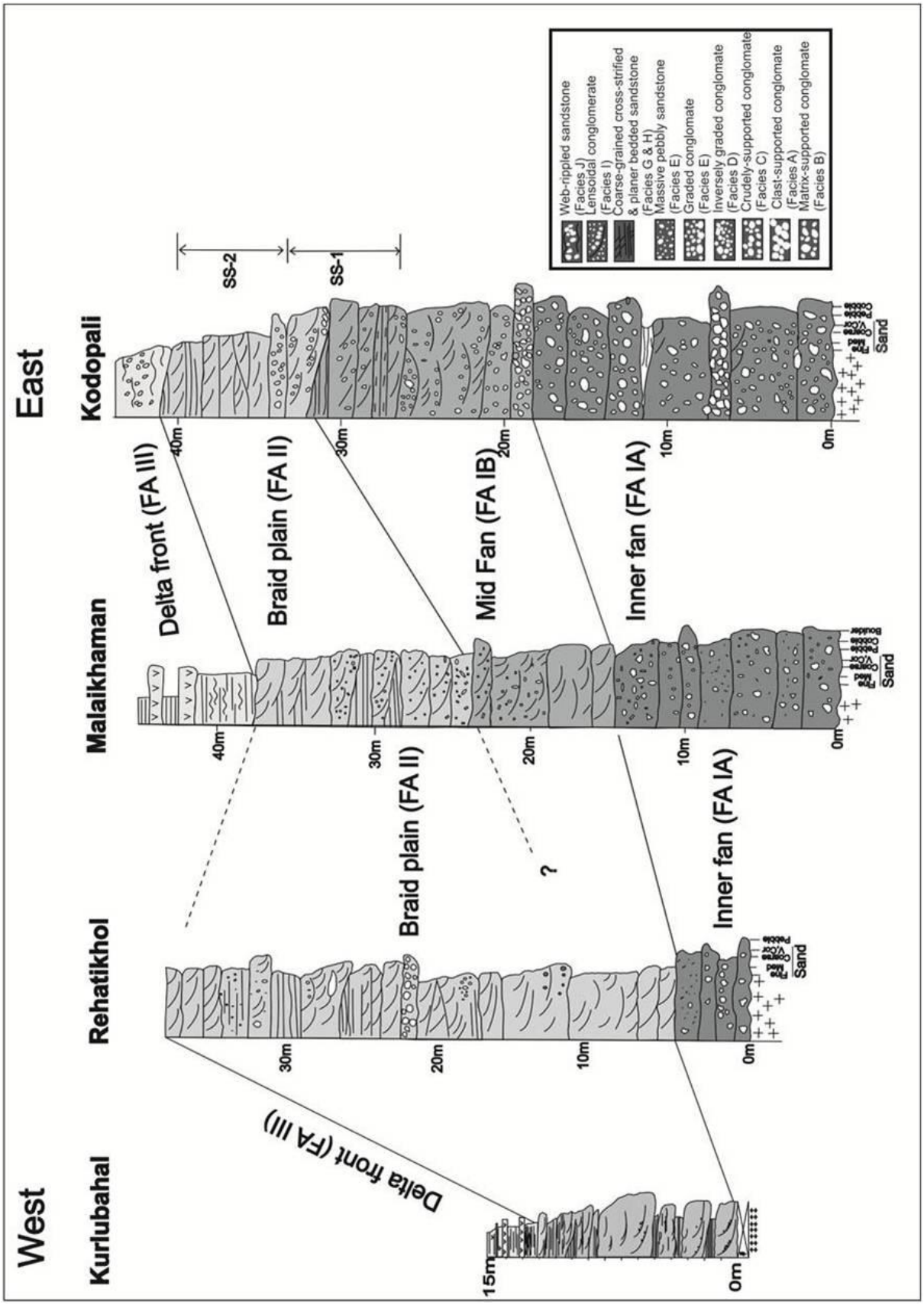

Fig..3.3. Detailed measured lithologs of Kodopali, Malaikhaman, Rehtikhol and Kurlubahal sections in an east–west transect. Relative positions of study locations are shown in inset. Note wedging out of alluvial fan (FA I) sediments and domination of braid-plain (FA II) sediments in the Rehtikhol section.

Table.3.1. Description and interpretation of dominant sedimentary facies in the Rehtikhol – Saraipalli fan delta-shelf complex

Facies type	**Description**	**Interpretation**	**Facies thickness (meters)**
Nonmarine facies associations: Alluvial fan (FA-I)			
A. Clast supported (boulder) conglomerate (Fig.3.4a)	I. Poorly sorted, angular, granule to boulder size clasts, smaller clasts have disorganized, near random fabrics. II. Ungraded matrix-infilled beds, basal bed contacts flat to deep scoured. Occasional single boulder train of well-rounded clasts with ungraded character.	Rock fall deposition Boulder lags from hyperconcentrated flood flows, or megaflood flow boulder beds.	0.22 – 1.32m
B. Matrix supported (cobble - pebble) Conglomerate (Fig.3.4b)	Generally thick; disorganized, poorly sorted; angular, granule to cobble size clasts of granite, amphibolite and vein quartz with occasional megaclasts (> 15cm in diameter); ungraded, partly crudely stratified; brownish, poorly sorted sandy matrix	Subaerial cohesive debris flow	0.30 – 1.6m
C. Crudely stratified conglomerate (Fig.3.4c)	Thin to thick (7.5 cm to several meters); partly a-axis imbricated; granule to pebble size clasts; poorly sorted sand matrix with clay content less than 1%; matrix or clast supported.	Cohesionless debris flow	0.4 – 1.2m
D. Inversely graded conglomerate (Fig.3.4d)	Matrix or clast supported with poorly sorted sand matrix; inverse concentration grading of granule to pebble size clasts, upper part of the unit mostly clast supported.	Seive deposit.	0.25 – 1.3m
E. Graded (Pebble-cobble) conglomerate (Fig.3.4e)	Granule- to boulder- size clasts; partly a-axis imbricated; poorly sorted sand matrix with clay content less than 1%; rip-up mud clasts.	Gravelly high-density turbidity current; cohesion-less debris flow.	0.3 – 1.6m

F. Massive pebbly sandstone (Fig.3.4f)	Moderately sorted medium to coarse sand; Featureless except some concretion layers. Rarely the beds are draped by parallel-laminated sandstone (max. thickness ~5cm)	Gradual aggradation from sustained high-density turbidity current (cf. Branney and Kneller, 1992). Gradual aggradation and upward migration of the depositional flow boundary due to grain hyper-concentration and hindered settling in a steady/quasi-steady current.	0.4 – 1.25m
Braided alluvial plain (FA-II) (Architectural element and facies code adapted from *Miall, 1978, 1985, 1996*)			
G. Cross-stratified sandstone (pebble, cobble and siltstone intraclasts) (Fig.3.5)	Solitary or grouped sets with high-angle trough cross-bedding (pebbly Gt, sandy St) and planar bed (Sh); planar cross beds (Sp) climbing or stacked over the top. Sporadic granule/pebble lags (Gh). Rare overturned cross-beds. Erosively based with lags and irregular to planar upper surfaces. Usually form a multi-storey complex that grades upward into SS. Trough cross-beds (St) show unimodal paleocurrent to west- northwest.	Braided fluvial channels and distributary channels (CH) with gravel/ sand bars and lags. Amalgamated channel deposits common.	0.15 – 0.82m
H. Medium to coarse grained sheet sandstone (Fig.3.6)	Sheet like bodies with erosive to slightly concave basal surfaces. Planar bed (Sh) with granule/pebble filled shallow scours (Ss) with occasional crude cross bedding (Sp and St).	Sand sheets (SS), Braided fluvial channel and distributary channels.	0.35 – 2.24m
I. Lensoidal Conglomerate (sandstone, siltstone and vein quartz intraclasts) (Fig.3.6)	Intraformational with cobble/ pebble size clasts. Lensoidal with strong erosional base (Ge). Commonly massive with occasional crude cross bedding.	Scour fill (SF)	~ 0.08m
Marine facies associations: Delta front (FA-III)			

J. Sandstone with wave generated bedforms (Fig.3.7)	Solitary or amalgamated beds of medium to coarse-grained sandstone. Internally massive Bedding surface replete with symmetrical bedforms with straight and bifurcated crests. Av. wave length and amplitude 54 to 80cm, and 6 to 14cm respectively.	Wave reworked, mouth bar sandstone.	2.5 to 6m
K. Sandstone-shale alternation (Fig.3.8)	Graded couplets of greenish sandstone and silty mudstone, occasionally tuffaceous, with sand: mudstone ratio 1: 0.85, Bouma (1962) T_{ae} to T_{ce}, Truncated T_{abe}, T_{bce} and T_{abce} sequences; C divisions ripple trains commonly loaded into exaggerated lenticules. Framework grains within sandstones include quartz, k-feldspar, lithic clasts and glass shards.	Silty sand turbidites with truncated sequences produced by variable axis to margin flow dynamics or hydraulic jumps where currents encountered bathymetric irregularity.	3.5 to 5m
L. Felsic tuff (Fig.3.9)	Buff coloured very fine-grained bedded tuffaceous rock; amalgamated or with thin shale intervention, glass shards and phenocrysts of quartz, k-feldspar, zircon, monazite, rutile and rare lithic fragments set within glassy groundmass. Signatures of grain welding.	Subaquous pyroclastic fall	Folded succession, at least > 2.5m thick
Prodeltaic Shelf (FA-IV)			
M. Reddish shale with scour-based sandstone lenses (Fig.3.10)	Approximately equal amounts of sandstone and mudstone interbedded, Sandstones with lenticular geometry, gutter or channel form, width: thickness varying between 3.8: 1and 13.2: 1. Sharp concave-up base, occasionally stepped and planar/wavy top, shale partings. Both symmetric and asymmetric filling. Grooves and prods at the sole of beds. Mud clasts are concentrated at the base of sandstone beds.	By-passed storm-dominated shelf. Strong erosional shore-parallel storm driven current.	35- 60m
N. Green/black Shale with micro-hummocky sandstone (Fig.3.11)	Interbedded shale, siltstone, and very fine to fine grained well-sorted sandstone. Common shale partings and thin beds; uneven, sharp, planar and sometimes scoured bases; sharp to gradational top; common wave ripple lamination, hummocky cross-stratification (av. wavelength and amplitude 42cm and 6.5cm). Bedding surfaces replete with asymmetric ripples (av. wave length 12 cm, amplitude 0.25cm).	Strong oscillatory flow within fair weather wave base. Absence of gutter implies relative weakening of the flows through distal travel.	> 12 m

O. Fissile green/black shale (Fig.3.12)	Shale with minor interbedding of siltstone. Siltstone lenses range in thickness from 2 to 5.5 cm, and in lateral extent from 8 to 12 cm; massive or planar laminated and wave rippled at the top. Grading is conspicuous and some ripples resemble the fading ripples of Pedersen (1985). Overall grading, although weak, is locally discernible within the beds.	Distal offshore	Several tens of meter
P. Stromatolitic limestone (Fig.3.13)	Bedded stromatolitic limestone; Stromatolitic columns attached with one another, circular in bedding plane projection; av. Column height and diam. Are 3.5cm and 1.2cm, respectively	Proximal shelf	3 – 5 meter

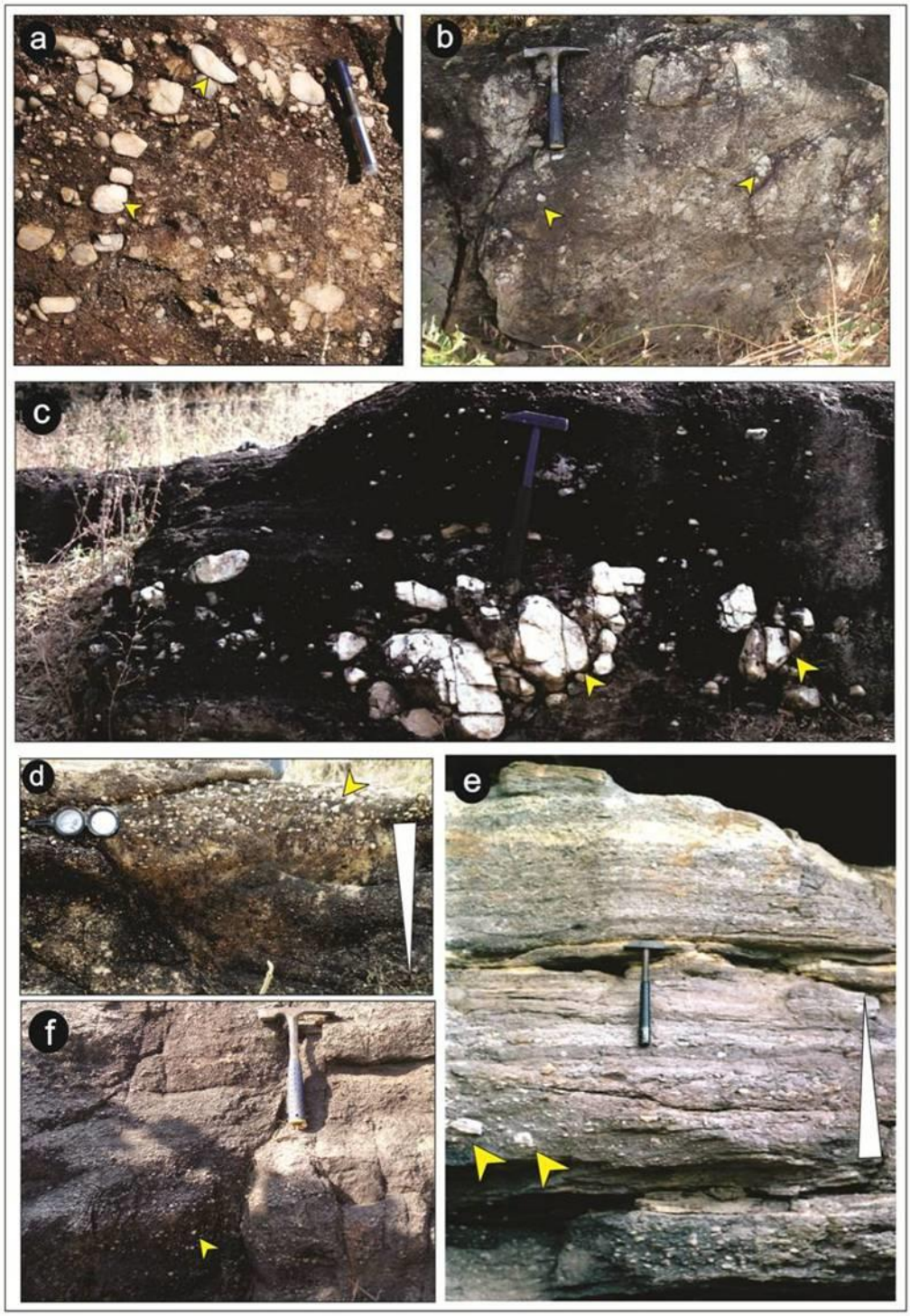

Fig.3.4. a) Clast supported boulder conglomerate of facies A (pen length 14cm), b) Granular sandy matrix-supported cobble-pebble (arrowed) conglomerate of facies B (hammer length 27cm), c) Clast- to matrix-supported crudely stratified conglomerate of facies C (hammer length 27cm), d) Inversely graded conglomerate of facies D (Brunton length 15cm), e) Graded pebble-cobble (arrowed) conglomerate of facies E (hammer length 27cm), and f) Pebbly (arrowed) sandstones of facies F (hammer length 27cm)

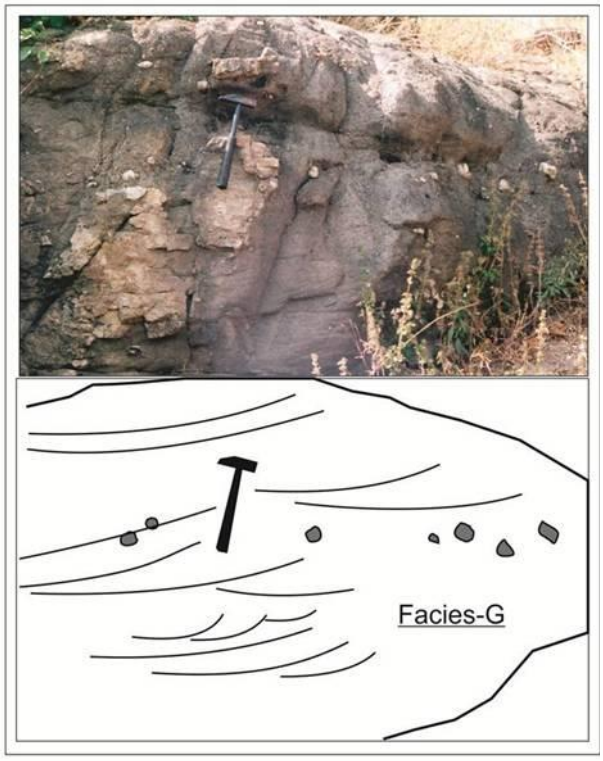

Fig.3.5. Granite intraclasts of pebble/cobble size within cross-stratified sandstones of facies G (hammer length 27cm)

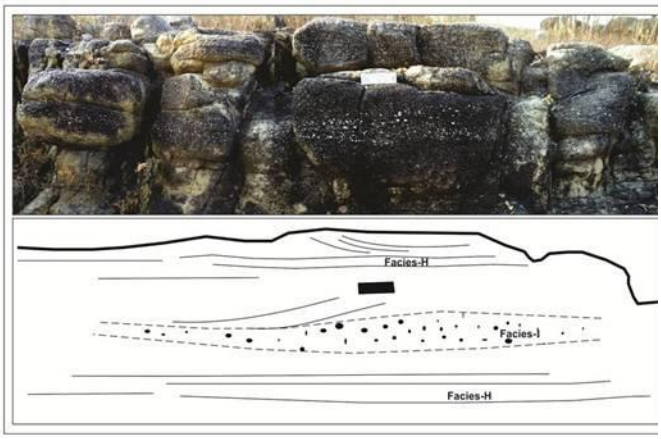

Fig.3.6. Lenticular intraformational conglomerate (Ge) with strong erosional base (facies I) (scale length 15cm).

Fig.3.7. Symmetrical bedforms on the bedding plane of facies J. Note their NE-SW oriented crest lines (hammer length 27cm).

Fig.3.8. Facies K; Sandstone intrabed with sharp base and gradational top encased within Saraipalli Shale (coin diameter 23mm)

Fig.3.9. a) Bedded tuff of facies L (hammer length 27 cm), b) Well laminated character of the tuff unit (Coin diam. 23cm).

Fig.3.10. a) Sandstone-Shale interbedding in facies M; Note lenticular geometry of sandstone interbeds (b).

Fig.3.11. Green/Black shale of facies N with presence of hummock (pen length 14cm)

Fig.3.12. Fissile green/black shale (Sh) of facies O. Note rare siltstone interbed. Sandstone (height of man 1.6m)

Fig.3.13. Bedded stromatolitic limestone of facies P (Man height 1.6 m). Bedding plane projection of column geometry is shown in the inset.

3a.1. Facies Associations (FA)

3a.1.1. Subaerial Facies Associations

3a.1.1a. FA I: Alluvial fan:

Represented by disorganized, poorly stratified, inversely or inversely to normally graded conglomerates (facies types A, B, C, D and E) and massive/stratified sandstone (facies F) with lenticular or sheet-like bed geometry. Depending on relative dominance of mass flow and channel flow products, the association is subdivided into two sub-associations, viz., inner fan and middle fan.

a. Inner fan:

Disorganized, poorly stratified, inversely or inversely to coarse-tail normally graded conglomerates (facies types A, B, C and D; Table.3.1) and subordinate crudely stratified to massive pebbly sandstone (facies F) constitute this sub-association (Fig.3.14; maximum 34.5m thick). Rocks of the sub-association are present in a narrow belt (<0.4km in width) following the basin margin, where the basement is largely composed of Archean gneisses of the Bastar craton and is cross-cut by basalt, dolerite and amphibolites dyke swarms of more than one generation (*Srivastava and Singh*, 2003 and references therein). While facies A (Fig.3.4a) is exclusively restricted to the contact with the craton, the other facies varieties (B, C and D) (Fig.3.4b, c, d) are found to be in alternation with the rest of the association all through the exposed stratigraphy. Conglomerates are either matrix- or clast-supported in poorly sorted feldspathic sandy matrix; matrix-supported units are by far the dominant variety. Clasts are outsized boulders of granite (15–18%), vein quartz (58–67%), basalt and amphibolites (3–5%) or fragments of sedimentary rocks (5–10%); maximum and average clast sizes recorded are 38cm and 7.3 cm, respectively. While some outcrops have very high concentrations of quartz clasts (>80%), others contain abundant sedimentary rock clasts. At a few localities, clasts are also found penetrating into the substratum in the basal part of the sub-association. Common facies sequences include matrix-supported conglomerate overlain by inversely graded ones; inversely graded conglomerates successively overlain by normally graded, graded-stratified pebble–cobble

conglomerates and crudely bedded granular sandstones or alternation between matrix-supported and massive to normally graded conglomerates (Fig.3.15). Laterally and vertically this sub-association is transitional to sub-association 1b, dominated by the channel flow products.

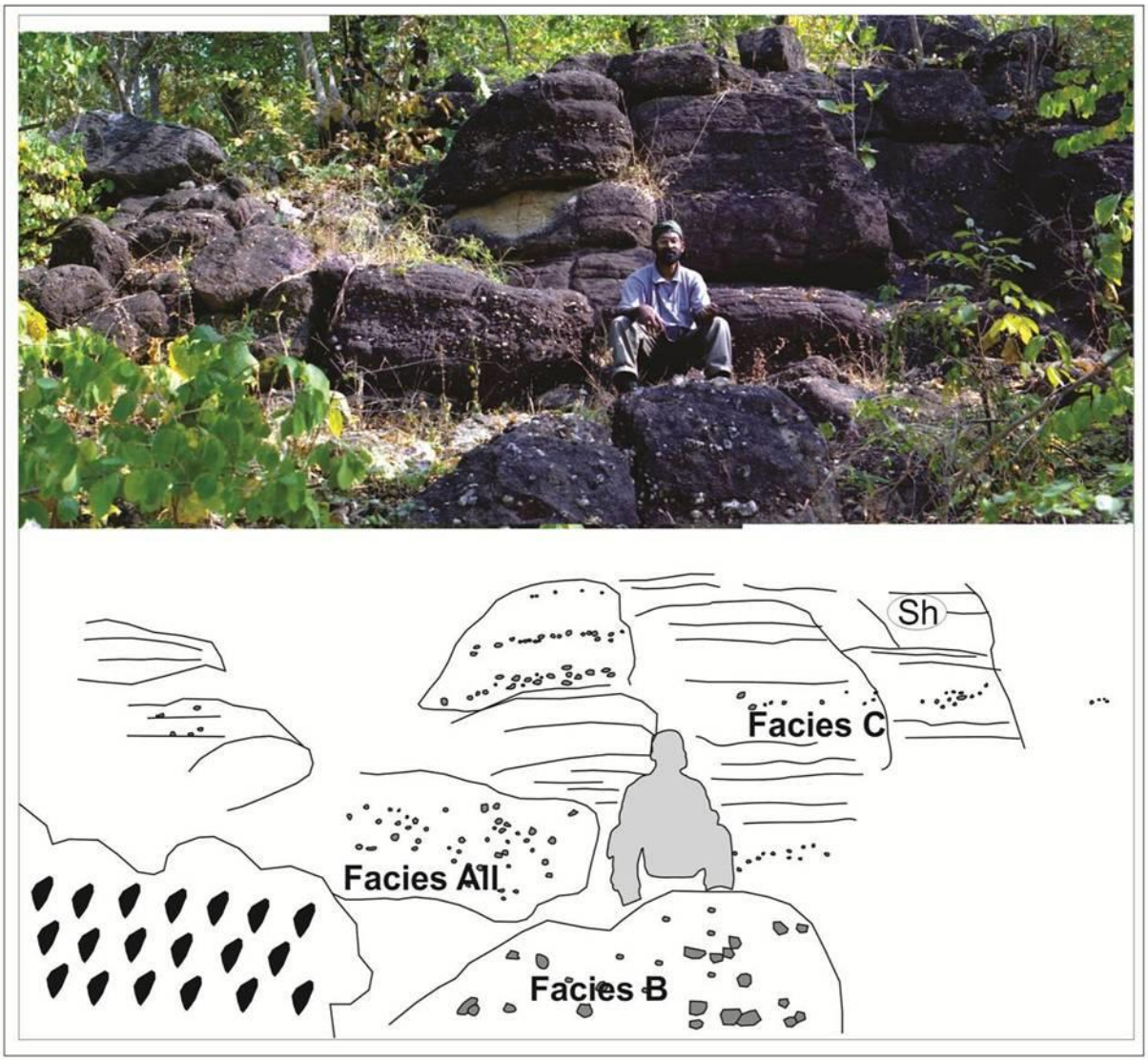

Fig.3.14. Profile of the FA IA (inner fan) section. (a) Photomosaic of study outcrop at Kodopali section, (b) interpretation of photomosaic. Facies AII represents clast-supported conglomerate (ungraded matrix-infilled beds), facies B represents matrix-supported conglomerate and facies C represents crudely stratified conglomerate. Sh represents planar stratified sandstone.

Interpretation:

Conglomerates are interpreted as the products of rock fall or hyperconcentrated flows (Fig.3.16). Penetration of clasts into the underlying substrata indicates freefall of clasts (*Bose et al.,* 2008). Hyperconcentrated flows are variously interpreted in literature as cohesive and transformed cohesive

flows (*Mulder and Alexander,* 2001) or cohesionless debris flows and sand flows (*Allen,* 1997). Whereas boulder (>35%) conglomerates of facies A1 with angular, poorly sorted clasts are interpreted as products of rock fall, clast-supported facies A2 conglomerates with disorganized clasts, non-erosional base, coarse sandy matrix (with5–8% mud) are most probably formed from sub-aerial pseudoplastic flows with high sediment concentration (*sensu hyperconcentrated flow*; *Sohn et al.,* 1999; *Saula et al.,* 2002). Sand: mud ratio >>1:1and presence of 8-15% disorganized gravel to boulder-sized clasts bear telltale features in support of a high concentration flow character (*Van Weering et al.,* 1998; *Mulder and Alexander,* 2001; *Bera et al.,* 2008). Preponderance of facies A in a narrow belt along the basin margin suggests derivation of these units from a line source (*Alexander and Leeder,* 1987; *Gawthorpe and Colella,* 1990). A multipoint character of the source is also attested to by the local variation in clast composition (cf., *Hwang and Chough,* 2000). Low mud content in such cohesive pseudoplastic flows is suggestive of subaerial origin. Unlike subaquous flows, subaerial flows with very low percentage of mud may behave as debris flows, as interstitial water aids (i) by adding additional mass, and thereby contributing to the density contrast between flow and ambient fluid, and (ii) by holding the flow together by surface tension effects (*Major and Iverson,* 1999; *Vallance* 2000). *Coussot and Muunier* (1996) suggested that clay content of 4–10% by volume would cause a sub-aerial poorly sorted matrix to behave as a pseudoplastic fluid regardless of the maximum particle size. Matrix-supported disorganized conglomerates (facies B; discussed later) with very low content of mud (<3%) are products of subaerial debris flows (*Lowe,* 1982; Iverson, 1997; *Major and Iverson,* 1999).

Clast-poor crudely stratified conglomerates (facies C), the reverse graded and the inverse to normal graded conglomerates(facies D, E) are interpreted as products of non-cohesive density-flows, in which cohesion is overcome by increased shear rate due to higher flow velocity or flow over a rough surface (*Mulder and Alexander,* 2001). *Iverson* (1997) suggested that in subaerial condition at a critical value (~2000) for the friction number, the cohesive debris flows transform to hyperconcentrated non-cohesive flows in which grain collision stresses exceed grain frictional stresses. It has been suggested that debris flows can transform to non-cohesive flows at a higher velocity with no change in water content or clay fraction. The reverse graded units (facies D) with clast-supported character in their uppermost part resemble sieve deposits and possibly resulted from transport and segregation of large clasts; upward movement of particles is not prevented in non-cohesive matrix (*Todd,* 1989; *Major,* 1997). Upward velocity gradient and a laminar regime, in

combination, resulted in the reverse graded character. Development of normal grading, though not very common in such hyperconcentrated flows, is ascribed to relatively uniform suspension fall-out;

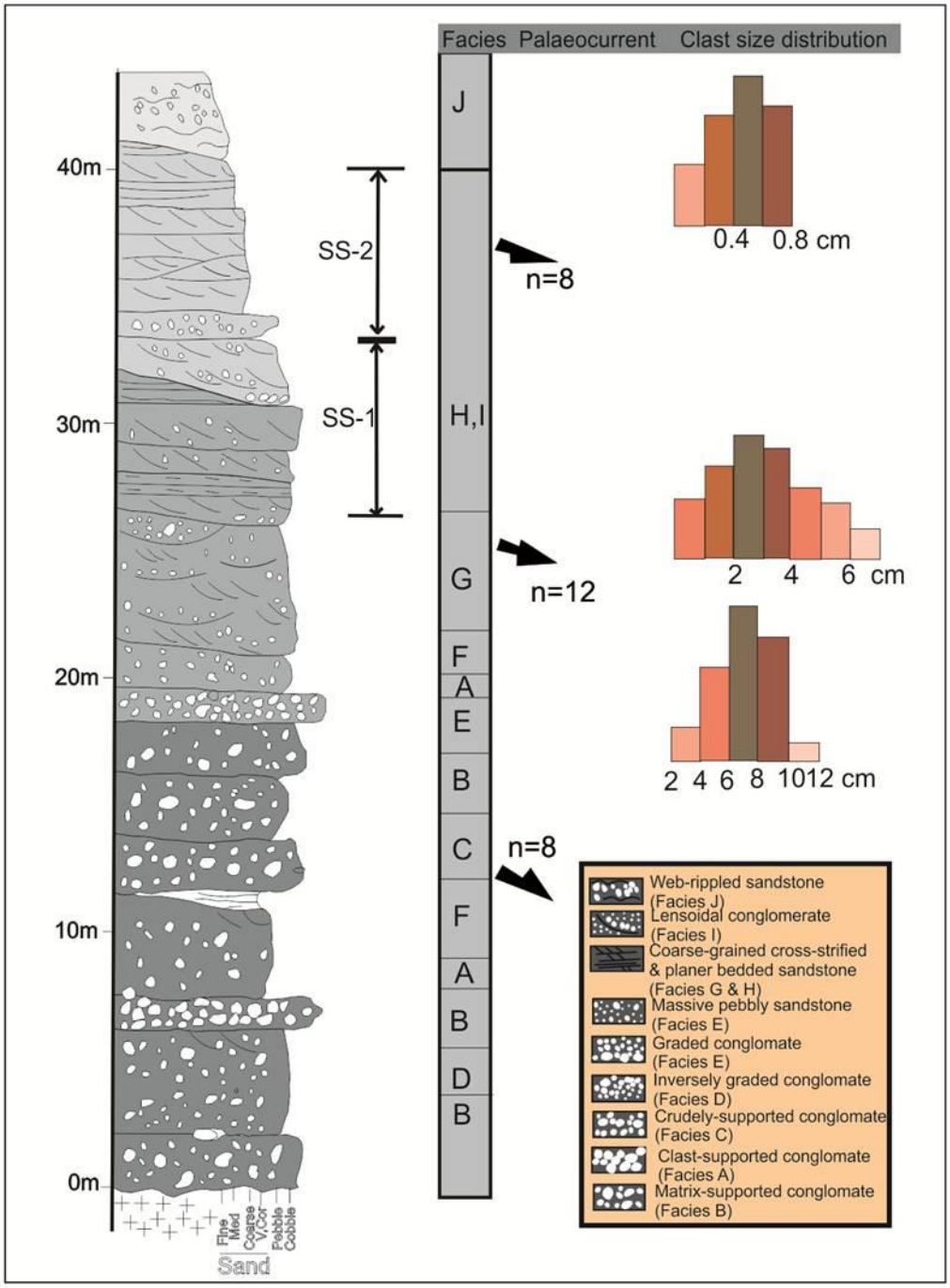

Fig.3.15. Detailed measured litholog of alluvial fan and braid-plain succession exposed at Kodopali section. Facies types, paleocurrent directions at different stratigraphic levels and variation in clast size and population up the succession within the fan are shown on the right. SS represents sand sheet element.

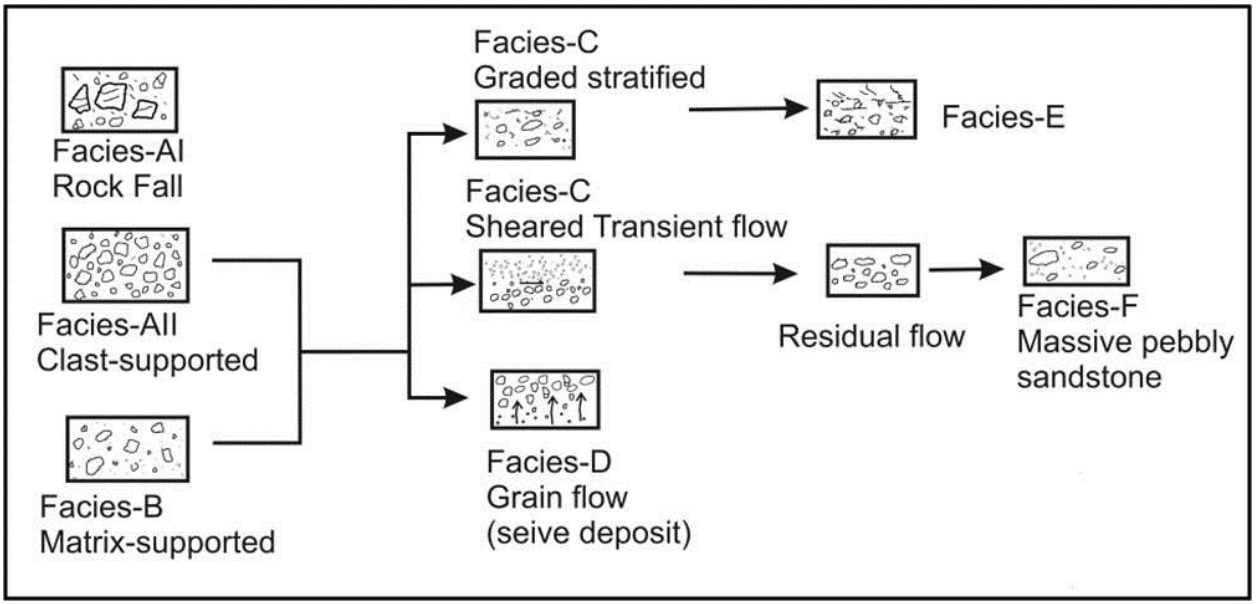

Fig.3.16. Summary of deposit types formed from the sediment gravity flows within Singhora alluvial fan system.

reports are available (*Pierson and Scott,* 1985; *Best,* 1996) for the presence of coarse-tail normalgraded units, particularly in subaerial conditions. Occurrence of normally graded units (facies E) in association with crudely stratified sandstones further supports the subaerial interpretation.

b. Mid-fan:

Channelized alluvial and non-channelized mass flow products together constitute this sub-association. The alluvial products are analyzed using the 'Architectural Element' concept of *Miall* (1983, 1985, 1988a). Sheet sandstones (SS; facies types F and H), sheet conglomerates (facies B, C and E) and channelized conglomerate (CH; facies L, A and C) in decreasing order of abundance constitute this sub-association (maximum recorded thickness 22 m). Within the sheet sandstone units about 80% of the structures comprise horizontal lamination (Sh), trough crossbeds(St) making up about 18% and scour-fills (average width 0.18m, depth 0.08m) with crude crossbedding constitute the remaining 2%. The thickness of SS units and horizontal laminations within them, vary between 1.2m and 4.5 m, and 2.5mm and 4.5 cm, respectively. Convolution and low-angle truncation of laminae are common observations. The presence of parting lineation is noted rarely on the bedding surfaces. The conglomerates with sheet-like bed geometry are matrix or clast-supported and with clasts arranged either in disorganized (facies B) or inversely graded (facies D) fashion. Individual conglomerate units commonly range in thickness from 28cm to 1.25m and maximum

clast size recorded is 13.5 cm. The small-scale fining-upward clast-supported conglomerate units have broad lenticular geometry, erosive bases and are interbedded with sheet sandstones (Fig.3.17). The lenticular units are decimetric to a few meters deep, more than several tens of meters wide and are filled with clast-supported conglomerates, crudely stratified (facies C) or normally graded (facies E), and massive/plane- stratified sandstone(facies F). Clast-supported, matrix-in filled, massive or normally graded conglomerate with rare well-sorted, openwork conglomerate lenses at the basal part of lenticular units, grades upward to massive pebbly sandstone (facies F) and further fines upward to crudely stratified (facies G) sandstone (Fig.3.17). In some small-scale lenticular units, a crudely stratified conglomerate body (facies C) in the center grades laterally to several units of conglomerate and sandstone facies (facies E, F and G) with concave-up lower and planar upper boundaries. On lateral tracing, the lenticular units are found to inter-finger with the coarse-grained/granular sheet sandstone units (facies H).

Interpretation:

The horizontal lamination within sheet sandstone units may represent either lower or upper plane bed processes (*Boggs,* 1995). Presence of parting lineation, low-angle truncation of laminae and occurrence of scours support prevalent upper flow regime plane bed condition (cf. *Eriksson et al.,* 1995). The granules to pebble sized clasts in many of the scour-fills suggest that the flow conditions at certain times were rapid and were even perhaps flashy. Occasional association of trough cross-stratifications may imply intervention of low-energy conditions attributable to weak, variable current action. Signatures of such fluctuating energy and water level conditions are common in products of both ephemeral fluvial and tidal channel systems (*Tirsgaard,* 1993; *Chakraborty and Paul,* 2008). *Shanmugam et al.* (2000) discussed the distinction between channels with fluvial and with tidal influences and emphasized several clues, viz.: (i) presence of cross-beds with mud drapes, and (ii) association with heterolithic facies and flaser bedding, as distinguishing criteria for identification of a tidal channel. *Eriksson et al.* (1995) based on their study of the Lower Proterozoic Magaliesberg Formation, South Africa used distinctive paleocurrent signatures (bimodal–polymodal) for identifying tide-dominated settings. The absence of any undoubted feature indicative of tidal action allowed interpretation of sheet sandstone units as the products of ephemeral fluvial channels. The sheet conglomerates are interpreted as the products of unconfined flows related to sheet flood events (*Hogg,* 1982; *Mcpherson et al.,* 1987). Clast-supported nature in conjunction with sheet-like bed

geometry indicates deposition from high-energy tractive flow (*Walker,* 1984). *Rust and Koster* (1984) considered the inter-gradational relationship between stream channel and sheet flood

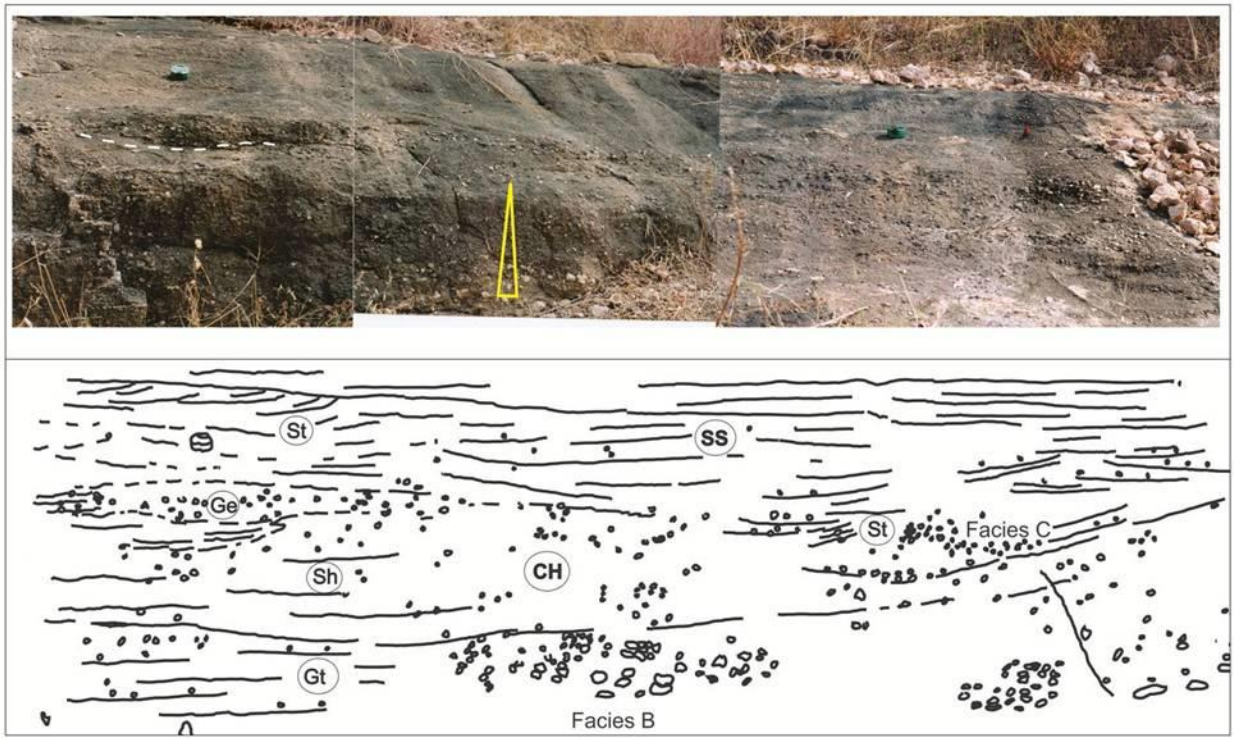

Fig.3.17. Profile of the FA IB (mid-fan) section. (a) photomosaic of study outcrop at Malaikhaman section, (b) interpretation of photomosaic. Facies B represents matrix-supported conglomerate and facies C represents crudely stratified conglomerate. White triangle indicates fining-upward character of CH (braided fluvial channels and distributary channels) element. Gt represents pebbly sandstone with cross-bedding, Ge represents lensoidal unit with strong erosional base, SS represents sheet sand, St represents sandy beds with high angle trough cross-stratification and Sh represents planar stratified sand bed.

deposits in most of the alluvial fan sequences. The small-scale, fining-upward, clast-supported, conglomerate-dominated lenticular units with scoured bases represent the channel-fills (cf., *Jones et al.,* 2001). Surges of coarse-grained highly concentrated flows generated during high-magnitude flood events may either remain confined within channels or spread out beyond the margins of shallow ephemeral channels (*Benvenuti,* 2003; *Deynoux et al.,* 2005).Widening of flow with concurrent decrease in water depth and flow velocity may result in the sheet-like geometry of resultant conglomerate units.

3a.1.1b. FA II: Braid-plain:

Horizontal- and cross-stratified granule-rich, coarse-grained, poorly sorted sheet sandstones (facies types Sh, St and Sp), clast-supported conglomerates (facies types Gh, Ge), and granule-free coarse-grained sandstones constitute this association; sandstones by far constitute the major volumetric proportion. In some sections viz. Malaikhaman and Kodopali sections this association is dominated by massive and horizontally stratified granule bearing coarse-grained sandstones and conglomerates with minor granule-free medium-grained sandstones. Stacked decimeter- to meter-thick fining-upward successions, averaging 0.85m in thickness and traceable in outcrop for lengths exceeding tens of meters, define the association (Fig.3.18). With erosive, scalloped or scoured base, each succession begins with a SS or CH element (cf., *Miall,* 1985; *Eriksson et al.,* 1995; *Jones et al.,* 2001) constituted of Ge, Gt and Sh lithofacies and, in turn, changes upward to amalgamated sheet sandstones dominated by Sh and Sp elements (Fig.3.18). Conglomerates are polymictic with clasts of granite, gneiss and vein quartz, lenticular (width ranging from16cmto1.83mand thickness ranging from 6 cm to 1.35m) and with base being either erosional, concave-up or planar, sharp/diffused. The planar-base units commonly show maximum elongation in paleocurrent direction. The large trough cross-stratifications (within facies Gt, average set-thickness 38 cm) record west–northwestward paleocurrent directions (Fig.3.19a). The Sh facies units are often intervened by thin (1.5–3.2 cm) pebble beds, composed dominantly of vein quartz clasts. Separated by planar or broad, undulated master erosion surfaces, extensive over the outcrop areas, medium- to coarse-grained sheet sandstone units are stacked vertically at the Kodopali and Rehtikhol sections, and are internally constituted of various combinations of facies types (Sh, St and Sp;). Sheet thicknesses in these sections vary between 0.54m and 0.87m and the maximum thickness recorded for the amalgamated sheet units is 4.75 m. Solitary lenticular cross-stratified units are up to22cm thick (facies Sp) and rest on planar master erosion surfaces; length of cross-strata in flow-parallel dimension ranges from0.24m to 0.86 m, width (flow transverse dimension) of which is indeterminable due to outcrop constraints. Foreset shapes are predominantly tangential, with lesser planar and convex-upward shapes; topsets are rarely preserved. While downcurrent transition from cross-bed sets to planar bedding is prevalent with sigmoidal foresets in between, the absence of ripple forms on the upper surfaces of horizontally stratified beds is noteworthy. Cosets of trough cross-stratifications (facies St, average set thickness 5.5 cm) are separated from the planar cross-stratified units by interfacies with curved or less commonly flat and locally scalloped, erosion surfaces. Paleocurrents from trough

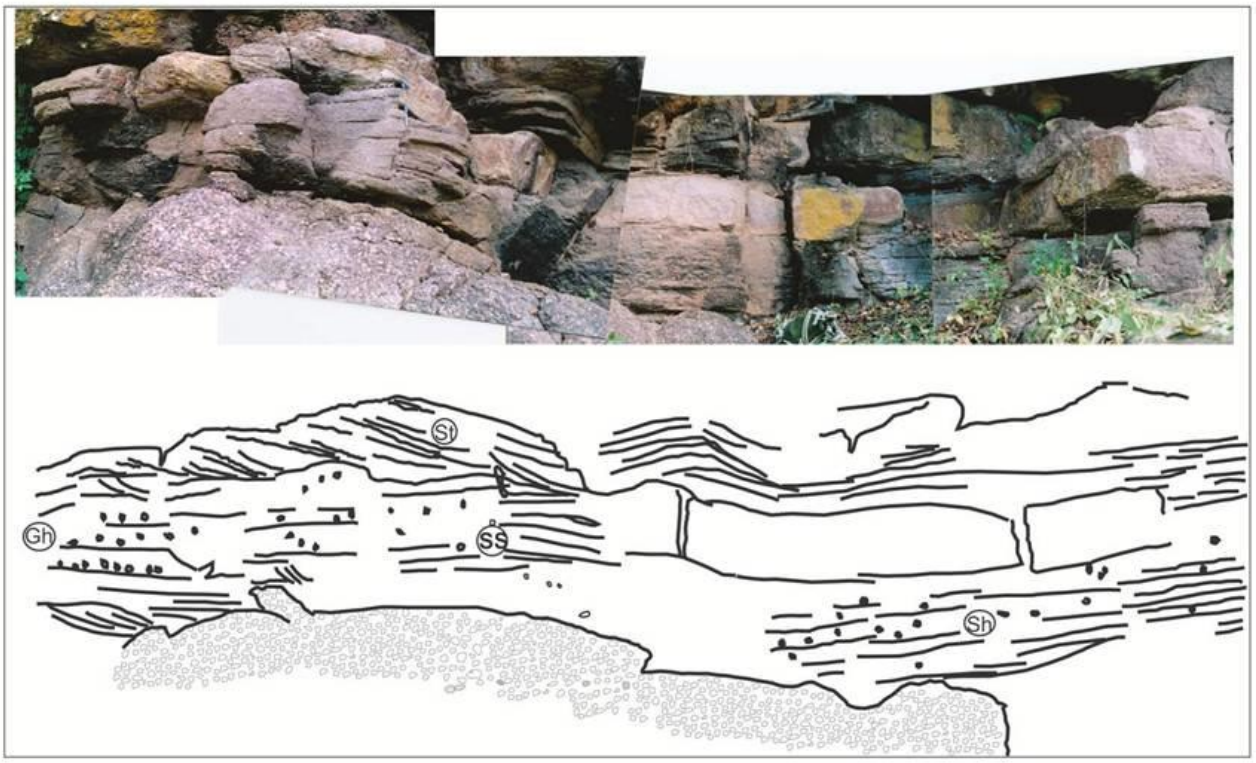

Fig.3.18 Decimeter-thick amalgamated SS (sheet sand) units of FAII; (a) photomosaic of study outcrop, and (b) interpretation of photomosaic.Note sharp contact with underlying conglomerate of FA IB. St represents sandy beds with high angle trough cross-stratification, Sh represents planar stratified sand bed and Gh represents granule-pebble lags.

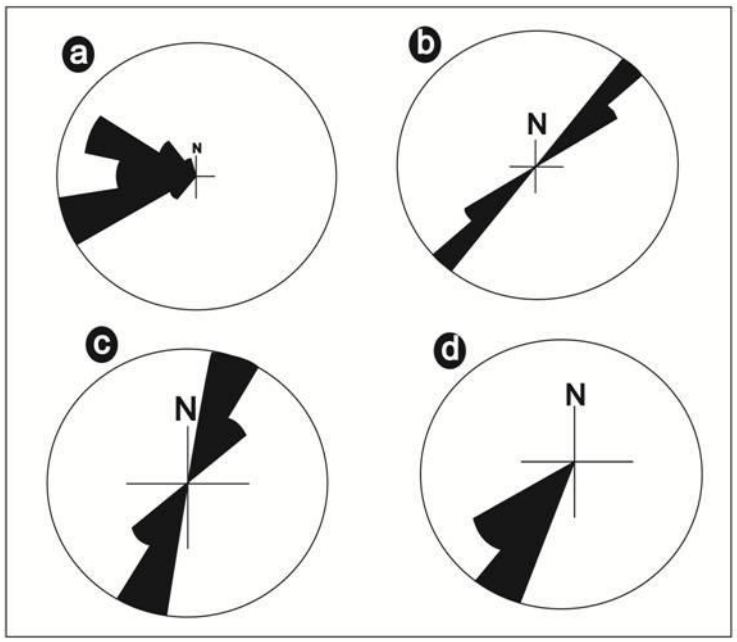

Fig.3.19. Paleo-directional/current data recorded from (a) trough cross-stratifications within FA I and FA II, (b) mega-ripple crest line orientation within facies J, (c) gutter orientation within FA IVa, and (d) asymmetric ripple migration direction within FA IVb.

cross-stratifications follow the same unimodal, low-dispersed pattern with predominant west–northwestward direction, similar to those from the large trough cross-stratified Gt units.

Interpretation:

Poor sorting, fining-upward sequences and presence of clast-supported conglomerates are suggestive of a fluvial origin (*Boggs,* 1995; *Bridge,* 2006). The absence of overbank fines and general lack of channel morphology is suggestive of broad (~150m wide), shallow (<2m deep), unconfined braided channel systems (sinuosity value 1.04–1.2; after *Le Roux,* 1992). The lenticular Ge and Gt units in many of the basal scours suggest that the flow conditions, at certain times, were rapid and perhaps even flashy (cf. *Jones et al.,* 2001). The planar-base conglomerate units in lateral transition with Sh and with maximum elongation in the current direction, are interpreted as products of mid-channel longitudinal bars, initiated and grown by competence failure at stages of high flood (*Cant and Walker,* 1978; *Boggs,* 1995). The thin sheets of pebble/gravel within the Sh facies units possibly represent sheet flood events, which inundated large parts of the alluvial plain during high flood stages. Interbedded with gravels and pebbles, the coarse-grained sandstone lenses at Malaikhaman and Kodopali sections represent deposition in abandoned channels or sand wedges at the edges of bars. The multistory sheet sandstone units at Rehtikhol section, characterized by horizontal lamination (Sh) and lesser low-angle planar cross-bedding (St), suggest a series of sandstone channel-fills, with only small-scale bar development, probably under flood conditions (cf., *Miall,* 1977, 1978; *Dam and Andersen,* 1990; *Eriksson et al.,* 1995). The occurrence of planar cross-bedded units in lateral and vertical association with horizontally laminated units suggest variable energy conditions, with transition from lower flow regime dune bedforms to upper flow regime plane bed conditions. The weakly dispersed paleocurrent pattern favors this view.

➢ 3a.1.1b(i). Paleo-hydraulics of Rehtikhol fluvial system

It is widely accepted that Precambrian rivers were mainly braided with non-perennial flow because of rapid channel shifting, as a result of bank instability in absence of vegetative cover (*Schumm,* 1968; *Rainbird,* 1992; *Long,* 2004, 2011). It is also argued that most of the Precambrian fluvial systems had higher paleoslope gradient i.e > 0.007° in contrary to the claim of *Blair and McPherson* (1994) from their studies in modern settings that braided fluvial systems naturally assume

gradient less than that (*Eriksson et al.,* 2008; *Sarkar et al.,* 2012). In this backdrop it is felt necessary that the paleo-hydrological condition of Rehtikhol braided river system be estimated to check the validity continuous of higher paleoslope gradient of Precambrian river systems. Various formulae for calculation of hydrological parameters of ancient river systems are based on sandstone grain-size analysis, clast sizes in conglomerate deposits and cross-bed set thicknesses (*Vander Neut and Eriksson,* 1999; *Eriksson et al.,* 2006). It is important to note that all these calculations are only estimates and unavoidable errors associated with these estimations are significant (*Eriksson et al.,* 2008). Despite this, necessity of such exercise is recommended by several workers in ancient fluvial systems so as to get a reasonable idea about their hydrological conditions, more specifically when it is done on comparative basis (cf. *Miall,* 1976; *Eriksson et al.,* 2008). The height of dunes, the most common type of bedforms that develop within river channel, is considered as reflective of channel flow parameters. Empirical relationships have been established between set thickness of dune cross-strata and channel parameters on the basis of observations in modern rivers (*Allen,* 1968; *Vander Neut and Eriksson,* 1999; *Eriksson et al.,* 2006). The aqueous cross-set thickness has been used in this study and estimation were carried out different hydraulic parameters of the Rehtikhol fluvial channels (Table.3.2) by using different formulas (given below) as proposed by different workers.

- The mean water depth (d_m) can be calculated by the empirical equation prescribed by *Allen* (1968):

  $$\mathbf{h = 0.086(d_m)^{1.19}} \quad (1)$$

  where 'h' is the mean cross-set thickness in meter.

- Channel width (W_c) in meters is calculated from the empirical regression equation of *Bridge and Mackey (*1993):

  $$\mathbf{W_c = 8.88d_m^{1.82}} \quad (2)$$

- Mean annual discharge (Q_m) is calculated from *Williams* (1984):

  $$\mathbf{Q_m = 0.06w^{1.66}} \quad (3)$$

- Bankfull channel width (W_b) is calculated from *Osterkamp and Hedman* (1982) and *Sarkar et al.,* (2012):

  $$\mathbf{Q_m = 0.027W_b^{1.71}} \quad \mathbf{or,\ W_b = \sqrt[1.17]{(Q_m/0.027)}} \quad (4)$$

- Bankfull channel depth (d_b) is calculated from *Leeder* (1978) and *Sarkar et al.,* (2012):

  $$\mathbf{d_b=(W_b/8.9)^{0.71}} \quad (5)$$

- The slope (S) is calculated from *Schumm* (1968):

  $$\mathbf{S=30\ (F^{0.95}/W_c^{0.98})} \quad (6)$$

  Where F= Channel width (W_c)/Channel depth (d_m).

- Bankfull channel discharge (Q_b) is calculated from *Williams* (1978):

  $$\mathbf{Qb= 4A_b^{1.21}S^{0.28}} \quad (7)$$

  Where, $A_b=W_b \times d_b$

- The drainage area (catchment area) of a river system can be estimated by:

  $$\mathbf{Q^b=A_d^{0.75}} \quad (8)$$

  Where, A_d is the drainage area in Km^2 (*Leopold et al.,* 1964).

- Principle steam length (from source to depotional site) can be estimated by:

  $$\mathbf{L=1.4A_d^{0.6}} \quad (9)$$

  Where L is the stream length in Km (*Leopold et al.,* 1964).

➢ 3a.1.1b (ii). Paleohydraulic result:

Paleohraulics estimation has been carried out on braid-plane deposits exposed at the Malaikhaman, Kodopalli and Rehatikhol village sections reveals paleoslope values more than 0.007 but less than 0.026 (average paleoslope values of Malaikhaman Section 0.015 m/m, Kodopalli section 0.018 m/m and Rehatikhol Section is 0.024 m/m). Such observation is worth noticing as *Blair and McPherson* (1994) in their fig. 6 showed modern rivers having slope values less than 0.007 and modern alluvial fans having values more than 0.026. Although it is argued that such observation is essentially an artifact of studies of those workers in rivers and fans belonging to arid climate (*Blair and McPherson*, 1994), it is significant to notice that the values obtained under present study invariably fall in the gap between the two demarcated fields, which as *Blair and McPherson* (1994) described as "Natural slope gap".

Table.3.2. Paleohyological data derived from set thickness of cross-bedding in the Rehatikhol braid-plane system.

	h [cm]	10% Decom-paction	h [m]	d_m [m]	W_c [m]	Q_m [m^3/S]	W_b [m]	d_b [m]	S [m/m]	Q_b [m^3/S]	Ad (Km^2)	L (Km)
Malaikhaman section	17	18.7	0.187	1.921	29.131	16.180	42.105	3.035	0.015	433.243	3278.252	180.100
	11	12.1	0.121	1.332	14.969	5.358	22.062	1.913	0.021	125.657	629.387	66.908
	16	17.6	0.176	1.825	26.551	13.872	38.481	2.846	0.015	364.645	2605.119	156.901
	13	14.3	0.143	1.533	19.327	8.188	28.272	2.283	0.018	202.056	1185.665	97.837
	17	18.7	0.187	1.921	29.131	16.180	42.105	3.035	0.015	433.243	3278.252	180.100
	18	19.8	0.198	2.015	31.792	18.707	45.834	3.224	0.014	509.698	4071.460	205.106
	13	14.3	0.143	1.533	19.327	8.188	28.272	2.283	0.018	202.056	1185.665	97.837
	15	16.5	0.165	1.729	24.055	11.775	34.965	2.657	0.016	303.513	2039.712	135.478
	20	22	0.22	2.202	37.351	24.444	53.595	3.605	0.013	687.725	6070.435	260.651
	23	25.3	0.253	2.476	46.252	34.855	65.954	4.181	0.011	1023.286	10311.678	358.200
Average	**16.3**	**17.93**	**0.1793**	**1.849**	**27.174**	**14.416**	**39.357**	**2.892**	**0.015**	**380.714**	**2759.297**	**162.408**
Kodopalli section	11	12.1	0.121	1.332	14.969	5.358	22.062	1.913	0.021	125.657	629.387	66.908
	17	18.7	0.187	1.921	29.131	16.180	42.105	3.035	0.015	433.243	3278.252	180.100
	14.5	15.95	0.1595	1.680	22.840	10.804	33.248	2.564	0.017	275.622	1793.709	125.424
	9.5	10.45	0.1045	1.178	11.963	3.693	17.747	1.637	0.024	82.824	361.031	47.935
	11	12.1	0.121	1.332	14.969	5.358	22.062	1.913	0.021	125.657	629.387	66.908
	9	9.9	0.099	1.126	11.013	3.219	16.378	1.546	0.025	71.022	294.121	42.388
	10.5	11.55	0.1155	1.281	13.941	4.761	20.590	1.820	0.022	110.089	527.625	60.190
	19	20.9	0.209	2.109	34.532	21.459	49.665	3.415	0.013	594.397	4997.681	231.947
	12.5	13.75	0.1375	1.483	18.202	7.412	26.673	2.190	0.019	180.734	1021.851	89.487
	8	8.8	0.088	1.020	9.198	2.387	13.750	1.364	0.028	50.810	188.193	32.426
	13	14.3	0.143	1.533	19.327	8.188	28.272	2.283	0.018	202.056	1185.665	97.837
	10.5	11.55	0.1155	1.281	13.941	4.761	20.590	1.820	0.022	110.089	527.625	60.190
	12	13.2	0.132	1.433	17.100	6.682	25.104	2.097	0.020	160.928	875.340	81.552
	14	15.4	0.154	1.632	21.647	9.883	31.560	2.470	0.017	249.449	1570.277	115.801
	13	14.3	0.143	1.533	19.327	8.188	28.272	2.283	0.018	202.056	1185.665	97.837
	14.5	15.95	0.1595	1.680	22.840	10.804	33.248	2.564	0.017	275.622	1793.709	125.424
	12.5	13.75	0.1375	1.483	18.202	7.412	26.673	2.190	0.019	180.734	1021.851	89.487

	14	15.4	0.154	1.632	21.647	9.883	31.560	2.470	0.017	249.449	1570.277	115.801
	10.5	11.55	0.1155	1.281	13.941	4.761	20.590	1.820	0.022	110.089	527.625	60.190
	13.5	14.85	0.1485	1.583	20.475	9.011	29.901	2.376	0.018	224.944	1368.041	106.607
	12.5	13.75	0.1375	1.483	18.202	7.412	26.673	2.190	0.019	180.734	1021.851	89.487
	19	20.9	0.209	2.109	34.532	21.459	49.665	3.415	0.013	594.397	4997.681	231.947
	27	29.7	0.297	2.833	59.106	52.367	83.681	4.956	0.010	1614.332	18937.546	515.849
	17	18.7	0.187	1.921	29.131	16.180	42.105	3.035	0.015	433.243	3278.252	180.100
	16	17.6	0.176	1.825	26.551	13.872	38.481	2.846	0.015	364.645	2605.119	156.901
	13	14.3	0.143	1.533	19.327	8.188	28.272	2.283	0.018	202.056	1185.665	97.837
Average	**13.61**	**14.97**	**0.149**	**1.586**	**20.560**	**9.074**	**30.022**	**2.383**	**0.018**	**226.685**	**1382.177**	**107.267**
Rehatikhol section	15	16.5	0.165	1.729	24.055	11.775	34.965	2.657	0.016	303.513	2039.712	135.478
	6	6.6	0.066	0.801	5.924	1.150	8.970	1.006	0.035	22.424	63.234	16.854
	7	7.7	0.077	0.911	7.499	1.701	11.277	1.184	0.031	34.759	113.436	23.932
	6	6.6	0.066	0.801	5.924	1.150	8.970	1.006	0.035	22.424	63.234	16.854
	16	17.6	0.176	1.825	26.551	13.872	38.481	2.846	0.015	364.645	2605.119	156.901
	13	14.3	0.143	1.533	19.327	8.188	28.272	2.283	0.018	202.056	1185.665	97.837
	12	13.2	0.132	1.433	17.100	6.682	25.104	2.097	0.020	160.928	875.340	81.552
	6	6.6	0.066	0.801	5.924	1.150	8.970	1.006	0.035	22.424	63.234	16.854
	7	7.7	0.077	0.911	7.499	1.701	11.277	1.184	0.031	34.759	113.436	23.932
	7	7.7	0.077	0.911	7.499	1.701	11.277	1.184	0.031	34.759	113.436	23.932
	13	14.3	0.143	1.533	19.327	8.188	28.272	2.283	0.018	202.056	1185.665	97.837
	12	13.2	0.132	1.433	17.100	6.682	25.104	2.097	0.020	160.928	875.340	81.552
	14	15.4	0.154	1.632	21.647	9.883	31.560	2.470	0.017	249.449	1570.277	115.801
	15	16.5	0.165	1.729	24.055	11.775	34.965	2.657	0.016	303.513	2039.712	135.478
	4	4.4	0.044	0.569	3.186	0.411	4.913	0.654	0.049	7.080	13.595	6.701
	4	4.4	0.044	0.569	3.186	0.411	4.913	0.654	0.049	7.080	13.595	6.701
	6	6.6	0.066	0.801	5.924	1.150	8.970	1.006	0.035	22.424	63.234	16.854
	6	6.6	0.066	0.801	5.924	1.150	8.970	1.006	0.035	22.424	63.234	16.854
Average	**9.3**	**10.32**	**0.103**	**1.151**	**11.476**	**3.447**	**17.045**	**1.591**	**0.024**	**76.669**	**325.704**	**45.063**

3a.1.2. Transitional facies association

3a.1.2a FA III: braid-delta:

Deposits of this association form a facies belt that ranges in grain size from mud-free coarse-grained sandstones (amalgamated beds or in alternation with siltstone; facies type J), interbedded medium- to fine-grained sandstone-silty mudstones (facies type K) to very fine-grained felsic tuffs (facies L), which are all arranged sequentially in order of superposition. The coarse sandstones are of tabular bed geometry, internally massive, sub-horizontal, laminated, asymptotically-based planar cross-stratified or trough cross-stratified. Arrangement of cross-stratifications often replicates chevron geometry. Bedding plane surfaces are replete with weakly asymmetrical mega-ripple bedforms having frequent bifurcation of crest lines (Fig.3.7). Wavelength and amplitude vary from 54cm to 80cm and from 6 cm to 14 cm, respectively (n=12) with bedform index between 8.5 and 12. Crest lines of bedforms, though occasionally curved, have a consistent average orientation, trending northeast–southwest (Fig.3.19b). Granules (maximum 2.5mm in diameter) are concentrated along the crests of bedforms. Although a weakly developed fining-upward character is recorded at places, stacked bed sequences within facies J are commonly without any definite trend in grain size variation. Measurements of cross-stratifications recorded a bimodal (northwest–southeast) paleocurrent pattern. The interbedded siltstones, although poorly exposed, display planar or wave-ripple laminated character. Overlying facies J, the sandstone–mudstone heterolithic facies K is observed only in detached quarry sections and is traceable overstrike lengths not exceeding 8–10m. The sandstone interbeds are greenish in color, tabular, centimeters to decimeters thick, normal coarse-tail graded, and massive or plane laminated (with truncated Bouma T_{abe}, T_{ace}, T_{bce}, T_{ae} subdivisions). The bases of the interbeds are invariably sharp, occasionally erosional, and upper surfaces are rippled and gradational. The presence of rip-up mud clasts is occasionally observed at the base of sandstone interbeds. Soft sediment deformation features such as imbricated convolute and orientated flames are common observations towards the upper parts of beds. Folded character of this facies unit at the outcrop scale did not allow reconstruction of depositional dip for the bedding surfaces. Bedded tuff or an interbedded tuff-mudstone succession (facies L) replaces facies K up-section. Occurrence of facies L is noted through the entire east–west transect of the basin, demarcating the contact between essentially arenaceous Rehtikhol and dominantly argillaceous Saraipalli Formations. The facies is buff colored, very fine-grained, evenly bedded, folded, and with beds being internally massive or plane laminated (Fig.3.9; discussed in detail in chapter 6).

Interpretation:

Sheet sandstones with horizontal lamination are reported from widely different environmental conditions, viz., beach, eolian, ephemeral fluvial or tidal channel environments (*Clifton,* 1969; *Mckee et al.,* 1967; *Tirsgaard,* 1993; *Eriksson et al.,* 1995). In absence of inverse grading, beach accretion cross-bedding, eoliantranslatant strata or tidal symmetrical, bipolar paleocurrent pattern, the sheet sandstones of facies J are interpreted as products of ephemeral braided sandy channel systems (*Nemec and Steel,* 1988; ephemeral stream deltas, *Dam and Andersen,* 1990).The mega-ripples of facies J with straight, occasionally bifurcated crests and wavelength:amplitude ratio >8:1 closely replicate shore-parallel swash bedforms (*Johnson,* 1977; *Sarkar et al.,* 1996; *Clifton,* 2006; *Chakraborty and Paul,* 2008). Concentration of granules along the crests supports wave churning (*Galloway,* 2002; *Catuneanu,* 2002). Bimodal paleocurrent patterns obtained from the trough cross-stratifications also support this contention. Nevertheless, strong asymmetry of the mega-ripples indicates dominance of currents over the wave component in the nearshore zone. Such wave reworking of coarse-grained alluvial sediments resembles a wave-dominated non-barred near shore condition, wherein the surf–swash transition resulted in planar lamination along with land ward- and seaward-dipping trough cross-stratification (cf., *Clifton,* 2006). The predominance of wave ripple forms within poorly sorted coarse-grained sheet sandstones point towards an interactive zone where the inferred channel systems entered an extensive shallow basin. The occasional weakly fining-up wards tacking possibly resembles aggrading or retrograding sequences, generally related to transgressive episodes. Normally graded sandstone beds with top-truncated Bouma cycles within facies K represent deposition from low-density turbulent flow dispersion (*Dickie and Hein,* 1995; *Chakraborty and Pal,* 2001). Incorporation of clasts from the substrate indicate strong shear at the base of the flows, a character of proximal turbidite deposition. The intervening massive or plane laminated greenish shale intervals lacking evidence of exposure and without any current or wave features, resembles open ocean deposition below wave-base (*Bera et al.,* 2008; *Chakraborty and Paul,* 2008). The inferred turbidites are analogous to the delta-fed turbidite fan sediments described from the Lower Proterozoic Timeball Hill Formation, South Africa (*Visser,* 1972; *Eriksson,* 1973; *Eriksson and Reczko,* 1995, 1998) and the Upper Carboniferous Crackington and Bude Formations, southwestern England (*Melvin,* 1986).The evenly bedded character and uniform thickness of the felsic tuff unit of facies L over a large area suggests the deposit is an ash-fall product. Occurrence of soft sediment deformation structures, however, indicates that the settlement of elutriated ash particles was associated with basin-scale instability. Absence of current or wave features also

supports the deep-water emplacement. Absence of welding, lack of vesicles and presence of undeformed glass bubbles indicate deposition of ash in a cold state. Rarity of glass shard sand their blocky form instead of cuspate shapes, suggests phreatic or phreatomagmatic explosive eruption (*Seif and Sparks,* 1978; *Cas,* 1983; *Chakraborty et al.,* 1996; *Pal et al.,* 2005), although generation of cuspate shards in phreatomagmatic phases is also not uncommon (*Seif and Sparks,* 1978).

3a.1.3. Marine association

3a.1.3a. FA IV: Shelf:

a) Proximal (inner) shelf:

The subassociation is ~55m thick and conformably overlies facies association III, and is constituted of wavy bedded, parallel laminated shale, contorted silty shale and medium-grained sandstones (facies types M and N). Numerous shallow scour surfaces (depth varies from 4 cm to 19 cm) define the bases of sandstone inter beds. These basal surfaces are commonly rounded and flat, occasionally stepped, gradually or abruptly (Fig. 3.20a, b) with planar or convex-up top surfaces, the inter beds assume lenticular geometry (width 18cm to 2.24m, depth 4–19 cm; length indeterminable because of sectional constraint) resembling gutter- or channel-fill geometry. They are straight or slightly meandering, commonly with steep to overhanging

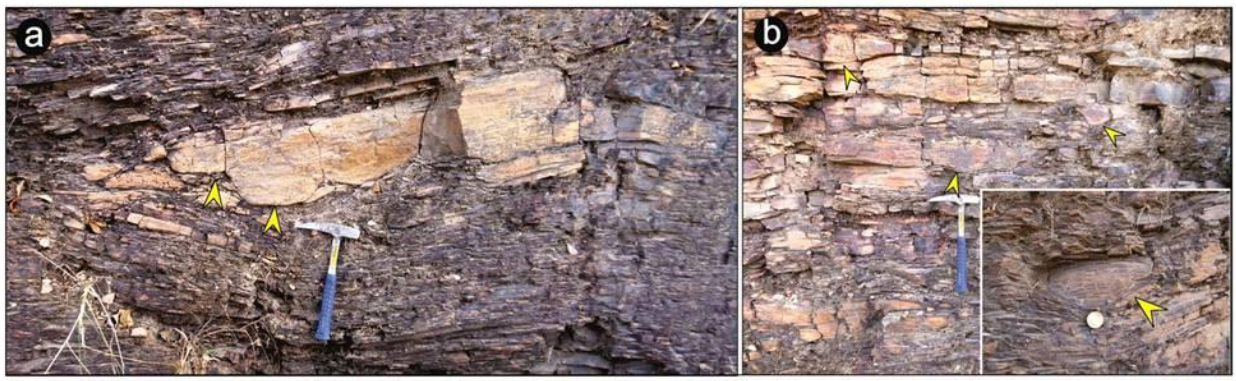

Fig.3.20. Facies M: gutter casts; stepped (a), symmetric/asymmetric (b) wave ripple laminations at the top. Length of coin is 27.5mm and that of hammer is 27 cm.

side walls and internally massive, or fining-upward, with top surfaces rippled. In general, they show a consistent NNE–SSW trend (Fig.3.19c). In cross-section, they are dominantly 'U'-shaped, shallow to

deep, both symmetrical and asymmetrical and with structure less or plane-laminated infill and ripple laminated towards the top. Preserved ripples on the bedding surfaces locally show profound asymmetry in profile. The wavelength and amplitude vary between 12.5 cm and 18.9 cm, 0.7 cm and 1.2 cm, respectively. Wavy bedded silty argillites drape the ripples and are followed upwards by contorted or parallel-laminated argillites. Detailed logging (Fig.3.21) within the facies unit revealed varying sandstone: shale ratios. Amalgamated gutters with width:depth (w:d) ratio (average 3.8:1; n = 8) constitute the sandy intervals. The gutters present within the shale-dominated parts are isolated, detached, thinner and wider (maximum w:d ratio up to 13.2:1). The width:depth ratio of gutters, averaged from 10 measurements through the section, shows a periodic variation in gutter geometry concomitant with lithological variation. In contrast to the massive or parallel-laminated character of isolated gutter-fill sandstones in mud-dominated parts, the gutters within the sand-dominated parts invariably show overall grading with the mud-clast concentrations at their bases. Wave ripples are less abundant in the latter case and convolute laminations are present locally. Overall, the association shows a fining-upward character with domination of mudstone in place of sandstone.

Interpretation:

Predominance of non-amalgamated sandstone beds with abundant wave structures coupled with interbedded silty and wavy bedded red mudstones; place this faciesassociation above fair weather wave base in a prodeltaic inner shelf setting (*Brenchley,* 1985; *Macnaughton et al.,* 1997). The shale (facies M) is considered to be a shelf suspension deposit, while the sandstone gutter and channel casts formed during high-energy events, viz., storms (cf., *Myrow,* 1992). Steep to overhanging sides of the gutters indicate that they were filled soon after being incised (*Goldring and Aigner,* 1982). Pervasive wave features within the shale indicate a wave-dominated shelf condition with intermittent encroachment of tempestites. The 'U' shapes of the gutters support their combined flow origin (*Beukes,* 1996). Grading within the sandstones suggest steadily waning character of the flows. The ripples at the top of sandstone interbeds are interpreted as the products of reworking either by fair weather waves or at the waning phase of storm events.

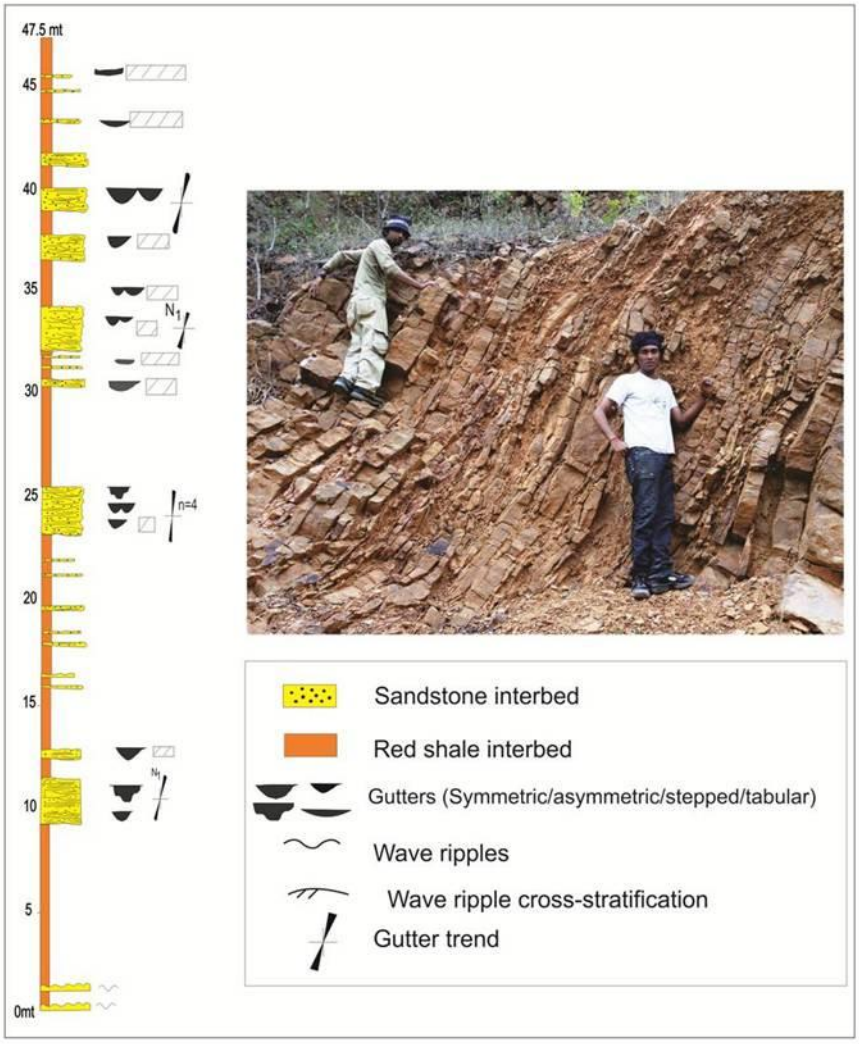

Fig.3.21. Photomosaic showing stacking pattern within sub-association IVa. Detailed measured litholog is provided alongside. Note stacking of fining- and thinning-upward hemicycles. Height of the person is ~1.6m.

presence of interstratified dark and relatively lighter colored irregular sub-laminae with average thickness of 4–6mm. Individual sub-laminae, however, do not persist for more than 2–3 cm. Sandstone layers are sporadic, lenticular, typically centimeters-thick, internally micro-hummocky cross-stratified (HCS; Fig.3.10) and with occasional current ripple caps. Individual HCS beds are sharp based, and the internal laminae typically intersect and truncate at low angles, and may be very gently curved. Occurring either as single beds, 4–18 cm thick, encased in mudstone, and as amalgamated beds, the HCS sandstone units constitute the swelling parts of hummocky sandstone bodies that are up to 1.2m thick. The overriding ripples are asymmetric (Fig.3.22), straight-crested and occasionally cuspate. Average wavelength and amplitude of hummocks and overriding ripples

are 42cm and 6.5 cm, and 12cm and 0.25 cm, respectively. The current ripples show southwest ward paleocurrent directions (Fig.3.19d).

Interpretation:

Black/gray color, higher shale: sandstone ratio and patchy sandstone beds with lenticular geometry–all indicate greater bathymetry for this sub-association, possibly in a distal shelf domain compared to sub-association IV a (*Diaz and Rozenberg,* 1995; *Fitzsimmons and Johnson,* 2000; *Bera et al.,* 2008). The intertwined irregular light and dark colored sub-laminae within the shales possibly reflect seasonal cycles alternately favoring and disfavoring growth of well preserved microbial mat in the general absence of bioturbation. The HCS units reflect the growth of vertically accreting bedforms with high sedimentation fall-out from upper flow regime currents (*Cheel and Leckie,* 1993). Lack of wave reworking on top of the inferred storm-laid beds indicates deposition between the fair weather and storm wave bases. This is well consistent with the non-erosional base of HCS units, which is more frequent in deeper shelves below fair weather wave base (*Bose et al., 1988*). The occurrence of current ripples at the top of HCS beds is particularly interesting in such a setting. Shore-parallel current direction obtained from the ripples can be best explained by the operation of unidirectional currents associated with a combined flow operative on the distal shelf.

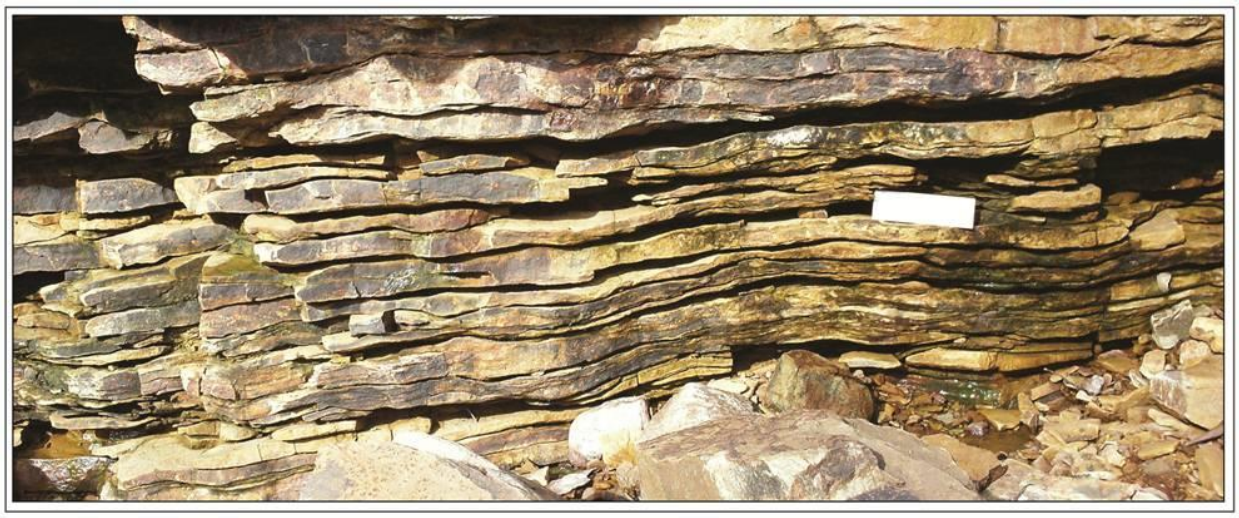

Fig.3.22. Distal shelf shale of sub-association IVb. Note occurrence of asymmetric ripples (scale length 15cm).

SUB-CHAPTER-III B

FACIES AND PALEOENVIRONMENTAL STUDY OF BHALUKONA FORMATION

Bounded between argillaceous marine shelf of the Saraipalli Formation below and the Chuipalli shelf shale at the top, the Bhalukona sandstone exhibits fourteen facies types (Table.3.3), clubbed under five different facies associations (FAs) belonging to nonmarine and marine settings. Absence of sediments belonging to this Formation in the eastern and northeastern part of the basin suggest wedge-like geometry for the Bhalukona formation; the thick part of the wedge is in the southern and southwestern part of the basin and the wedge tapers towards east and northeast. Facies associations constituting the wedge are distinctive in average grain size, stratification style, facies motif, paleocurrent pattern and direction. Documentation of facies associations and their mutual interrelations has been carried out from studies in seven best exposed outcrops spread over the basin viz. Bhalukona village, Padampur road cutting, Bhalugungri, Dongrijharan, near Singhora temple, Sishupal hill and Deodhara temple sections(Fig.3.23). The dominant structural characteristics and stratigraphic positions of the facies associations are illustrated from the Bhaludongri and Dongrijharan sections where most of them (except for FA I and FA V; discussed later) are present in a near-complete succession. All the associations are not present in all the sections studied, but they invariably maintain their relative stratigraphic succession. Like Rehtikhol Formation, specific depositional processes and events within the fluvial system of Bhalukona Formation are also identified through delineation of genetically related package of strata i.e 'architectural elements' following *Miall* (1978, 1985 and 1996).

Bhalukona sandstone is mature (matrix content varies from ~1.7% to ~7.7%), medium (Mdφ~0.23φ) to fine (Mdφ~2.47φ) grained, polymodal to unimodal sandstone, where the feldspar content varies between ~7.00% and ~0.50%. However, spatio-temporal variation has been observed based on modal abundance of framework minerals, matrix contents and size & shape of grains e,g poorly sorted and arkosic sandstone of Padampur road and Bhalukona village (western part of Bhalukona) is composed of mono and poly-crystalline quartz grains, feldspars and glauconite (detailed perteography has been described in FA-1) whereas, in rest of the locations the Bhalukona

sandstones are present with matured, arenitic, well sorted and well rounded character. Decrease in feldspar and matrix contents up the stratigraphic column is evident (Fig.3.24).

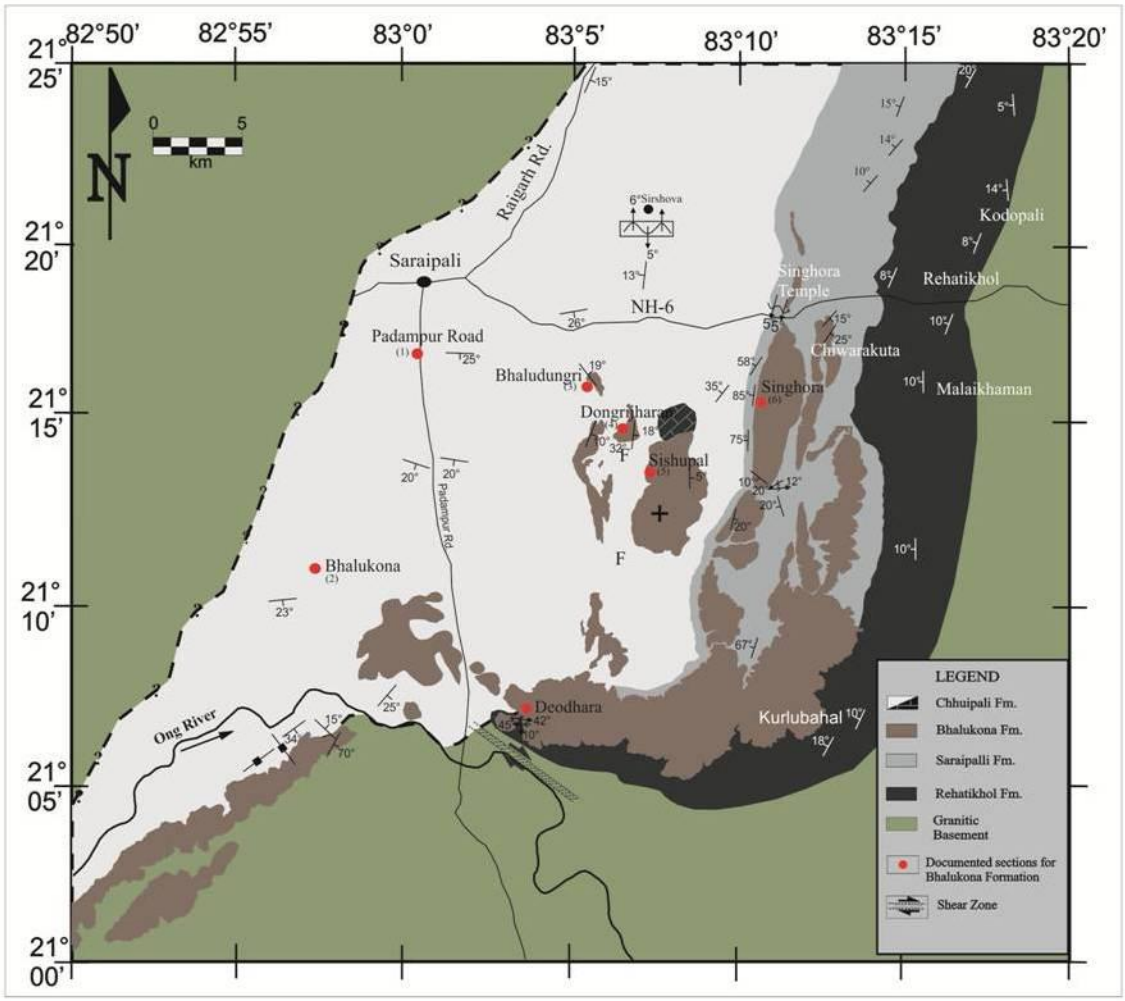

Fig.3.23. Aerial distribution of exposures of Bhalukona Formation in the Singhora basin. The study area locations are marked in red dots.

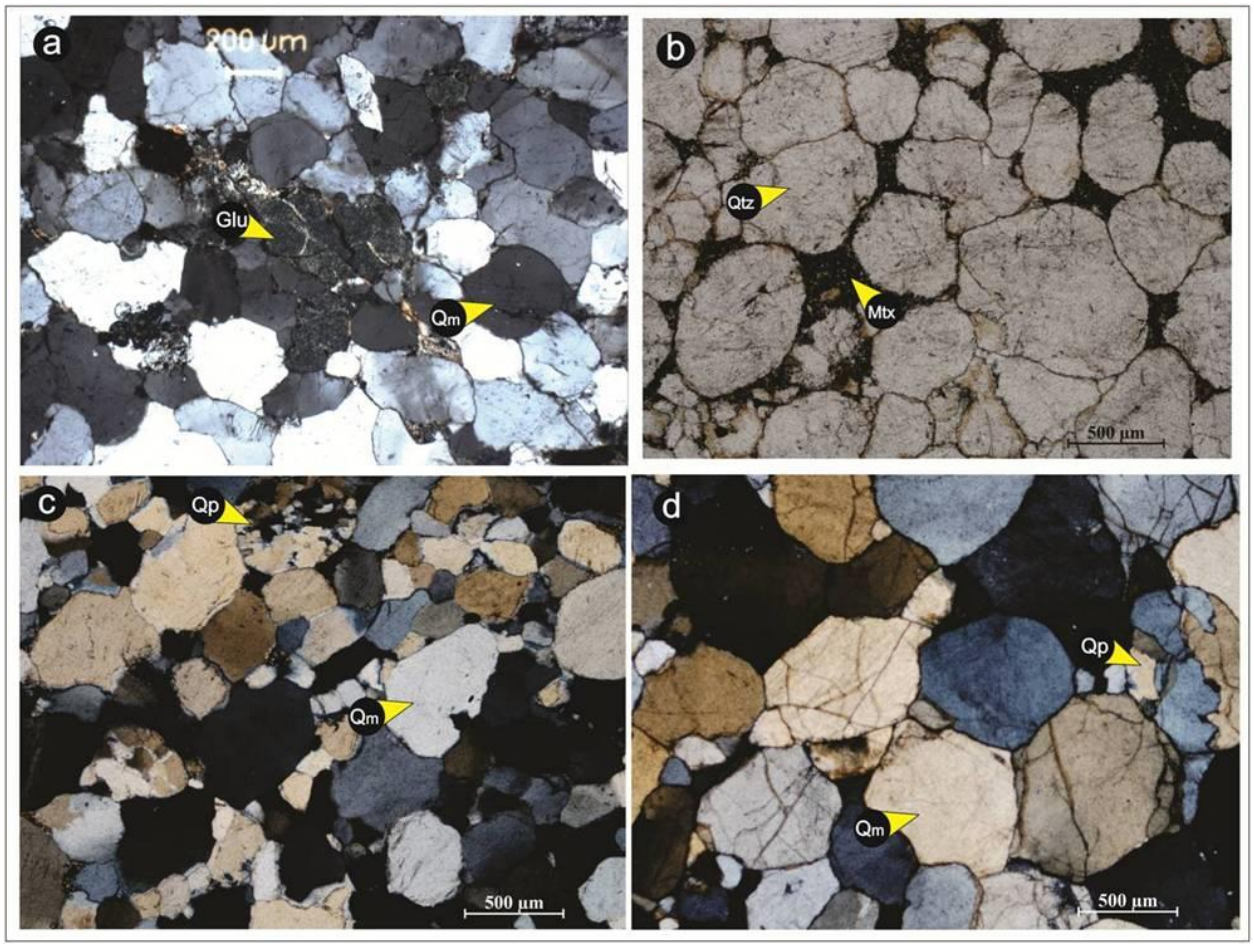

Fig.3.24. Glauconitic, poorly-sorted sandstone of FA I (a, b) and well-sorted mature sandstones in rest of the associations (c). Note the presence of matrix in sandstones of FA I (b). Q_m: Monocrystalline quartz, Q_p: Polycrystalline quartz M_{tx}: Matrix, Glu: Glauconite.

Table.3.3. Lithofacies of Bhalukona Formation and their inferred depositional environment

Architectural elements	**Description**	**Associated elements**	**Interpretation**	**Facies thickness**
Non-marinefacies association **FAB - I: Braided fluvial system** (architectural element and facies code adapted from *Miall* (1978, 1985, 1996)				
A. Medium- to coarse-grained cross-stratified poorly sorted sandstone (with mudstone and siltstone intraclasts) (CH)	Solitary or grouped sets with high-angle trough cross-bedding (sandy, St) and horizontal laminated bed (Sh); planar cross bed (Sp) climbing or stacked over the top. Rare overturned cross-beds. Usually solitary and rare multi-storey complex. Trough cross-beds (St) show unimodal paleocurrent towards southeast	Associated with SS, LA and OF elements. Upward thinning and fining packages	Braided fluvial channels and distributary channels (CH) with sporadic lags. Amalgamated channel deposits common	1.8 to 3.2m
B. Medium grained sheet sandstone (SS)	Sheet-like bodies with erosive to slightly concave basal surfaces. Planar (Sh) and cross-stratified (St) bed; granule/pebble filled shallow scours (SF) with occasional crude cross-bedding (Sp, St)	Overlies and laterally associated with CH element	Sand sheets (SS), braided fluvial channel and distributary channels, shallow scour fills	Sheet like bodies may extend >80m laterally with 0.8 to 1.35m thickness. Scours are with 24 cm width and 7.5 cm depth on average.
C. Lateral accretion macroform (LA)	In cross-section wedge-shaped sandstone lenses constituted principally of Sp and St. Distinctive internal grading from granule to coarse- and medium-grained sandstones. Cross-beds show easterly paleocurrent direction, at high angle to the paleocurrent obtained from the CH units	Laterally associated with CH element; also occasionally overlain by CH element	Accretion laterally across channel	Lenticular unit, laterally traced maximum for 4.3m, av. thickness 0.85m
D. Overbank fines	Red coloured, fine grained sand, silt and mud (Fh) with	Underlain by CH element.	Overbank and/or waning	Laterally extensive in specific

(OF)	minor Sh, Sp and rare St. Sandstones of broad lenticular geometry with average width and thickness 2.12 m and 0.26 m, respectively	Exposure constraint did not allow documentation of lateral and upper contact relationship for this element	flood deposits	locations viz. Bhalukona section. Varying between 2.23m and 4.35m in thickness
Marine facies association (FA)s				
FAB - II: Foreshore-beach				
E. Medium-grained tabular sandstone	E1. Tabular units of well-sorted sandstone; trough cross-stratified. Rare small-scale planar cross-strata with tabular geometry. Average set thicknesses of trough and tabular cross-stratification are 0.15 m and 0.08 m, respectively	Overlies wave ravinement surface (facies I) and overlain by the rocks of FA II	Traction current deposition under lower flow regime conditions, deposited from sinuous-crested ripple and linear-crested dune bedforms	0.07 to 1.16m
	E2. Parallel-stratified sandstone with ungraded stratification bands. Low angle truncations		Upper flow regime tractive transport of sand grains. Common in beach environment	0.035 to 0.86m
FAB - III: Upper shoreface				
F. Thick-bedded lenticular sandstones	Lenticular beds (av. width 0.78 m) with planar base and convex-up top, massive or planar-curved cross-laminated (Average set thickness 9.4 cm). Symmetrical ripple forms (av. wave length 11.4 cm, amplitude 0.9 cm; Ripple Index (RI = 12.6) on the bedding surfaces. Amalgamated beds constitute packages (average 1.35 m in thickness)	Facies F and G change over laterally or alternate vertically with one another	Lower flow regime dune deposits in a wave dominated setting, bedform index >8 suggestive of swash origin	0.22 to 0.87 m in thickness; width varying between 23 cm and 1.46 m
G. Thin-bedded lenticular sandstones	Smaller scale lenticularity in comparison to facies F, rare siltstone stringers		Relatively lower energy interdune deposits in wave dominated	0.08 to 0.38 m in thickness; width varying between 23 cm and 1.46m.

			shoreface setting	
FAB - IV: Lower shoreface				
H.	Lenticular beds (av. width 0.28 m) internally constituted of H1. Cosets of trough cross-stratification with average set thickness 4.5 cm; rare planar lamination. H2. Planar tabular/curved cross-strata arranged in chevron pattern. Average set thickness 4.3 cm Tops of sandstones commonly reworked by ripples	In association with facies types I and J	Mixed wave/current two- and three-dimensional bedforms	0.12–0.29 m
I. Quasi-planar laminated sandstone	Thin (<4 cm) planar-laminated sandstone. Multiple low-angle truncation surfaces; lower laminae commonly downlap onto basal surface	Associated with facies H	Combined flow (?) plane bed related to high energy (storm) event	0.24–0.68 m
J. Bi-directional cross-stratified sandstone	Herringbone cross-stratified sandstone, Laterally and vertically discontinuous. Surfaces of reactivation	Dominant in the upper part of the association in alternation with facies H	Reversing unsteady flow related to tidal action	Set and coset thickness 7.5 and 19.3 cm respectively
FAB - V: Wave dominated Delta front				
K. Tabular, parallel-sided massive/normal-graded sandstone	Decimetre- to meter-thick parallel sided sandstone beds; base of beds sharp, nonerosional/feebly erosional and top varying between sharp and gradational. Bed tops are often replete with symmetrical wave ripples (av. wave length and amplitude 3.5 cm and 0.6 cm, respectively). Beds thicken and amalgamate upwards through the succession. Observed with two internal structural sequences: K1 and K2			
	K1. Poorly sorted coarse to medium grained sandstone.		Rapid deposition from sandy	Decimetre to meter thick.

	Ungraded to coarse-tail normal graded, with flat basal contacts, rarely scoured. Crude horizontal or wavy laminae; climbing current ripple cross-laminations only in the uppermost part (Bouma Ta, Tab, Tbc)	Occur in amalgamation or in alternation with facies k	dispersions associated with waning turbulent flow. Near bed suspension generated by mixing with ambient fluid along the upper surface of the basal dense flow.	Traceable for more than 500 m in exposure
	K2. Featureless (massive, lacking any grading), rarely the beds are draped by parallel-laminated sandstone (maximum thickness 0.26 m)		Gradual aggradation from sustained high density turbidity current (cf. Branney and Kneller, 1992) and upward migration of depositional flow boundary due to grain hyperconcentration and hindered settling in a steady and quasi-steady current.	Decimeter (0.35 to 0.76m) thick, laterally traceable for more than 500m
L. Ripple laminated siltstone/mudstone	Siltstone with lesser very fine arenite. Sporadic current ripple	Alternates with facies K with gradational and sharp contacts at its base and top, respectively	Offshore fines	0.03 to 0.13m

3b.1 Facies Associations of Bhalukona Formation (FAB):

3b.1.1. Non-Marine Facies Associations:

3b.1.1a. FAB - I: Braided Fluvial System.

Granule rich, coarse grained (Mdφ = 0.16φ), poorly-sorted sandstones of this association, constituted of facies types A-D (Table 3.3), overlies the argillaceous inner shelf sediments of Saraipalli Formation with interpreted erosional contact, and are exposed in the western and northwestern parts of the basin viz., Padampur road and Bhalukona village sections (Fig.3.23). Although exposure limitation did not allow documentation of physical contact between sediments of this association and its underlying Saraipalli Shale, the coarse granular and pebbly grain size of sediments in the association and occurrence of rip-up mud clasts in variable size within it allowed interpretation for an erosional base for the association. Maximum thickness for the association observed is ~10 m. Following *Miall* (1978, 1985, 1996) facies types are clubbed under four different types of architectural elements (Table.3.3). In the best exposed section (Bhalukona village and Padampur Road), stacking of four meter-thick tabular fining upward (grain size varies between granule (average −1.40φ) and medium sand (average 1.47φ) size from base to top) successions is observed (Fig.3.25). Each succession begins with a 'Channel' (CH) or 'Lateral Accretion' (LA) element, and in turn, topped by thin bedded sheet like medium-grained sandstones (SS element) dominated by horizontal laminated (S_h), planar cross-stratified (S_p) and trough cross-stratified (S_t) lithofacies (Figs.3.25a, 3.26c). Planar or broadly undulated master erosion surface, extensive over ~75 m wide outcrop area, is found to separate vertically stacked tabular units. Coarse sandstone with dispersed rip-up mud intraclast pebbles (max. diam. 8.1 cm) (G_m; Fig.3.25a) with cosets of S_t and S_p characterizes the CH element (Figs.3.25a, 3.26a and b). The SS elements are found marginally to the CH units or overlying and typically arranged in a multi-storey fashion (Fig.3.26c). The paleocurrent readings (from S_p and S_t) from both CH and SS element are towards a mean azimuth of 167° (Fig.3.25a). The LA macroforms (Fig.3.25a), consist of medium- to coarse-grained sandstone, are only a maximum 2.40 m long, 0.55 m thick and recognized with foresets dipping towards east. Broad, shallow scours (average width: depth ratio 6.4:1), filled with very coarse and granular sandstone (SF), disrupt the fining-upward tendency (Fig.3.26d). Occasionally, lensoidal bodies of cross-stratifications (average set thickness 8.6 cm) with granules concentrated at foreset bases are found to fill the scours. In Padampur road section, the top of the association is replete with large-

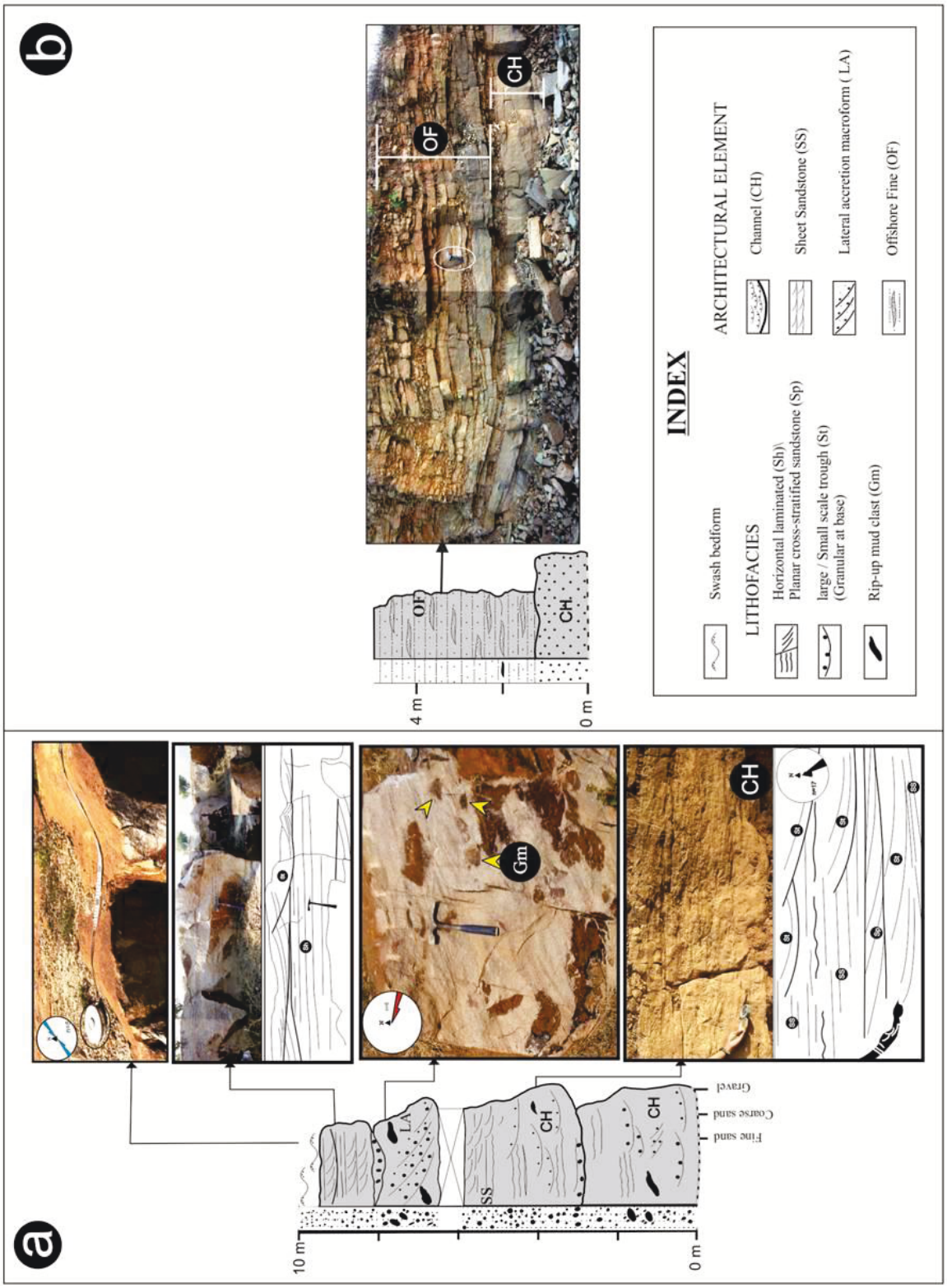

Fig.3.25. Measured lithologs of FA-B 1 from Padampur village (a) and Bhalukona village (b) sections. Note amalgamated channels (CH) with G_m units at Padampur and OF element at Bhalukona section. Paleocurrent indicators show eastward orientation.

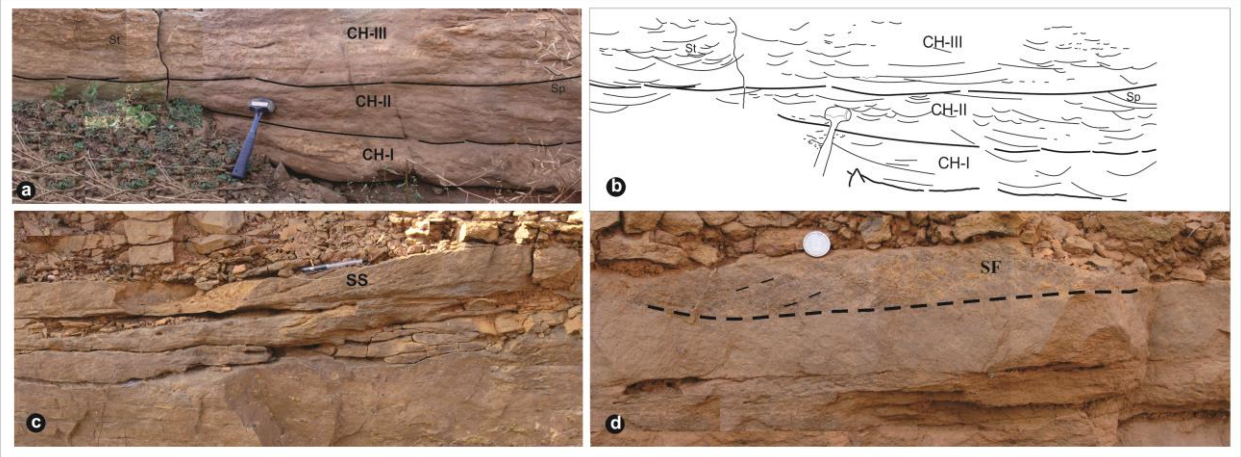

Fig.3.26. Photographs revealing different architectural elements within FAB - 1. (a) Amalgamated CH [field sketch alongside (b)], (c) Sand Sheet (SS), and (d) granule/pebble filled shallow scours (SF) (Hammer length 27cm, pen length 12cm and coin diam. 23cm).

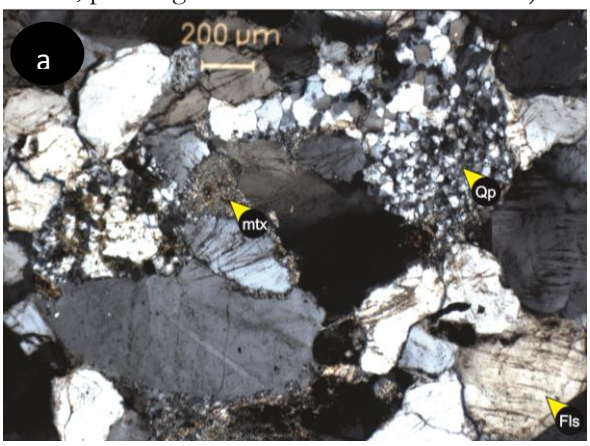

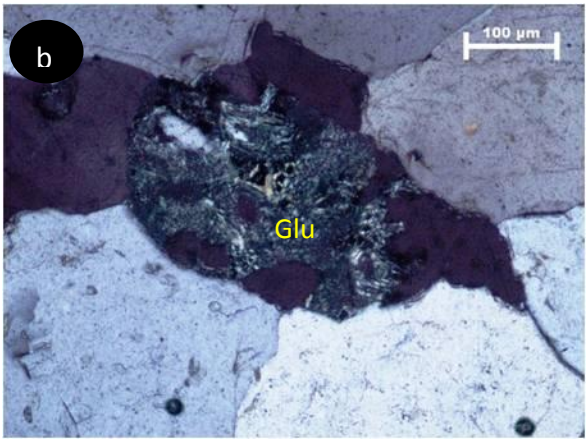

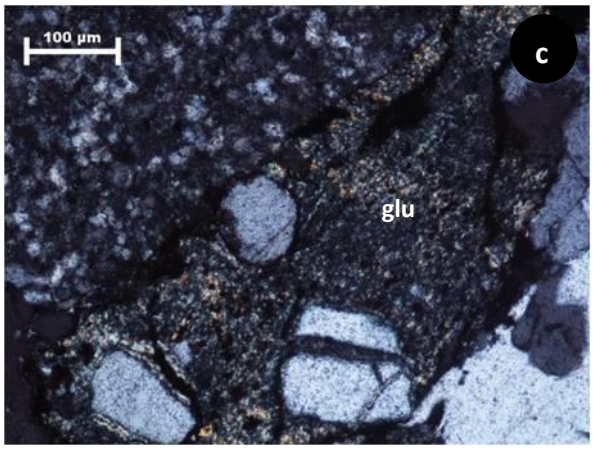

Fig.3.27.a. Poorly sorted sandstones of FAB-1. Note formation of pseudo-matrix from decomposition of feldspar. b. Replacement of feldspar detrital grain by glauconitic clay with a few unaltered patches c. Glauconitisation along grain fracture progressively engulfing the entire grain.
Qp = polycrystalline quartz, Fls= Feldspar, g= glauconite, mtx= matrix

scale symmetrical bedforms (average wave length and amplitude 70 cm and 8.9 cm, respectively) with straight, bifurcated crest lines; concentration of coarsest grains observed on the crest lines (Fig.3.25a). In the Bhalukona village section, 'Overbank Fine' (OF) element, constituted of alternation between thinly bedded and laminated fine-grained lenticular sandstone and siltstones, are exposed with up to 4.35 m of thickness (Fig.3.25b).

Thin section study on sandstone of this association reveals poorly-sorted, clast-supported sub-arkose to sub-litharenite characters for the sandstones. Matrix is generally rare; wherever present is <8% in volume and identified as opaque iron oxide or clayey pseudomatrix formed by squashing of labile lithic fragments. In addition to quartz [monocrystalline (Qm) and polycrystalline (Qp)], feldspar and lithic fragments (quartzite, siltstone and shale) constitute the clast population of the sandstones (Fig. 3.27a). Many of the feldspar grains are found to be relaced by glauconitic clay (Fig. 3.27b). Initiating as veins and patches along the grain fractures and cleavages, glauconitisation progressively engulfed the entire detrital feldspar grains, with occasionally left out remnants (Fig. 3.27c). Quartz (Qm) grains are subangular, coarse- to fine-grained and with occasional ironoxide coatings and overgrowths. Polycrystalline quartz grains (Qp) are subordinate, consist mainly of sutured, semicomposite crystals with preferred crystallographic fabric, probably of metamorphic origin. Muscovite, rutile and zircon (rare) are the main heavy minerals.

Interpretation:

Features supporting the fluvial interpretation include poor sorting; sharp based fining-upward sequences and predominance of cross-beds with a unimodal south-eastward paleocurrent direction (cf. *Bridge,* 2006). Overbank fines are rare and restricted to thin units of red siltstone. Defining the channel pattern is problematic because local lateral continuity of outcrops is limited. The general lack of channel morphology and low dispersion of paleocurrent, however, are suggestive of a broad, shallow (<2 m deep) and unconfined braided channel system (sinuosity value 1.03; after *Le Roux,* 1992). The dominant trough cross beds are related with megadune migration, whereas the minor planar cross-bedded units represent smaller dunes migrating over the banks. The downstream migrating dune fields are commonly overlain by poorly-defined laterally extensive sand sheets. The relatively larger-scale lateral accretionary foresets are the results of marginal bar migration. Coarse grained, solitary nature of the unit, with erosional top and base, is comparable with simple cross-bedded bars described from the low-sinuosity braided systems in the Brownstones (Lower

Devonian) Welsh Borders (*Allen,* 1983). Rapid variability in discharge is documented in form of scours filled with coarse sediments including granules and commonly present reactivation surfaces within the S_t units. In fact, the granule-filled scours incised on top of all other fluvial facies presumably represent a stage of strongest turbulence and bed shear. Occasional side-filling of the scours suggests emergence, thus we are inclined to take scours as ultimate products of sheet flow during a falling water stage when bed shear and grain entrainment capacity are at maximum (cf. *Bose and Chakraborty,* 1994). The overbank fine grained siltstones and sandstones present at the Bhalukona village section are interpreted as deposits of flood stages and following waning stages (cf. *Jones et al.,* 2001). From wavelength: amplitude ratio (>8:1), the large scale bedforms present at the top of the association at Padampur road section are identified as of swash origin (*Clifton,* 1969, 2006). Concentration of coarse grains at the bedform crests corroborates wave churning (*Galloway,* 2002; *Catuneanu,* 2002). Reworking of fluvial sediment by marine agent is inferred.

3b.1.2. Marine facies association of Bhalukona Formation (FAB):

3b.1.2a. FAB - II: Beach-Foreshore:

Beach-Foreshore Sandstones of this association are observed at the Bhaludungri and Dongrijharan sections overlying granular/pebbly ravinement deposit (discussed later) with sharp, erosional contact. Tabular (tens of meter wide) beds of medium-grained sandstone, made up of subfacies E1 and E2 of FAB-II, often in amalgamation (maximum thickness recorded ~2.23 m), constitute the association. Individual bed thickness varies between 0.65 and 1.32 m. The sandstones preserve horizontal lamination (parting lineated and with low-angle truncations), very low-angle trough cross-stratifications (set thickness ranging between 10 cm and 45 cm; average ~15 cm) and rare tabular cross-stratifications. Paleocurrent measurements from troughs reveal bimodal west-southwest orientation (Fig.3.28).

Interpretation:

Horizontal-laminated sheet sandstones with parting lineation suggest upper flow regime condition. Such sandstones are reported from widely different environmental conditions, viz. beach, eolian, ephemeral fluvial or tidal channel environments (*Clifton,* 1969; *McKee et al.,* 1967; *Tirsgaard,* 1993; *Eriksson et al.,* 1995). Absence of inverse grading, eolian translatant strata or tidal symmetrical and bipolar paleocurrent pattern allows us to negate those possibilities. On the contrary, good

sorting, plane lamination (with parting lineation), low-angle truncation, alteration with trough cross-stratified units and stratigraphic position below shoreface facies association (FAB - III) suggest deposition of these sandstones in a beach condition. The trough cross-stratified units, in association, are interpreted as the product of shallow-marine currents on the foreshore associated with the beach. In the foreshore waves transport water onshore; when they break on the beach they drive a thin sheet of water rapidly up the beach face. This swash is capable of moving sand and gravel, and typically produces plane lamination parallel to the beach face. Commonly on a foreshore there are two dominant current systems - longshore currents produced by oblique wave approach to the shoreline and a cell circulation of rip currents and longshore currents (*Komar,* 1976; *Walker,* 1984).Similar products are recorded from several modern wave-dominated clastic shorelines, wherein the surf-swash transition results in planar lamination along with landward and seaward-dipping trough cross stratification (cf. *Bose and Chaudhuri,* 1990; *Bose and Chakraborty,* 1994; *Clifton,* 2006).

3b.1.2b. FAB - III: Upper Shoreface.

From landward to basin-ward, sandstones of this association overlie the beach- foreshore sandstones (FAB - II), ravinement lag (RL) or gray shale of the Saraipalli Formation with thickness varying between 0.12 m and 0.23 m (Fig.3.28). Either in amalgamation or separated by centimeter-thick mudstone partings, stacked sets of decimeter-to meter-thick tabular units of fine- to medium-grained moderate- to poorly-sorted sandstones make up this association (Fig.3.29a). Internally each tabular unit is constituted of intermingling between two different sub-associations (I and II) at various scales (Fig.3.29b), both sub-associations are constituted of lenticular beds of medium (Md_{φ}~ 0.23 φ) to fine (Mdφ~2.47φ) grained sandstones, but differ in grain size sorting (σ), bed thickness and degree of lenticularity. Despite intermingling, dominance of sub-associations I and II is observed in the lower and upper parts of the tabular units, respectively. Sub-association-I sandstones are moderately-sorted (σ = 0.87), uniformly thick bedded (average bed thickness ~46 cm), broad lensoid (width 0.28 m, maximum length 1.46 m) in geometry, internally structureless, and trough cross-stratified (average set thickness 18 cm) or low-angle planar curved cross-stratified (average set thickness 12 cm). In contrast, sandstones of sub-association II are either sandwiched between units of sub-association I, or present in amalgamation towards the upper parts of the tabular units. Constituted of thin (average thickness ~11 cm) bedded, poorly-sorted (σ = 1.22) sandstones, the

sub-association II units internally comprise alternations of trough cross-stratification (average set thickness ~5.4 cm) and plane laminations. Trough cross-stratifications from both sub-associations show a bimodal west northwest- west southwest orientation (Fig.3.28). Sub-association I, when directly overlies the Saraipalli shale, show presence of rip-up shale clasts at its basal part. Oscillation ripples, in trains, represent the dominant surface bedforms (Fig.3.30a). The ripples are symmetrical in profile, straight-crested (rarely three-dimensional) and occasionally with crest bifurcations (crest line orientation ~NNE-SSW) (Fig.3.30a). On average, wavelength and amplitude of the ripples are 12.8 cm and 1.2 cm, respectively. Confined at the basal part of this association soft-sediment deformations in form of crumpled and distorted beddings are recorded. Sandstones of this association are sub-arkose to quartz arenite [$Q_{(total)}$ = 87.53–92.66%, F = 8.34–4.84%, L = 0.00–0.53%, glauconite and heavies = 0.00–0.42%; matrix content, in general, <8%] in composition and show variable grain size sorting. Glauconites are present both as clast and matrix. Rutile and zircon are most common heavy minerals.

Interpretation:

Dominance of trough cross-strata with bimodal foreset orientations and frequent occurrence of wave generated bedforms indicate deposition in a shallow, wave-dominated environment above fair-weather wave base (*Walker and Plint,* 1992). Wave length: amplitude ratio (>8:1) for the wave ripples suggest their swash origin (*Clifton,* 1969, 2006; *Sarkar et al.,* 1996) in upper shoreface set-up. Bimodal, land (west) ward directed paleocurrent recorded from trough cross-stratifications within sub-associations-I and II suggest landward migration of lunate bedforms, varying in scale (centimetre to decimetre high). Similar landward migrating decimetre-high lunate megaripples are described from the area of most intense wave build-up just seaward from the surf zone in medium to coarse-grained sandy non-barred nearshores in southern Oregon (*Clifton,* 1976; *Posamentier and Walker,* 2006). Whereas the thick beds (average cross-bed set thickness 18 cm) with broad lenticular geometry are interpreted as products of bar migration, the thin bedded units (average set thickness 5.4 cm) with overriding small-scale ripple bedforms are possibly of interbar origin (*Tamura et al.,* 2007).

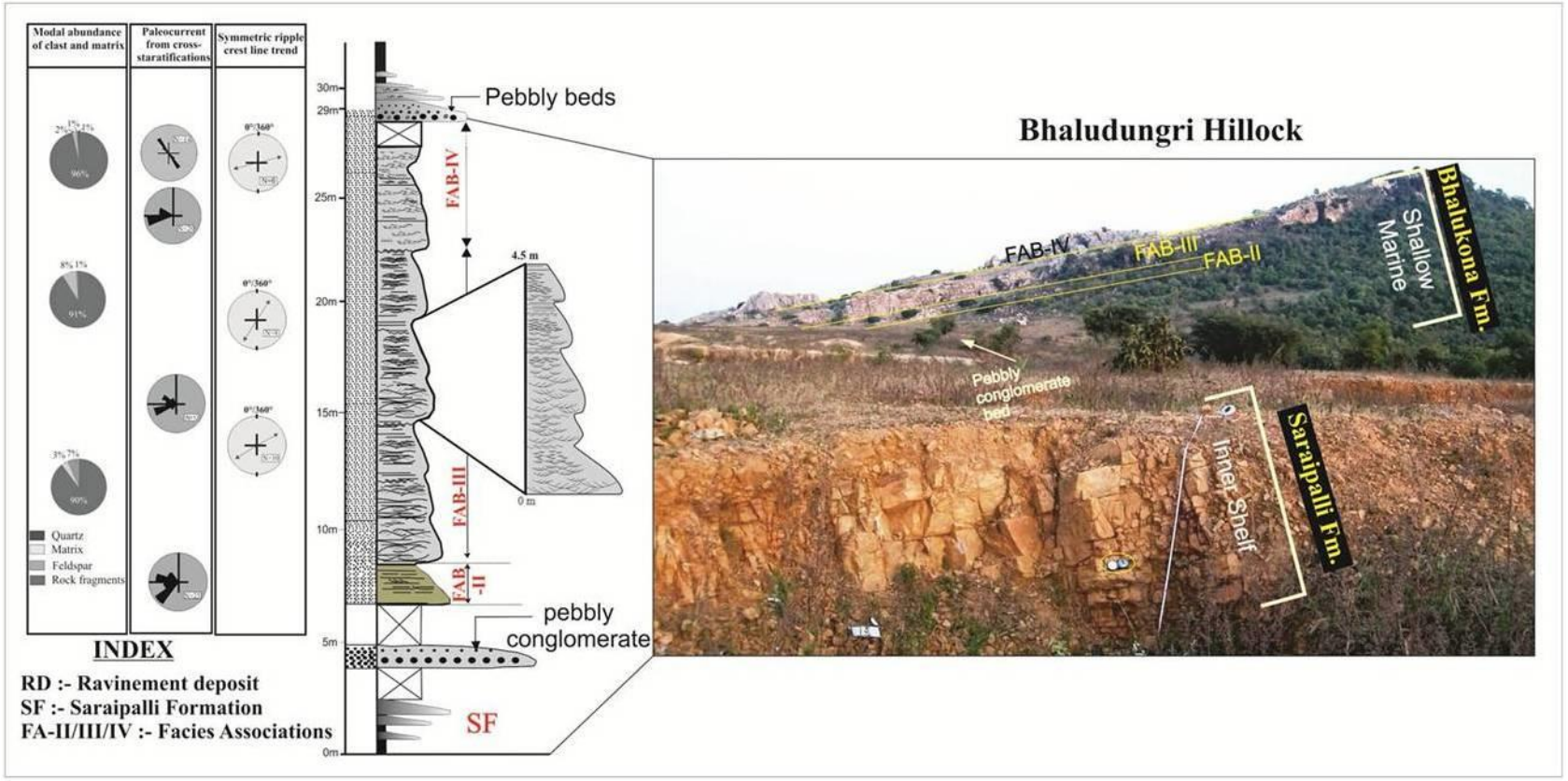

Fig.3.28. Detailed measured litholog of FAB - II, III and IV exposed at the Bhaludungri section. Note occurrence of intraformational conglomerate layer at the base and top of the section, respectively. Detailed architecture of stacked tabular unit is shown on the right. Paleocurrent directions, paleoshoreline trend and variation in modal abundance of framework elements and matrix content of sandstones at different stratigraphic levels are shown on the left. Note steady decline in feldspar content up the stratigraphic column.

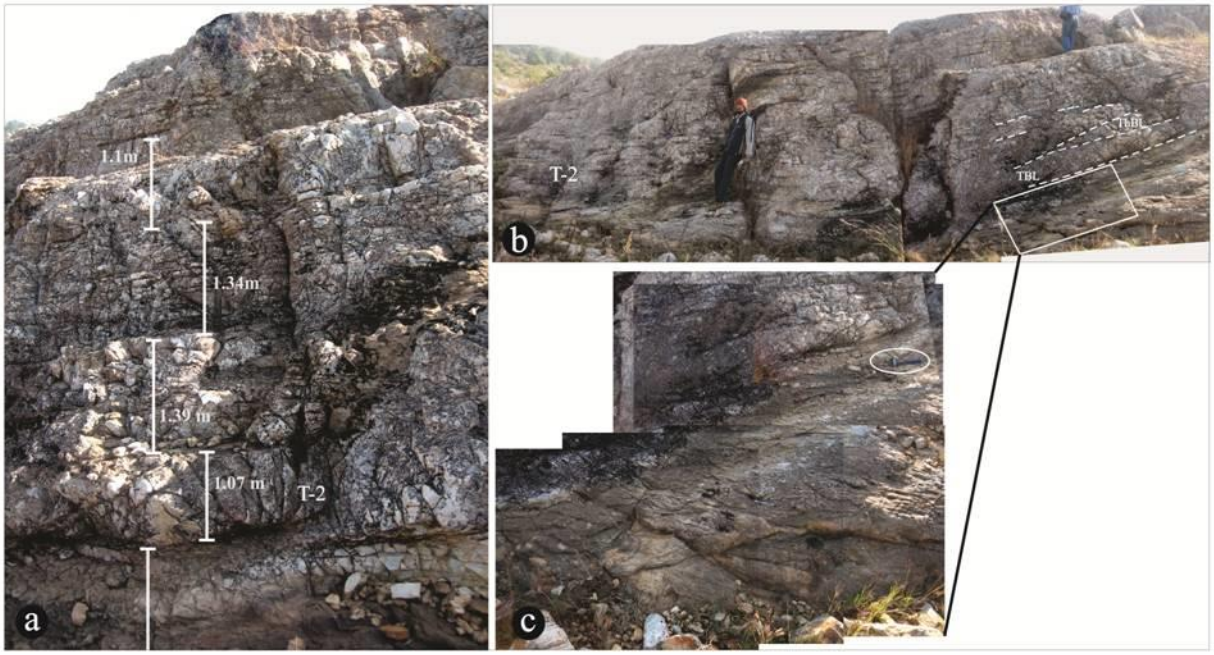

Fig.3.29. Stacked meter-thick tabular units within FAB - III (a). Photomosaic detailing the internal structures of one such tabular unit (T2) is shown on the right (b). Note intermingling between thick- (TBL) and thin-bedded (ThBL) lenticular units within FAB - III. A detailed view representing chevron cross-stratification pattern within the TBL units are shown in (c). Larger scale cross strata within TBL represents the bar bedforms and thin ripple laminated bedforms within ThBL represent the interbar.

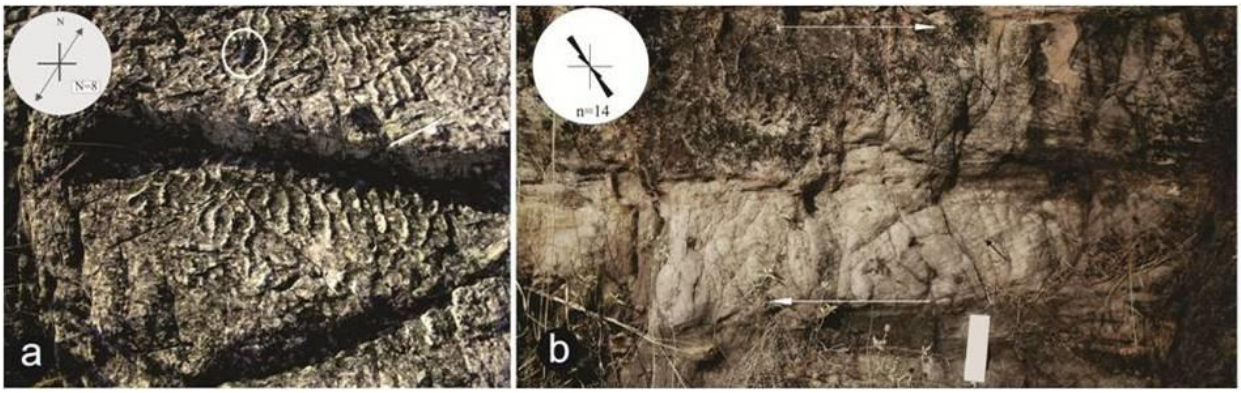

Fig.3.30. Plan view of facies J showing trains of wave ripple. Rose diagram showing NNE–SSW trend for the ripple crest lines (a). Bipolar cross-stratifications within facies J of lower Shoreface facies association (FAB - IV) (b).

3b.1.2c. FAB - IV: Lower Shoreface.

This association comprises the uppermost part of Bhalukona succession at Bhaludungri, Dongrijharan, Sishupal and Singhora sections and is represented by stacked sets of tabular units constituting facies types H, I and J of FABs. While lower boundary of this association with FAB - III is gradational and difficult to delineate in field, the upper boundary is sharp and can easily be demarcated by centimeter-thick bed/s of clast-supported coarse granular sandstone. Two laterally equivalent facies, H1 (cosets of troughs capped by wave rippled sheets) and H2 (tabular cross-strata arranged in crisscross chevron pattern) constitute the basic motif of tabular units. The troughs are with average set and coset thickness 4.5 cm and 11.6 cm, respectively and their paleocurrent measurement indicate unimodal westward direction of migration (Fig.3.28). The associated wave ripples show north northeast - south southwest crest line orientation. The bedform size decreases steadily upward in the stratigraphic section (set thickness recorded ~1.85 cm at the top). At places, the cross-laminated units are cut by shallow, concave-up erosional surfaces. The concordant laminations (facies I of FAB) overlying these surfaces are intermittently intervened by truncation surfaces. Bipolarity in the orientation of cross-stratifications is observed at some selected intervals in the upper part of the association (facies J of FAB; Fig.3.30b). Sandstones of this association are bimodal in grain size distribution (Mdφ1 = 0.096φ, Mdφ2 = 4.02φ) and quartz arenite in composition [Q(t) = 97.79%, F = 0.45%; matrix content <2%].

Interpretation:

A perpetually wave-agitated relatively deep neritic environment is inferred. Meter-thick chevron cross-stratification co-set suggests that the water depth was sufficient to accommodate vertically accreted bedforms~2 m or more in height, possibly encompassing middle and lower shoreface domain. In an overall wave-dominated set up, the vertically accreted bedforms might have acted as barriers that led to local enhancement of tide represented by bipolar cross-stratified units in the upper part of the association. Although the association lacks any definite signature of hummocky cross-stratification, the low-angle truncations with conformable overlying laminae are suggestive of possible storm action (*Tamura et al., 2007*). The coarser grain fraction in the bimodal grain population was possibly carried by storm currents within the relatively deeper neritic domain where otherwise fine sand size grains equilibrated with fair weather waves (*Clifton, 2006*).

3b.1.2d. FAB - V: Wave influenced delta front.

This is best exposed at the Deodhara section in the south-eastern part of the study area and FAB-V constituted of facies types K and L (Table.3.3). Rocks of this association are deformed and folded. Despite being folded, the gently dipping limb (average dip < 10°) of asymmetric folds allowed documentation of detailed sedimentological characters. Non-amalgamated (separated by cm-thick silty grey shale intervals; facies L of FAB-V) to amalgamated decimeter- to meter-thick parallel sided sandstone beds (facies K of FAB-V) made up the general framework for the association (Fig.3.31). Individual bed, with indistinct coarse-tail normal grading, is characterized by a distinctive vertical succession of structures: massive successively followed upward by planar-parallel laminations and non-climbing current ripple crosslamination (Bouma T_a, T_{ab}, T_{bc}). Beds are invariably planar, sharp at the base and their upper boundaries vary between sharp and gradational. Continuity of the beds with unchanged thickness is traced in the outcrop for more than hundred meters. Adjacent coarser (sandstone beds; facies K of FAB-V) and finer (facies L of FAB-V) interbeds show poor correlation ($r = 0.12$) between their thickness values. Bed tops are reworked by symmetric ripples with average wave length and amplitude 4.2 cm and 0.8 cm, respectively. Massive (unstratified) sandstone beds, without any grading, are also common. Sandstones of this association are silica-cemented, quartz arenite (Q(mc) > 90%; matrix content <5%) in composition, poorly-sorted with variation in grain size between 9.96φ and 0.45φ.

Interpretation:

The sandstone beds are interpreted as products of gravity flows ranging in rheology between highly concentrated granular dispersion and dilute noncohesive turbidity current. Low correlation coefficients ($r = 0.12$) between adjacent coarser (sandstone beds, facies K of FAB-V) and finer (facies L of FAB-V) interbed thicknesses suggest their independent origin (*Schwarzacher and Fischer,* 1982). The massive, unstratified beds are interpreted as products of gradual aggradation and consequent upward migration of the depositional flow boundary due to grain hyperconcentration and hindered settling in a sustained steady and/or quasi-steady, high-concentration current (*Branney and Kokellar,* 1992; *Kneller and Branney,* 1995). Amalgamated mass-flow units, separated infrequently by facies L (of FAB-V) shale, resemble delta front sandstone lobes (shale encased, thickening up, Bouma Ta, Tab, Tbc beds, etc.) ahead of the coeval alluvial system (FAB-I) present at the landward part of the basin (*Pattison,* 2005). Deposition within fair weather wave base is attested by the

presence of wave-formed symmetrical ripples on the bedding surfaces. The stacked event beds (i.e., Bouma-like Tab, abc beds) with diffuse contacts between the ripple-laminated division and overlying massive (Ta) or plane-laminated (Tb) divisions, are interpreted as evidences for waning to waxing to waning flow conditions. Very high sandstone: shale ratio and medium- to coarse-grain size in these sandstones allowed us to confirm their derivation within a river-delta fed by a low-sinuosity, bedload channel system (FAB-I).

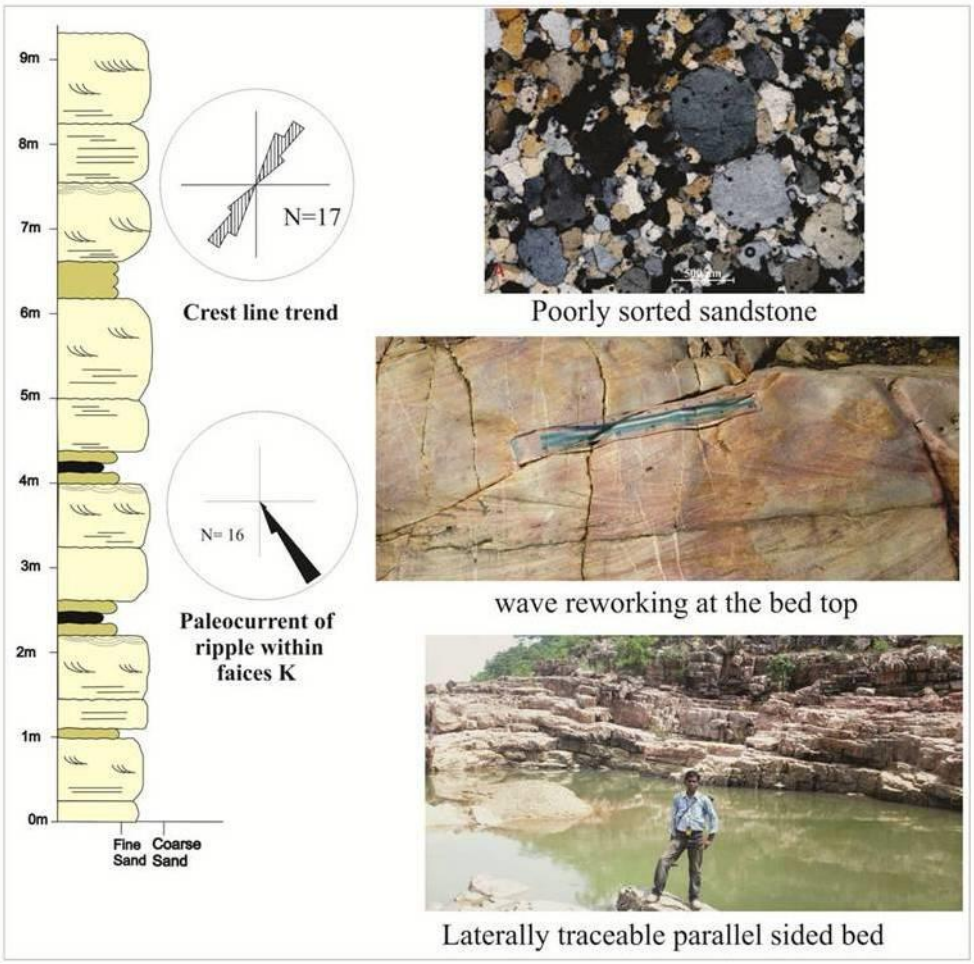

Fig.3.31. Measured litholog of FAB - V exposed at the Deodhara section. Whereas the solid rose in the right demarcates south-easterly paleocurrent measured from the current ripple cross-stratifications within facies K, the stippled rose indicates crest line trends of wave generated bedforms. Photographs on the right (from base to top) illustrates laterally traceable parallel-sided character of beds, wave reworking at the bed top and poorly sorted character for the sandstone.

CHAPTER-IV:

PALEOGEOGRAPHIC SHIFTS IN SEQUENCE STRATIGRAPHIC FRAMEWORK

The stratigraphic record is fundamentally discontinuous and this has profound implications for the interpretation of Proterozoic earth history (*Von der Borch et al.,* 1988; *Christe-Blick et al.,* 1988, 1995). Although approximate continuity has long been the practical paradigm in Proterozoic studies, it is also appreciated that concordant strata are not necessarily being conformable (*Chakraborty et al.,* 2012). Unconformities are more likely to be overlooked in strata of Proterozoic age than in Phanerozoic counterparts owing to poor biostratigraphic resolution and hence, there is a need to rely on physical stratigraphic evidence for breaks, evidence that is commonly only locally preserved. The study of sedimentary successions in terms of repetitive facies and associated discontinuities has become known as 'sequence stratigraphy' (*Vail,* 1987; *Van Wagoner et al.,* 1988), which became widely employed in last two decades in understanding a sedimentary basin filling motif in space-time framework. In fact, sequence stratigraphy as developed by the Exxon Production Research Group, provides a methodology for recognising sedimentary successions into a hierarchy of genetically related sedimentary packages (*Van Wagoner et al.,* 1990), based on the recognition of a number of key bounding discontinuities, and on regressive or transgressive facies characteristics. A transgression is defined as a landward migration of the marine shoreline, preserved in the stratigraphic record as a retrogradational shift of facies and a marine regression results in progradational stacking patterns related to the seaward shift of facies. Base level is the surface to which subaerial erosion proceeds, usually approximated with the sea-level (*Schumm,* 1993). The rise and fall in the base level are independent from sedimentation, hence, the three main factors those control the marine transgression and regression are eustatic oscillation, vertical tectonism (subsidence, uplift) and sedimentation.

4.1 Sequence stratigraphy: A brief preamble

Sequence stratigraphy is the most recent and revolutionary paradigm in the field of sedimentary geology that strives towards understanding a sedimentary succession in spatio-temporal framework by identifying key surfaces of chronostratigraphic importance in the basinal scale viz. Unconformity, flooding and maximum flooding surface/s, ravinement surface etc. and characterize the pattern of stratal packaging bounded between those key surfaces. The various types of sequences and bounding surfaces are illustrated in Fig.4.1. The depositional sequence (*Jervey,* 1988; *Van wagoner et al.,* 1990, *Hunt and Tucker,* 1992) is defined in relationship to the relative sea-level (base-level) curve, and it is bounded by the subaerial unconformity and its marine correlative conformity. The timing of

the subaerial unconformity is generally related to the stage of base level fall (*Posamentier et al.,* 1988), whereas the correlative conformity was initially considered to form during early sea level fall, which was later revised to the end of relative fall (*Hunt and Tucker,* 1992; *Helland-Hansen and Martinsen,* 1996). The depositional sequence consists of four systems tracts with distinct stratal stacking patterns: the highstand systems tract (HST) forms during late relative rise, when the sedimentation rate exceeds the rate of relative sea level rise in the shoreline area (normal regression); the falling stage systems tract (FSST) forms during relative fall (forced regression); the lowstand systems tract (LST) forms during early relative sea level rise, when the sedimentation rate exceeds the rate of relative rise in the shoreline area (normal regression); and the transgressive systems tract (TST) which forms when the rate of relative sea-level rise in the shoreline area exceeds the sedimentation rate. The former three systems tracts (HST, FSST and LST) form together a progradational package known as a regressive systems tract (RST; *Embry and Johannessen,* 1992). A RST followed by a TST form together a genetic stratigraphic sequence (*Galloway,* 1989), bounded by maximum flooding surface (MFS). The combination of a TST followed by a RST gives the Transgressive-Regressive (T-R) sequence, bounded by conformable transgressive surface (CTS) in the marine portion of the basin. The nonmarine correlative of the CTS is either unidentifiable within the fluvial succession, or eroded by the ravinement surface. In either case, the subaerial unconformity is conveniently chosen to represent the T-R sequence boundary in the nonmarine succession. The central assumption in all models is that the predictable stacking pattern of systems tracts and stratigraphic surfaces are mainly controlled by the interplay of base level change and sedimentation at the shoreline. Owing to the interest of oil sector in the Phanerozoic basins good-quality subsurface data (well log and seismic) as well as well-constrained chronological data base were available, which helped in framing many of the basic concepts of sequence stratigraphy. Scenario is much complex for Proterozoic basins in absence of both subsurface and chronological data. Sedimentological logging and facies mapping at local to regional scales are the most important tool for application of sequence stratigraphic concepts in Proterozoic successions, which can help in identifying stratal discordances and discontinuities in facies succession. Any abrupt change in paleogeography can be picked up as a key surface and the arrangement/hierarchy of such surfaces can help in sequence stratigraphic interpretation. Subsidiary evidences for a sequence boundary may include marked changes in sediment provenance, changes in paleocurrent trends, and diagenetic exposure fabric, if any. A suitable paleogeographic setting involving both continental and marine agents and their interaction in space-time frame with relative rise/fall in sea level can also be of

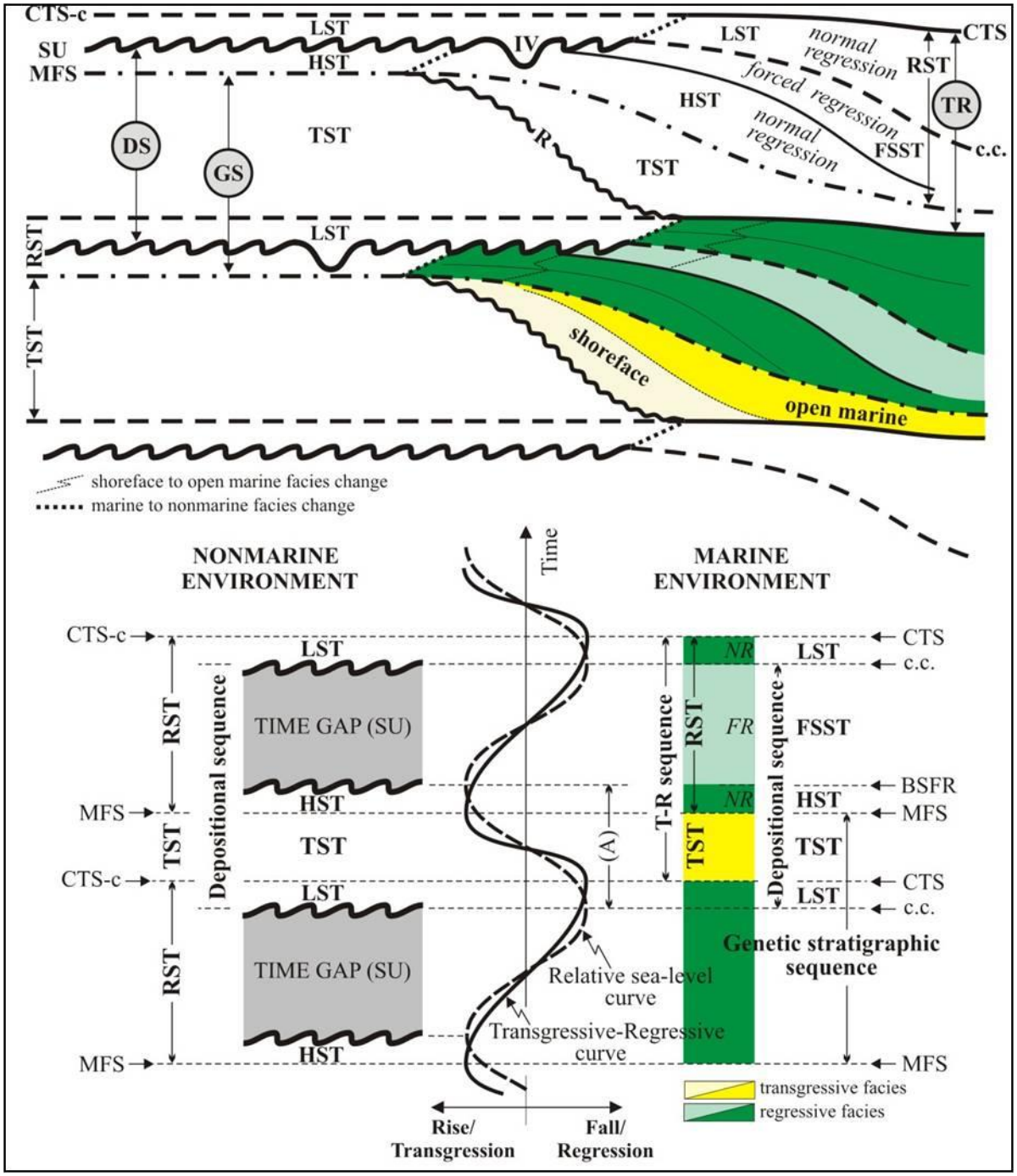

Fig.4.1. Types of sequences, bounding surfaces and systems tracts, defined in relation to the relative sea-level and Transgressive-regressive curve (modified after *Catuneanu et al.*, 1998). DS = Depositional sequence, GS = Genetic stratigraphic sequence, T-R Transgressive-Regressive sequence, LST = Lowstand Systems Tract, TST = Transgressive Systems Tract, HST = Highstand Systems Tract, FSST = Falling Stage Systems Tract, RST = Regressive Systems Tract, SU = Subaerial Unconformity, C.C = Correlative conformity, CTS = Conformable transgressive surface, MFS = Maximum flooding surface, R = Ravinement surface, BSFR = Basal Surface of forced regression, IV = Incised valley, NR = Normal regression (sediment supply driven), FR = Forced (base level fall driven) regression.

immense help in establishing the sequence stratigraphic rationale in Proterozoic stratigraphic sections.

4.2 Application of Sequence stratigraphic rationale under the present study

A wide range of paleo-environmental products varying between continental (alluvial fan, braided fluvial), transitional (foreshore, beach, shoreface, delta etc) and marine (inner to outer shelf) and their interaction in space and time, as recorded within the studied stratigraphic interval, allowed application of sequence stratigraphic concepts under the present study. Based on the stratal packaging and identification of unconformity from abrupt transition of facies belt, two depositional sequences viz. DS -1 and DS -2 are delineated within the studied section. Complete profile of first 'sequence' (DS -1) and basal (involving only records of forced regression and lowstand) portion of second 'sequence' (DS - 2) fell under the purview of presently studied stratigraphic interval (Fig. 4.2). Above the granitic/gneissic basement the Rehtikhol and Saraipalli Formations, in combination,

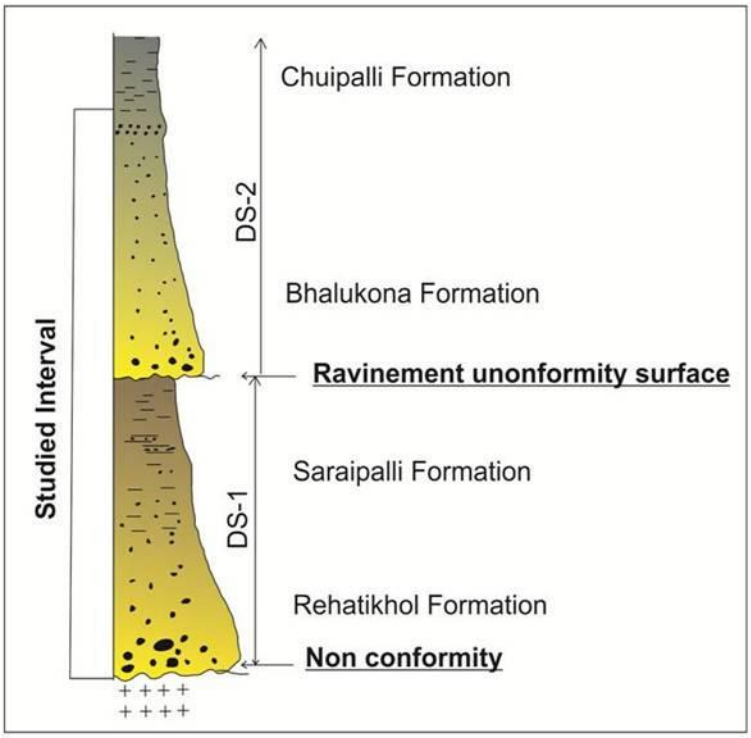

Fig.4.2. Framework of two depositional sequences (DS-1 & DS-2) under the present study. While DS-1 is bounded between non-conformity at its base and type-1 unconformity at its top, the DS-2 has unconformity at its base that transforms into ravinement surface basinward.

constitute the DS -1, bounded at its base and top by basal unconformity and Type-1 unconformity, respectively. Overlying the Type-1 unconformity and its correlative conformity the Bhalukona Sandstone Formation constitutes the basal part of DS - 2. The following section discusses the Key surfaces used in demarcating and characterising the two depositional sequences and stratal architecture within each 'sequence' from the nature of litho-packaging recorded in between the interpreted key surfaces.

4.2.1. Key surfaces

Besides the nonconformity that marks the base of Rehtikhol succession (i.e its contact with the basement) the other significant depositional discontinuity that allowed making division of studied stratigraphic interval into two depositional sequences is the inferred unconformity at the base of fluvial association (FAB - I) of Bhalukona Formation. A drastic basin-ward dislocation of facies belt demarcates this unconformity that brought the coarse, granular alluvial sandstone of FAB - I right onto the Saraipalli highstand shelf. Besides these two surfaces of basin-scale importance, the present study identifies two other key surfaces; both are erosional in character (Fig.4.3). Out of these one is present at the base of beach-foreshore association (FAB - II) of Bhalukona Formation and the other at the top of lower shoreface association (FAB - IV) of Bhalukona Formation. While the surface at the base of FAB - II is traced in outcrop for 3.5 km between Bhaludungri and Dongrijharan sections, that at the top of FAB - IV is traced between the Bhaludungri and Sisupal sections, spanning in space for more than 7.5 km. Clast-supported, polymictic conglomerate beds containing clasts of vein quartz, chert and sandstone demarcate the key surface at the base of FAB - II and glauconitic granular sandstone beds containing clasts of sandstone constitute the other at the top of FAB - IV (Fig. 4.3). The surface at the base of FAB - II is interpreted as an erosion surface produced by wave ravinement at the lowstand of relative sea level (*Dominguez and Wanless,* 1991). Occurrence of ~23 m thick shallow marine succession on this surface suggests that the unconformity and its overlying forced regressive products are reworked by wave ravinement, resulting in a situation where the unconformable contact is directly overlain by marine facies (discussed below). Landward, the sequence boundary is marked by alluvial incision. At the base of FAB - II the sequence boundary is cut within a marine setting (*MacEachern et al.,* 1999). The surface at the top of FAB - IV represents the boundary where shallower marine strata are sharply overlain by deeper marine strata without significant erosion. Such surface correlates landward to

Transgressive Surface of Erosion (TSE), and is interpreted here as near conformable marine flooding surface (FS) formed at the base of transgressive systems tract of relative sea level. Above this surface, the occurrence of storm-infested middle-to distal-shelf succession of Chuipalli shale records the history of transgression.

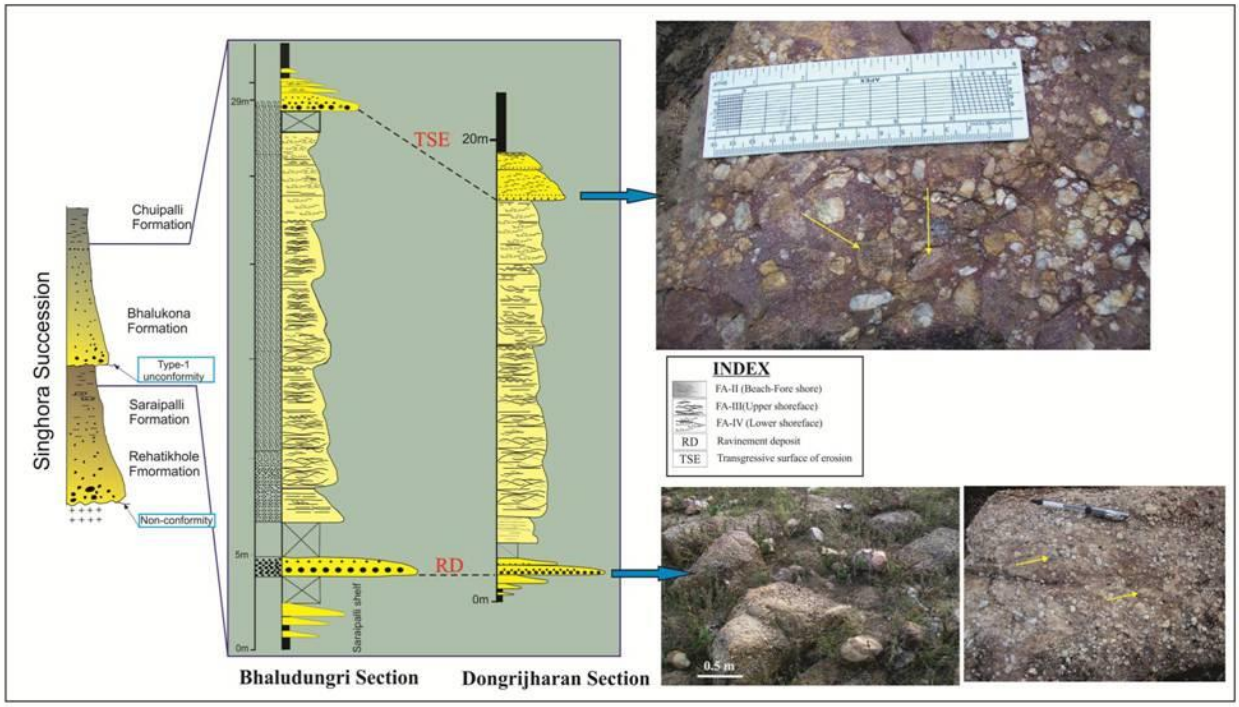

Fig.4.3. Detailed litholog of Bhaludungri and Dongrijharan sections showing positions of key (diachronous) surfaces viz. ravinement deposit (RD) and Transgressive surface of Erosion (TSE) with field photographs for the both. The yellow arrows in the photograph at the top indicate sandstone clasts. Both scale and Pen have length of 14 cm.

4.2.2 Paleogeographic shifts and making of DS-1

Studies of measured sections (Fig.3.3) reveal sediments of marine associations succeeding the continental (subaerial) ones up the stratigraphic column within DS-1 and thereby suggest an overall retrogradational stacking pattern. In the stratigraphic record such fining-upward alluvial–coastal strata are used to establish transgressive sequences and are interpreted as a signature of progressive upward-deepening (*Bourgeois,* 1980; *Emery and Myers,* 1996). For a braid-delta fringed by an alluvial fan such deepening-up tendency is related either to declining sediment supply caused by retreat of scarp front and lowering of source area relief (*Kingsley,* 1984; *Rigsby,* 1994) or to rising bathymetry induced by relative rise in sea level (*Benvenuti,* 2003) or a combination of both. Steady decrease in grain size up the stratigraphic column in the studied sections strongly suggests steady

wearing down of the source area and in turn, decreasing supply of detritus. The role of eustasy could not be assessed in absence of any record of the Mesoproterozoic–Neoproterozoic sea level stand. However, the irreversible transition from the subaerial to the submarine condition in all the studied sections without any basin-scale discontinuity, and the presence of wave-reworked granule-topped mega-ripples in the delta system (FA III) bear support of a local increase in sea level. Both extrabasinal and intrabasinal events possibly contributed to the deepening-upward trend.

The increase in channelized flow up the section within the subaerial part of Rehtikhol succession may be related to change in sediment dispersal processes attributed to the geomorphic evolution, i.e., an enlargement of the fan catchments yielding greater volume of water (cf., *Blair,* 1987). The increasing geomorphic maturity of the hinterland might then indicate a declining tectonic activity. Alternatively, the change in dispersal processes might also indicate a regional climatic change from semi-arid conditions characterized by brief torrential rainfall, to more humid conditions, perhaps characterized by a more pronounced seasonality and less ephemeral water runoff. Braid-delta associations are generally reported from regressive settings with commonly coarsening- and thickening-upward sequences of sandstones and conglomerates. However, in the present case the overall fining-upward sequence development pattern, lack of thickening-upward pattern or large-scale low-angle cross-stratification, and abundance of sub-horizontal stratification, suggest a retrogradational sequence development motif, generally related to transgressive episodes. Under rising base level, trapping of sediment within the alluvial realm resulted in a heterogeneous coastline character in the Singhora basin in Rehtikhol-Saraipalli time. The stacked fluvial succession of FAII suggests channel aggradation, presumably as a result of slow rise of river base profile in tune with rising sea level (cf., *Blum and Tornqvist,* 2000). The fining upward trend and onlapping of distal facies onto proximal facies is attributable to loss of slope gradient through aggradation (cf., *Catuneanu,* 2004; *Bose et al.,* 2008). The rising base level/ sea level finally resulted in transgression on the Rehtikhol coastline with establishment of Saraipalli shelf system (FA IVa and b). The base of inner shelf sub-association (FA IVa) is interpreted as a flooding surface. The basal part of Saraipalli Shale Formation, represented by FA IVa, records overall upward-fining stacking pattern and identified as the product of Transgressive Systems Tract (TST). Within its overall upward-fining character the FA IVa, made up of facies types M and N, can be further subdivided into a number of vertically stacked upward-deepening facies packages/cycles ranging in thickness between 6.8m and >12m (Fig.4.4). A complete cycle shows gradual upward transition from facies M to N and is

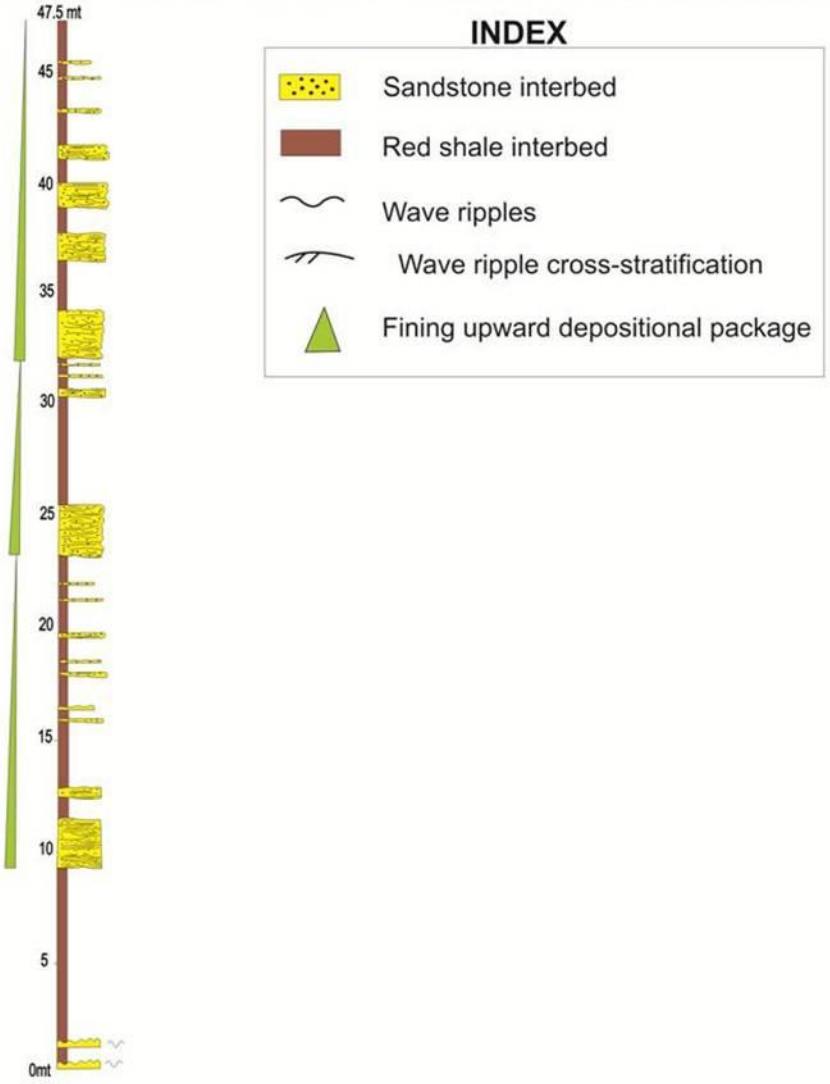

Fig.4.4. Fining- and thinning-upward hemicycles within FA IV; illustrating the stacking pattern within Transgressive Systems Tract (TST).

interpreted as record of waning history of storm pulse/s invading the muddy shelf. The sandy intervals with deeper and amalgamated gutters represent the highest energy condition in the main storm pulse; thin, wider and isolated gutters within the shale dominated intervals reflect progressive weakening of erosive power with gradual waning of the storm event. Upward in the stratigraphic column sediments belonging to sub-association IVb, constituted of gray to black fissile shale (facies O) with shale: sandstone ratio of 9.5:1, represents the products of maximum flooding (MFS). Patchy and inconsistent exposure condition did not allow complete documentation of stratal geometry through the entire Saraipalli succession. However, the thickening- and coarsening-upward stratal stacking pattern recorded at the upper part of the Saraipalli Shale Formation (*Chakraborty et al.,* 2009) bear indication that the Saraipalli shelf attained highstand sea level condition at its terminal sedimentation history. That the shelf attained near-equilibrium physiographic profile with progradation by the end of Saraipalli time with appreciable reduction in clastic supply is attested in the growth of patchy, biohermal stromatolites in the uppermost Saraipalli succession (Sisupal section).

4.2.3 Architecture of DS-2

The present work dealt only with the basal part of DS- 2 represented by the Bhalukona Formation. Process-based facies, facies association analyses and delineation of key surface/s allowed identification of 'Systems tract's within the Bhalukona Formation and delineate two-stage subdivision within the regressive Bhalukona depositional history viz. forced regressive and lowstand. An interpreted sequence stratigraphic framework for the Bhalukona succession is presented in Fig. 4.5. A drastic basin-ward dislocation of facies belt is inferred that brought the coarse, granular alluvial sandstones (FAB - I) of the Bhalukona Formation right onto the Saraipalli highstand shelf. Exposure limitation and non-availability of borehole data did not allow physical documentation of contact relationship between the alluvial Sandstone and its underlying shelf deposits. However, occurrence of mud clasts, boulder-sized at times, within the sand-stones of FAB - I suggests that the Bhalukona fluvial system encroached the Saraipalli shelf with incision. Such alluvial incision of shelf is attributed to the fall in the base level of erosion and formation of Type-I sequence boundary (*Posamentier et al.,* 1992; *Posamentier and Allen,* 1993; *Hunt and Gawthorpe,* 2000). That there was subaerial exposure and unconformity formation gets support from petrographic evidence as well i.e replacement of detrital feldspar grains by glauconitic clay within the sandstones of FAB-I (Fig. 3.27

b,c). Relacement of unstable detrital grains and cement viz. feldspar, calcite by secondary minerals such as glauconite, given availability of sufficient amounts of K, Al and Fe that may be derived from weathering of clays, is used by workers as a proxy to recognise sequence bounding unconformities (Khalifa, 1983; Catuneanu, 2006). The interpretation is also favoured by the presence of correlative deltaic system (FAB - IV) in basinward part of Bhalukona shoreline. From the preserved thickness of FAB - I, it is estimated that the Bhalukona fluvial system incised more than 10 m on the Saraipalli shelf. Recognition of decimetre-thick channel- bar complexes stacked within meter-thick alluvial succession (FAB - I) suggest that the erosional relief is greater than the single channel fill, a criteria commonly used for identification of incised valleys. The occurrence of wave generated bedforms and sandstones with glauconitic matrix in the uppermost part of FAB - I at the Padampur Road section (Fig.3.25) indicate reworking of alluvial sediments by marine agents on the forced regressive shoreline of the Bhalukona Sea. The sediment gravity flow units within FAB - IV reflect deposition from hyperpycnal density underflows generated at the river mouth during high discharge floods (*Mulder and Syvitski,* 1996; *Chakraborty et al.,* 2009). Coarse grain size (medium to coarse sand) and evidences of fair weather wave reworking suggest that the delta system, developed ahead of the Bhalukona river system, was essentially restricted in shallow water within the shelf domain. Poor grain sorting of FAB - IV sandstones and restriction of wave reworking signatures only at the top of beds imply fluvial dominance in the delta. The mixing of wave- and current-produced structures is typical of wave-influenced delta front (*Bhattacharya and Walker,* 1991), but relative scarcity of wave-produced structures suggests wave influence rather than dominance. Though a physical link between marginal fluvial system (FAB - I) and related delta front (FAB - IV) cannot be established, it can be appreciated that the hyperpycnal flow deposits in the delta front relate to the time during which sediment flux to the sea attains its maximum. The base of FAB - IV is demarcated as correlative conformity related to the Type-I unconformity inferred at the base of FAB - I association in the landward direction. Offlapped and aerially separated from the fluvial association (Padampur section), the delta front sandstone lobe is deposited at the distal part of the basin (Deodarah section). The gentle dip of Bhalukona sea floor provoked such long-distance regression of deltaic sandstone (~15 km southeastward) in course of forced regression (cf. *Posamentier and Morris,* 2000).

The cessation of forced regression and inception of stillstand or slow rise of base level established wave-dominated lowstand coastline. The soft sediment deformation features at the basal part of FA-B III bear indication of basinal instability that contributed in the turn over from the

forced regression to the lowstand of sea level. The amalgamated pebble bedset at the sole of FAB -- II, traced basin-ward for more than 3.5 km between Bhaludungri and Dongrijharan sections, demarcate the diachronous ravinement deposition formed by wave reworking associated with slow landward retreat of the coastline truncating deposits of preceding forced regression (cf. *Cattaneo and Steel,* 2003). Backstepping incised shorefaces are described in literature from several stratigraphic sections pre-serving nearshore successions (Cardium E4, E5; *Walker and Eyles,* 1988; *Pattison and Walker,* 1992; Shannon sandstone, *Bergman,* 1994; Beaverhill Lake shoreface, Viking Formation, *Walker and Wiseman,* 1995). It is inferred that the forced-regressive shoreline trajectory became steeper than the shelf dip in the Bhalukona Sea because of increased wave stress on the sea bed (cf. *Carey et al.,* 1999). To regain the equilibrium geometry as a function of prevailing wave energy during subsequent base level rise, wave erosion and ravinement resulted in the coastal areas, where forced regressive profile gradient was steepest and waves are also with highest energy. Occurrence of anomalous coarse sized grains, unavailable in both underlying and overlying sediment column, within the ravinement lag bears proof for complete reworking of fluvial products. This is also supported by steady decline in feldspar content up in the stratigraphic column of nearshore succession from the foreshore-beach (FAB- II) and basal part of upper shoreface (FAB- III) sandstones to the lower shoreface sandstones (FAB- IV). Absence of lag at the base of nearshore sandstones at the Sisupal and Singhora sections and in lieu, gradational transition between the Saraipalli shelf and Bhalukona shoreface in these sections represent basin-ward correlative conformity. In the east and northeast of the basin, absence of Bhalukona rocks and juxtaposition of Saraipalli and Chuipalli argillaceous sediments suggest wedge out of regressive sediment package in the basin-ward direction. The cms-thick cycles represented by bar-interbar stacking within FAB - III (Fig.3.29) are interpreted as 'parasequences' sensu lato (*Van Wagoner et al.,* 1988). The meter-tick tabular units bounded by planar surfaces, occasionally overlain by shale, represent the parasequence sets with large-scale linkages of facies or systems tracts (*Brown and Fisher,* 1977; *Proust et al.,* 2001). The surfaces bounding the units without significant erosion or clear break in lithology represent within-trend conformable marine flooding surfaces (FS; *Catuneanu,* 2006). The stacking of tabular units with near-uniform thickness is indicative of the aggradational to weakly retrogradational nature at in the early lowstand history as the rate of sediment supply matched or occasionally fell behind the slow but steady creation of accommodation on flattened shoreface profile (*Posamentier and Morris,* 2000; *Hampson,* 2000). With slow, steady rise in relative sea level and concomitant increase in bathymetry, the sediments of lower shoreface (FAB-IV) overlie the sediments of upper shoreface

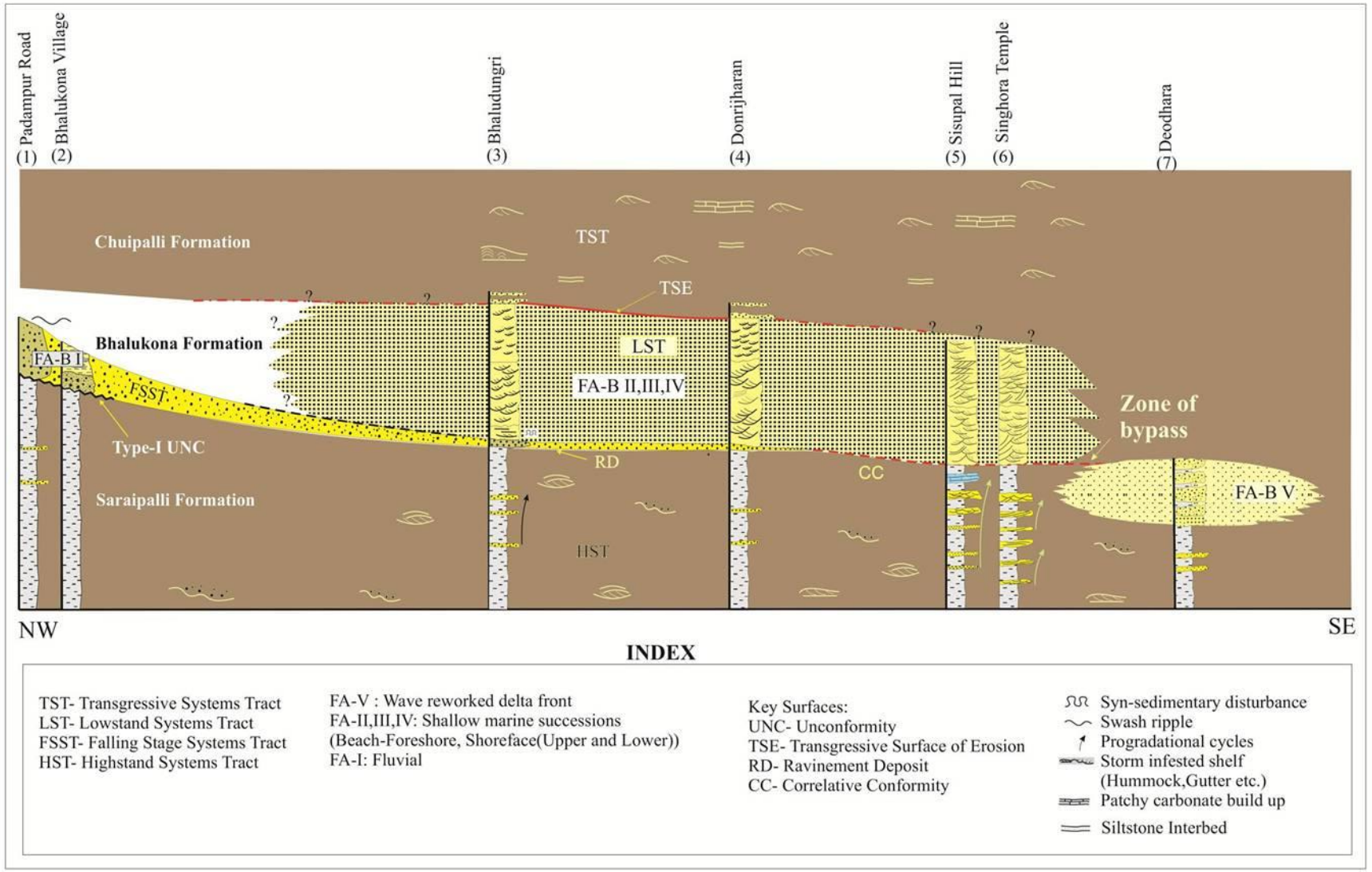

Fig.4..5. Graphic log correlation in depositional-dip profile across the Bhalukona Formation showing transition from underlying Saraipalli to overlying Chuipalli sediments in Singhora basin, central India; numbers of log locations are from Fig. 3.23. Locations of 'key surfaces' viz. unconformity, ravinement surface and Transgressive surface of Erosion are shown. Note the presence of unconformity in the western part of the basin, which turns into correlative conformity basinward; development of ravinement within the wave base. The distally pinching foreshore-beach-shoreface facies associations indicate its wedge nature. Top of the Bhalukona sandstone represents the Transgressive surface of erosion.

(FAB-III) association. The rise in base level and increase in the accommodation space marginally exceeded the sedimentation rate in the lower shoreface and thereby a time-equivalent, landward onlap back across the irregular lowstand topography resulted in the enhanced strength of tidal currents, recorded as bipolar cross-stratified beds in the upper part of FAB-IV association (cf. *Mellere and Steel,* 1995). Further, steepening in the gradient of relative sea level rise resulted outpacing of sediment supply, increase in bathymetry and flooding at the shore-line. The glauconite-bearing granular sandstone beds at the top of FAB - IV represents ravinement deposition associated with the establishment of transgressive Chuipalli shelf system. Following the Transgression-Regression (T-R) sequence model (*Embry and Johannesen,* 1992), the upper boundary of the lowstand section marks the point between regression and following transgression and is termed as 'maximum regressive surface'. The occurrence of shelf shale of Chuipalli Formation above is surface confirms its 'maximum regression' status (cf. *Catuneanu,* 2002). The coupling of the surface of maximum regression with the interpreted surface of transgression and ravinement allowed us to pick it as a 'Systems Tract' boundary. Lying above forced regressive fluvial deposit (FAB - I) and bounded between the wave ravinement deposit at its base and transgressive ravinement deposit at the top, the nearshore sedimentary package, constituted of FAB - II, III and IV, records the lowstand depositional history of Bhalukona Sea.

Although the exposures of some stratigraphic intervals are not continuous enough to physically trace the key surfaces for long distance, their process-driven interpretations as well as documentation of strata stacking patterns within successions present both below and above these surfaces allowed 'sequence stratigraphic' interpretation for the studied stratigraphic interval.

CHAPTER-V:

NEW AGE CONSTRAINTS FROM SINGHORA BASIN

The study of magmatic rocks in Precambrian setups has special emphasis as they can be used judiciously to date the magmatic events and put age constraints on the events happened before and after the crystallization of magma. The magmatic rocks in the form of dykes, sills and pyroclastic in Precambrian sedimentary basins are of special importance as there is no other precise way to date the near-surface processes during this time period. Moreover, the petrogenetic study based on geochemistry of major, minor trace elements and isotopes leads us to trace the tectonic settings, conditions of melt-generating depths and also the way crust and mantle interact during such events. Hence, on a broader aspect, delineation of coupled deeper and shallower processes operative in old continental crusts provide importatnt clues towards the global-scale events related to continental drift and supercontinental cyclicity. Magmatic rocks occurring in continental cratonic blocks, particularly the dyke swarms provide important clues towards the correlation of continental blocks using their geochemistry, age and paleomagmetic pole data.

The above-mentioned uses of magmatic rocks necessiate an application of those in Indian continents, which is known to have several Precambrian cratonic nuclei grown through addition of crustal material and accretion of craton-margin orogenic belts during this time. Moreover, it has been felt to be extremely important to know the exact age of the regional-scale near-surface events expressed by the development of several large to small sedimentary basins and their related tectonics during Precambrian time. The magmatic inputs at the basement, at the margin and inside the sedimentary basins are considered to be important lithounits to establish the age constraints, tectonic setup and regional to global correlatibility.

5.1. Proterozoic magmatic events in cratonic India:

In view of the present study, magmatic activities in and around the Proterozoic sedimentary basins are under scanner. Study of different magmatic events in Precambrian India had been adopted since the end of last century; and presise rediometric geochronological and geochemical data of Proterozoic magmatic events from Indian cratons have been widely documented in literature e.g., 1.78–1.71Ga granitoid plutons in the Delhi fold belt of NW India (*Biju-Sekhar et al.* 2001), ~1.61Ga basic-ultrabasic intrusives from Dalma volcanic of Singhbhum craton, eastern India (*Roy et al., 2002*), ~2.1-1.97 Ga and ~1.1 Ga mafic dyke swarms in Bundelkhand craton of north India (*Pradhan et al.,* 2012, *Mallikarjuna Rao,* 2004), ~1.88 Ga mafic dyke swarms of central Indian Bastar

craton (*Srivastava and Gautam,* 2009); ~1.36 Ga, Kotakonda kimberlite, Ramannapeta lamproite and younger (~1.1 Ga) Muligiripalle kimberlite in Dharwar craton (near the margin of Cuddapah basin) (*Chalapathi Rao et al.,* 1996); ~1.45 Ga of alkaline magmatism and anorthositic intrusions at the cratonic boundary with adjacent high grade granulites e.g. Eastern Ghats Mobile Belt (EGMB) (*Upadhyay et al.,* 2009), ~1.40 Ga rhyolitic to doleritic dykes at the cratonic margin (*Ratre et al.,* 2010) and ~1.65-1.70 Ga mafic dyke intrusion in southern Indian granulites (*Radhakrishna and Joseph,* 1995). Moreover, the evidences of magmatic activities in the form of mafic dykes and sills, ultramafic kimberlite pipes, volcanic ash flow and fall deposition in craton hosted Proterozoic sediment cover are not in exception; and age clusters of different magmatic episodes are also available from sedimentary basins e.g., ~1.62 Ga porcellanite from lower Semri Group of Vindhyan basin (*Ray et. al.* 2002; *Rasmussen et. al.,* 2002); ~0.97-1.1 Ga Majhgawan-Hinota kimberlite of Vindhyan basin (*Gregory et al.,* 2006; *Sankar et al.,* 2001); ~1.35 Ga Chelima lamproite (*Chalapathi Rao et al.,* 1996) and ~1.9 Ga mafic sill (*Bhaskar Rao,* 1995; *Anand et al.,* 2003) in Cuddapah basin; ~1.0 Ga Sukda and Dhamda tuff, from the upper part Chhattishgarh basin (*Patranabis-Deb et. al.,* 2007, *Bickford et al.,* 2011c); ~1.4 Ga from the lowermost group of Chhattisgarh Supergroup (*Bickford et al.,* 2011); ~1.0 Ga from the rhyolitic tuff unit (*Mukherjee et al.,* 2012) and ~0.62 Ga Tokapal kimberlite (*Lehmann et al.,* 2007) in Indrãvati basin. Narrowing down to the eastern cratonic block of Bastar region, *Ramakrishnan* (1990) recognized three major basic magmatic events in the southern Bastar shield with variable rock types, *viz.*, amphibolite dykes, greenstone dykes/sills, and dolerite/metadolerite dykes on the basis of field relationship. However, *Sarkar et al.* (1990) suggested four episodes of mafic/ultramafic activity *i.e.*, 2.7 Ga, 1.8 Ga, 1.5 Ga, and 1.2 Ga. Recently, two major episodes of thermal activities *viz.*, Meso-Neoarchaean (<3.0Ga) sub-alkaline (BD1) and boninitic (BN) dykes and Paleoproterozoic (~1.8Ga) sub-alkaline (BD2) dykes have been identified and detail geochemical study has been carried out by *Srivastava et al.* (1996, 2000, 2004); *Srivastava and Verma,* 1998; *Srivastava and Singh,* (1999, 2001, 2003a,b,c, 2004); *Srivastava* (2005a,b, c, 2006a, b, 2008); *French et al.* (2004, 2008); *Srivastava and Gautam,* (2007, 2009) and *Singh et al.* (1997). Recent reports of i) ultramafic intrusive of Neoproterozoic time (~620Ma) from Indrãvati basin, (Tokapal–Bhejripadar kimberlite system, *Lehmann et al.,* 2007); ii) Mainpur kimberlite of end-Cretaceous/Deccan ages (~65 Ma) (*Lehmann et al.,* 2010) and iii) mafic dykes (63.7-66.6 Ma) bear indication that thermal events continued even up to end-cretaceous time on Bastar craton and Chhattisgarh basin, in particular (*Chalapathi Rao et al.* 2011a). The occurrences of kimberlite and related magmatic rocks in Bastar craton and East

Dharwar craton and their genetic implications have been reviewed thoroughly by *Chalapathi Rao et al.* (2011b).

5.2. Magmatic rocks in and around Chhattisgarh Basin:

The available database on the magmatic inputs within the craton and marginal orogenic belt and those present within the sedimentary covers are scantily attended and await studies in terms of geochemistry and geochronology. Indeed, such geochemical and geochronological appreciation of the magmatic inputs (either in the form of dykes or as conformable lithodemic units) present within the Chhattisgarh and its adjoining basins will have multifold implications, *viz.* (1) identification of isochronous markers those may help in correlating the lithotectonic domains in regional and global perspective, (2) the spatio-temporal evolution of magma chamber(s) taking into consideration the secular chemical variation in the mantle source, (3) the exhumation-erosional episodes of the orogenic hinterland and its cause-effect relationship, if any, with the coeval events in adjacent craton. During Proterozoic time, growth of the continents took place by the addition of mantle-derived material to pre-existing continental blocks. Majority of such material addition was associated with continental crustal growth under different tectonic environments like, accretionary orogens, collisional orogens and within supercontinents undergoing rifting and break-up (*Windley,* 1995). Major and trace element signatures in each case are unique and show the chemical character of the prevailing mantle sources.

In the present study area, *i.e.* the Chhattisgarh and associated basins, very few age data was available even a decade ago (possibly the only report of 700-750 Ma K-Ar dating of authigenic glauconite from the lower part of Chhattisgarh basin by *Kreuzer et al.,* 1977). Precise age-bracketing of thousands-of-meter thick unmetamorphosed sedimentary successions (with absence of age-connoting fossils) is a long-standing challenge in Indian Proterozoic stratigraphy. However, the broad descriptions of volcanic activities in the form of pyroclastic or tuffaceous (including porcellanite) rocks and basic intrusive of the Chhattisgarh basin, hornblende granodiorite intrusion in the Ampani basin, ultramafics from Indrãvati succession (cf. *Das et al.,* 2001) and mafic dykes of Sukma basin (*Ramachandra et al.,* 1995; *French et al.* 2008) are available in publications. In recent years, several reports with precise age data have started to pour in that implies that Bastar craton has also witnessed a major rhyolitic volcanism at ~1.0 Ga, *e.g.* Sukhda, Sapos and Dhamda rhyolitic tuff of

Chhattisgarh and Indrãvati basin (*Patranabis-Deb et al.,* 2007; *Bickford et al.,* 2011, *Mukherjee et al.,* 2012). As far as Chhattisgarh basin and its adjacent small basins are concerned, all the reported magmatic rocks and their dates are mostly from the stratigraphically upper part of the Chhattisgarh Supergroup. Hence, in terms of age and tectonic settings retrieved, all these magmatism are related to the closure of Chhattisgarh Main basin at the eastern margin of Bastar craton. Initiation of the Chhattisgarh basin and the adjacent small basins like Khariar and Ampani basins was, however, speculative as of Mesoproterozoic age. Moreover, the correlatability of sedimentation history of the small basins with respect to the Chhattisgarh main basin was also speculative, particularly due to the absence of datable rocks/events at the stratigraphic bottom. This prompted a search of datable rocks in the Singhora basin (known to be the proto-basin of Chhattisgarh basin) and also at the adjacent Khariar and Ampani basins. The present study which was initiated as a part of the Department of Science and Technology (DST, Govt. of India) sponsored research project had been aimed to look for and study the basal units of Singhora basin and Khariar basin, with special emphasis on the occurrences of magmatic rocks in and around these basins. The earlier GSI field reports suggested presence of tuffaceous rocks and basaltic rocks in these basins (*Subrata Chakraborti, pers. com.*; *Chakraborti et al.,* 1997). During the initial reconnaissance field trips, several horizons of tuffaceous rocks have been identified from the eastern and south-eastern parts of the Singhora basin and from the eastern parts of Khariar basin. Moreover, several mafic bodies (some unmetamorphosed) have been identified in and around Singhora basin. Apart from the age dating (using appropriate methods for each types of rocks) all these units are studied for their geochemical characters, tectonic framework of these magmatic activities. Part of these data has been published for timely understanding of the Proterozoic basin development at the eastern fringe of Indian craton (*Das et al.,* 2009; *Das et al.,* 2011). Here is a detailed account of the study of magmatic rocks in and around Singhora basin.

5.3. Magmatic rocks in and around the studied Singhora basin:

Singhora basin occupies a crucial position in terms of overall Chhattisgarh Supergroup. Though there is some amount of controversy (*Bickford et al.,* 2012b; *Chakraborty et al.,* 2012), it is broadly accepted to be the proto-basin (*Das et al.,* 2001; *Saha et al.,* 2013) and marks the initiation of Chhattisgarh basin fill. Hence, a precise age data can fix the age of initiation of Chhattisgarh basin as a whole. This has become of paramount importance after the discovery of ~1000 Ma tuff and

suggestion that the upper age limit of Chhattisgarh Supergroup of this age by *Patranabis-Deb et al.,* (2007). Furthermore, the geochemical character of magmatic rocks might be useful to highlight the conditions of the source region and erstwhile tectonic framework at the eastern margin of Indian craton with clues to the tectonic development of the basin(s). Moreover, it is intended to mark the age bracket of the sediments deposited in between the two magmatic events, *i.e.* Saraipalli Formation of Singhora Group.

The lower most Singhora group has experienced two major volcanic activities, one in the form of bedded tuff, which makes a concordant relationship with coarse grained Rehatikhol Formation and fine grained Saraipalli Formation; and the other as a mafic intrusive, which was emplaced within the basin with cross-cutting at least the lowermost Rehtikhol Formation and the overlying Saraipalli Formation. A detail exposure-based study, petrography, mineral chemistry and geochemical characterization (including major, trace and rare-earth elements) have been carried out. U-Th-Pb Electron Probe Microanalyzer (EPMA) data was used to date the monazite grains of the Singhora tuff and, Sm-Nd mineral-whole rock isochron technique for the dating of basic intrusive. The detail documentation of the data has been made in the following sections for both the units separately.

5.4. Porcellanitic tuff beds: Megascopic observations:

The bedded tuff is exposed at several places in the Singhora basin. Study and sampling was carried out at Chiwarakutta (N 21°19'30'' E 83°13'45''), Murmuri (N 21°19'50'' E 83°14'10''), Singbahal dam site (N 21°19'55.5'' E83°14'40'') and Balenda village (N 21°21'35'' E 83°14'58''), all in the eastern part of the basin; and at Kurlubahal (N 21°6'42'' E 83°14'25''), from the south-eastern part of the basin (Fig.5.1). As far as the known established stratigraphy is concerned, the bedded porcellanitic tuff unit of Singhora Group occurs at the boundary between Rehatikhol Formation and its overlying Saraipalli Formation. However, at places it is found to alternate with thin argillaceous beds of Saraipalli Formation just above the pebbly sandstone units of Rehtikhol Formation. At the outcrop scale, this complexly folded tuffaceous unit shows variable thickness and lateral continuity. The thickness at the eastern side

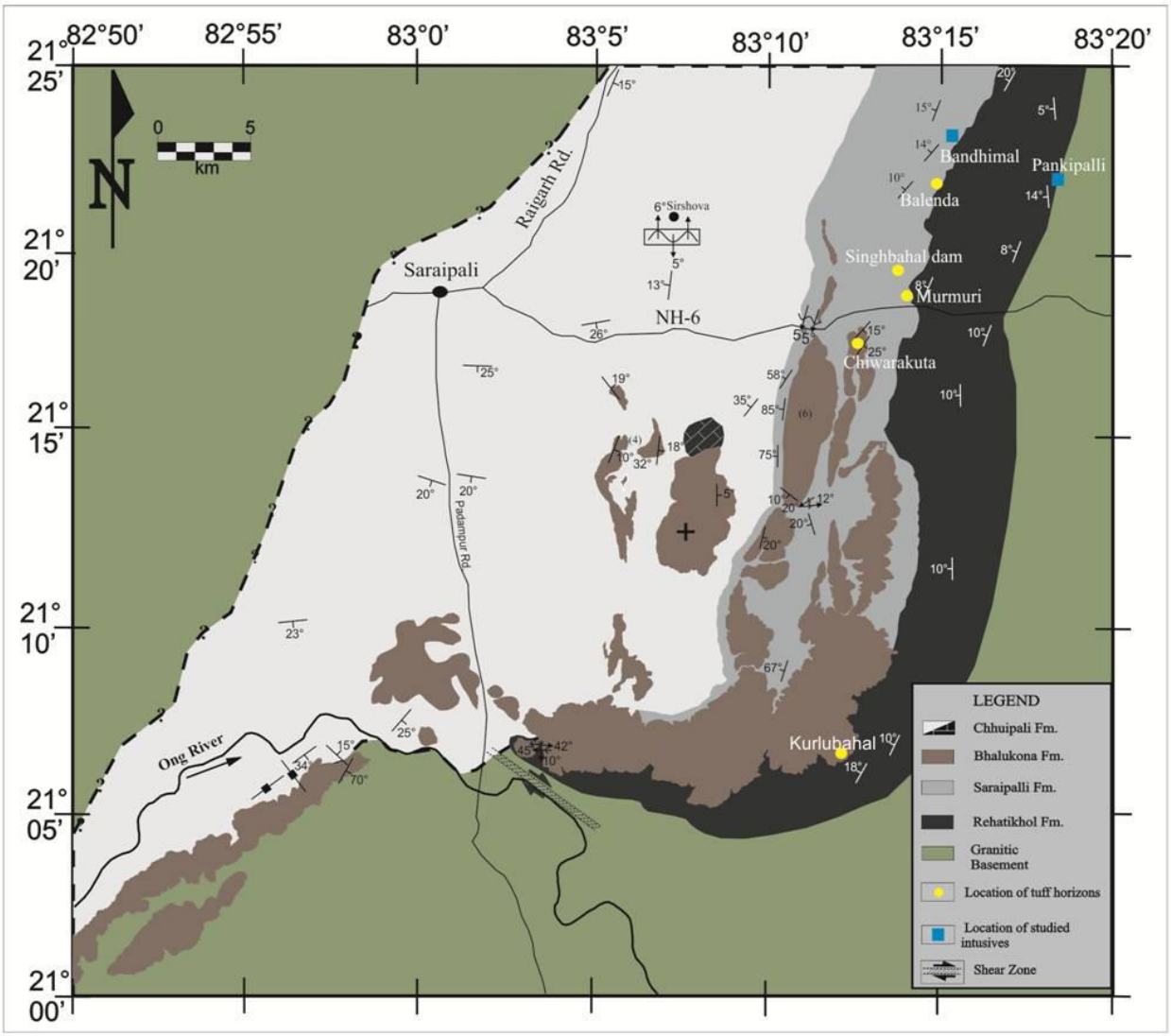

Fig.5.1. Map showing the location of tuff units (yellow circles) and mafic intrusives (blue squares).

of the basin varies between 2 and 5 m. On the outcrop-scale, two varieties of porcellanite tuff are identified, *i.e.* buff colored and thinly bedded (thickness 2-5 mm) found in alternation with reddish shale which is best exposed near Chiwarakutta village (Fig.5.2a) and another one is the dark colored, massive to plane laminated, and inter-bedded with fissile gray to black massive/plane laminated shale exposed near Balenda village (Fig.5.2b). Near Murmuri and Singhbahal outcrops, the tuff beds exhibit plunging upright fold where the plunge of the fold axes varies from 22° to 31° towards north and south (Fig.5.2c). Quartz venation at high-angle to the bedding plane has also been observed.

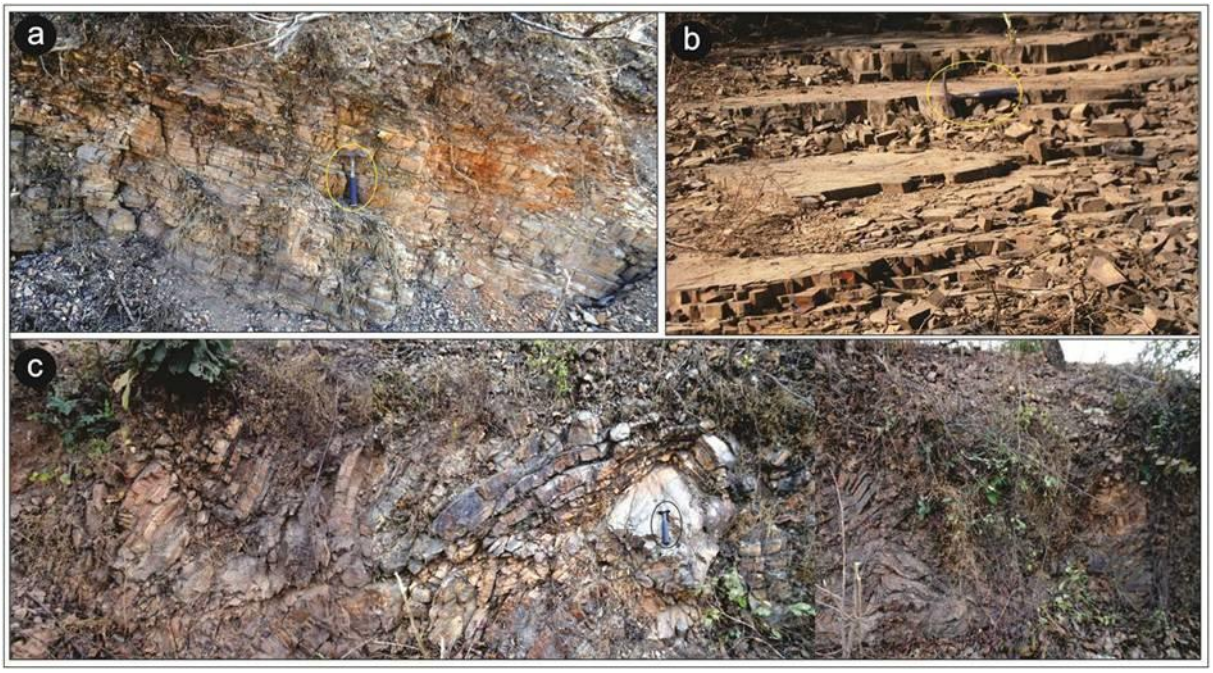

Fig.5.2. Bedded tuff within the Singhora basin. 2-5m thick, thinly bedded, buff colour, westerly dipping tuff layers at the road cutting section near Chiwarakutta village **(a);** dark colour varity of bedded tuff near Balenda village **(b);** and **(c)** showing complexly folded exposure of the tuff unit along E-W trending road cutting section near Murmuri village.

*5.4.1 Microscopic observations***:**

More than twenty samples were collected from field for their petrographic analysis. Detail thin-section study has been performed using polarized microscope and scanning electron microscope (SEM). All the samples are very fine-grained in nature and that forced us rely on the SEM observations for better identification, instead of polarized microscope study. Detailed petrographic study reveals that quartz and feldspar are set in a microcrystalline and glassy matrix with zircon, monazite, rutile and apatite in subordinate presence (Fig.5.3a). The rocks contain microscopic banding defined by alternating coarse and fine grain size. Coarse grained band contains silt size quartz, feldspar, rutile and glass shards (Fig.5.3b), whereas fine-grained layers contain microcrystalline quartz, kaolinite and sericite. Extensive late-stage quartz venation is observed in both the varieties. Blob-, sickle- and cuspate-shaped morphologies of glass shards indicate their volcanic affinity (Seif and Sparks 1978; Cas 1983). Also, few grains of white mica have been observed, particularly in the buff-colored variety. There are circular fine-grained portions in the dark colored variety of samples from Balenda and Singbahal dam site (Fig.5.3.a). All of the tuff samples revealed the presence of zircon and monazite grains.

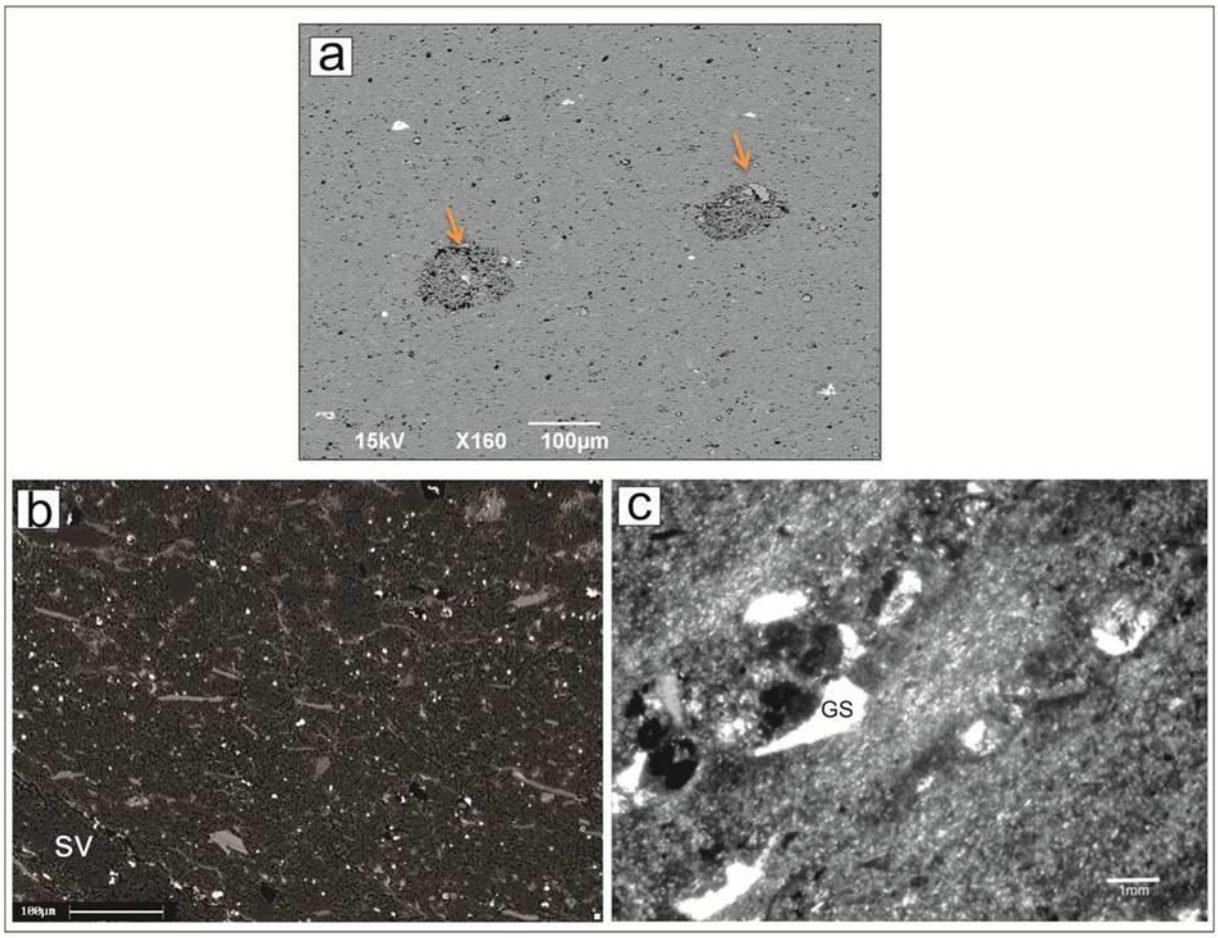

Fig.5.3. (a) Backscattered electron image of the dark colored variety of samples from Balenda and Singbahal, circular fine-grained portions are marked by arrow. **(b)** Tuff from Chiwrakutta. Note the quartz and feldspar phenocrysts set within fine-grained groundmass. The brighter spots represent clusters of rutile and grains of monazite and zircon. Also present is a secondary quartz vein (SV) at the lower left corner of the photograph. **(c)** Photomicrograph of the tuff showing various morphologies of glass shards (GS), including the sickle shape.

Zircon grains are mostly subhedral in shape, fragmented and also abraded. Occasionally, euhedral grains are observed. The zircon grains range in size from 20 to 100 μm (Fig.5.4). Oscillatory compositional zoning is observed in the back-scattered electron image (BSE image) of a euhedral grain. In many cases the cores are mantled by either single or multiple rims of varying thickness. Monazite grains in tuff samples from all the areas occur in two modes: (i) well-formed grains (10-30 μm) having a core with an irregular rim and (ii) clusters (6-20 μm) of fine grains (Fig.5.5). In well-formed grains, cores display various morphologies ranging from subhedral to subrounded.

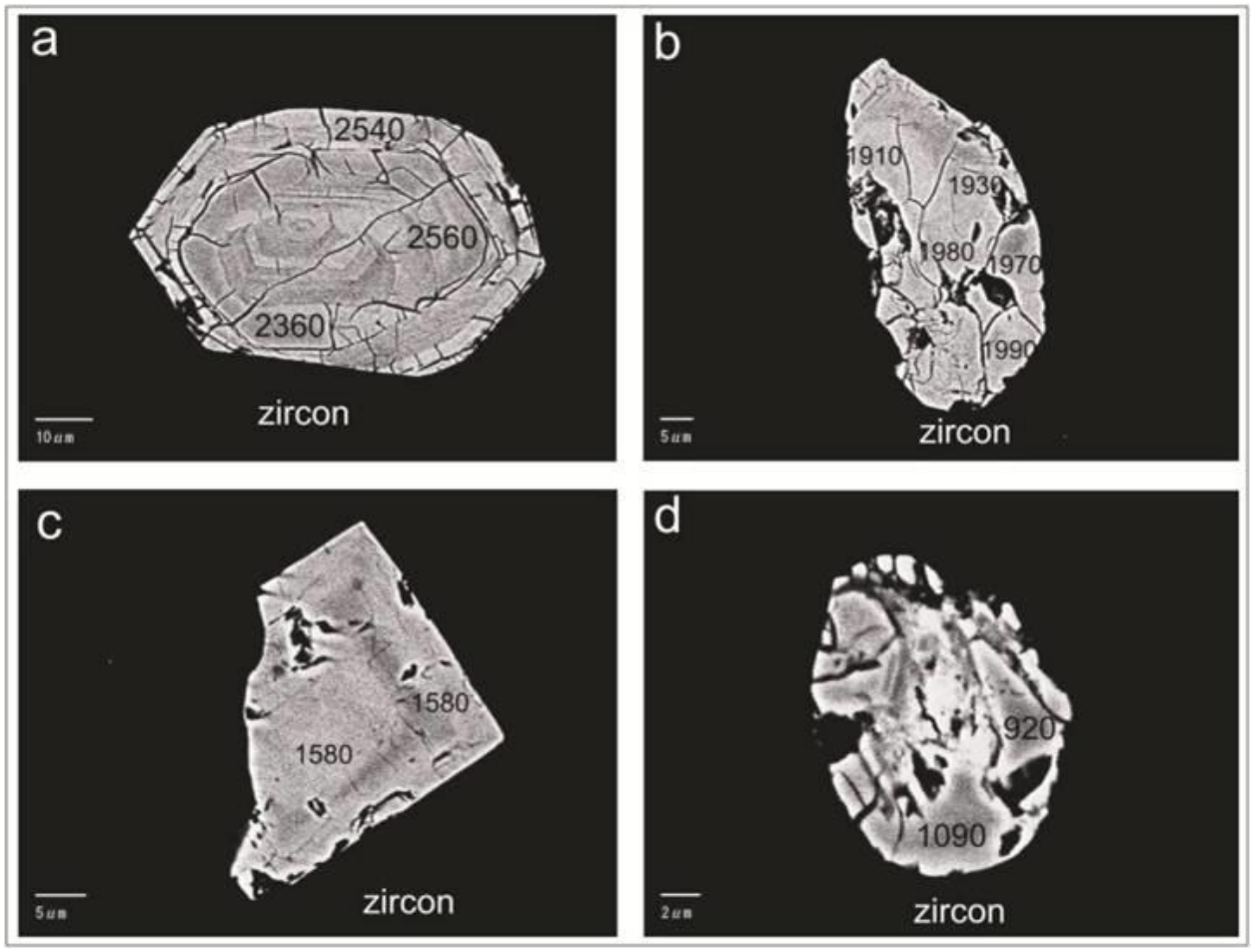

Fig.5.4. Backscattered electron images of zircons in the Singhora tuff (Chiwrakutta and Singbahal) showing age values (in Ma) determined by the U-Th-Pb electron probe method. Note subhedral to euhedral morphology of zircon grains present in the studied samples **(a–d)**. Also note concentration of ~1000-Ma date in subhedral grains with resorbed boundaries **(d).**

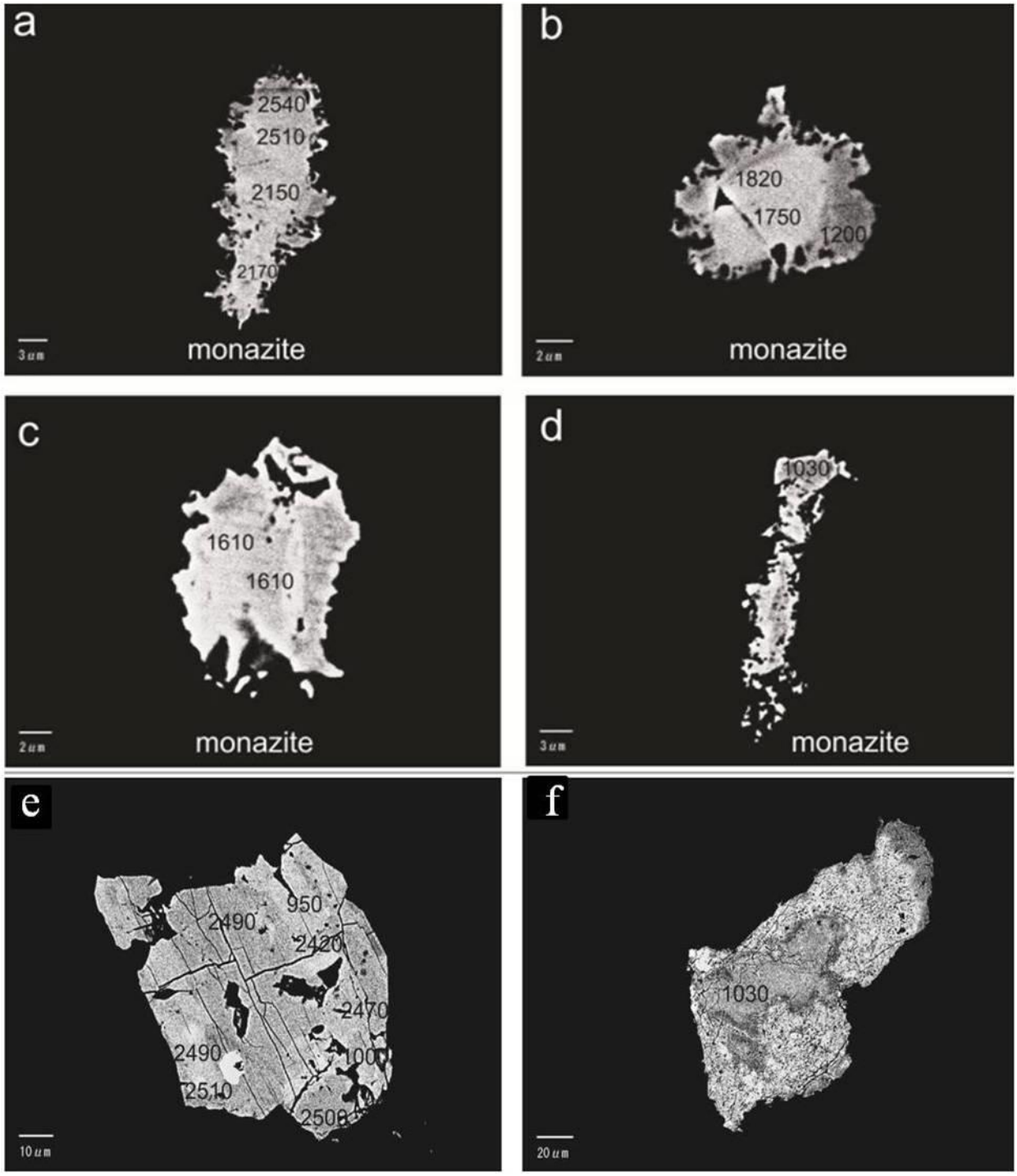

Fig.5.5. Backscattered electron images of monazites in the Singhora tuff (Chiwrakutta and Singbahal) showing age values (in Ma) determined by the U-Th-Pb electron probe method. Note larger grains with resorbed rims **(a–c)** and cluster of fine monazite grains **(d)** present in the studied samples. The ~1000-Ma age is noticed from the fine-grained cluster. **(e-f)** Monazite of from the sandstone unit underlying the tuff unit of the Singhora Group (i.e., from the Rehatikhol Formation).

5.4.2. Whole-rock geochemistry:

Eight representative samples from two varieties were analyzed for whole-rock geochemistry and the data has been listed in table.5.1. Samples show very high silica content (89-91 wt%), low A/CNK ratio (molar $Al_2O_3/(CaO+Na_2O+K_2O)$), *i.e.* varies from 0.90 to 1.1. Comparatively less mobile major oxides like Al_2O_3 contents vary within a short range *e.g.*, 4.5 to 5.9 wt% and 0.20 to 0.27 wt% for TiO_2. On the other hand, iron oxide content varies widely *i.e.*, Fe_2O_3 ranges between 1.05 to 3.80 wt%. The carbon content for Balenda sample is higher than other three samples that have been analyzed for it.

Primitive mantle normalized trace element values are shown in fig.5.6a and characterized by distinct overall enrichment of large ion lithophile elements (LILEs) (Rb, Ba, Th, etc.) with respect to the high-field-strength elements (HFSE) (Nb, Zr and Y) but, Ba, Nb, Ti and Sr are shows clear depletion. Only one sample (CH1c) shows depletion in Pb. The normalized values of all the HFSE elements like Nb, Zr and Y are quite uniform. However, in sample CH2a, Zr is slightly depleted. Keeping the overall trend, the normalized values of Ba, Th and Sr also show large dispersion in their range. Chondrite-normalized trace element plot (Fig.5.6b) also reveals that all the elements are one to two orders higher than the chondrite compositions and the overall LILE-enriched pattern is quite distinct. While plotting the trace elements normalized to the average continental crustal values, it is observed that the trend is flat and most of the values are very close to the crustal compositions (Fig.5.6c). Th, U and rare earth elements (REE) are having higher than crustal values, whereas Ti, Nb and Sr values are distinctly below those of the average crustal values. Interestingly, slight LILE element enriched trends are also characteristic for all the samples while normalized against lower continental crustal values with nearly similar patterns of enrichment and depletion of individual elements as those of primitive mantle-normalized plot (Fig.5.6d). The chondrite-normalized REE pattern (Fig.5.6e) for the Singhora tuff samples is shown an overall enrichment in light rare earth element (LREE) with an average $(La/Nb)_N$ value of 8.9. All of the samples are also characterized by a negative Eu anomaly, $Eu/Eu^* = Eu/ (Sm \times Gd)^{0.5}$, ranging from 0.17 to 0.25.

Table 6.1. Major, minor and trace element composition of tuff.

	CH 1a Chiwrakutta	**CH 1b Chiwrakutta**	**CH 1c Murmuri**	**CH 2a Singbahal**	**CH 2b Balenda**
SiO_2	89.74	90.45	90.64	92.61	87.83
TiO_2	0.27	0.26	0.27	0.20	0.22
Al_2O_3	5.84	5.95	5.73	4.55	5.96
Fe_2O_3	1.83	1.97	1.87	1.05	3.80
MnO	0.020	0.024	0.024	0.019	0.025
MgO	0.47	0.48	0.47	0.32	0.55
CaO	0.19	0.17	0.22	0.21	0.17
K_2O	1.38	1.36	1.37	0.96	1.17
Na_2O	0.09	0.09	0.09	0.08	0.07
P_2O_5	0.124	0.110	0.131	0.077	0.169
LOI	2.04	2.01	2.09	1.35	2.78
Sum	**99.95**	**100.87**	**100.80**	**100.07**	**99.97**
Cr	37	96	98	61	111
V	24.51	134.70	27.19	16.71	15.21
Co	12.66	17.94	15.25	31.30	15.98
Ni	14.3	15.0	15.2	9.5	42.3
Cu	32.2	32.2	34.0	25.6	46.1
Zn	24.2	23.8	18.3	13.0	41.9
Ga	6.2	6.8	6.8	5.9	7.6
Pb	5.3	5.5	1.1	3.5	4.1
Th	6.27	6.60	6.71	5.46	11.97
Rb	103.1	101.2	101.8	73.3	82.9
U	3.3	4.4	3.6	2.4	5.7
Sr	62	60	61	55	164
Y	21.00	22.47	22.34	27.44	41.23
Zr	73	74	73	59	63
Nb	8.1	8.3	7.9	6.5	7.9
Sc	6.84	8.44	7.34	5.00	7.36
U	2.14	2.91	2.52	2.68	2.09
Hf	1.93	4.15	1.94	1.19	1.71
La	29.23	30.43	28.37	19.14	45.01
Ce	54.57	54.93	56.15	32.80	62.91
Pr	6.59	6.73	6.48	3.89	10.43
Nd	27.27	27.48	26.66	16.34	44.07
Sm	5.36	5.25	5.51	4.21	8.52
Eu	0.79	0.87	0.88	0.96	1.41
Gd	3.90	4.07	4.17	3.26	6.95
Tb	0.66	0.67	0.72	0.69	1.17
Dy	3.54	3.59	3.91	4.31	6.45

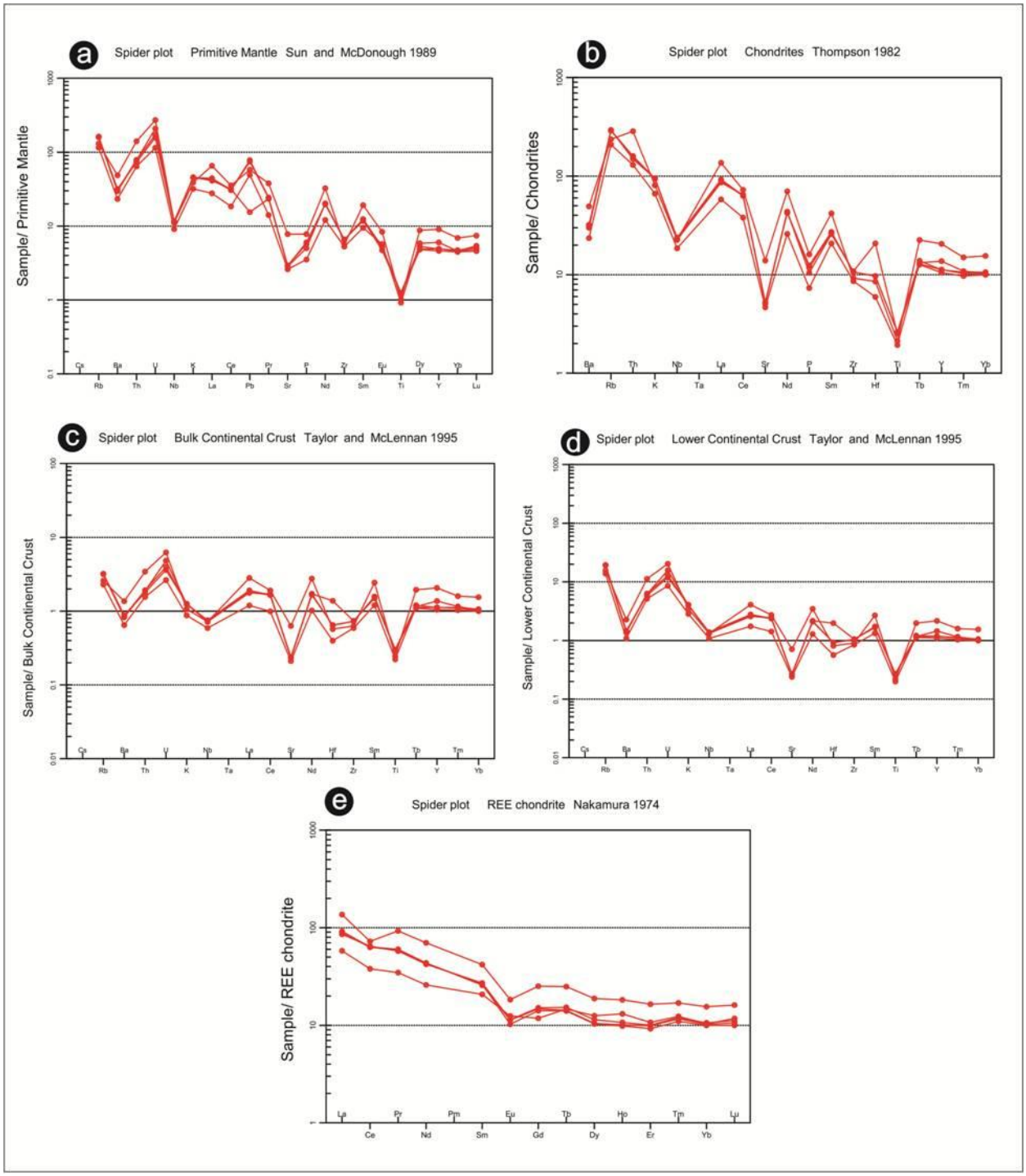

Fig.5.6. (a) Primitive Mantle normalized trace elements plots showing overall enrichment of LILEs and clear depletion of Ba, Ti, Sr, Nb. **(b)** Chondrite normalized trace element plot showing overall LILE-enriched pattern. **(c)** Flat-trend trace elements pattern of bulk continental crust normalized plot, most of the values are very close to the crustal compositions. **(d)** Lower crust normalized trace element pattern exhibits nearly similar patterns of enrichment and depletion of individual elements as those of primitive mantle-normalized plot. **(e)** Showing overall enrichment in light rare earth element (REE) in chondrite normalized REE spider plot.

5.4.3. Geochemical character of the studied samples:

Samples revealed anomalously high silica content (*i.e.* 89-91 wt%) as compared with that of the normal felsic tuff of different tectonic settings worldwide (~65-80 wt%; GEOROC database; http://www.georoc.mpchmainz.gwdg.de). This anomalous value is due to the presence of numerous secondary micro veins of quartz cutting across the primary layering of the rock. Such secondary silica enrichment prevents the characterization of the studied tuff samples on the basis of major element chemistry and also possibly the reason of variation of some relatively more mobile trace elements. However, the samples are showing an affinity towards rhyolite and dacite field in the major elements triangular diagram of *Jensen* (1976) (Fig.5.7a). In spite of that, more reliance is given on trace elements, particularly those showing lesser dispersal among the studied samples collected from all over the basin. A classification scheme based on more immobile element ratios, Nb/Y and Zr/Ti (*Winchester and Floyd,* 1977 and that of modified by *Pearce,* 1996), indicates a composition in between rhyodacite and andesite (Fig.5.7b, c) and also showing a marginal affinity of high calc-alkaline shoshonite in Co/Th plot (Fig.5.7d). The tectonic discrimination plots using the parameters based on major elements show a post-orogenic granite affinity (*e.g.* those of *Maniar and Piccoli,* 1989) (Fig.5.8a). However, as mentioned earlier it would be prudent to use more immobile elements. In the discrimination diagram for A-, I- and S-type granitoids, all the samples show the affinity towards the I- and S-type granitoids (*Whalen et al.,* 1987) (Fig.5.8b). Moreover, the tectonic discrimination of granitic rocks (*Pearce et al.* 1984) shows that all samples fall in the volcanic arc granite field (VAG) (Fig.5.8c). On a more inclusive tectonic discrimination scheme in Y vs. Rb space, however, the data plot in the field of syncollisional granite and volcanic arc granite (Fig.5.8b).

5.5 Geochronology

5.5.1 Monazite and zircon age dating of the bedded tuff:

Small size of datable minerals available in the tuff samples of all the studied locations debars to use higher resolution techniques like LA-ICPMS or SHRIMP. Hence, keeping in mind the volcanogenic pyroclastic origin of this rock type a frantic effort had been given to date monazite and zircons using the U-Th-Pb EPMA technique which is known to be not that robust at this age of

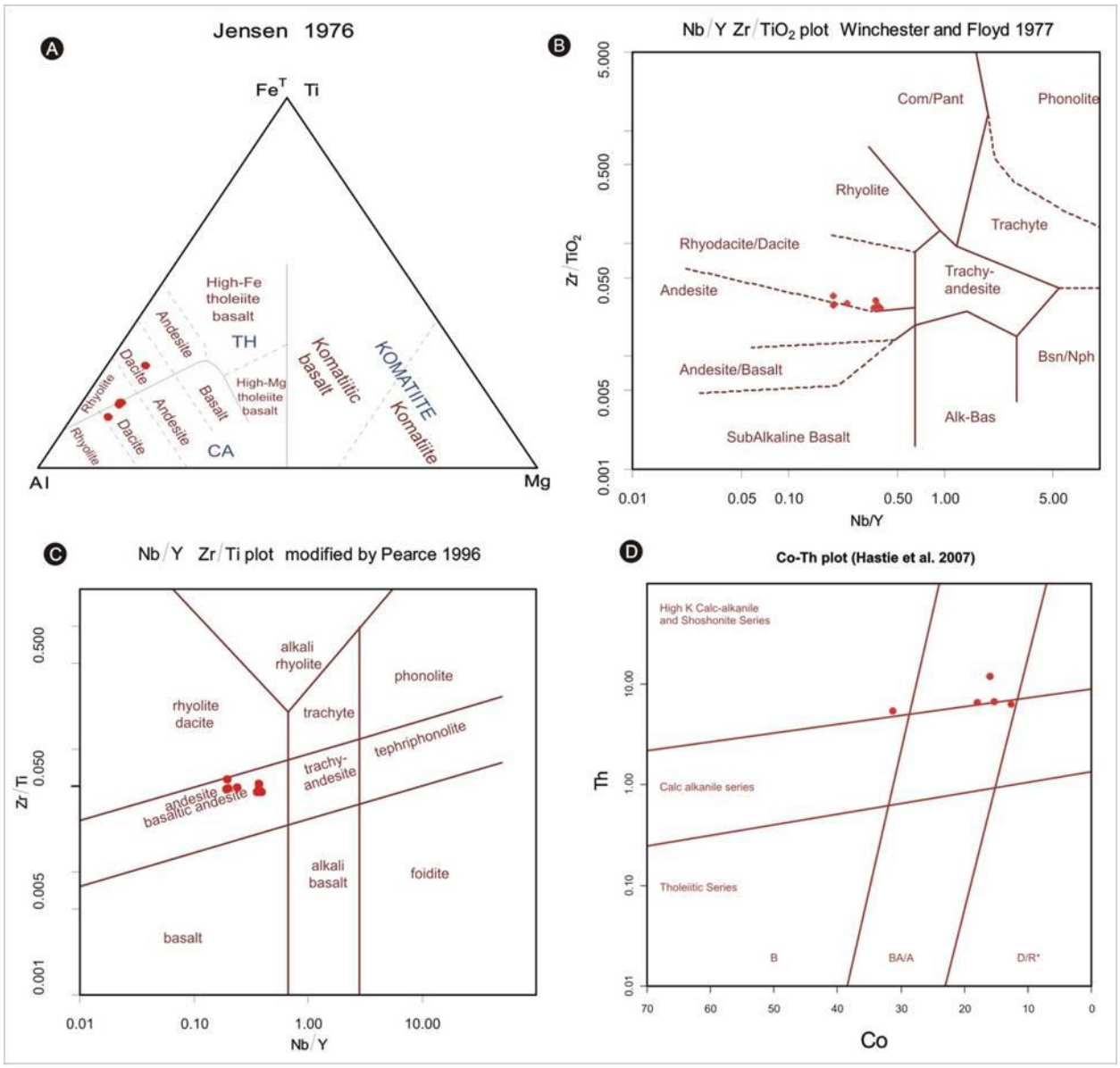

Fig.5.7. Sample showing rhyolite to dacite affinity in major and trace elements plots**.**

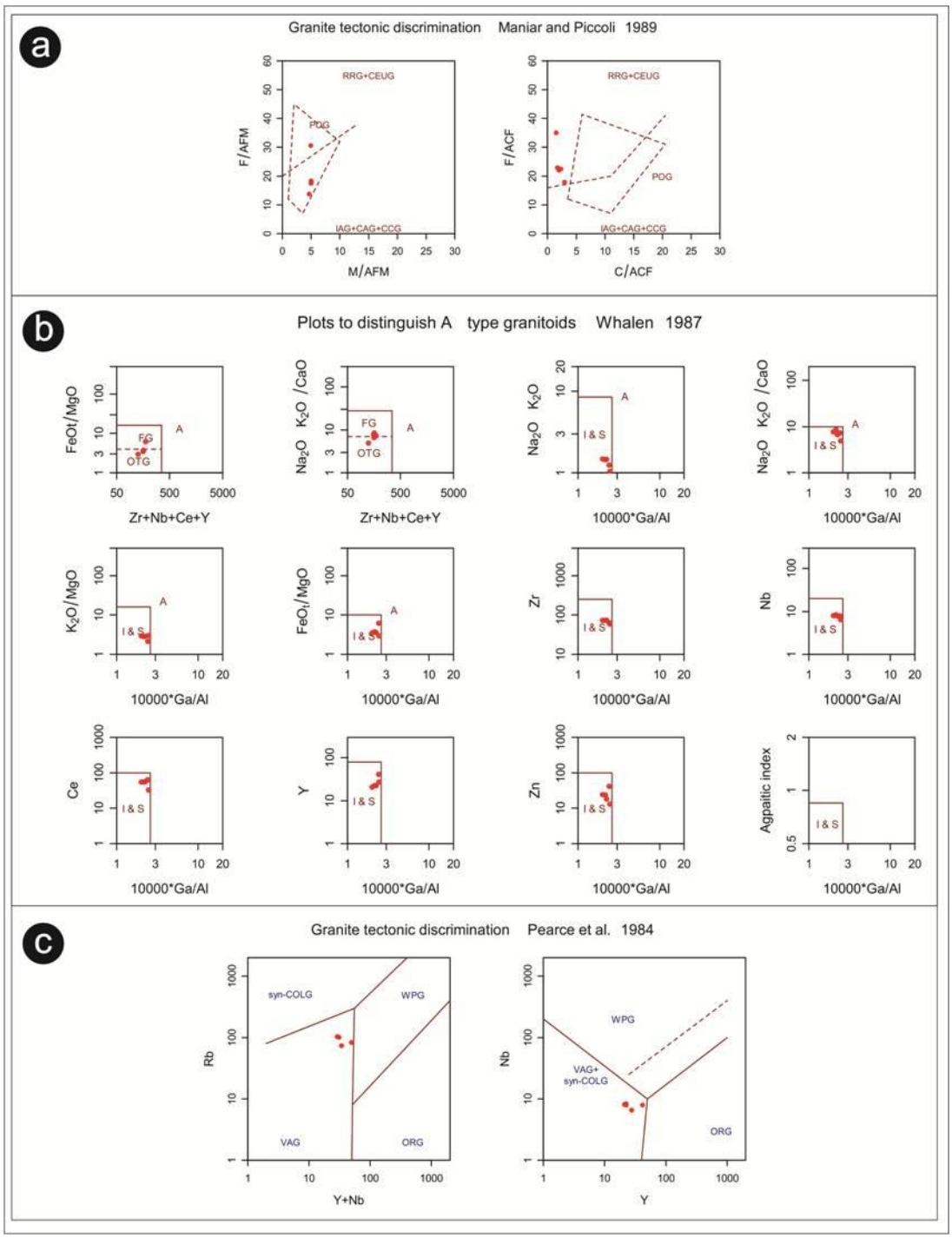

Fig.5.8. Samples are showin post-orogenic granite affinity (a), I & S type granitoid character (b) and volcanic arc to syn- collisional volcanic arc granite in composition in different tectonic discrimination diagrams.

earth science practices. Problems are particularly more for zircon analysis using this technique that too for the Precambrian rocks. Though the results have already been published (*Das et al.,* 2009), here is a detailed account of the raw data and data processing. Analyses have been carried out on total 139 spots on monazite grains and 103 spots on zircon grains identified in several thin sections. Back scattered electron images (BSI) of grains from the Singhora tuff with analytical spots and age data are shown in Fig.5.4. The probability diagram of ages for 139 points on monazite grains shows several age clustures as represented by peaks in probability diagram at 2500, 2100, 1870, 1720, 1500 (3 closed-spaced peaks), 1230 and 1000 Ma (Fig.5.9). Out of these, the well-formed monazite grains (6-40 μm) register the highest peak in the frequency distribution diagram at ~1500 Ma, with subordinate peaks at 2500, 2100, 1870, 1720, 1230 and 1000 Ma. The youngest peak of 1000 Ma age is obtained from nearly decomposed/resorbed irregular aggregrates of fine-grained monazites (Fig.5.5d). The 2500 and 1800 Ma ages are obtained from the exotic monazite grains (with or without a rim), whereas the ~1500 Ma age is yielded from the monazite grains having a core with distinct irregular rims. Due to multiple age clusters in the probability diagram, a need was felt to do further statistical analyses to characterize each of the peaks better. Gaussian peak fittings have been carried out using two different fit parameters. The results are shown in the fig.5.9. In these fits

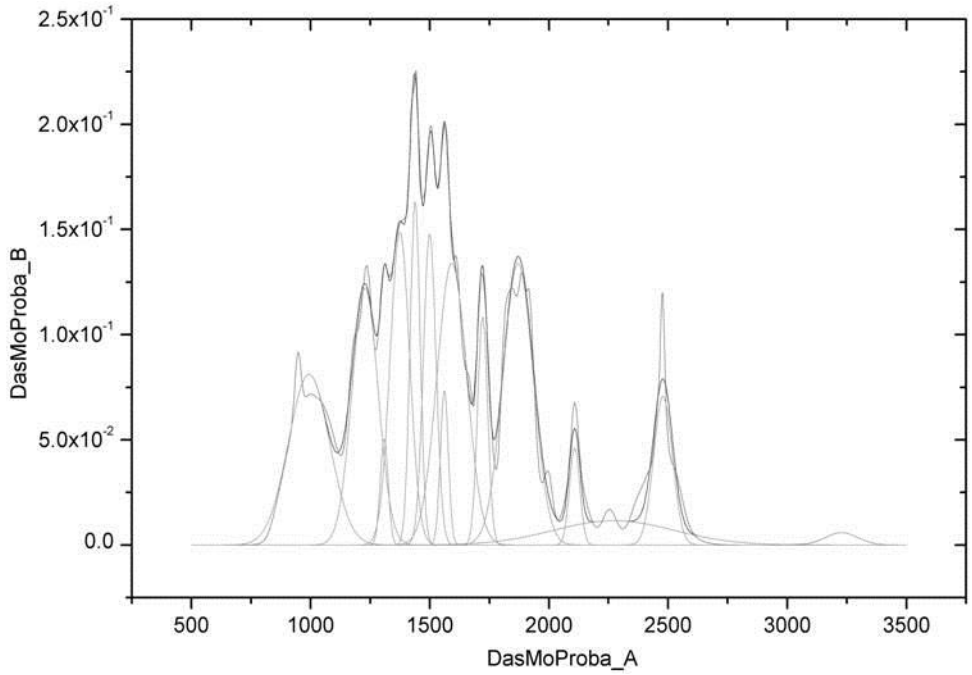

Fig.5.9. Deconvoluted probability peaks from the age spectra of monazite grains from Singhora tuff.

the centre of gravity for each calculated peaks represents the age value, while the full width at half maximum (FWHM) values imply the 2σ error ranges. The first fit with higher chi-square but lesser correlation coefficient values reveals 8 overall peaks at 988, 1214, 1477, 1722, 1876, 2108, 2257, and 2472 Ma with an artifact at 3228 Ma. The three observed peaks at the probability density diagram around 1500 Ma yields one Gaussian curve with centre of gravity at 1477 Ma and FWHM of 337 Ma. There is not much clubbing of peaks during this curve fitting in other age spectram. However, to get a better individualistic curve fit, a renewed calculation with lower chi-square but higher correlation coefficient values yield 14 best fit curves (Fig.5.9). This actually separates the three peaks around 1500 Ma. The three gaussian best-fit curves yield age values of 1437 ± 50 Ma, 1499 ± 62 Ma and 1592 ± 145 Ma from respective values of centre of gravity and FWHM. Among these three 1437 ± 50 Ma peak stands for the highest probability curve. The youngest peak yields a best fit curve with age value of 993 ± 202 Ma. There are several satellite peaks in between 993 Ma peak and 1437 Ma peak. Older peaks are distinct at 2478 ± 92 Ma, 2108 ± 51, 1870 ± 148 and 1721 ± 50 Ma from as revealed by the centre of gravity and FWHM values of each best fit curves.

With such multiple peak values from monazite analyses, the first problem was to check and identify the age clusters which are inherited before crystallization and those which represent the later thermal pulses in and around the basin. Hence, to check the inheritance of age data and the effect of any later pervasive thermal event, monazites grains were separated from units above and below this tuff layer in Singhora basin. The monazite grains from the underlying sandstone unit *i.e.*, Rehtikhol Formation has been analyzed (44 spots). Similarly, sandstone units belonging to the overlaying Saraipalli Formation has been processed with low yield of only one monazite grain (3 spots). The lower sandstone unit (Rehatikhol Formation) contains two types of monazite grains: (i) detrital monazite yielding a ~2500 Ma age (Fig.5.5e) and (ii) decomposed and recrystallized detrital monazite yielding a 1000 Ma age (Fig.5.5f). Zircons from the same sandstone are mostly older than 2400 Ma, with a distinct peak around 2600 Ma. Monazite grain from the upper sandstone (Saraipalli Formation) has an age around 1740 Ma.

Most of the zircon grains are too low in PbO content to obtain ages with a low standard deviation. Only selected ages of zircons are shown in fig.5.4. Large zircon grains from the Singhora tuff yield ages somewhat similar to those for monazite, *i.e.* 2500, 2100, 1800 and 1500 Ma (Fig.5.4). No ages younger than 1500 Ma is revealed from large euhedral zoned zircon grains. The younger

ages obtained from zircons (~900 Ma), are clearly from grains with decomposed, recrystallized, and resorbed grain boundaries.

5.6 Mafic intrusives: Megascopic observations

During detailed field mapping, several mafic dykes with different degrees of alteration have been observed at the boundary of the basin but intruding the basement. Such intrusives were evident in north-eastern part, eastern, southern and south-eastern parts of the basin. However, only one mafic intrusive is identified intruding the sediments and direct contact with the sedimentary units of Saraipalli Formation. Intriguingly, along the strike orientation of this intrusive another small occurrence of mafic body has been traced at the boundary between lowermost Rehtikhol Formation and the granite gneiss of Bastar craton. The present study has been done on these two spatially separated mafic units (Fig.5.1). One of them is exposed at northern part of the Singhora basin, *i.e.* near the Bandhimal village (N 21° 22′ 36.6′′ E 83° 15′ 2.6′′) and the other one is found to occur at the basin-margin (contact with Rehatikhol sandstone) near Pankipalli village (N 21° 22′ 45.60′′ E 82° 57′ 43.06′′). The exposed length of Bandhimal intrusive is nearly 455 m and width of 200 m at the maximum; trending southeast (SE)-northwest (NW) (120°-300°), which is at high angle to the strike of sedimentary beds (20°/15°→W) of this area. Here the mafic body has direct contact with the shale layers of Saraipalli Formation (Fig.5.10). There is no chilled margin effect developed at the boundary between the mafic body and shale. On the other hand, the Pankipalli intrusive unit has cut across the boundary between basement granitic/granite gneiss and the Rehatikhol Formation. However, it is not traceable further down-dip in the Saraipalli Formation *i.e.*, towards further east in the basin. Hence, the mafic body, exposed at Bandimal and Pankipalli is interpreted as a discordant body at least till the Saraipalli Formation and is preferred to term it as an intrusive body. In the absence of any conclusive field data on the present erosional surface, it is difficult to term it either as a dyke or a sill. The petrographic observations, mineral chemical character, bulk rock geochemical character (including isotope geochemistry) and geochronological data have been published in *Das et al.* (2011). Here is a detailed account of all these.

Fig.5.10. Field photograph showing **(a)** contact relationship between the diabasic intrusive body and the Saraipalli shale and **(b)** a closer view to note that there is not much contact effect. The scales (white) in both the figures are of 15 cm in length.

5.6.1. Petrography and mineral chemistry

Thin sections of the collected samples of both the intrusives reveal presence of plagioclase and pyroxene crystals. Most of the plagioclase grains are 40-50 μm in width and less than 70-80 μm in length (Fig.5.11a). Rare large (longer than 150μm) plagioclase laths have also been observed. The clinopyroxene grains, in general, are less than 50μm in size and occasionally form aggregates of smaller grains (Fig.5.11a). Such size distribution of major minerals imparts medium to fine grained character for the studied rock samples. There is no systematic variation of grain size or modal abundances of the minerals in the studied diabasic units from the central part of the body towards its rim. In terms of grain shape, plagioclase and pyroxene grains are euhedral to subhedral with presence of distinct grain boundary. Differently oriented plagioclase laths enclose clusters of pyroxene grain showing intergranular texture (Fig.5.11a). Plagioclase and clinopyroxene grains often exhibit ophitic to subophitic texture. Lath-shaped plagioclases are rarely zoned. Besides, there are magnetite, ilmenite and sphene with minor calcite, biotite and glass. Occurrence of calcite is local

even in microscopic scale and principally confined within the micro-fractures suggesting its secondary origin. Despite local sericitization the plagioclase grains are mostly fresh and often show well preserved twin lamellae (Fig.5.11b). The rock unit is overall fresh except along the joint and fracture planes where some amount of alteration of the rock unit is noticed. Representative compositional data of all the analyzed minerals are tabulated in table 5.2.

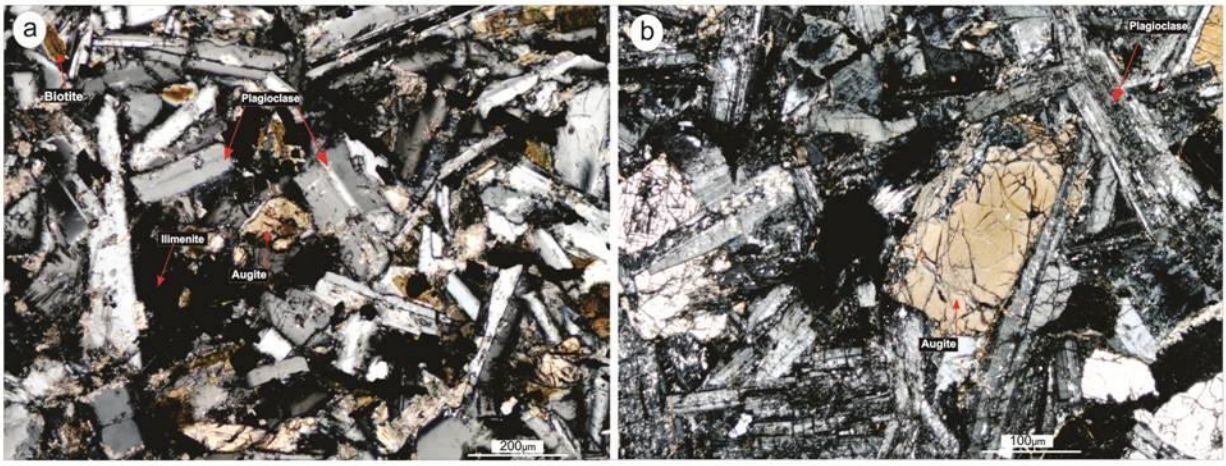

Fig.5.11. Photomicrograph of the diabasic intrusive. Note the preservation of magmatic textures and mineralogy defined dominantly by plagioclase laths, pyroxene and opaque minerals (a). Despite local sericitization the plagioclase grains are mostly fresh and often show well preserved twin lamellae (b).

Table.5.2. Representative mineral compositions of pyroxene, plagioclase and ilmenite of the studied rock. Compositional values are recalculated from raw electron microprobe analysis data.

Pyroxene X_{Mg}	0.57	0.56	0.55	0.61	0.62	0.65
Wo (mole%)	46.34	45.3	43.04	42.19	42.77	43.96
En (mole%)	30.77	30.46	31.56	35.16	35.52	36.52
Fs (mole%)	22.89	24.24	25.4	22.65	21.7	19.52
Plagioclase						
Ab (mole%)	41.82	42.34	45.24			
An (mole%)	56.73	56.34	53.56			
Or (mole%)	1.45	1.32	1.2			
Ilmenite						
Ilm (mole%)	73.57	89.52	19.45			
Hm (mole%	26.43	10.48	80.55			

Several points from core to rim of plagioclase phenocrysts are showing almost uniform composition and they are labradoritic with narrow range of chemical variability in terms of end member mole% i.e., $Ab_{41-45}An_{53-56}Or_{1.2-1.4}$. In spite of the slight chemical variation in plagioclase phenocrysts, there is

not much chemical zoning present in most of the plagioclase grains. However, in some grains the core is slightly anorthite-rich in comparison to the rim. Subhedral clinopyroxene grains are not zoned, relatively less altered and compositionally augitic in nature ($Wo_{42-46}En_{30-36}Fs_{19-25}$ and X_{Mg} = 0.57–0.65). Opaque minerals are mostly Fe–Ti oxides and composition recalculation on 3-oxygen basis indicates a solid solution between ilmenite and hematite ($Ilm_{19-73}Hm_{80-10}$).

5.6.2 Whole-rock geochemistry, Rb-Sr and Sm-Nd isotope study:

Several samples were collected from both the bodies, particularly from the central part and from the boundary part of the respective bodies. Samples studied under microscope for degree of alteration and weathering. Those with least alteration effects were selected for geochemical analysis. The studied samples of the intrusive units display small variation in major oxide compositions. Normative calculation based on CIPW scheme is shown in Table.5.3. This shows that the studied samples are quartz-normative basalt with the presence of major normative minerals of ternary feldspar, hypersthene (and small amount of diopside), ilmenite, hematite, sphene and apatite. Normative calculation involving hydrous phases show presence of normative biotite and hornblende, apart from quartz, binary feldspar, calcic-pyroxene and Fe-Ti oxides. The major elemental chemistry is characterized by SiO_2 = 50-53 wt%, total alkalis (Na_2O+K_2O) of 4 wt% with K_2O/Na_2O of 0.21-0.26 (Table 2). The TiO_2 content is low and varies between 1.67 to 2.12 wt%. The magnesium number *i.e.*, Mg # ranging between 42 and 46 is moderately low and Cr, Ni contents vary between 13-21 ppm and 38-47 ppm, respectively. Classification has been done on the basis of bivariate and multivariate plots using the major and trace elements (Figs.5.12). On the basis of major oxides abundance the intrusive is classified as basaltic andesite to basalt and plots on the boundary between tholeiite and calc-alkaline series (Fig.5.12a,b,c). Depending on the Shand's index, all of the studied samples can be termed as metaluminous. *Jensen* (1976) plot, however differentiates the rocks studied from two different location i.e., Bandimal intrusive being andesitic basalt the Pankipalli sample plots in the field of high Fe tholeiite. Some selective trace elements of the studied samples show alkali basalt to sub-alkaline basalt nature in Zr/TiO_2 vs. Nb/Y plot (Fig.5.12d). Recent classification scheme using Co and Th content (*Hastie et al.,* 2007) classify these rocks as marginally high K calc-alkaline to shoshonitic basalt (Fig.5.12e).

The trace element data show overall enrichment (one to two orders) with respect to the composition of primitive mantle. Multi-trace element diagram indicates characteristic enrichment of large ion lithophile elements (LILE) such as Sr, K, Rb, Ba and Th, in comparison to high field strength elements (HFSE) such as Nb, P, Zr, Ti, and Y. A definite enrichment of Pb and Ba with slight depletion of Nb and P are characteristic of this rock (Fig.5.13a). On the other hand, chondrite-normalized trace element distribution though show overall similar trend of LILE enrichment, the two bodies show differences in certain elements. Th-ratio is somewhat more depleted for Pankipalli intrusive, while Zr-ratio is enriched in Bandimal intrusive (Fig.5.13b). Similar exercise has been carried out with respect to the values of bulk continental crust. The normalized plot shows flat trend for the whole spectrum with slight high values than the average continental crust (Fig.5.13c). However, there is sharp enrichment of Ba and depletion of K. Some of the incompatible trace element ratios (LILE/HFSE and LILE/REE) have been calculated in Table.5.4 and are compared to reported average values of crust and mantle (*Hofmann,* 1988). The ratios like Nb/Th and Nb/La are of particular importance due to the relative immobility of these elements and their ability to test the degree of crustal contamination during the passage through crust enriched in Th and LREE. These ratios are in the range of 0.56-0.75 for Nb/La and 2.9-3.4 for Nb/Th, and these values fall in between the average crustal and mantle values. Chondrite-normalized REE plot (Fig.5.13d) shows overall enrichment of LREE in contrast to HREE [$(La/Yb)_N$ = 6.45-8.64]. In the LREEs, slope is moderate *i.e.* $(La/Sm)_N$ = 2.30-2.97 which is similar in the HREE spectrum [$(Eu/Yb)_N$ = 2.56-2.65]. The pattern is almost devoid of any Eu anomaly (Eu/Eu^* = 1.0-1.04).

The results of whole rock Rb-Sr and Sm-Nd isotope analyses are listed in Table.5.5. The initial Nd value is in the range of 0.510815 to 0.510919 and initial Sr is in the range of 0.709377 to 0.706672. The initial Sr ratio is higher than the general trend of the depleted mantle through time. The epsilon (ε) values are a measure of the deviations of the isotopic ratios in the samples from the expected value in a uniform reservoir. The epsilon values for both Sr and Nd isotopes have been calculated, as these values can be used to test the cogenetic character and contamination in the samples, or can be a measure of the extent to which the magmas, when they cooled to form the rocks, had fractionated relative to their postulated depleted mantle source(s). The calculated epsilon (ε) values are $\varepsilon^t Nd$ = +(0.3-2.3) and $\varepsilon^t Sr$ = +(54.56-92.91), where t=1421 Ma (this is the age value from this basalt as discussed later). In $\varepsilon^t Nd$ vs. $\varepsilon^t Sr$ isotope correlation diagram (Fig.5.14) the studied samples plot in the field of positive $\varepsilon^t Nd$ and positive $\varepsilon^t Sr$. The T_{DM} ages refers to the depleted

mantle model ages calculated from the Nd isotope ratios, and is a measure of the length of time of the sample has been separated from the mantle from which it was originally derived. The calculated depleted mantle model age for this intrusive is 1.7 Ga.

Table. 5.3. Representative bulk rock analysis data of the intrusive and their calculated CIPW norms (as in *Das et al.,* 2011)

	10/L7	7/21	10/L7b	7/21 _2	7/25	HB1* standard
SiO_2	53.489	52.225	52.886	52.312	50.109	50.30 (50.187)
TiO_2	2.07	2.032	2.12	2.108	1.67	1.02 (1.024)
Al_2O_3	16.111	16.11	15.99	16.14	14.991	16.60 (16.556)
Fe_2O_3	12.159	12.277	12.289	12.235	13.971	10.56 (10.497)
MnO	0.157	0.159	0.154	0.162	0.27	0.17 (0.172)
MgO	4.635	5.096	4.596	4.935	6.055	8.73 (8.726)
CaO	7.563	6.92	7.58	6.98	7.319	9.28 (9.279)
Na_2O	3.326	3.423	3.318	3.385	2.82	3.13 (3.182)
K_2O	0.714	0.892	0.702	0.884	1.74	0.73 (0.730)
P_2O_5	0.358	0.336	0.355	0.328	0.264	0.26 (0.254)
Total	100.582	99.47	99.99	99.469	99.209	100.77 (100.606)
LOI	2.64	2.59	2.61	2.56	2.37	
Ba	600.536	747.738	641.445	742.8	893.966	188.748 (193.566)
Rb	22.382	32.792	22.105	30.126	47.1	19.688 (19.154)
Sr	435.73	422.949	432.29	420.824	290.742	382.356 (375.954)
Zr	248.268	233.386	247.683	235.468	129.56	104.842 (103.634)
Nb	17.935	17.355	17.857	17.297	19.643	5.154 (5.207)
Ni	38.613	46.631	39.718	47.215	46.327	168.778 (168.128)
Co	45.962	56.831	46.287	55.836	55.269	42.688 (43.541)
Zn	111.901	111.453	110.826	110.58	97.862	79.512 (77.196)
Cr	21.987	14.793	20.84	13.896	59.371	310.621 (306.529)
La	32.16	29.61	23.809	28.371	23.65	–
Ce	64.95	60.01	55.379	59.65	49.75	–
Pr	8.13	7.53	7.56	7.56	6.43	–
Nd	32.39	30.66	31.57	30.68	25.62	–
Sm	6.8	6.63	6.5	6.35	5.34	–
Eu	2.29	2.27	2.24	2.26	2.1	–
Gd	7.19	6.88	7.05	6.92	5.66	–
Tb	1.01	0.99	1.05	1.02	0.84	–
Dy	5.37	5.44	5.41	5.41	4.75	–
Ho	1.08	1.06	1.04	1.03	0.99	–
Er	2.76	2.66	2.65	2.7	2.57	–
Tm	0.39	0.38	0.36	0.37	0.38	–
Yb	2.51	2.44	2.49	2.46	2.47	–
Lu	0.38	0.37	0.37	0.35	0.38	–
Y	30.096	29.434	30.102	29.681	26.055	25.026 (25.080)
Sc	22.485	22.04	20.528	21.657	41.221	31.557 (30.936)
V	155.374	161.07	152.684	160.524	272.981	211.658 (210.598)
Cu	30.5	33.199	30.1	32.098	126.443	65.023 (62.146)
Pb	14.125	11.206	14.06	11.134	7.314	3.514 (3.524)
Th	6.173	5.268	5.983	5.161	3.465	3.779 (3.977)
Ga	22.374	22.049	21.481	21.756	14.798	14.864 (15.462)
Q	11.09	8.76	10.67	9.20	5.56	
Or	4.22	5.27	4.15	5.22	10.28	
Ab	28.14	28.96	28.08	28.64	23.86	
An	26.92	25.96	26.66	26.23	23.11	
Di	1.30	0.00	1.43	0.00	5.23	
Hy	10.94	12.69	10.78	12.29	12.66	
Ilm	0.34	0.34	0.33	0.35	0.58	
Hm	12.16	12.28	12.29	12.24	13.97	
Tn	4.65	4.35	4.78	4.41	3.35	
Ru	0.00	0.08	0.00	0.13	0.00	
Ap	0.85	0.80	0.84	0.78	0.63	

*HB1 is basalt from Rishiri volcanic and used as the internal standard. Average values of standard before and after the unknown analyses are given. Values in parenthesis indicate the reported value of HB1.

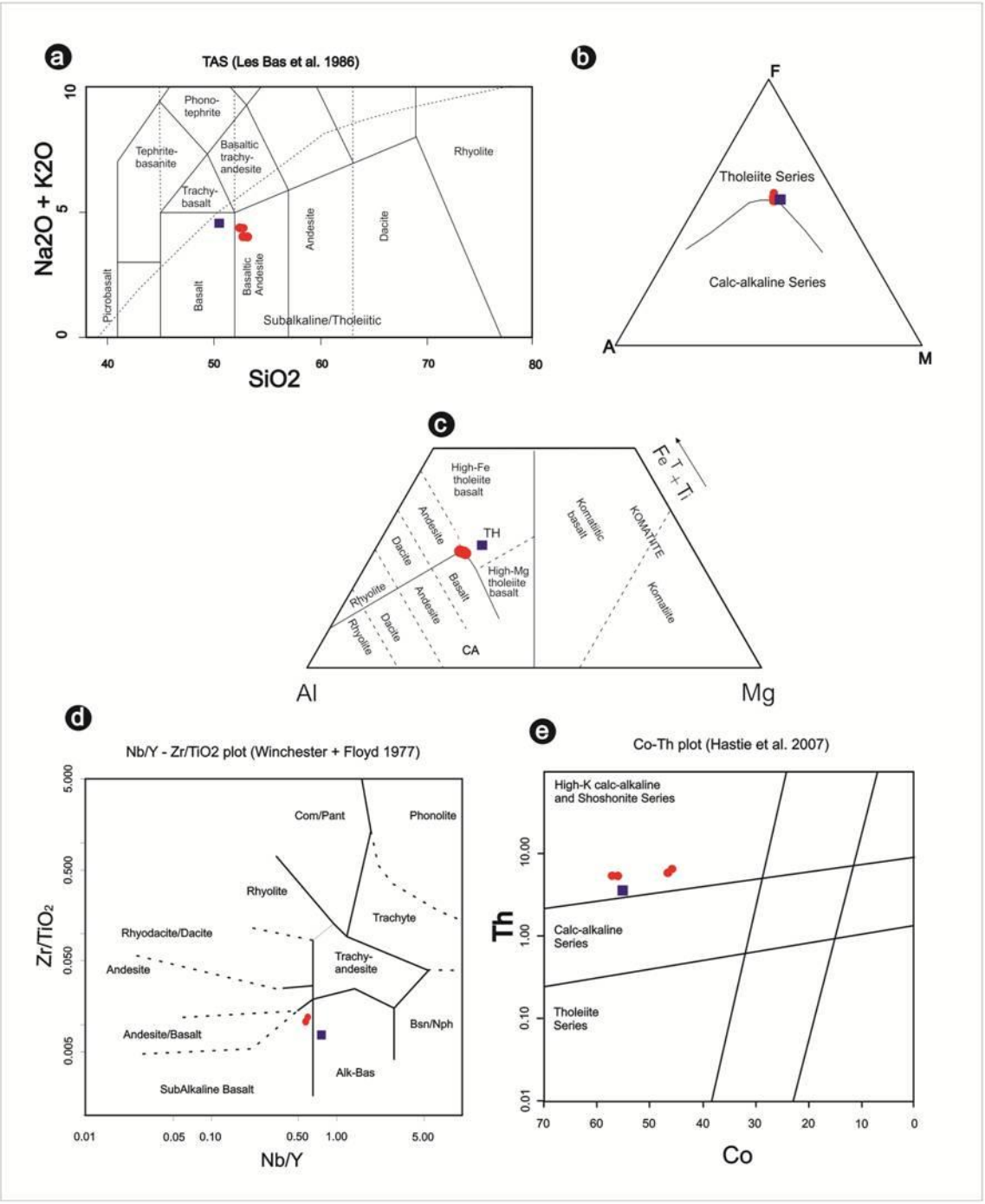

Fig..5.12. Major element classification shows **(a)** basaltic-to-basalt andesitic composition in TAS diagram, **(b)** marginally tholeiitic in AFM diagram of *Irvine and Baragar* (1971), and **(c)** while basalt-alkali basalt to tholeiitic in the plot of *Jensen* (1976). **(d)** Some trace *vs.* major element plots show the subalkaline basalt in character (Nb/Y *vs.* Zr/TiO2 plot). **(e)** Classification scheme of *Hastie et al.* (2007) using Co and Th exhibits marginally high K calc-alkaline to shoshonitic basalt. Solid red circles represent Bandimal unit and solid blue-square represents Pankipalli unit.

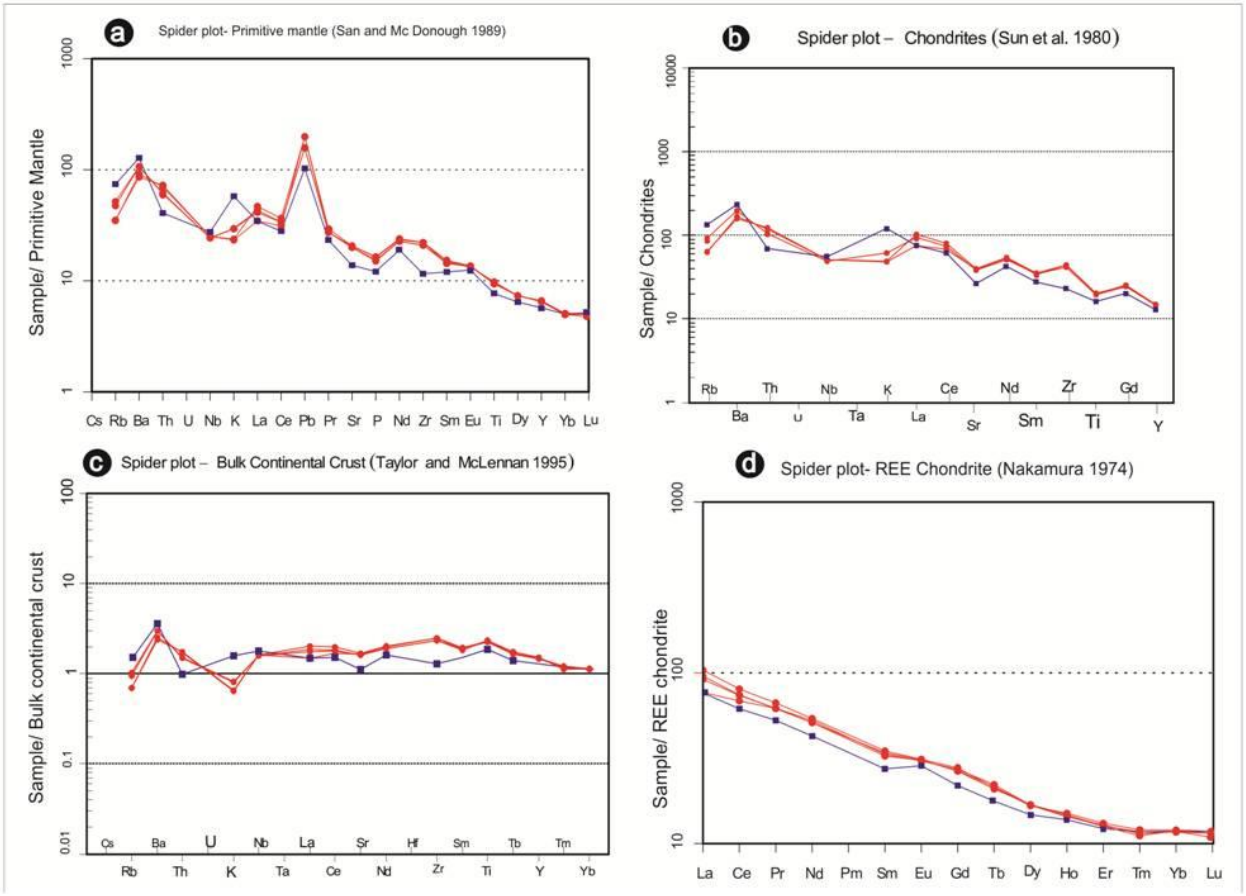

Fig.5.13. (a) Primitive Mantle-normalized multiple trace element pattern; note the enrichment of Pb and Ba and slight depletion of Nb and P in both the plots. **(b)** Chondrite normalized trace elements pattens; overall enrichment of LILEs. **(c)** Bulk continental crust normalized plot; showing slight high values than the average continental crust and enrichment of Ba and depletion of K **(d)** Chondrite normalized rare earth element (REE) pattern showing LREE enriched character.

Table.5.4. Selected incompatible trace element ratio for diabasic rock of Bandimal. The average crust and mantle values are given from Hofmann 1988.

Sample	Th/La	Nb/La	Nb/Th	Ba/Nb	Ce/Pb
10/L7	0.19	0.56	2.9	33.5	4.6
7/21	0.18	0.59	3.3	43.1	5.4
10/L7b	0.25	0.75	3	35.9	3.9
7/21_2	0.18	0.61	3.4	42.9	5.4
7/25	0.16	0.81	5.6	45.5	6.8
Mantle*	0.13	1	8	10	9
Crust*	0.22	0.7	3	22	4

Table .5.5. Rb-Sr and Sm-Nd isotope ratios analysed for the studied samples. Initial εNd values calculated using the present-day values of ($^{143}Nd/^{144}Nd$) = 0.512638 and ($^{147}Sm/^{144}Nd$) = 0.1966 for the chondritic uniform reservoir (*Jacobsen and Wasserburg*,1980); Depleted mantle model ages calculated using the two-stage model of *Liew and Hofmann* (1988).

Sample no.	Sample location	Sm (μg g^{-1})	Nd (μg g^{-1})	$^{147}Sm/^{144}Nd$	$^{143}Nd/^{144}Nd$	Nd (initial)	ε^tNdt = 1420 Ma	T_{DM} (Ga)	$^{87}Sr/^{86}Sr$	$^{87}Rb/^{86}Sr$	Rb (μgg^{-1})	Sr (μg g^{-1})	Sr (initial)	ε^tSr
10/L7 (Whole rock)	Bandimal	6.586496	30.016149	0.1161	0.512004 ± 2.1	0.510919	+2.3	1.7	0.713394 ± 6	1.143	31.73112	466.132	0.709377	+93.05
10/L7 (Pyroxene)	Bandimal	6.866607	26.864702	0.1353	0.512187 ± 2									
10/L7 (Plagioclase)	Bandimal	0.597598	3.699139	0.0881	0.511746 ± 9									
7/25 (whole rock)	Pankipalli	5.049551	23.543071	0.1135	0.511875 ± 2.9	0.510815	+0.3	1.9	0.716740 ± 4.6	0.4939	60.93179	357.224	0.706672	+54.56

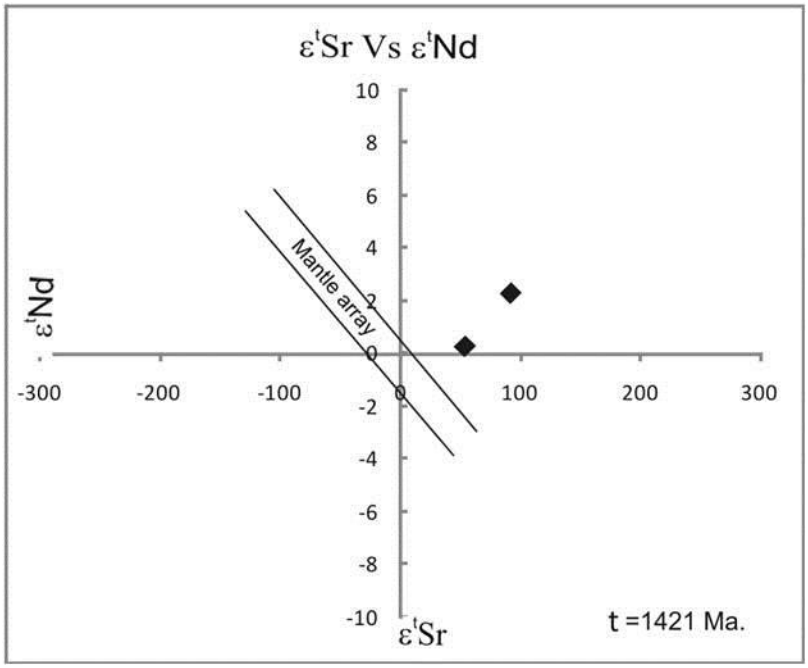

Fig.5.14. ε^tNd *vs.* ε^tSr plot. The values are calculated at t = 1421 Ma. Note the positive displacement away from the mantle values and the whole rock samples plot in the upper right quadrant as both εSr and εNd are positive. This can be due to the contamination of basaltic magma by crustal components that had high Sr abundances yielding R values > 1, where R = (Sr/Nd)basalt /(Sr/Nd)contaminant (*DePaolo and Wasserburg*,1979). The arkosic sediments rich in feldspars could have been the potential contaminant that increased the εSr much more rapidly relative to decreasing the εNd values in the magmas parental to the diabasic intrusive rock.

5.6.3 Geochronology

Fresh rock samples are collected from the central part of the intrusive body, which have been analyzed for Rb-Sr and Sm-Nd isotopic composition. The data are presented in Table 4. Whole rock powder sample was used for both Rb-Sr and Sm-Nd analysis, where as fresh mineral grains of pyroxene and feldspar have been separated for Sm-Nd isotopic analysis. Detailed procedure of mineral separation has been described in Chapter 2.

Sm-Nd mineral and whole rock data define a linear array with reasonable spread in $^{147}Sm/^{144}Nd$ ratios yielding an isochron (Fig.5.15) which corresponds to an age of 1421 ± 23 Ma. (2σ, MSWD = 1.6) with an initial $^{143}Nd/^{144}Nd$ = 0.510922 ± 0.000017 (2σ). As the rock is megascopically and petrographically least altered and unmetamorphosed, this age is considered as the emplacement age of the intrusive.

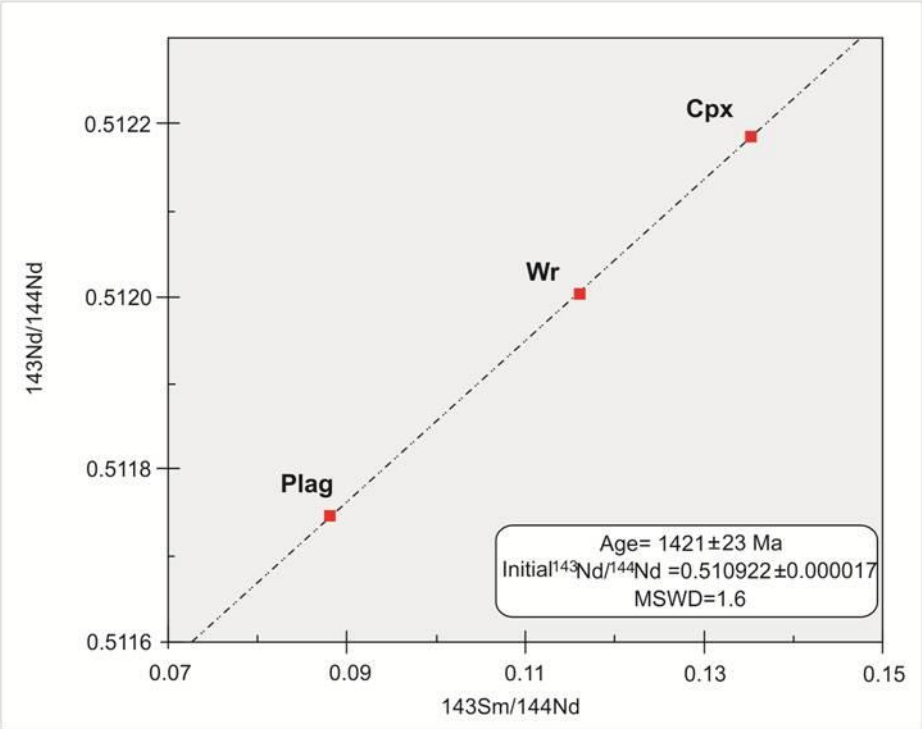

Fig.5.15. Whole rock-mineral Sm–Nd isochron plot yielding an age of 1421 ± 23 Ma (MSWD = 1.6) which is interpreted as the emplacement age of the diabasic intrusive.

5.7 Implications from the geochemical and geochronological data

The major observations from the above data are as follows.

(1) The felsic tuffaceous rock showing a porcellanitic character is rhyolitic to dacitic in composition. The presence of glass shards of different shapes is indicative of their volcanogenic origin. Their bulk rock composition indicates a LILE-enriched and LREE-enriched magma type with indications of deep crustal source or crustal contamination. Chemical character implies this to be volcanic arc granite. Post-depositional silicification

related to some later tectonothermal event debars use of many of the petrogenetic characterizations using geochemistry of the rock.

(2) The felsic tuffaceous unit occurs above the Rehtikhol Formation (the lowermost unit of Singhora basin) all over the exposed eastern and south to southeastern parts of the basin. This field observation implies it to be a part of the basal units of Singhora basin and Chhattisgarh sedimentation. Detailed geochronological study using EPMA chemical age dating has been carried out on monazite and zircon grains. Monazite shows several age clusters in the probability density diagram. However, as the peak(s) around 1500 Ma is showing highest statistical probability, this age is considered to be the age of crystallization of this tuff unit. Further peak fitting analyses yield three strong peaks at close interval *viz.*, 1437 ± 50 Ma, 1499 ± 62 Ma and 1592 ± 145 Ma. There is a possibility that volcanic eruptions occurred in a close time interval. However, the peak values are all within their cummlative error ranges and hence, a particular value is difficult to choose for the age of crystallization. It is noteworthy that commonly the yongest one *i.e.*, 1437 ± 50 Ma (which is incidentally the strongest peak among all) is considered to be the age of crystallization. Recent data of Singhora tuff though predicts even younger age of ~1405 Ma (*Bickford et al.,* 2011b). The age data of the porcellanitic tuff from the present study is decisively ~1500 Ma, but possibly around 1437 ± 50 Ma, on the basis of statistical regression.

(3) All older dates from the monazite and zircon grains of the the studied tuff and their underlying and overlying formations are inherited from the older tectonothermal events in Mesoproterozoic India and its erstwhile neighbors. Euhedral zircon age data (though not very high resolution data) also imply no event younger than 1500 Ma. However, the small grain cluster of monazite and resorbed grain boundaries of some monazite grains yield an age of *ca.* 1000 Ma. Recrystallized zircon grains also yield the similar age. The shapes of monazite and zircon in tuff is indicative of a thermal/hydrothermal event around 1000 Ma. The experimental works also suggest dissolution and reprecipitation of these minerals at different physico-chemical conditions (*Oelkers and Poitrrason,* 2002; *Harlov et al.,* 2011). With all these, it is considered that this basin experienced a hydrothermal activity around 1000 Ma which is the cause of extensive silicification of the rock and can be correlated with the

reported ignimbritic volcanic activity in this basin and the surrounding basins (*Patranabis-Deb et al.,* 2007; *Mukherjee et al.,* 2012).

(4) The mafic rock, on the other hand, has intrusive contacts with the Saraipalli Formation, one unit further above in Chhattisgarh stratigraphy. From the existing field evidence this is considered to be at least younger than the Saraipalli Formation. The studied intrusive bodies at Bandimal and Pankipalli are diabasic in character with ophitic to subophitic texture shown by plagioclase lath and intercrystalline augitic pyroxene and Fe-Ti oxides. The overall geochemical character is of basalt to basaltic andesite with LILE-enrichment against the primitive mantle and LREE-enriched character against chondrite. The trace element distribution against average continental crust, however, does not show any tend implying some amount of contribution of the crust in the magma. The intrusive shows a prominent affinity towards within-plate basalt at Zr/Y vs Zr plot (Fig.5.16) with strong evidence in favor of nonplume-recycled magma as a possible source (Nb/Y *vs.* Zr/Y plot, *Condie,* 2005) (Fig.5.17). Some selective trace element ratios (Th/La, Nb/La, Nb/Th, Ba/Nb and Ce/Pb) are compared with the average crustal and mantle values (Hofmann, 1988). The HFSE elements which are less immobile *e.g.*, Nb, Th and La have their ratios closer to the average crustal values. The incompatible-element enriched basalts have ratios of several strongly incompatible trace elements, including Nb/U and Ce/Pb ratios close to those of the continental crust suggesting that crustal contribution during the genesis of the magma for this studied intrusive. The present data have been compared with the available data of plume related basalts for different other HFS elemental ratios (*e.g.*, Ce/Pb, Nb/La, Ba/La). It has been observed that present data is plotted far away from plume-related rocks. Instead, they have an affinity towards the field of sediment mixing or continental crustal assimilation. Moreover, the positive epsilon values of $Nd_{(t)}$ and $Sr_{(t)}$ imply that this rock has greater $^{143}Nd/^{144}Nd$ and $^{87}Sr/^{86}Sr$ ratios than those in the depleted mantle source of the magma from which it is derived. Using the Sr, Rb, K, Pb, abundance, ratios of Th/La (0.18-0.25), Nb/La (0.56-0.75), Nb/Th (2.9-3.4), Ba/Nb (33.5-43.1) and Ce/Pb (3.9-5.4) (Table. 5.4) in the studied rocks and high $^{87}Sr/^{86}Sr$ ratio partial assimilation of continental crust or sedimentary material within the magma is interpreted. It may reflect derivation of these magmas from incompatible element enriched regions of the sub continental mantle.

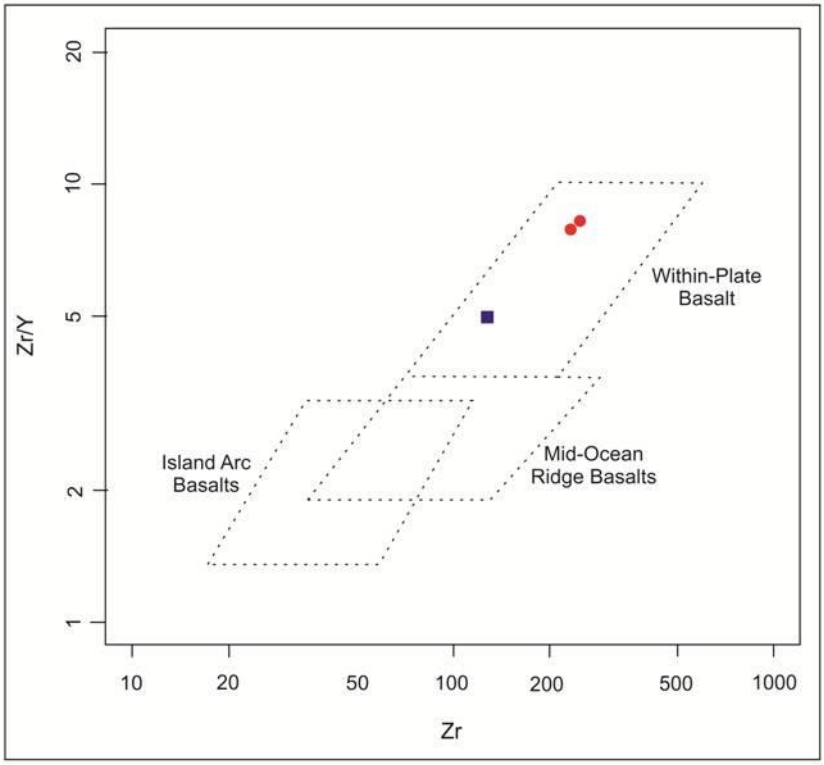

Fig.5.16. Tectonic discrimination diagram using immobile trace elements Zr and Y shows an affinity towards within plate basalt.

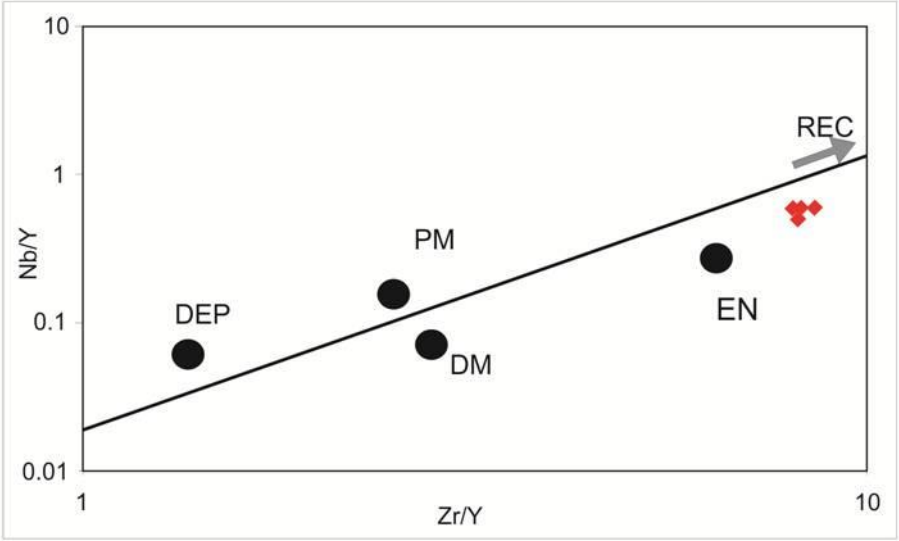

Fig.5.17. Diagram showing mantle composition components and fields for basalts of different tectonic settings. The diagram is after Condie (2005). ♦ : Studied samples, EN: enriched component, PM: primitive mantle, REC: recycled component, DM: shallow depleted mantle, DEP: deep depleted mantle. Note the non-plume recycled magma is the source character for the studied intrusive.

(5) Sm-Nd mineral-rock isochron age yields a value of 1421 ± 23 Ma. (2σ, MSWD= 1.6) with an initial $^{143}Nd/^{144}Nd$ = 0.510922±0.000017 (2σ). This age is considered to be the emplacement age of the studied intrusive. Moreover, the discordant field relationship of the studied intrusive with the Saraipalli strata, an age older than ca. 1420 Ma is proposed for the Saraipalli Formation of Singhora Group

(6) The two studied magmatic rock types in the Singhora Basin offer a unique opportunity to reconcile the ages of their respective crystallization and in turn the relative ages of the overlying and underlying formations. Occurring at the basal part of the basin, this set of information proves useful to fix the age of near-initiation of this particular basin, and as a matter of fact the initiation of Chhattisgarh basin, second largest Precambrian sedimentary basin in India. Moreover, their geochemical characterizations allow narrowing down on the prevailing tectonic setting in this region and their evolution through time. The felsic volcanics imply an operative arc at the margin of the Indian craton at some time between 1400 and 1500 Ma. This cratonic fringe zone was also magmatically active at least till *ca.* 1420 Ma when this basin experienced diabasic magmatism. Interestingly, the heterolithic sediments of Saraipalli Formation lie in between these two events. Now, this may tentatively imply the time taken for deposition of Saraipalli succession, can be either ~80 Ma (considering the crystallization age of tuff to be ~1500 Ma) or lesser, i.e. ~20 Ma (considering the crystallization age of tuff to be ~1440 Ma as revealed from the statistical analyses).

CHAPTER-VI:

BASIN EVOLUTION

Interpretation of basin sediment-fills has evolved with increasing sophistication of stratigraphy and sedimentology over past half century. The current approach is integrative and interdisciplinary and is categorized as a sedimentary geological approach. This interdisciplinary approach focuses on the formation of basins, the nature of their sedimentary fills, maturation of the sediment fills, and timing of events. Certain events clearly show a correlation between process of formation and sedimentary responses. In fact, analysis of timing of events in sedimentary basins plays a crucial role in integrative mode of basin analysis where an attempt is made to determine the geological events and interpreted processes occurred in specific times and how, in fact, they are linked in a causal way (*Klien and Lee,* 1984; *Allen and Allen,* 1990). It must be emphasized that just because certain events occur coincidentally, it does not mean that a correlation of processes exists within a sedimentary basin. The integrative effort to correlate events permits evaluation of processes and responses within basins and isolation of associated variables. Crucial to a reasonable basin evolution model, then, is the accuracy of dating methods used to establish timing of specific events and processes. While biostratigraphy is commonly used for establishing a temporal framework for correlating time-equivalent facies and systems in Phanerozoic successions and to constrain timing of specific events, isotope geochronology serves the only recourse in Precambrian succession that can constrain both event stratigraphy and history of changing chemical processes and their associated petrologic responses.

Along with delineation of events and putting age-bracket for them, a successful basin evolution model should also embody the interpretative basis of sedimentology (sedimentary processes), stratigraphy (spatial relations of sedimentary rock bodies belonging to different time slices), facies and depositional systems (organized response of sedimentary products and processes into sequences and rock bodies of a contemporaneous or time-transgressive nature), paleooceanography, paleogeography and paleoclimatology, sea level analysis (local, global, eustatic), sedimentary petrology and mineralogy of sedimentary rocks to determine source areas and in turn, to constrain the paleocurrent analysis and diagenesis. As many of these aspects are not well constrained for Precambrian basins, for ex. Paleooceanography, paleoclimatology, sea level stand etc., modeling of filling history in basin of this time period is relied mostly on documentation of facies association stacking motif and its variability in space and time (*Criste-blick et al.,* 1988). The present study is also no exception.

SUBCHAPTER-VI-A

6a.1. EVOLUTION OF REHATIKHOL ALLUVIAL FAN AND BRAID-DELTA DEPOSITIONAL SYSTEM

The facies associations across the Rehtikhol-Saraipalli Formations indicate an overall continental to marine depositional system through a coastal set up showing varying interplay between riverine and wave processes (Fig.6.1). Within the continental subaerial part, sediment dispersal on the alluvial fan surfaces was the most widespread and spatially most varied. Depending on the drainage basin morphology and destabilized slope character (bed rock or colluvium), *Blair and Mcpherson* (1994) categorized alluvial fan sedimentation processes into three primary types, viz.: (i) sediment gravity flows triggered by (a) collapse of bedrock cliffs or (b) destabilization of colluvial slopes, and (ii) fluidized gravity flows generated by destabilization of colluvial slopes. Clusters of angular, poorly sorted, granular to bouldery granitic and gneissic fragments (facies A of FA-I) in the Malaikhaman section resemble talus or colluvial cone deposition at the frontal parts of bedrock cliffs. However, detailed field observations revealed that such rock fall deposition was aerially restricted and that the Rehtikhol fan system was dominantly fed by sediment and fluid gravity flows generated in the colluvial slopes. Except for the Malaikhaman section, rock fall fragments can only be observed as outsized clasts present within the sediment gravity flow products (cf., *Beaty and Depolo,* 1989). Such bias towards granular and sandy (occasionally pebbly) sediment gravity flow deposition suggests that the drainage basin was a colluvium covered gently sloping (1–7°) beveled plain with only occasional presence of stiff cliffs (Fig.6.1). The spatial variation in the depositional pattern, i.e., the rock fall deposition at the Malaikhaman section, sediment and fluid gravity flow deposits at the Kodopali and Murmuri sections and medium- to coarse-grained sheet sandstone elements of FA-II (i.e., braid-plain) at the Rehtikhol section, offered scope for interpreting the proximal–distal relationship within the alluvial fan–braid-plain system. The Malaikhaman, Kodopali and Murmuri sections represent the inner and middle fan parts, where sediment and fluid gravity flows (facies types A, B and D of FA-I) were supplied by relatively higher gradient, lower order streams that funneled over short distances resulting in rapid transfer of overland flow and flash flooding (cf., *Patton,* 1988; *Blair and Mcpherson,* 1994). The observed association with sieve conglomerates depicts water percolating down rapidly from the channels in the inner fan part, the more rapidly incising channels consuming most of the water, leaving the shallower ones high and dry. Facies types C and E within the mid-fan part reflect

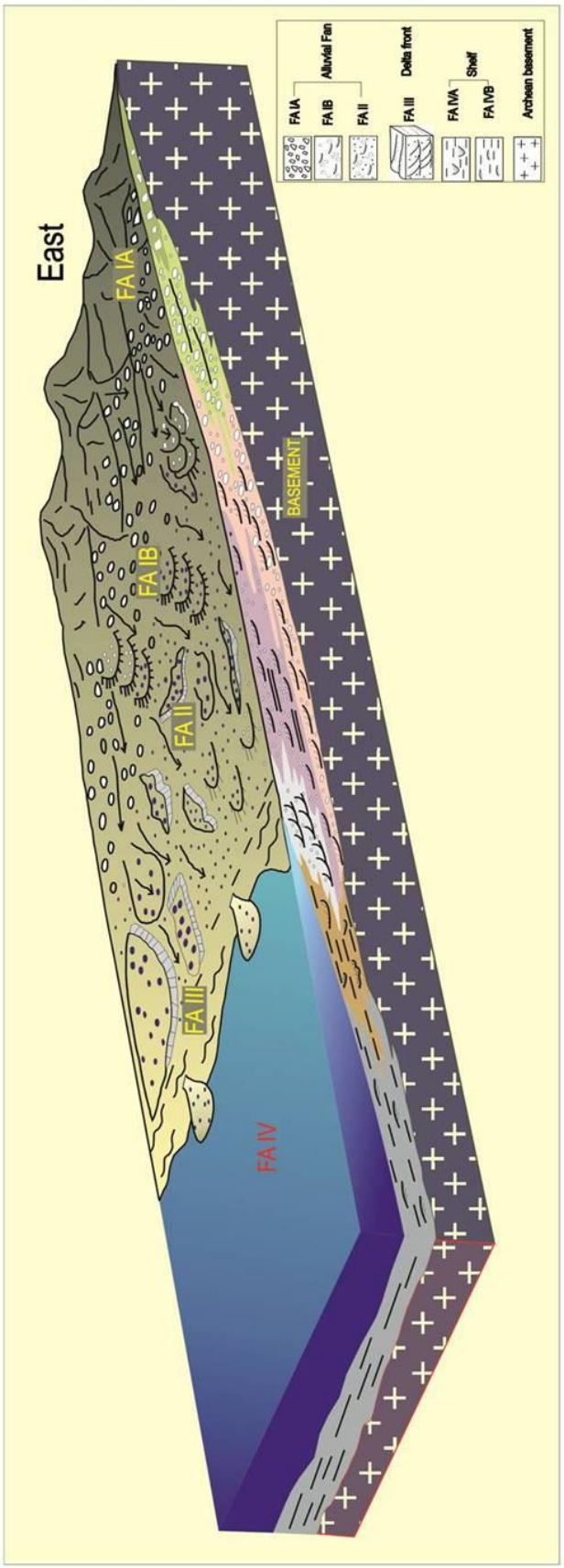

Fig.6.1. Inferred depositional model and resulting facies distribution of the conglomerate/coarse-grained sandstones of the Rehtikhol Formation and mudstones of the Saraipalli Formation. The arrows on the block indicate inferred flow vector from the paleocurrent analysis.

the down-flow equivalents of facies types A and B of the inner (proximal) fan (Fig.3.16). The flows turned increasingly steady and weaker with loss of slope. The predominance of sheet sandstone elements at the Rehtikhol section represents deposition within low-gradient laterally shifting streams attaining a near braid-plain character. One can assume a relatively low depositional gradient at the Rehtikhol section with poor development of FA 1a and complete absence of FA 1b.

In this backdrop, it becomes imperative to discuss distinction between the products of alluvial fan and braided fluvial system in rock record as it, more often than not, remains uncertain in absence of debris flow and sheet flood products (*Bose et al.,* 2008). Fluvial systems belonging to middle or distal fan environments may appear tantalisingly similar with braided fluvial systems, particularly when they are flashy, ephemeral and sheetflood dominated. As Rehtikhol alluvial fan and braid plain system are found mutually associated, it was felt necessary to evaluate the Rehtikhol braided river system through independent paleohydrological estimation so as to decipher whether it represents an independent braid plain system or fluvial-dominated subdivision i.e the mid- or distal part of the Rehtikhol alluvial fan. Addressing similar issue, *Blair and McPherson* (1994) in their seminal paper argued in favour of apparent gap in slope between fans (minimum slope for modern fans 0.026m/m) and rivers (maximum slope for modern rivers 0.007m/m) in nature and suggested distinctiveness of alluvial fans in terms of morphology, hydraulic processes, sedimentological processes and facies assemblages. Subsequent works (*Saito and Oguchi,* 2005; *Hashimoto et al.,* 2008; *Eriksson et al.,* 2006, 2008) involving calculation of hydraulic parameters in modern fans and fluvial systems as well as in their ancient analogues, contradicted the view of *Blair and McPherson* (1994) and opined in favour of a continuum of slopes between humid region fans and flood plain rivers; the observation of *Blair and McPherson* (1994) was considered as an artifact of preferential use of data only from arid and semiarid regions (cf. *Long,* 2011). Notwithstanding possible climatic control on distinctive slope generation that may provoke development of fan and fluvial systems in modern settings, the other important issue is its uniformitarianian application in the vegetation-free Precambrian setting. In particular, the 2.00 – 1.8 Ga. paleoproterozoic time window that has been projected by *Van der Neut and Eriksson* (1999) as an unique sedimentary paleo-environmental window when aggressive weathering in extreme and changing climatic condition led to a higher gradient style of sandy braided channel system (*Eriksson et al.,* 2006) and thereby, making the slope controlled paleohydrolic distinction between the two environments difficult. An unanimous

acceptance of this view, however, could not become possible as paleohydrological data provided by *Els* (1990), first of its kind, from 3.1 - 2.8 Ga Witwatersrand rocks revealed clear separation of slope between fan and fluvial fields. Recent studies by *Eriksson et al.* (2006) and *Sarkar et al.* (2012) on paleohydrolics of fluvial systems belonging to different time domains of Proterozoic provided support in favour of steep channel gradients of fluvial systems transcending the lower slope bound of fan systems making the claim of *Van der Neut and Eriksson* (1999) for unique fluvial style specific to 2.00 - 1.80 Ga time slice further weak. However all available data in literatures on paleohydraulics of river Precambrian systems comes from studies either in Paleoproterozoic basins (Waterberg Group, South Africa; *Van der Neut and Eriksson,* 1999; *Eriksson et al.,* 2006, 2008) of basin belonging to Neoproterozoic time (Sonia Formation, Marwar Supergroup, *Sarkar et al.*, 2012). Signatures from Mesoproterozoic fluvial succession escaped attention so far. Such knowledge gap posed as major constrained in offering a generalized view on high gradient nature of Precambrian river systems. In this backdrop the paleohydrologic study carried out on Mesoproterozoic Rehatikhol fluvial system may offer a significant data based that is helped in developing a generalized perception of nature of Precambrian river system.

The estimated hydraulic parameters for the Rehtikhol fluvial system present at the Malaikhaman, Kodopali and Rehtikhol village sections are provided in Table 3.2 (Chapter-III). Figure.6.2. illustrates binary plots involving average values of bankful water discharge (Q_b in M^3/S) and paleoslope (S in m/m) estimated from the fluvial deposits at the Malaikhaman, Kodopali and Rehtikhol village sections in the backdrop of maximum gradient of rivers (0.007m/m) and minimum gradient for alluvial fans (0.026m/m), earmarked by Blair and McPherson (1994). Also plotted are the estimated paleohydrological data from fluvial deposits belonging to the Paleoproterozoic Boulberg Formation (*Eriksson,* 2006) and Neoproterozoic Sonia Formation (*Sarkar et al.,* 2012) to get a comparative understanding on the nature of Precambrian river systems, in general. It is noteworthy that none of the values from the Rehtikhol fluvial system fall below the gradient of 0.007m/m (i.e in the field of river), neither above the slope value of 0.026m/m i.e in the field of alluvial fan. The values from all the three sections fall within the 'natural depositional gap', demarcated by *Blair and McPherson* (1994) from their studies in modern rivers and alluvial fans, showing consistency with the observations of *Eriksson et al* (2006) and *Sarkar et al.* (2012) made from Boulgerg Formation and Sonia Formation, respectively. Although it is appreciated by workers that

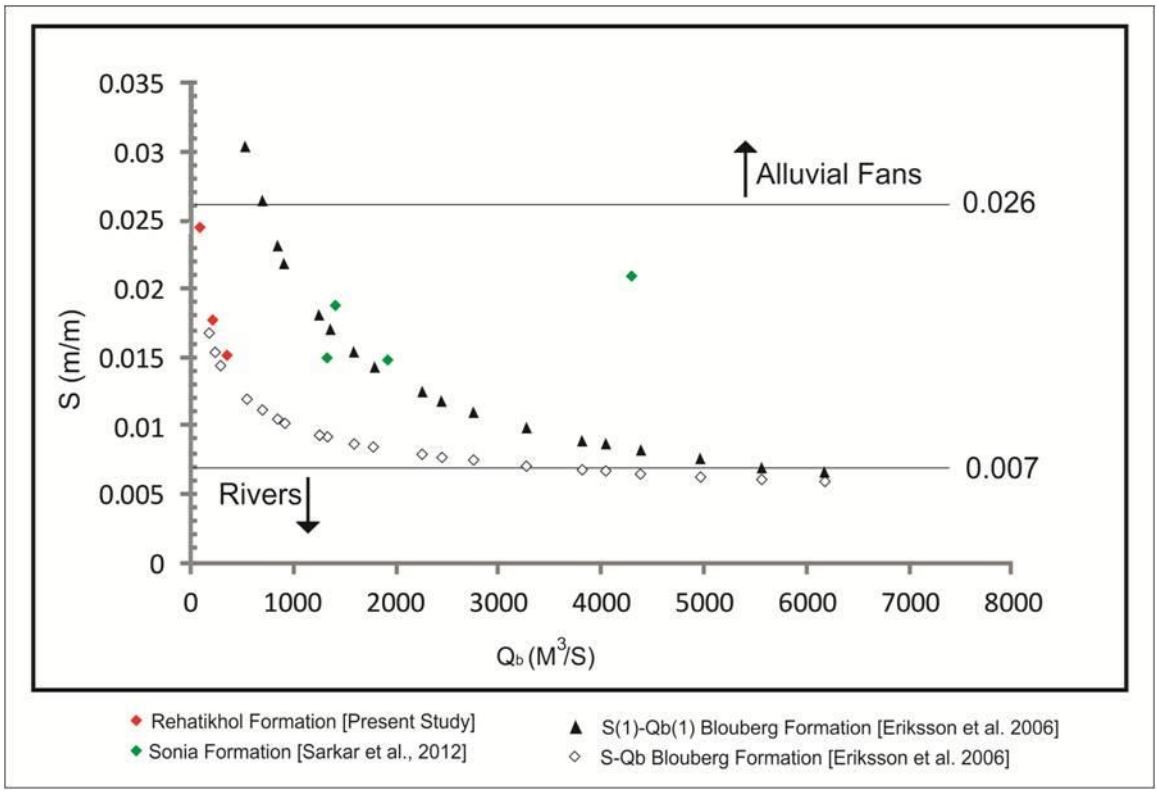

Fig.6.2. Binary plot of paleoslope (S) and mean annual bankful discharge values (Qb) calculated for the Rehtikhol fluvial system present at Malaikhaman, Kodopali and Rehtikhol village sections. Maximum gradient for rivers (0.007 m/m) and minimum gradient for alluvial fan (0.026 m/m) are shown after *Blair and McPherson* (1994). Also plotted are the paleoslope values available in literature from the Boulberg Formation, South Africa and Sonia Formation, India. Note paleoslope values from the Rehtikhol fluvial system fall in 'natural depositional gap', earmarked by Blair and McPherson.

the values obtained through such paleo-hydrolic analyses should not be considered as absolute, yet it is noteworthy that similar results are obtained by researchers from other Paleoproterozoic (2 - 1.8 Ga Waterberg Group, South Africa; Van der Neut and Eriksson, 1999, Eriksson et al., 2006, 2008;) successions and interpreted as of high-gradient braided fluvial signature, unique for the Proterozoic time period. Our data from the Rehtikhol fluvial system match well with paleohydrolic data generated from of Proterozoic river systems in other parts of the World and in the process strengthen the view that Proterozoic river systems, in general, had steep channel gradients, higher than the upper limit of modern river systems. At the same time, restriction of the values below the lower limit of alluvial fan *i.e.* 0.026m/m allowed rejecting the possibility of Rehtikhol fluvial system as an integral part of Rehtikhol alluvial fan system. The scale of the channels in Rehtikhol fluvial system is estimated from the known width: depth relationship using channel-fill thickness as a minimum approximation of channel depth. Modern braided rivers have width: depth ratios from 50:1 to 900:1 (*Roe and Hermansen,* 1993; *Macnaughton et al.,* 1997). In the Rehtikhol braided stream

system, 23 channel-fills yielded a mean thickness of 0.85 m, with a maximum measured thickness of 2.24m. Thus, mean channel widths of the order of 0.04–0.76 km are probable, with some channels perhaps exceeding 2 km in width.

From the paleocurrent direction (Fig.3.19 ; chapter-III) of fluvial system it is inferred that the braid-plain system entered the basin from east–southeast. The deltaic channel systems resemble *Miall's* (1985) distal braid-plain model, and are analogous to modern ephemeral stream systems, and thus were subjected to episodic floods (cf., *Eriksson et al.,* 1995).The tabular deposits were laid down either as turbidites or as tractive current deposits with diffused horizontal and subordinate low-angle cross-stratification. Wave reworking often modified the original depositional character and resulted in (1) lags of coarsest grain sizes produced by the 'washing' out of finer grained sediments, (2) cross-stratifications and laminations as products of bedform migration (a) on the shoreface parallel to the coast (northeast–southwest) or (b) from the sea to the land (northwest to southeast), and (3) low-angle laminations and wave ripples of inferred foreshore origin. The lack of grain rounding and absence of evidence for extensive reworking, however, suggests that the wave energy was only moderate. The gravity flow units (facies K of FA-II) within this setting are products of occasional flood events in the feeder system with the supply of denser sediment–water mixture, as documented from many other Proterozoic shallow water epeiric basin systems (*Button,* 1973; *Van der Neut et al.,* 1991). As such, fluvially influenced units make up most parts of the Rehtikhol braid-delta deposits. The Rehtikhol braid-delta sequence is interpreted essentially as a fluvially dominated, wave-influenced system.

Stratigraphically the Rehtikhol braid delta is overlain by the Saraipalli shelf system. From documentation of retrogradational facies stacking pattern it has been inferred that the Rehtikhol-Saraipalli succession represents a transgressive sequence (Fig.6.3 a & b) deepening upward up to distal shelf domain, beyond storm wave base. The contact between the braid-delta and the shelf associations is conformable, albeit marked by the pyroclastic tuff unit (facies L of FA-III) bearing signatures of basin-scale instability. All through the study area, the invariable presence of this unit at a key stratigraphic level strongly suggests a process–product relationship between

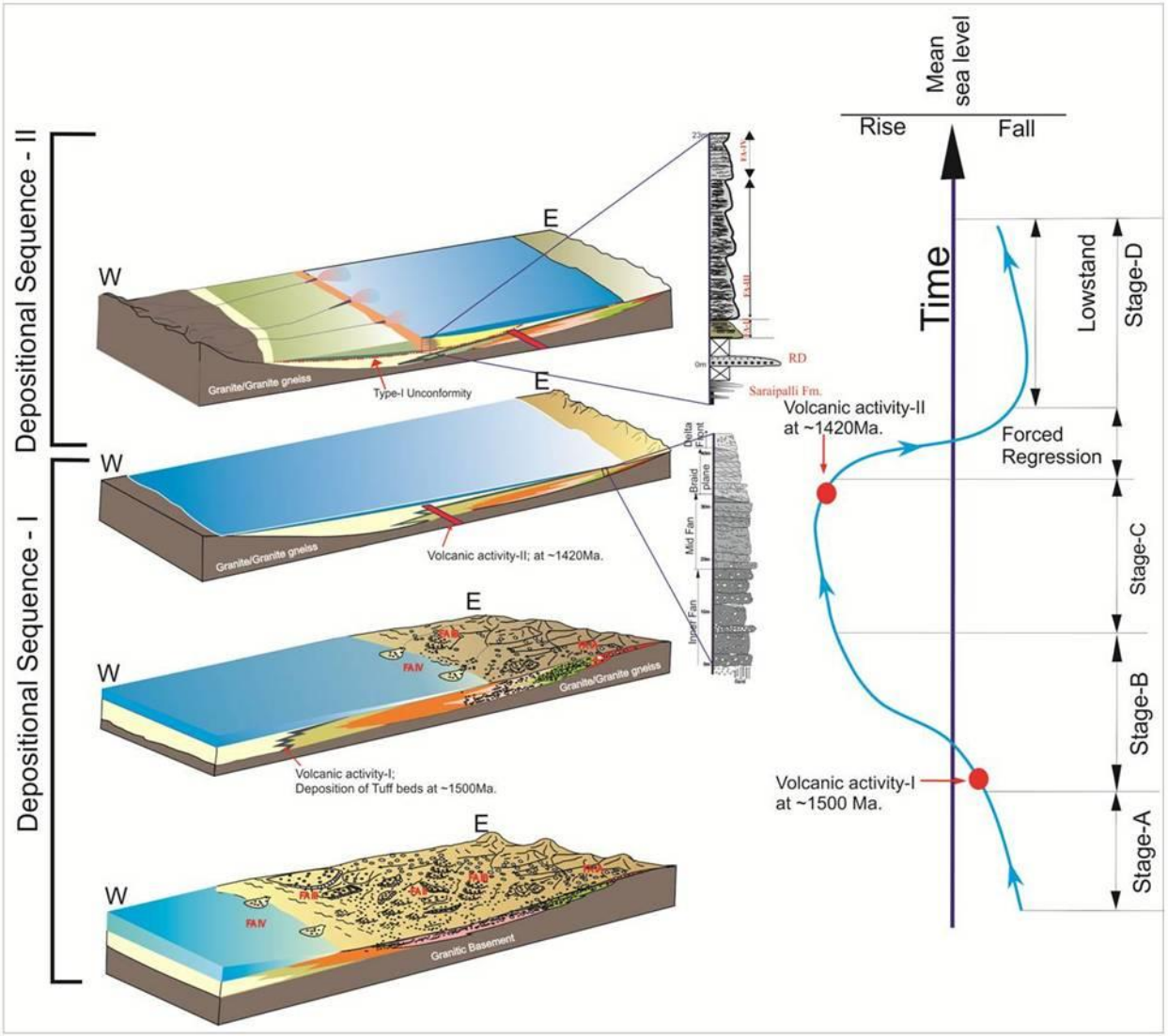

Fig.6.3. Cartoon illustrating palaeoenvironmental setup of Singhora basin in different time slices and its evolution through time. Depositional sequences (DS-1 & DS-2) are marked on the left. The interpreted relative sea level curve reconstructed from palaeoenvironmental shift is shown on the right. Note, timing of magmatic activity projected on the relative sea level curve (discussed in the text).

the eruptive event in the hinterland and the transgression within the Singhora basin. The ~1500 Ma (1470 Ma, to be precise) U-Th-Pb monazite date obtained from the tuff unit allowed constraining the timing of this transgressive event. Possibly the sea level rise in the basin was accomplished by volcanically induced collapse/lowering of the hinterland. The transgression brought the shelf sediments above the continental products without any intervening unconformity.

6a.2. SARAIPALLI SHORELINE AND SHELF CIRCULATION:

Orientation of the mega-ripple crest lines as measured from bedding planes within the facies J sandstone units gave a mean orientation of northeast–southwest, suggesting a NE–SW strike of the paleoshoreline, in as much as swash-bedform crests generally form parallel to the shoreline or the bathymetric contours (*Leckie and Krystinik,* 1989). This is also consistent with the orientation of wave ripple crest trends within the shale/siltstone interbeds of facies M of FA-IV. Paleocurrents from the underlying FA II fluvial unit show a predominant west–northwest transport direction indicating the land was in the east or southeast. Against this backdrop, the nearly shore-parallel orientation (NNE–SSW) of gutters indicates that the seaward or westward downwelling flow was deflected to the left due to geostrophic veering and was dominantly shore-parallel. This is well consistent with the coriollis force in the original southern hemisphere location of the depositional basin (*Williams and Schmidt,* 1996). Operation of such shore-parallel geostrophic currents with strong unidirectional flow component is noticed in modern shelves and shorelines as well (*Swift and Niedoroda,* 1985; *Duke,* 1990). Wave-cum-current ripples mantling the lenticular sandstone units also show migration paralleling the gutter orientation, i.e., southwestward.

Preponderance of erosive features (gutters, channels) and absence of depositional features like hummocky cross-stratification (HCS) in the inner shelf part suggest that it behaved as a 'zone of bypass' under the storm action (*Reading,* 1996; *Einsele,* 2000). Gutter casts are described both in association with unidirectional flows beneath turbidite beds (*Allen,* 1982) as well as with storm generated hummocky cross-stratified (HCS) beds (*Brenchley,* 1985; *Myrow,* 1992; *Martel and Gibling,* 1994) in wave-dominated shorelines. Absence of undoubted unidirectional flow-related erosional features such as flutes or current crescents and occurrence of pervasive wave features within the interbedded shale units, point towards oscillatory or combined flow origin for the inner shelf gutters and channels. *Duke* (1990) suggested that apparent unidirectional structures can be produced by waves with a stronger stroke towards the offshore, and that the unidirectional components in fact run oblique or near parallel to shoreline. Nearshore-parallel gutter orientation and shore-parallel migration of asymmetric ripples mantling the sandstone units suggest a combined flow character for the geostrophic current on the Saraipalli inner shelf; additionally, a strong unidirectional current was superimposed on the wave-generated oscillatory motion.

HCS units were deposited in the distal shelf, i.e., at the farthest offshore limit of sand transport. Despite the presence of hummocky cross-stratification, most of the ripples indicate the dominance of a unidirectional current during the waning stages of storms. However, local wave ripples possibly relate to residual oscillatory motion of the waning storms. Storm events and their influence on the seafloor can be divided into episodes of erosion, bypass and deposition. The depositional event can be further described as a result of spatial and temporal changes in the velocity of unidirectional and oscillatory flow components and their relative magnitudes (*Myrow and Southard,* 1991). On an otherwise muddy, sediment starved distal shelf, hummocky sandy bedforms were initiated and formed when sufficient quantity of sand was locally available, with flows attaining suitable conditions during the storms (*Midtgaard,* 1996). For the duration of single storm events, erosion on some parts of a shelf together with sporadic and patchy sedimentation in the other (distal) part, have been interpreted from several storm-infested Phanerozoic siliciclastic shelves (*Brenchley et al.,* 1993; *Siringanand Anderson,* 1994; *Sarkar et al.,* 2002).

6a.3. RATIONALE BEHIND BOTH ALLUVIAL FAN AND DISTAL BRAID-DELTA MODELS INSTEAD OF A SIMPLE FAN DELTA MODEL.

Distinction between the two depositional models of a coarse grained delta system, i.e., fan-delta and braid-delta, is essentially hinged on characterization of their subaerial part, i.e., alluvial fan or braided river/braid-plain, as shoreline and subaquous components of both may be similar (*Holmes,* 1965; *Mcpherson et al.,* 1987). These systems unconformably overlie stratigraphic basement, and fan deltas, in particular, are bounded by fault systems in many cases (*Ethridge and Wescott,* 1984; *Nilsen,* 1982). Considering the water flow conditions (supercritical and subcritical in the alluvial fan and river systems, respectively), *Blair and Mcpherson* (1994) distinguished critical slope requirements for the two, i.e., $\geq 1.5^{\circ}$ in the case of the former and $\leq 0.4^{\circ}$ for the latter. In the absence of geomorphological attributes, the paleohydraulic estimations carried out from the Rehtikhol fluvial system allowed its interpretation as an independent braid plain system unrelated to the associated alluvial fan system. In sedimentological parlance the dominance of sediment gravity flow (cohesive and non-cohesive types) and unconfined sheet flood deposits along with limited presence of channel flow products in the Malaikhaman, Kodopali and Murmuri sections, have been considered as earmark signatures in favor of an alluvial fan (cf., *Mcpherson et al*., 1987; *Blair and Mcpherson,* 1994).

Distal to the alluvial fan, with the fall in depositional gradient (below the critical slope requirement for a fan development), the braid-plain system developed as a separate geomorphic entity between Malaikhaman and Rehtikhol.

In the studied sections, the subaerial and subaquous units share comparable volumetric proportions. The subaerial sectionis represented by (a) massive/stratified channelised to sheet-like conglomerate units resulting from the non-tractional deposition from cohesive and non-cohesive pseudoplastic flows (FA 1a), and(b) poorly sorted tabular sandstones bearing telltale signatures of deposition within a braided channel system (FA Ib and FA II). As an intermediate between the plastic mudflow and non-Newtonian fluid flow, hyperconcentrated flows are described both from the subaerial and subaquous set-ups. Close mutual association with the alluvial facies, however, prompted us to favor the subaerial origin of the conglomerate units. Meter scale (thickness) braid-plain deposits (FA II) separate the fan conglomerates and the overlying marine strata. The deltaic nature of the strata described here is evident from the general stratigraphic relationships indicating that the coarse-grained clastics of braid-plain origin were debouched within the standing body of water in the west and northwest and reworked by shallow marine agents. The interplay of fluvial and marine processes resulted in a distinct deltaic facies that helped us to distinguish the braid-delta deposit from a classical fan-delta deposit. Going beyond the restrictive approach of putting the depositional framework within a fan-delta or a braid-delta model, the entire system from the Rehtikhol–Saraipalli section is documented, from its subaerial apex (alluvial fan) to subaquous toe (braid-delta) and further basinward, i.e., up to the distal shelf domain.

SUBCHAPTER VI-B

BREAK IN SEDIMENTATION (UNCONFORMITY FORMATION): EVIDENCES FROM PALEOCURRENT PATTERN AND SEDIMENT GEOCHEMISTRY

It is discussed in Chapter-IV that Bhalukona sedimentation commenced on Saraipalli shelf with an unconformable relation. In absence of any specific exposure depicting physical relationship between the Saraipalli argillaceous sediment and coarse, arenaceous Bhalukona sediment, the interpretation is based essentially on process-based facies association analysis and consideration of abrupt paleo-environmental shift across the Saraipalli-Bhalukona boundary. As an unconformity represents a significant hiatus in basin sedimentation history and bear signature for intrabasinal and extrabasinal forcing (individually or combinedly), it is felt that the interpretation be strengthened by other proxies, as well. In absence of any paleontological clue in Precambrian system, the present study undertook recourse of paleocurrent analysis and sediment geochemistry ('Nd' isotope study in particular) for validation of field based interpretation. The purpose was to verify whether there is any paleocurrent shift across the unconformity surface and further, if such shift can be corroborated by change if sediment geochemical signature.

6b.1. PALEOCURRENT STUDY:

Detailed mapping of Bhalukona Sandstone reveals confinement of continental alluvial sediments in the western and north-western corners of the study area; the shallow-marine and deltaic sediments dominate in the east and southeast (Fig.6.4). Distribution of facies types in space, paleocurrent directions measured form different facies associations and crestline orientation of swash bedforms present within FAB-I (Padampur road section) – these signatures together suggest that the Bhalukona Sea had ~northeast-southwest shoreline orientation and the basin opened to the east and southeast. This is also supported by the paleocurrent direction obtained from the FAB-I fluvial association, which shows predominant east–southeast directed sediment transport indicating the land was in the west and northwest. This inference is in striking contrast with the understanding of northwestward opening of Chhattisgarh basin, suggested from the works carried out in the Rehtikhol Formation of Singhora Group and also in the Lohardi and Kansapathar Formations of Chandarpur Group (*Paul and Chakraborty,* 2006; *Patranabis-Deb and Chaudhuri,* 2007; *Chakraborty and*

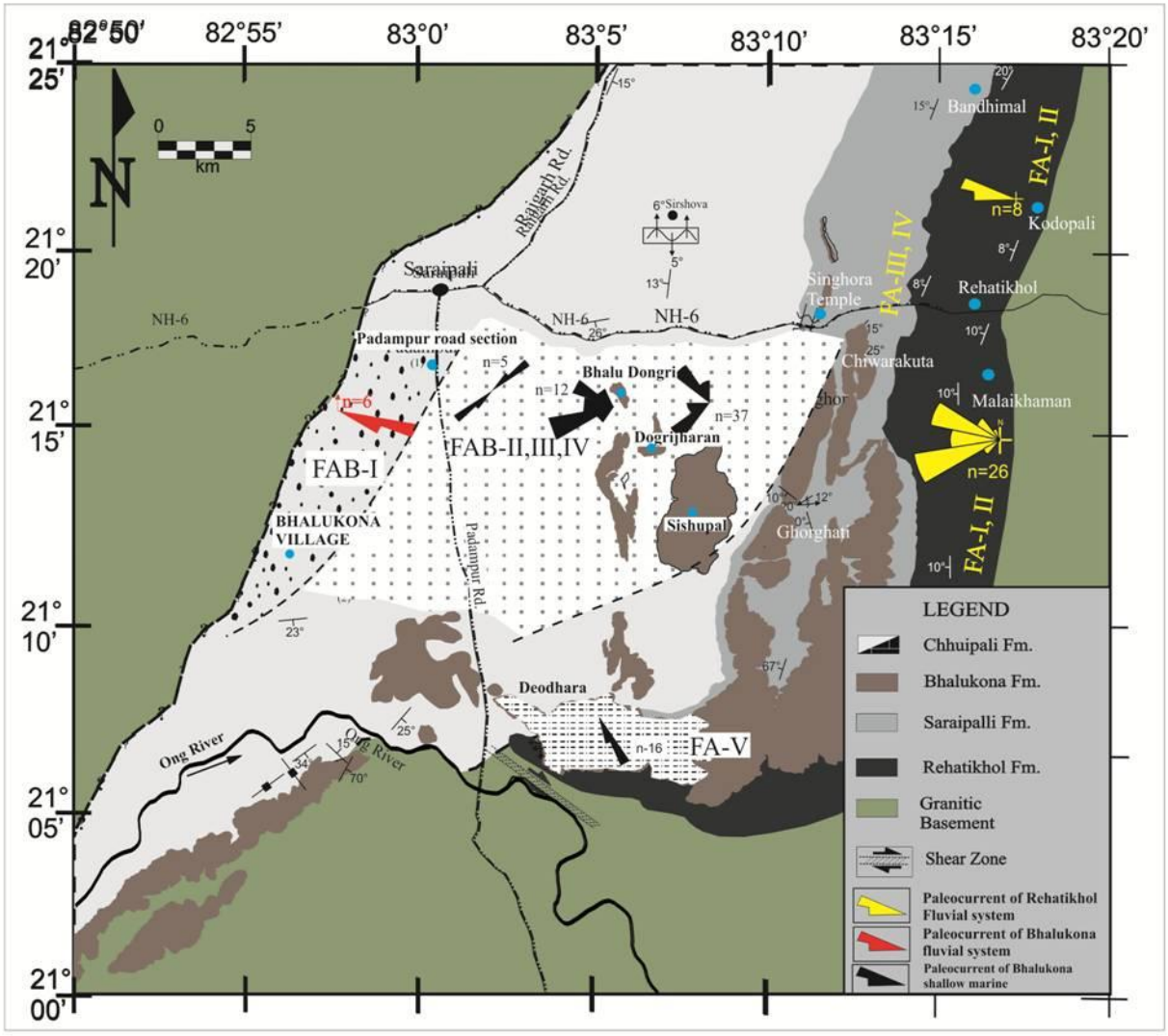

Fig.6.4. Facies association (FA) map of Singhora basin. Representative paleocurrent directions and directional attributes are given on the map. Also given the locations of measured lithologs of studied sections. Please note the proximal-distal relationship of different facies associations.

Paul, 2008), respectively. A reversal in sediment provenance in the Singhora basin during the Bhalukona deposition is inferred, corroboration of which is sought from independent geochemical study.

6b.2. `Nd ISOTOPE´ STUDY OF SEDIMENTS:

Total eleven samples involving all units of both the Saraipalli Formation (four samples from stratigraphic bottom to top) and the Bhalukona Formation (seven samples from stratigraphic

bottom to top) are analyzed for their Sm–Nd isotopes. In the absence of any evidence of post-depositional fractionation, the Sm/Nd ratio of the sediments could represent the source rocks (*Armendáriz et al.,* 2008). The initial Nd isotopic composition represented by $\varepsilon^{t}Nd$ is considered to be a robust parameter to identify the provenance as well as any sudden shift in the provenance. The $\varepsilon^{t}Nd$ values calculated for the time of formation of the Singhora Group (t = 1.42 Ga) for all the samples are showing negative values (Fig.6.5). For the Saraipalli Formation, these values range from −0.2 to −6.6, whereas six samples from the Bhalukona Formation range from −7.0 to −11.5 with exception of a sample having a value of −0.2 (Table.6.1). If the sediments of both the Saraipalli and Bhalukona Formations were derived from the same provenance then their $\varepsilon^{t}Nd$ values should be similar. However, sediments of the Saraipalli Formation and lowermost Bhalukona Formation (at the contact region) must have derived from rocks that had less negative $\varepsilon^{t}Nd$ values (−0.2 to −6.6), and major part of the sediments of the Bhalukona Formation (Middle and Top) were derived from distinctly different sources that had more negative $\varepsilon^{t}Nd$ values (−7.0 to −11.5). If we assume that the source rocks (or their protoliths) that supplied the sediments were of igneous parentage then they could have been similar in age and had different $\varepsilon^{t}Nd$ values. For example, sediments derived in different proportions from a granite ($\varepsilon^{t}Nd$ = −14) and gabbro ($\varepsilon^{t}Nd$ = +6), both formed at the same time, can also explain the variations observed in them. The granitoid rocks typically would have lower Sm/Nd ratios than the gabbro and in the sediments representing different proportions of granite and gabbro will have a range of Sm/Nd ratios correlated with $\varepsilon^{t}Nd$ values will be expected in the sediments. However, sediments of both the Saraipalli and the Bhalukona Formations have nearly uniform Sm/Nd ratio and show no correlation with $\varepsilon^{t}Nd$ values indicating that their provenance also had similar Sm/Nd ratios. The enrichment factor, fSm/Nd is the deviation of $^{147}Sm/^{144}Nd$ of the sample from the chondritic uniform reservoir (CHUR) value which is similar for these two formations in the range of −0.364 to −0.494 (Fig.6.5).Hence, the differences in the $\varepsilon^{t}Nd$ values can be explained if the provenances are made up of similar rocks but of different ages. The Nd model ages are useful to evaluate relative antiquity of the provenance (*Faure,* 1986). Depleted mantle Nd model age (T_{DM}) implies the time of extraction of the source rock of the sediment from a depleted mantle source. The T_{DM} ages are in the range of 1.9 to 2.5 Ga for the Saraipalli Formation, whereas, in the Bhalukona Formation this shows much higher values towards 2.5to 2.8 Ga excepting a sample from the base level (Table.6.1, Fig.6.5).The actual ages of the source rocks could be few hundred million years younger than their respective T_{DM} ages (*Dickins,* 2005). Thus, from the calculated $\varepsilon^{t}Nd$ values, more contributions from juvenile continental sources for the Saraipalli Formation that

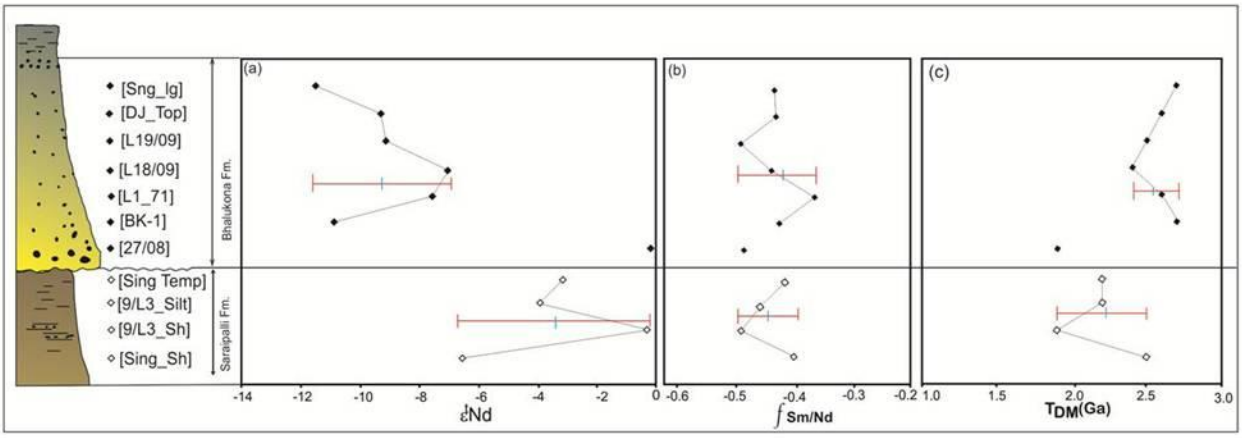

Fig.6.5. Nd isotopic composition of rocks from Saraipalli Formation and Bhalukona Formation. The time-corrected Nd isotopic compositions (ε^{t}Nd, t = 1.42 Ga), enrichment factors (fSm/Nd) and depleted mantle model ages (TDM) are plotted in (a), (b) and (c), respectively. The Y-axis represents the relative stratigraphic positions of the samples. The maximum error in calculation of ε^{t}Nd is ±0.2. The samples collected from continuous exposures are connected by thin line. Note that there is a change of Nd isotopic composition in the early Bhalukona sedimentation history, possibly indicating a sudden provenance change.

Table 6.1. Sm–Nd isotopic compositions of representative samples from the Saraipalli and Bhalukona Formations.

Sample Description	Stratigraphic position	Sm (μg g^{-1})	Nd (μg g^{-1})	^{143}Nd/^{144}Nd**	^{147}Sm/^{144}Nd	(^{143}Nd/^{144}Nd)$_{Initia\ 1}$	ε^{0}_{Nd}	T_{DM} (Ga)	ε^{t}_{Nd}	$f_{Sm/Nd}$
Sng_lg	Bhalukona SSt	1.084	5.843	0.511253±4.0	0.1110	0.510217	-27.0	2.79	-11.5	-0.4356
DJ_Top	Top most Bhalukona SSt	0.220	1.113	0.511369±7.0	0.1116	0.510328	-24.7	2.64	-9.3	-0.4326
L19/09	Top Bhalukona SSt	1.114	5.912	0.511267±2.8	0.0998	0.510335	-26.7	2.51	-9.1	-0.4927
L18/09	Top Bhalukona SSt	0.358	1.726	0.511471±8.4	0.1100	0.510444	-22.8	2.46	-7.0	-0.4406
L1_71	middle Bhalukona SSt	2.881	13.900	0.511581±6.0	0.1250	0.510415	-20.6	2.68	-7.6	-0.3645
BK_1	middle Bhalukona SSt	0.377	1.935	0.511300±13.0	0.1128	0.510247	-26.1	2.77	-10.9	-0.4263
27/08	bottom Bhalukona SSt	0.401	2.106	0.511731±3.8	0.1008	0.510790	-17.7	1.91	-0.2	-0.4877
Sing Temp	contact zone Saraipalli Sst.	3.175	15.791	0.511594±5.0	0.1064	0.510600	-20.3	2.21	-4.0	-0.4589
9/L3_Silt	Saraipalli Sst.	8.837	46.672	0.511711±5.0	0.1146	0.510642	-18.1	2.20	-3.2	-0.4173
9/L3_Sh	Saraipalli Shale	7.883	41.886	0.511721±3.0	0.0996	0.510791	-17.8	1.90	-0.2	-0.4935
Sing_Sh	Saraipalli Shale	2.684	13.667	0.511570±5.0	0.1185	0.510464	-20.8	2.51	-6.6	-0.3976

****The errors quoted are 2 x S.E.**

changes upward in stratigraphy with contributions from older upper continental crustal material are apparent. However, within Saraipalli and Bhalukona Formations variations in the ε^{t}Nd values to extent of 3 and 2 units are seen, respectively. This could be as a result of variations in relative

contributions of sediments from rocks of slightly different crustal residence ages that occurred in their provenance.

The southeasterly paleocurrent measured from the fluvial association of Bhalukona Formation, in striking contrast with the northwestward paleocurrent documented from the underlying Rehtikhol river system (*Chakraborty et al.,* 2009), is noteworthy. Changes in regional drainage patterns associated with unconformity formation associated with the development of incised valleys are documented in literature (*Dalrymple et al.,* 1994; *Fitzsimmons and Johnson,* 2000). In such instances, the distributary channels are pulled towards the vector of maximum base level fall, and accordingly, the progradation direction of associated shoreline may also get realigned. However, near-reversal of paleocurrent (about 180° out of phase), as documented in the present study, cannot be accounted by this reasoning and calls for operation of some allokinetic forcing. A tectonic perturbation possibly caused the reversal of basinal slope and change in sediment provenance from east-southeast to west-northwest in the Bhalukona time. The idea finds support in the shift of Nd- isotope values in course of deposition of Bhalukona succession. The $\varepsilon^{t}Nd$ change recorded from the lower part of Bhalukona succession (except one sample from the contact zone) can be caused either due to lack of sequence preservation, or, merely as an artifact of post-depositional diagenetic alteration. Overlapping and similar *f*Sm/Nd values across the boundary between Saraipalli and Bhalukona Formations suggest no perceptible loss of record (or hiatus) and hence, the sharp change of T_{DM} and $\varepsilon^{t}Nd$ values are interpreted as characters of their respective sources. The contact zone sample at the base of Bhalukona yielding anomalous data, though show the mixing of isotopic characters of Saraipalli Formation, could also be explained by its derivation from greenstone belt rocks, particularly basaltic type. These rocks present at the western part of the studied basin will have higher εNd values than the surrounding granites. With the present database such provenance correlation would be speculative. However, a change in the provenance right in the early history of Bhalukona sedimentation is distinct. Contribution of relatively juvenile materials during the deposition of Saraipalli rocks changed to more contributions from older and less radiogenic crustal components during the depositional history of the Bhalukona Formation. Further, there is an increase in the proportion of older materials added upward within the Bhalukona succession. We interpret this provenance change in the early history of Bhalukona sedimentation and subsequent progressive change during Bhalukona basin-fill history as a result of protracted tectonic disturbance in and around the basin. Corroborative evidence in favor of this contention can be drawn from the

diabase dyke that intruded the Saraipalli Formation prior to Bhalukona sedimentation. The ~1420 ma age obtained from the dyke provide a possible age for this tectonic perturbance in the Singhora basin that caused relative sea level fall in the Bhalukona Sea vis-à-vis shift in sediment provenance. Here, it is noteworthy that the Singhora basin is structurally disturbed and the tectonic disturbance was pulsative with superposition of at least two phases of deformation. With such a background, the above-mentioned provenance shift is a possibility.

SUBCHAPTER VI-C

6c.1. ESTABLISHMENT OF BHALUKONA FLUVIO-DELTAIC SYSTEM AND ITS SPATIO-TEMPORAL EVOLUTION

Fig. 6.3.c illustrates the establishment of Bhalukona shoreline on Saraipalli shelf with fall in relative sea level. From process-based analyses within the Bhalukona succession (chapter-III) a fluvio-deltaic model is proposed with delineation of paleo-environmental products ranging between continental fluvial (FAB-I), beach-foreshore (FAB-II), upper shoreface (FAB-III), lower shoreface (FAB-IV) and wave-dominated delta front (FAB-V). The sediment gravity flow units of FAB-V reflect deposition from hyperpycnal density underflows generated at the river (FAB-I) mouth during high discharge floods (*Mulder and Syvitski,* 1996; *Chakraborty et al.,* 2009). Coarse grain size (medium to coarse sand) and evidences of fair-weather wave reworking suggest that the Bhalukona delta system developed in shallow water, essentially restricted within the shelf domain. Poor grain sorting of FAB-IV sandstones and restriction of wave reworking signatures only at the top of beds imply fluvial dominance in the delta. The mixing of wave- and current-produced structures is typical of wave-influenced delta front (*Bhattacharya and Walker,* 1991), but relative scarcity of wave-produced structures suggests wave influence rather than dominance. Though a physical link between marginal fluvial system (FAB-I) and related delta front (FAB-IV) cannot be established, it can be appreciated that the hyperpycnal flow deposits in the delta front relate to the time during which sediment flux to the sea attains its maximum. Studies in the modern settings revealed that the degree of shelf incision by a forced regressive river system is driven by the exposure of convex-up coastal profile that occurs either at the shelf edge or at the preceding highstand coastline (the coastal prism) (*Posamentier et al.,* 1992; *Talling,* 1998). In absence of shelf-slope break and slope control in the Proterozoic basins, downstream increase in the stream power of Bhalukona incised fluvial system is unlikely. Hence, it is possible that the Bhalukona fluvial system incised the highstand coastal prism developed on the Saraipalli shelf and debouched sediment load ahead of channel confinement in the shallow water delta front setting (within fair weather wave base). The base of FAB-IV is demarcated as correlative conformity related to the Type-I unconformity inferred at the base of FAB-I association in the landward direction. Offlapped and aerially separated from the fluvial association (Padampur road section), the delta front sandstone lobe is deposited at the distal part of the basin (Deodarah section).

The gentle dip of Bhalukona sea floor provoked such long-distance regression of deltaic sandstone (~15 km southeastward) in course of forced regression (cf. *Posamentier and Morris,* 2000).

The cessation of forced regression and inception of stillstand or slow rise of base level established wave-dominated lowstand coastline (Fig. 6.3.d,e). The soft sediment deformation features at the basal part of FAB-III bear indication of basinal instability that contributed in the turn over from the forced regression to the lowstand of sea level. The amalgamated pebble bedset at the sole of FAB-II, traced basin-ward for more than 3.5 km between Bhaludungri and Dongrijharan sections, demarcate the diachronous ravinement deposition formed by wave reworking associated with slow landward retreat of the coastline truncating deposits of preceding forced regression (*Cattaneo and Steel,* 2003). Backstepping incised shorefaces are described in literature from several stratigraphic sections preserving nearshore successions (Cardium E4, E5; *Walker and Eyles,* 1988; *Pattison and Walker,* 1992; Shannon sandstone, *Bergman,* 1994; Beaverhill Lake shoreface, Viking Formation, *Walker and Wiseman,* 1995). It is inferred that the forced-regressive shoreline trajectory became steeper than the shelf dip in the Bhalukona Sea because of increased wave stress on the sea bed (cf. *Carey et al.,* 1999). To regain the equilibrium geometry as a function of prevailing wave energy during subsequent base level rise, wave erosion and ravinement resulted in the coastal areas, where forced regressive profile gradient was steepest and waves are also with highest energy. Occurrence of anomalous coarse sized grains, unavailable in both underlying and overlying sediment column, within the ravinement lag bears proof for complete reworking of fluvial products. This is also supported by steady decline in feldspar content up in the stratigraphic column of nearshore succession from the foreshore-beach (FAB-II) and basal part of upper shoreface (FAB-III) sandstones to the lower shoreface sandstones (FAB-IV). Absence of lag at the base of nearshore sandstones at the Sisupal and Singhora sections and in lieu, gradational transition between the Saraipalli shelf and Bhalukona shoreface in these sections represent basin-ward correlative conformity. In the east and northeast of the basin, absence of Bhalukona rocks and juxtaposition of Saraipalli and Chuipalli argillaceous sediments suggest wedge out of regressive sediment package in the basin-ward direction.

The cms-thick cycles represented by bar-interbar stacking within FAB-III are interpreted as 'parasequences' sensu lato (*Van Wagoner et al.,* 1988). The meter-tick tabular units bounded by planar surfaces, occasionally overlain by shale, represent the parasequence sets with large-scale linkages of

facies or systems tracts (*Brown and Fisher,* 1977; *Proust et al.,* 2001). The surfaces bounding the units without significant erosion or clear break in lithology represent within-trend conformable marine flooding surfaces (FS; *Catuneanu,* 2006). The stacking of tabular units with near-uniform thickness is indicative of aggradational to weakly ret-rogradational stacking in the early lowstand history as the rate of sediment supply matches or occasionally falls behind the slow but steady creation of accommodation on flattened shoreface profile (*Posamentier and Morris,* 2000; *Hampson,* 2000).

With slow, steady rise in relative sea level and concomitant increase in bathymetry, the sediments of lower shoreface (FA IV) overlie the sediments of upper shoreface (FA III) association. The rise in base level and increase in the accommodation space marginally exceeded the sedimentation rate in the lower shoreface and thereby a time-equivalent, landward onlap back across the irregular lowstand topography resulted in the enhanced strength of tidal currents, recorded as bipolar cross-stratified beds in the upper part of FA IV association (cf. *Mellere and Steel,* 1995). Further steepening in the gradient of relative sea level rise resulted outpacing of sediment supply and transgression at the shore-line. The glauconite-bearing granular sandstone beds at the top of FA IV represents ravinement deposition associated with the establishment of transgressive Chuipalli shelf system. Following the Transgression-Regression (T-R) sequence model (*Embry and Johannesen,* 1992), the upper boundary of the lowstand section marks the point between regression and following transgression and is termed as 'maximum regressive surface'. The occurrence of shelf shale of Chuipalli Formation above the surface confirms its 'maximum regression' status (cf. *Catuneanu,* 2002). The coupling of the surface of maximum regression with the interpreted surface of transgression and ravinement allowed us to pick it as a 'Systems Tract' boundary. Lying above forced regressive fluvial deposit (FAB-I) and bounded between the wave ravinement deposit at its base and transgressiveravinement deposit at the top, the nearshore sedimentary package, constituted of FAB-II, III and IV, records the lowstand depositional history of Bhalukona Sea.

6c.2. How far was the retreat of Bhalukona Sea?

Sequence stratigraphic models *(Plint,* 1988; *Plint and Nummedal,* 2000; *Posamentier et al.,* 1992; *Van Wagoner,* 1995; *MacEachern et al.,* 1999) involving forced regressive and lowstand shoreface succession often document fairly thin character for the deposits. The thin deposit character is commonly tagged with, (i) decline in accommodation space and (ii) horizontal TransgressiveSurface of Erosion (TSE)

that cause large-scale transgressive erosion and removal of shoreface succession. While decreasing accommodation can be well-perceived for forced regression, theslow base level rise in lowstand goes against the idea. Also, thepresumption of horizontal TSE cannot be unequivocal unless sediment supply to the shoreface is reduced to zero and sea level rise is an absolute minimum (cf. *Walker and Wiseman,* 1995). In this context, the ~23 m thick foreshore-shoreface succession in a lowstand depositional motif demands analysis for the extent of shoreface retreat on the Bhalukona coastline that allowed its preservation. Working on Joarcham sandstone of Alberta *Walker and Wiseman* (1995) considered 1 mm rise in relative sea level per year, in consistence with the rate of present day eustatic risein sea level, and 1 m per year as the rate of shoreface retreat, as observed in the east coast of USA and estimated 15 m risein TSE with a gradient of 0.04° for 20 km retreat of shoreface. Recognising geographic and chronologic variations, it is generally agreed upon from average global conditions that the continental freeboard remained constant since 2.5 Ga in the entire Proterozoic and Phanerozoic time (*Eriksson,* 1999 and references therein). Considering continental crustal growth, the freeboard and sealevel changes as interdependent variables, we assume that the rate of present day eustatic rise in sea level can be extended to Proterozoic systems as well. However, we differ from *Walker and Wiseman* (1995) in making estimation for rate of shoreface retreat. Working on the muddy (sand <1% in volume) Amazon river mouth, *Allison et al.* (1995) estimated shoreface retreat rate varying between 0.5 and 1 m per year with highest rates recorded in areaswith dentate or terraced shorelines with large tidal amplitude.Sandy (medium to coarse-grained) Bhalukona coastline without (i) any large-scale tidal signature and (ii) evidences favouring terraced shoreline character allowed us to favour the lower bound of shoreface retreat rate, i.e., 0.5 m per year. Though the exposure constraint and deformed nature of the terrain did not allow us estimation of net shoreface retreat in the Bhalukona Sea that allowed preservation of ~23 m of shoreface succession, if we go by present day rate of eustatic rise, i.e., 1 m per year and average rate of shoreface retreat 0.5 m per year, it requires ~11.5 km retreat of the shoreline (Fig.6.6). It may be pertinent to mention here that the measured total exposure width of FAB-II and FAB-III rocks in the studied area in paleoshoreline (NNE-SSW) perpendicular section is also consistent with the obtained value i.e., around 12 km (Fig.6.4).

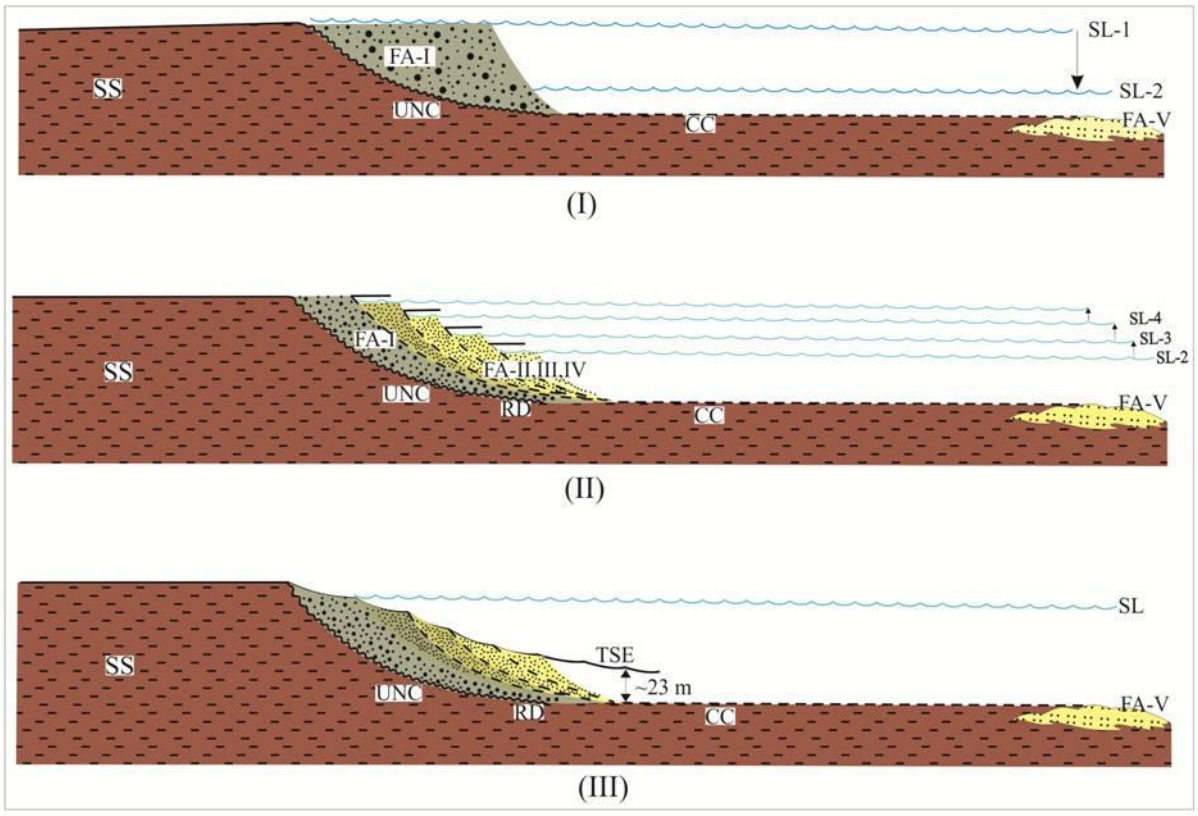

Fig.6.6. Interpretation of the events that led to the formation of Bhalukona regressive succession (i) base level fall, formation of incised fluvial valley and detached delta lobe (Type-I unconformity), (ii) slow, stepwise increase in relative sea level, landward and upward migration of shoreface causing erosion of underlying alluvial sediment and formation of ravinement deposit and (iii) the landward and upward migration of shoreface during transgressive erosion formed a TSE. Vertical double-headed arrow shows the section preserved as a result of transgression.

CONCLUSION

- Facies and paleoenvironmental analysis revealed presence of environmental products ranging between continental alluvial fan and braid plain system to distal marine shelf beyond storm wave base in Rehatikhol and Saraipalli Formation with transitional delta in between. A gently sloping source area in east-southeast of the study area is inferred.

- Cross-set thickness based paleohydraulic estimation on the products Rehatikhol braided alluvial system show paleoslope values higher (0.015m/m of Malaikhaman section, 0.018m/m of Kodopalli section and 0.024m/m of Rehatikhol section) than the modern river systems (0.007m/m). Such observation is well consistent with results obtained from alluvial deposits of Precambrian time preserved in other parts of the world. The present study from Mesopropetrozoic system, in a way, fills the informational gap as the available studies in literature are either from deposits of Paleoproterozic or Neoproterzozoic time.

- The coastline of the Singhora basin in Rehatikhol and Saraipalli time was trending NNE-SSW and river system entered the basin from east-southeast. The Saraipalli shelf was wave influenced with intermittent insurgence of storm action. Inner shelf mostly acted as a bypass zone whereas most of storm derived sedimentation was in outer shelf domain.

- Operation of geostrophic currents on the Singhora shelf has been inferred from the directional relationship of gutters with the inferred orientation of the shoreline.

- From facies sequence development pattern a transgressive buildup history is suggested for the Rehatikhol-Saraipalli package. Geochronology of tuffaceous unit present at the boundary of two Formations allowed fixing of ~ 1500 Ma age for the transgressive event. Denudation of the source area, increasing bathymetry with relative rise in sea level, or a combination of both forced the transgression. Collapse of hinterland physiography under the forcing of volcanic event possibly acted as a triggering event. As such, both extrabasinal and intrabasinal forcings contributed to the deepening-upward trend.

- Incursion of Bhalukona fluvial system on Saraipalli shelf mark the history of base level fall and formation of incise valley. A Type-I unconformity (with ~10m incision) is inferred at the base of Bhalukona fluvial deposit. The unconformity changes basinward to correlative conformity. In shallow marine part wave reworking of fluvial deposits formed ravinement deposit that got merged with the unconformity surface.

- Shift in neodymium isotope (avarage ε^{t}Nd: -3.5 to -7.9; avarage T_{DM}: 2.20Ga to 2.53Ga) and reversal in paleocurrent direction (from WNW to ESW) across the Saraipalli - Bhalukona boundary demarcate the unconformity surface. A possible reversal in source area is presumed.

- Tectonic forcing is suggested behind the unconformity formation. Evidences put forward in favor of this argument are i) Shift in 'Nd' isotope value across the Saraipalli-Bhalukona contact ii) Reversal of paleocurrent across the unconformity and iii) emplacement of diabase intrusive within the Saraipalli Formation immediately before the onset of Bhalukona sedimentation.

- As far as the magmatic rocks, occurring in and around the Singhora basin are concerned the present study clearly reveals that the basin was tectono-magmatically active in course of its sedimentation history. There is a possibility of arc-related tectonism at the eastern margin of erstwhile Indian craton. Global-scale volcanic arc magmatism of similar age is also indicated from some other continental blocks where subduction-related continental outgrowth was ongoing (*Zhao et al.,* 2009). Though, further geochemical, in particular isotopic studies are needed. The present at the present undestanding suggest that the east Indian cratonic margin was possibly a part of that global-scale accretionary process. The pulsative tectono-magmatically active east Indian cratonic margin is evident felsic volcanic-arc granitic magmatisim at 1500 Ma (present study) and within plate basaltic intrusion at ~1420 Ma (present study) in course of Singhora sedimentation. Possibily this tectonomagmatic activity continued till the emplacement of Sukhda tuff at ~1000 Ma (*Patranabis-Deb et al.,* 2007).

- A regressive history is documented from the arenaceous Bhalukona package, which reveals presence of paleo-environmental products ranging from fluvial through shallow marine (beach shoreface) to delta. The regressive history is further divided into two Systems Tracts viz. forced regression and low stand. While the Bhalukona fluvial system represent the product of forced regression, the aggradational and weak retrogradational stacked beach-foreshore, upper- and lower-shoreface sediments, in order of superposition, record the lowstand depositional history.

- Taking into consideration ~23 m preserved shoreface succession, 1 m per year eustatic rise consistent with present day rate and average rate of shoreface retreat 0.5 m per year, ~11.5 km retreat for the Bhalukona shoreline is estimated in its lowstand history.

- Increase in sea level rise and flooding of Bhalukona coast line terminated the Bhalukona sedimentation and set the Chuiaplli shelf systems in operation.

- Application of sequence stratigraphic rationale allowed divisioning of studied stratigraphic interval into two depositional sequences viz. DS-1 and DS-2. The intraformational unconformity at the base of Bhalukona Formation divides two sequences. Bounded between nonconformity at its base and Type-I unconformity at its top, DS-1 involving both Rehtikhol and Saraipalli Formations records a transgressive history, while the DS-2, studied only for its basal parts, records products belonging to forced regression and lowstand.

ACKNOWLEDGEMENT

With great pleasure I take this opportunity to express my deep sense of gratitude to Dr. Kaushik Das and Dr. Partha Pratim Chakraborty for their academic guidance. Their ability to come up with solution for problem is beyond compare. Apart from there scientific acumen, cool temperament and positive attitude are the qualities that I would wish to presses. There approach to both scientific research and life are exceptional and admirable. I am fortunate to have had them as my Ph.D supervisor.

I am grateful to Prof. Hiroshi Hidaka, Department of Earth and Planetary System Science, Hiroshima University for his constant support and help.

I thank to Prof. S. Balakrishnan for his guidance in the Isotope Geochemical Lab, Pondicherry University and all his advice that ware always motivating. I would like to say thanks to my lab-meets and faculty members of Pondicherry University and Delhi University for their kind cooperation and supports. I also thank to the faculty members of Presidency University specially Drs. Sankar Bose, Arijit Ray and Kalyan Halder for their fruitful suggestions and supports during the entire tenure of my work.

I duly acknowledge the help rendered by Drs. Subrata Karmakar, Ashish Sarkar and Tapash Gongopadhyay and several master's and Ph.D students of ISM Dhanbad (Bukun, Shruti, Arun, Atri, Pubali), IIEST Shibpur (Narayan, Arindam, Subhojit, Arijit and students of 2013 batch) IIT-Bombay (Avijit), Delhi University (Manoranjan and Pritam) during the field works at Chhattisgarh and even after that. Especially I would like to express my special thanks to Subhojit for his useful contributions and supports. I am feeling very fortunate to get him as co-worker.

You do not get to do good work, or for that matter anything, if you do not have good support from your friends, seniors and juniors around you. I am lucky to have several of them who had propelled me to whosever I am their constant love and encouragement. My Seniors, friends and juniors of T.D.B College- Ranigunj, Presidency College- Kolkata, ISM- Dhanbad, IIEST- Shibpur, Delhi University, IIT-Kharagpur, IIT-Bombay and Geological Survey of India, specially Mr. Supriya Chakraborty, Sandeep Neogi and Dr. Bibhas Karmakar, I think you for being with me always.

The financial support I received from Department of Science and Technology (DST), India (as a project Junior Research Fellowship) and later from Council of Scientific and Industrial Research (CSIR), India (as a Senior Research Fellowship) is duly acknowledged. I also thanks to DST for necessary travel support to attend the 29th Meeting of International Association of Sedimentologist, Austria in 2012. I thank to Balasore Alloys Limited (formerly Ispat Alloys Limited) where currently I am employed and my colleagues for their supports form last one year.

Words can not express how grateful I am to my parents and my wife for all of the sacrifices that you've made on my behalf. Without your efforts, I would not have come this far.

Date: (PRIYABRATA DAS)

REFERENCES

Alexander, J., Leeder, M. R., 1987. Active tectonic control on alluvial architecture. In: Ethridge, F.G., Flores, R.M., Harvey, M.D. (Eds.), Recent Developments in Fluvial Sedimentology. Society of Econ. Paleont. Mineral, Tulsa, special publication 39, 243–252.

Allen, J. R. L., 1965. Finning upward cycles in alluvial succession. Geol. Jour. 4, 229-246.

Allen, P. A. Allen, J. R., 1990. Basin analysis: principles & applications. Blackwell sciences. Oxford.

Allen, J. R. L. 1982. Mud drapes in sand-wave deposits: a physical model with application to the Flokestone Beds (Early Cretaceous south England). Philosophical Transaction of Royal society, London, 23, 65-80.

Allen, J. R. L., 1983. Studies in fluviatile sedimentation: bars, bar complexes and sandstone sheets in low sinuosity braided streams) in the Brownstones (L. Devonian) Welsh Borders. Sedimentary Geology 33, 237–293.

Allen, P. A., 1997. Earth Surface Processes. Blackwell, Oxford, p. 404.

Allison, M. A., Nittrouer, C. A., Faria Jr., L. E. C., 1995. Rates and mechanisms of shoreface progradation and retreat downdrift of the Amazon River mouth. Marine Geology 25, 373–392.

Anand, M., Gibson, S. A., Subbarao, K. V., Kelley, S. P., Dickin, A. P. 2003. Early-Proterozoic melt generation processes beneath the intra-cratonic Cuddapah Basin, Southern India. Journal of Petrology 44, 2139–2171

Armendáriz, M., López-Guijarro, R., Quesada, C., Pin, C., Bellido, F., 2008. Genesis and evolution of a syn-orogenic basin in transpression: insights from petrog-raphy, geochemistry and Sm–Nd systematics in the Variscan Pedroches basin (Mississippian, SW Iberia). Tectonophysics 461, 395–413.

Babu, R., Singh, V. K., 2011. Record of aquatic carbonaceous metaphytic remains from the Proterozoic Singhora Group of Chhattisgarh Supergroup, India and their significance. Journal of Evolutionary Biology Research 3, 47–66.

Banerjee, D. M., Mazumdar, A., 1999. On the late Neoproterozoic-early Cambrian transition events in parts of east Gondwanaland Neoproterozoic. In Roy A.B. (ed) special issue Neoproterozoic crustal evolution and India: Gondwana linkage. Gondwana Research 2, 199-211.

Beaty, C. B., Depolo, C. M., 1989. Energetic earthquakes and boulders on alluvial fan: is there a connection? Bulletin of Seismological Society of America 79, 219–224.

Benvenuti, M., 2003. Facies analysis and tectonic significance of lacustrine fan-deltaic successions in the Pliocene-PliestoceneMugello basin, central Italy. Sedimentary Geology 157, 197–234.

Bera, M. K., Sarkar, A., Chakraborty, P. P., Loyal, R. S., Sanyal, P., 2008. Marine to continental transition in Himalayan foreland. Geological Society of America Bulletin 120 (9–10), 1214–1232.

Bergman, K. M., 1994. Shannon Sandstone in Hartzog Draw- Heldt Draw fields rein-terpreted as
detached lowstand shoreface deposits. Journal of Sedimentary Research B64, 184–201.

Best, J. L., 1996. The fluid dynamics of small-scale alluvial bedforms. In: Carling, P.A., Dawson, M.R. (Eds.), Advances in Fluvial Stratigraphy. John Wiley and Sons, New York. 67–125.

Beukes, N. J., 1996. Sole marks and combined-flow storm event beds in the Brixton Formation of
the siliciclastic Archaean Witwatersrand Supergroup, South Africa. Journal of Sedimentary Research A66 (3), 567 576.

Bhadra, S., Gupta, S., Banerjee, M., 2004. Structural evolution across the Eastern Ghats Mobile Belt—Bastar craton boundary: hot over cold thrusting in an ancient collision zone. Journal of Structural Geology 26, 233–245.

Bhaskar Rao, Y. J., Pantulu, G. V. C., Damodara Reddy, V., Gopalan, K., 1995. Time of early sedimentation and volcanism in the Proterozoic Cuddapah basin, south India: evidence from the Rb–Sr age of the Pulivendla mafic sill. Mem. 33, Geol. Soc. India, 329–338.

Bhattacharya, J., and Walker, R. G., 1991. Facies and facies successions in river- and wave dominated depositional systems of the Upper Cretaceous Dunvegan Formation, northwestern Alberta: Bulletin of Canadian Petroleum Geology, v. 39, p. 165–191.

Bickford, M. E., Basu, A., Patranabis-Deb, S., Dhang, P. C., Schieber, J., 2011a. Depo-sitional history of the Chhattisgarh basin, central India: constraints from new SHRIMP zircon ages. The Journal of Geology 119, 33–50.

Bickford, M. E., Basu, A., Patranabis-Deb, S., Dhang, P. C., Schieber, J., 2011b. Depo-sitional history of the Chhattisgarh basin, central India: constraints from new shrimp zircon ages: a reply. The Journal of Geology 119, 553–556.

Bickford, M. E., Basu, A., Mukherjee, A., Hietpas, J., Juergen, S., Patranabis-Deb, S., Ray, R. K., Guhey, R., Bhattacharya, P., Dhang, P. C., 2011c. New U–Pb SHRIMP zircon ages of the Dhamda Tuff in the mesoproterozoic Chhattisgarh Basin, Peninsular India: stratigraphic implications and significance of a 1-Ga thermal-magmatic event. Journal of Geology 119, 535–548.

Biju-Sekhar, S., Yokoyama, K., Santosh, M., Pandit, M. K., Okudaira, T., Yoshida, M., 2001. EPMA chemical ages of Paleoproterozoic granitoids from NW India and their significance. Gondwana Research 4, 577–578.

Biswal, T. K., Sinha, S. 2003. Deformation history of the NW salient of the Eastern Ghats Mobile Belt, India. Journal of Asian Earth Sciences 22, 157–169.

Biswal, T. K., 2000. Fold-thrust belt geometry of Eastern Ghats Mobile Belt, a structural study from its western margin, Orissa, India. Journal of African Earth Science Special Issue 31 (1), 25–33.

Biswal, T. K., Biswal, B., Mitra, S., Roy Moulik, M., 2002. Deformation pattern of the NW terrane boundary of the Eastern Ghats Mobile Belt, India A Tectonic Model and Correlation with Antartica. Gondwana Research 5 (1), 45–52.

Biswal, T. K., De Waele, B., Ahuja, H., 2007. Timing and dynamics of the juxtaposition of the 442 Eastern Ghats Mobile Belt against the Bhandara Craton, India: a structural and zircon 443 U–Pb SHRIMP study of the fold-thrust belt and associated nepheline syenite plutons. Tectonics 26, 1–21.

Blair, T. C., 1987. Sedimentary processes, vertical stratification sequences, and geomorphology of the Roaring River alluvial fan, Rocky mountain National park, Colorado. Journal of Sedimentary Petrology 57, 1–18.

Blair, T. C., McPherson, J. G., 1994. Alluvial fans and their natural distinction from rivers based on morphology, hydraulic processes, sedimentary processes, and facies assemblages. Journal of Sedimentary Research 64, 450–489.

Blum, M. D., Tornqvist, T. E., 2000. Fluvial responses to climate and sea-level change: a review and look forward 47, 2–48.

Boggs Jr., S., 1995. Principles of Sedimentology and Stratigraphy. Prentice Hall, New Jersey, p. 774.

Bose, P. K, Chakraborty, P. P., 1994. Marine to fluvial transition: Proterozoic Upper Rewa Sandstone, Maihar, India. Sedimentary Geology 89, 285–302.

Bose, P. K., Chaudhuri, A. K., 1990. Tide versus storm in epeiric coastal deposition: two Proterozoic sequences Geol. J., 25 (1990), pp. 81–101

Bose, P. K., Sarkar, S., Mukhopadhyay, S., Saha, B., Eriksson, P., 2008. Precambrian basin-margin fan deposits: Mesoproterozoic Bagalkot Group, India. Precambrian Research 162, 264–283.

Bose, P. K., Eriksson, P. G., Sarkar, S., Wright, D. T., Samanta, P., Mukhopadhyay, S., Mandal, S., Banerjee, S., Altermann, W. 2011. Sedimentation patterns during the Precambrian: a unique record? Journal of Marine and Petroleum Geology 33, 34-68.

Bose, P.K., Chaudhuri, A., Seth, A., 1988. Facies, flow and bedform patterns across a storm-dominated inner continental shelf: Proterozoic Kaimur Formation, Rajasthan, India. Sedimentary Geology 59, 275–293.

Bourgeois, J., 1980. A transgressive shelf sequence exhibiting hummocky crossstratification: the Cape Sebastian Sandstone (upper Cretaceous), southwestern Oregon. Journal of Sedimentary Petrology 50, 681–702.

Brandl, G. and de Wit, M.J., 1997. The Kaapvaal Craton, South Africa. In: Greenstone Belts(M.J. de Wit and L.D. Ashwal, Eds), Oxford Monograph on Geology and Geophysics 35, 581-608.

Branney, M. J., Kokellar, B. P., 1992. A reappraisal of ignimbrite emplacement: progressive aggradation and changes from particulate to nonparticulate flow during emplacement of high-grade ignimbrite. Bulletin Volcanologique 54, 504–520.

Brenchley, P. J., Oickerili, R. K., Stromberg, S. G., 1993. The role of wave reworking on the architecture of storm sandstone facies, Bell Island Group (lower Ordovician), eastern Newfoundland. Sedimentology 40, 359–382.

Brenchley, P. J., 1985. Storm influenced sandstone beds. Modern Geology 9, 369–396.

Bridge, J. S., Mackey, S. D., 1993. A theoretical study of fluvial sandstone body dimen-sions. In: Flint, S.S., Bryant, I.D. (Eds.), Geological Modeling of Hydrocarbon Reservoirs. International Association of Sedimentologist, Special Publication 15, pp. 213–236.

Bridge, J. S., 2006. Fluvial facies models: recent developments. In: Posamentier, H.W., Walker, R.G. (Eds.), Facies Models Revisited. SEPM special publication, vol. 84, pp. 85–170.

Brown, L. F. Jr., Fisher, W. L., 1977. Seismic stratigraphic interpretation of depositional systems: Examples from Brazilian rift and pull-apart basins. In: Payton, C.E. (Ed.) Seismic stratigraphy - Applications to Hydrocarbon Exploration. AAPG Memoir 26, 213–248.

Button, A., 1973, A regional study of the stratigraphy and development of the Transvaal Basin in the eastern and northeastern Transvaal. Ph. D. dissertationWitwatersrand University, Johannesburg, South Africa (1973), p. 352

Cant, D. J., Walker, J. G., 1978. Fluvial processes and facies sequences in the sandy braided south Saskatchewan River, Canada. Sedimentology 25, 625–648.

Carey, J. S., Swift, D. J. P., Steckler, M., Reed, C. W., Niedoroda, A., 1999. High-resolution sequence stratigraphic modelling 2: effects of sedimentation processes. In: Har-bugh, J.W., Watney, W.L., Rankey, E.C., Slingerland, R., Goldstein, R.H., Franseen, E.K. (Eds.) Numerical Experiments in stratigraphy: recent advances in strati-graphic and sedimentologic computer simulations. SEPM Special Publication 62, 151–164.

Cas, R. A. F., 1983. Submarine crystal tuffs: their origin using aDevonian example from southwestern Australia. Geological Magazine 120, 471–486.

Cattaneo, A., Steel, R. J., 2003. Transgressive deposits: a review of their variability. Earth Science Review 62, 187–228.

Catuneanu, O., 2002. Sequence stratigraphy of clastic systems: concepts,merits and pitfalls. Journal of African Earth Science 35, 1–43.

Catuneanu, O., 2004. Retroarc foreland systems e evolution through time. Journal of African Earth Sciences 38, 225e242. Geological Society of Africa Presidential Review No. 7.

Catuneanu, O., 2006. Principles of Sequence Stratigraphy. Elsevier, 375p.

Catuneanu, O., Willis, A. J., Miall, A. D., 1998. Temporal significance of sequence boundaries. Sedimentary Geology 121, 157–178.

Chakraborti, S., 1997. Eleucidation of the sedimentary history of the Singhora Group of rocks, Chattisgarh Supergroup, M.P. Records of Geological Survey of India 130 (6), 184–187.

Chakraborty, P. P., Banerjee, S., Das, N. G., Sarkar, S., Bose, P. K., 1996. Volcaniclastics and their sedimentological bearing in Proterozoic Kaimur and Rewa Groups in central India. In: Bhattacharya, A. (Ed.), Recent Advances in Vindhyan Geology, vol. 36. Memoir Geological Society of India, pp. 59–76.

Chakraborty, P. P., Pal, T., 2001. Anatomy of a forearc submarine fan: upper Eocene- Oligocene Andaman flysch Group, Andaman Islands, India. Gondwana Research 4, 477–486.

Chakraborty, P. P., Sarkar, A., Bhattacharya, S. K., Sanyal, P., 2002. Isotopic and sedimentological clues to productivity change in Late Riphean Sea: A case study from two intracratonic basins of India. Proc. Indian Academy of Science (Earth Planetary Science)111, 379-390

Chakraborty, P. P., Paul, S., 2005. Proterozoic braid delta deposits: Lohardih Formation, Chattisgarh Supergroup, India. Ind. J. Geol. 75, 233–253.

Chakraborty, P.P., Paul, S., 2008. Forced regressive wedges on a Neoproterozoic siliciclastic shelf: Chandarpur Group, central India. Precambrian Research 162, 227–247.

Chakraborty, P. P., Das, K., Sarkar, A., Das, P., 2009. Fan-delta and storm-dominated shelf sedimentation in the Proterozoic Singhora Group, Chattisgarh Supergroup, central India. Precambrian Research 70, 88–106.

Chakraborty, P. P., Dey, S., Mohanty, S. P., 2010. Proterozoic platform sequences of Peninsular India: Implications towards basin evolution and supercontinent assembly. Journal of Asian Earth Sciences 39, 589–607.

Chakraborty, P. P., Das, K., Tsutsumi, Y., Horie, K., 2011. Depositional history of the Chhattisgarh basin, central India: Constrints from new SHRIMP zircon ages by M.E. Bickford, A. Basu, S. Patranabis-Deb, P.C. Dhang, J. Scieber: A discussion. Journal of Geology 119, 549–552.

Chakraborty, P. P., Das, P., Das, K., Saha, S., Balakrishnan, S., 2012. Regressive depositional architecture on a Mesoproterozoic siliciclastic ramp: sequence stratigraphic and Nd isotopic evidences from Bhalukona Formation, Singhora Group, Chhattisgarh Supergroup, central India. Precambrian Research 200–203, 129-148.

Chalapathi Rao, N. V., Burgess, R., Lehmann, B., Mainkar, D., Pande, S. K., Hari K. R., Bodhankar, N., 2011a. $^{40}Ar/^{39}Ar$ ages of mafic dykes from the Mesoproterozoic Chhattisgarh basin, Bastar craton, Central India: Implication for the origin and spatial extent of the Deccan Large Igneous Province. Lithos 125, 994–1005.

Chalapathi Rao, N.V., Paton, C., Lehmann, B., 2011b. Origin and diamond prospectivity of Mesoproterozoic kimberlites from the Narayanpet field, Eastern Dharwar Craton, southern India: insights from groundmass mineralogy, bulk-chemistry and perovskite oxybarometry. Geological Journal. DOI: 10.1002/gj.1309.

Chalapathi Rao, N. V., Miller, J. A., Pyle, D. M., Madhavan, V., 1996. New Proterozoic K-Ar ages for some kimberlites and lamproites from the Cuddapah Basin and Dharwar Craton, South India: evidence for non-contemporaneous emplacement. Precambrian Research 79, 363-369.

Chatterjee (Jha)., N., Das, N., Ganguly (Das), M., Chatterjee, B., 1990.Stromtolised based biostratigraphic zonation of Chandi Formation, Raipur Group, Chattisgarh Supergroup, in and around Dhamda-Nandini area, Durg dist, M.P. Precambrain Centre Geological Survey india Special publication, 28, 400-410.

Chaudhuri, A. K., Mukhopadhyay, J., Patranabis Deb, S., Chanda, S. K., 1999. The Neoproterozoic cratonic successions of Peninsular India; Gondwana Research 2, 213-225.

Chaudhuri, A. K., Mukhopadhyay, J., Patranabis-Deb, S., Mukherjee, M. K., Ghosh, G., 2002. The purana basins of southern cratonic province of India—a case for Mesoproterozoic fossil rifts. Gondwana Research 5, 23–33.

Cheel, R. J., Leckie, D. A., 1993. Hummocky cross-stratification. In: Wright, V.P. (Ed.), Sedimentology Review, 1. Blackwell, Oxford, 103–122.

Christie-Blick, N., Grotzinger, J. P., and von der Borch, C. C., 1988. Sequence stratigraphy in Proterozoic successions: Geology 16, 100-104

Christe-Blick, N., Dyson, I. A., Von der Borch, C. C., 1995. Sequence stratigraphy and the interpretation of Neoproterozoic earth history. Precambrian Research, 3–26.

Clifton, H. E., 1969. Beach lamination: nature and origin. Marine Geology 7, 553–559.

Clifton, H. E., 1976. Wave-formed sedimentary structures—a conceptual model. In: Davis, R.A., Ethington, R.L. (Eds.), Beach and Nearshore Processes: Society of Economic Paleontologists and Mineralogists, vol. 24. Special Publication, pp. 126–148.

Clifton, H. E., 2006. A reexamination of facies models for clastic shorelines. In: Posamentier, H.W, Walker, R.G. (Eds.), Facies Models Revisited. SEPM special publication, vol. 84, Tulsa, Oklahoma, USA, pp. 293–337.

Condie, K. C., 2005. High field strength element ratio in Archean basalts: A window to evolving source of mantle plumes?; Lithos 79 491–504.

Conrad, J. E., Hein, J. E., Chaudhuri, A. K., Patranabis-Deb, S., Mukhopadhyay, J., Deb, G. K., Beukes, N. J., 2011. Constraints on the development of Proterozoic basins in central India from $^{40}Ar/^{39}Ar$ analysis of authigenic glauconitic minerals. GSA Bulletin 123, 158–167.

Cotter, E., 1978. The evolution of fluvial style, with special reference to the central Appalachian Paleozoic. In: Miall, A.D., (ed.), Fluvial Sedimentology. Canadian Society of Petroleum Geologists Memoir 5, 361-383.

Coussot, P., Muunier, M., 1996. Recognition, classification andmechanical description of debris flows. Earth Science Review 40, 209–227.

Dalyrymple, R. W., Zaitlin, B.A., 1994. High-resolution sequence stratigraphy of a complex, incised valley succession, Cobequid Bay -Salmon River estuary, Bay of Fundy, Canada. Sedimentology 41, 1069-1091.

Dalziel, I. W. D., 1997. Neoproterozoic-Paleozoic paleogeography and tectonics: review, hypothesis and environmental speculations. Geological Society of America Bulletin 109, 16-42.

Dam, G., Andersen, F., 1990. High energy ephemeral stream deltas: an example from the upper Silurian Holmestrand Formation of the Oslo region, Norway. Sedimentary Geology 66, 197–225.

Das, K., Yokoyama, K., Chakraborty, P. P., Sarkar, A., 2009. EPMA U–Th–Pb Monazite dating and trace element geochemistry of tuff units from the basal part of Chhattisgarh and Khariar basin, central India: implications for basin initiation and depositional contemporaneity. Journal of Geology 117, 88–102.

Das, N., Dutta, D. R., Das, D. P., 2001. Proterozoic cover sediments of southeastern Chattisgarh state and adjoining parts of Orissa. Geological Survey of India Special Publication 55, 237–262.

Das, D. P., Kundu, A., Das, N., Dutta, D.R., Kumaran, K., Ramamurthy, S., Thangavelu, C., Rajaiya, V., 1992. Lithostratigraphy and sedimentation of Chhattisgarh basin. Indian Minerals 46, 271–288.

Das, D. P., Dutta, N. K., Dutta, D. R., Thanavellu, C., BabuRao, K., 2003. Singhora Group: the oldest Proterozoic lithopackage of eastern Bastar Craton and its significance: Indian Minerals 57, 127-138.

Das, N., Ganguly Das, M., Arora, Y. K., 1990. Micro-facies assemblage of gypsum from Chattisgarh basin - a sabkha model of evaporotic formation. Geological Survey of India, Special Publication 28, 639–647.

Das, P., Das, K., Chakraborty, P. P., Balakrishnan, S., 2011. 1420 Ma diabasic intrusives from the Mesoproterozoic Singhora Group, Chhattisgarh Supergroup, India: Implications towards non-plume intrusive activity. Journal of Earth System Science 120, 1–14.

Dasgupta, S., Bose, S., Das, K., 2013. Tectonic evolution of the Eastern Ghats Belt, India. Precambrian Research 227, 247-258

Datta, B., 1998. Stratigraphic and sedimentologic evolution of the Proterozoic siliciclastics in the southern part of Chhattisgarh and Khariar, Central India. J. Geol. Soc. India 51, 345–360.

Deb, G. K., 2013. Discussion of Saha et al. (2012, Precambrian Research) Tectono-magmatic evolution of the MesoproterozoicSinghora basin, central India: Evidence forcompressional tectonics from structural data, AMS study and geochemistry of basic rocks, Precambrian Research 230, 248– 257.

DePaolo, D .J., Wasserburg, G. J., 1979. Petrogenetic mixing models and Nd–Sr isotopic pattern; Geochim. Cosmochim. Acta 43, 615–627.

Deynoux, M., Ciner, A., Monod, O., Karabiyikoglu, M.,Manatschal, G., Tuzcu, S., 2005. Facies architecture and depositional evolution of alluvial fan to fan delta complexes in the tectonically active Miocene Koprucay Basin, Isparta Angle, Turkey. Sedimentary Geology 173, 315–343.

Dharma Rao, C. V., Santosh, M., Wu Y.B, 2011. Mesoproterozoic ophiolitic mélange from the SE periphery of the Indian plate: U–Pb zircon ages and tectonic implications. Gondwana Research 19, 384-401.

Diaz, R. J., Rozenberg, R., 1995. Marine benthic hypoxia: a review of its ecological effects and the behavioral responses of benthic microfauna. Oceanography and Marine Biology: an Annual Review 33, 245–303.

Dickie, J. R., Hein, F.J., 1995. Conglomeratic fandelta and submarine fans of the Jurassic Laberge Group, Whitehorse Trough, Yukon territory, Canada: fore-Architectural Element sedimentation and unroofing of a volcanic island Architectural Element complex. Sedimentary Geology 98, 263–292.

Dickins, A. P., 2005. Radiogenic Isotope Geology, 2nd ed. Cambridge University Press, 492 pp.

Dickinson, W. R., 1970. Interpreting detrital modes of graywacke and arkose. Journal of Sedimentary Petrology 40, 695–707.

Dominguez, J. M. L., Wanless, H. R., 1991. Facies architecture of a falling sealevel strandplain, Doce River Coast, Brazil. In: Swift, D.J.P., Oerteal, G.F., Tillman, R.W., Thorne, J.A. (Eds.), Shelf Sand and Sandstone Bodies, vol. 14. International Association Sedimentologists Special Publication, pp. 259–281.

Donaldson, J. A., De Kemp, E. A., 1998. Archean quartz arenites in the Canadian Shield: examples from the Superior and Churchill Provinces. Sedimentary Geology 120, 153–176

Donaldson, J. A., Eriksson, P. G., Altermann, W., 2002. Actualistic versus nonactualistic conditions in the Precambrian: a reappraisal of an enduring discussion. In: Altermann W, Corcoran PL, editors. Precambrian Sedimentary environments: a modern approach to ancient depositional systems. IAS Spec Publ, vol. 33. Oxford7 Blackwell 3 –13.

Duke, W. L., 1990. Geostrophic circulation in shallow marine turbidity currents? The dilemma of paleoflow patterns in storm-influenced prograding shoreline systems. Journal of Sedimentary Petrology 60, 870–883.

Dutt, N. V. B. S., 1964. A suggested succession of the Purana Formations of the southern part of Chattisgarh, M.P. Rec. Geol. Surv. India 93-II, 143-148.

Einsele, G., 2000. Sedimentary Basins; Evolution, Facies and Sediment Budget. Springer-Verlag, Berlin, Heidelberg, Tokyo, p. 792.

Els, B. G., 1990. Determination of some palaeohydraulic parameters for a fluvial Witwatersrand successionSouth African Journal of Geology 93, 531-537.

Els, B. G., 1998. The auriferous Late Archaean sedimentation systems of South Africa: unique palaeoenvironmental conditions? Sedimentary Geology 120, 205– 224.

Embry, A. F., Johannessen, E. P., 1992. T–R sequence stratigraphy, facies analysis and reservoir distribution in the uppermost Triassic-Lower Jurassic succession, western Sverdrup Basin, Arctic Canada. In: Vorren, T.O., Bergsager, E., Dahl-Stamnes, O.A., Holter, E., Johansen, B., Lie, E., Lund, T.B. (Eds.), Arctic Geology and Petroleum Potential, vol. 2 (Special Publication). Norwegian Petroleum Society (NPF), 121–146.

Emery, D., Myers, K. J., 1996. Sequence Stratigraphy. Blackwell, Oxford, UK, pp-297.

Eriksson, P. G., Reczko, B. F. F., 1995. The sedimentary and tectonic setting of the Transvaal Supergroup floor rocks to the Bushveld complex. Journal of African Earth Science 21, 487–504.

Eriksson, P. G., Reczko, B. F. F., 1998. Contourites associated with pelagic mudrocks and distal delta-fed turbidites in the Lower Proterozoic Timeball Hill Formation epeiric basin (Transvaal Supergroup), South Africa. Sedimentary Geology 120, 319–335.

Eriksson, P. G., Reczko, B. F. F., Jaco Boshoff, A., Schreiber, M., Van Der Neut, M., Snyman, M. C. P., 1995. Architectural elements from lower Proterozoic braid-delta and high-energy tidal flat deposits in the Magaliesberg Formation, Transvaal Supergroup, South Africa. Sedimentary Geology 97, 99–117.

Eriksson, P. G, Martins-Neto, M. A, Nelson, D. R., Aspler, L. B., Chiarenzelli, J. R., Catuneanu. O., 2001. An introduction to Precambrian basins: their characteristics and genesis. Sedimentary Geology l 41–142, 1–35.

Eriksson, P. G., Altermann, W., Nelson, D. R., Mueller, W. U., Catuneanu, O., 2004. The Precambrian Earth: tempos and events. Amsterdam7 Elsevier. 941 pp.

Eriksson, P. G., Bumby, A. J., Brümer, J. J., Van Der Neut, M., 2006. Precambrian fluvial deposits: Enigmatic palaeohydrological data from the c. 2–1.9 Ga Waterberg Group, South Africa. Sedimentary Geology 190, 25–46.

Eriksson, P. G., Bose, P. K., Catuneanu, O., Sarkar, S., Banerjee, S., 2008. Precambrian clastic epeiric embayments: examples from South Africa and India. In: Pratt, B.R., Holmden, C. (Eds.), Dynamics of Epeiric Seas, vol. 48. Geological Association of Canada, St. Johns, Newfoundland, 119-136. Special Paper.

Eriksson, P.G., Mazumbar, R., Sarkar, S., Bose, P.K., Alterman, W., van dar Merwe, R., 1999. The 2.7-2.0 Ga volcano-sedimentary record of Africa, India and Australia: evidence for global and local changes in sea level and continental freeboed. Precambrian Research 97, 269-302.

Eriksson, K. A., 1973. The Timeball Formation—a fossil delta. Journal of Sedimentary Petrology 43, 1046–1053.

Ethridge, F. G., Wescott, W. A., 1984. Tectonic setting, recognition and hydrocarbon reservoir potential of fan delta deposits. In: Koster, E.H., Steel, R.J. (Eds.), Sedimentology of Gravels and Conglomerates, vol. 10. Canadian Society of Petroleum Geology Memoir, pp. 217–235.

Faure, G., 1986. Principles of Isotope Geology, 2nd ed. John Wiley & Sons, 589 pp.

Fitzsimmons, R., Johnson, S., 2000. Forced regressions: recognition, architecture and genesis in the Campanian of the Bighorn Basin, Wyoming. In: Hunt, D., Gawthorpe, R.L. (Eds.), Sedimentary Responses to Forced Regressions, vol. 172. Geological Society of London Special Publication, pp. 113–140.

Folk, R. L., 1974. Petrology of Sedimentary Rocks. Austin, Texas: Hemphills, 182p.

French, J. E., Heaman, L. M., Chacko, T., Rivard, B., 2004. Global mafic magmatism and continental breakup at 2.2 Ga: evidence from the Dharwar craton, India. Geological Society of America . Ann. Meet. Program Abstracts 36 (5), 340)

French, J. E., Heamana, L. M., Chackoa, T., Srivastava, R. K., 2008. 1891–1883 Ma Southern Bastar–Cuddapah mafic igneous events, India: A newly recognized large igneous province. Precambrian Research 160, 308–322

Fuller, A. O. 1985. A contribution to the conceptual modelling of pre-Devonian fluvial systems. Trans. Geological Society of South Africa 88, 189–194.

Galloway, W. E. 1989. Genetic Stratigraphic Sequences in Basin Analysis II: Application to Northwest Gulf of Mexico Cenozoic Basin. AAPG Bulletin 73, 143-154.

Galloway, W. E., 2002. Paleogeographic setting and depositional architecture of a sand dominated shelf depositional system, Miocene Utsira Formation,North Sea basin. Journal of Sedimentary Research 72, 476–490.

Gawthorpe, R. L., Colella, A., 1990. Tectonic controls on coarse-grained delta depositional systemsin rift basins. In:Gawthorpe, R.L., Colella,A. (Eds.), Coarse-Grained Deltas, special publication. lAS, vol. 10, Blackwell Science Publication, pp. 113–127.

Gazzi, P., 1966. Le arenarie del flysch sopracretaceo dell'Appenino modenese: correlazioni con il flysch di Monghidoro. Mineralogy Petrography acta 12, 69-97.

Ghosh, P. K., Shah, S. C., 1965. On the occurrence of stromatolites from the Raipur limestone (M.P.) Proc. 51st and 52nd Indian Science Congress Abstract 196.

Goldring, R., Aigner, T., 1982. Scour and fill: the signature of event separation. In: Einsele, G., Seilacher, A. (Eds.), Cyclic and Event Stratification. Springer-Verlag, Berlin, pp. 354–362.

Gregory, L., Meert, J. G., Pradhan, V., Pandit, M. K., Tamrat, E., Malone, S. J., 2006. A paleomagnetic and geochronologic study of the Majhgawan kimberlite, India:

Implications for the age of the Upper Vindhyan Supergroup. Precambrian Research 149, 65–75.

Gupta, S., Bhattacharya, A., Raith, M., Nanda, J. K., 2000. Contrasting pressuretemperature deformation history across a vestigial craton-mobile belt boundary: the western margin of the Eastern Ghats Belt at Deobhog, India. Journal of Metamorphic Geology 18, 683–697.

Gupta, S., Bose, S., 2004. Deformation History of the Kunavaram Complex, Eastern Ghats Belt, India: Implications for Alkaline Magmatism Along the Indo-Antarctica Suture. Gondwana Research 7, 1235–1241

Gupta, S., 2012. Strain localization, granulite formation and geodynamic setting of 'hot orogens': a case study from the Eastern Ghats Province, India. Geological Journal 47, 334-351.

Hallam, A., 1997. Estimates of the amount and rate of sea-level changes across the Rhaetian–Hettangian and Pliensbachian–Toarcian boundaries (latest Triassic to early Jurassic). Geololgical Society of London 154, 773–779.

Hampson, G. J., 2000. Discontinuity surfaces, clinoforms, and facies architecture in a wave-dominated, shoreface–shelf parasequence. Journal of Sedimentary Research 70, 325–340.

Harlov, D. E. Wirth, R., Hetherington, C. J., 2011. Fluid-mediated partial alteration in monazite: the role of coupled dissolution–reprecipitation in element redistribution and mass transfer. Contribution to Mineralogy and Petrology 162, 329–348.

Hashimoto, A., Oguchi, T., Hayakawa, Y., Linb, Z., Saito, K., Wasklewicz, T. A., 2008. GIS analysis of depositional slope change at alluvial-fan toes in Japan and the American Southwest. Geomorphology 100, 120–130.

Hastie, A. R., Kerr, A. C., Pearce, J. A., Mitchell, S. F., 2007. Classification of altered volcanic island arc rocks using immobile trace elements: development of the Th–Co discrimination diagram. Journal of Petrology 48, 2341–2357.

Helland-Hansen, W., Martinsen, O. J., 1996. Shoreline trajectories and sequence: description of variable depositional-dip scenarios. Journal of Sedimentary Research 66, 670–688.

Hessler, A. M., Lowe, D. R., 2006. Weathering and sediment generation in the Archean: An integrated study of the evolution of siliciclastic sedimentary rocks of the 3.2 Ga Moodies Group, Barberton Greenstone Belt, South Africa. Precambrian Research 151, 185-210.

Hoffman, P. F., Kaufman, A. J., Halverson, G. P., Schrag, D. P., 1998. A Neoproterozoic snowball Earth. Science 281, 1342–1346.

Hoffmann, A. W., 1988. Chemical differentiation of the Earth: The relationship between mantle, continental crust and oceanic crust; Earth Planetary Science Letter 90, 297–314.

Hogg, S. E., 1982. Sheetfloods, sheetwash, sheetflow, or . . .? Earth Science Reviews 18, 59–76.

Hokada, T., Misawa, K., Yokoyama, K., Shiraishi, K., Yamaguchi, A., 2004. SHRIMP and electron microprobe chronology of UHT metamorphism in the Napier Complex, East

Antarctica: implications for zircon growth at > 1000 °C. Contributions to Mineralogy and Petrology, 147, 1–20.

Holmes, A., 1965. Principles of Physical Geology. Ronald, New York, p. 1288.

Hunt, D., Gawthorpe, R. L. (Eds.), 2000. Sedimentary Response to Forced Regressions, vol. 172. Geological Society of London, Special Publication, p. 383.

Hunt, D., Tucker, M. E., 1992. Stranded parasequences and the forced regressive wedge systems tract: deposition during base level fall. Sedimentary Geology 81, 1–9.

Hwang, I. G., Chough, S. K., 2000. The Maesan fan delta, Miocene Pohang BASIN, SE KOREA: architecture and depositional processes of a high-gradient fan delta-fed slope system. Sedimentology 47, 995–1010.

Iverson, R.M., 1997. Physics of debris flows. Reviews in Geophysics 35, 245–296.

Jacobsen, S. T. B., Wasserburg, G. J., 1980. Sm–Nd isotopic evolution of chondrites. Earth Planetary Science Letter 50, 139–155.

Jairam, R., Banerjee, D. M.,1980. Preliminary studies of the stromatolites from Raipur area, Chhattisgarh Basin. Geological Survey of India Special Publication 44, 57-67.

Jensen, L. S., 1976. A new cation plot for classifying subalkalic volcanic rocks; Ontario Division of Mines, Miscellaneous Paper 66, 21.

Jervey, M. T., 1988. Quantitative geological modelling of siliciclastic rock sequences and their seismic expression. In: Sea-level Change -- an Integrated Approach (Eds C. K. Wilgus, B. J. Hastings, H. Posamentier, J. C. Van Wagoner, C. A. Ross and C. G. St. C. Kendall), Special. Publication Society Economical and Paleontological Mineral 42, 47-69.

Johnson, H. D., 1977. Shallow marine sand bar sequences: an example for the late Precambrian of North Norway. Sedimentology 24, 245–270.

Jones, S. J., Forstick, L. E., Austin, T. R., 2001. Braided stream and flood plain architecture: the Rio Vero formation, Spanish Pyrenees. Sedimentary Geology 139, 229–260.

Karmakar, S., Bose, S., Das, K., Dasgupta, S., 2009. Proterozoic Eastern Ghats Belt, India – A witness of multiple orogenies and its lineage with ancient supercontinents. Journal of Virtual Explorer 32, paper 3.

Kaufman, A. J., Knoll. A. H., Awramik, S. M., 1992. Biostratigraphic and chemostratigraphic correlation of Neopro terozoic sedimentary successions: Upper Tindir Group, northwestern Canada, as a test case; Geology 20, 181-185.

Khalifa, M.A., 1983. Origin and occurrence of glauconite in the green sandstone associated with unconformity, Bahariya Oases, Western Desert, Egypt. Journal of African earth sciences, 1, No. 34, 321-325.

Kingsley, C. S., 1984. Dagbreek fan-delta: an alluvial placer to prodelta sequences in the Proterozoic welkom Goldfield, Witwatersand, South Africa. Sedimentology of gravels

and conglomerates, Koster, E.H., Steel, R.J., (Eds), Memoir Canadian Society of Petroleum Geology 10, 321-330.

Klein, G. V., Lee, Y II., 1984. A preliminary assessment of geodynamic controls on depositional systems and sandstone diagenesis in back-arc basins, Western Pacific Ocean. Tectonophysics 102, 119–152.

Kneller, B. C., Branney, M.J., 1995. Sustained high density turbidity currents and the deposition of thick massive sands. Sedimentology 42, 607–616.

Knoll, A. H., 1994. Neoproterozoic evolution and environmental change. In: Bengston, S., (Ed.), Early life on Earth. Noble symposium, vol. 84, Columbia, New York, pp. 439–449.

Komar, P. D., 1976. Beach processes and sedimentation: Englewood Cliffs, New Jersey, Prentice-Hall, 429 p.

Rust, B.R., Koster, E.H., 1984. Coarse alluvial deposits. In: Walker, R.G. (Ed.), Facies Models, vol. 1. Geoscience Canadian Reprint Series, pp. 53–70.

Kruezer, H., Karre, W., Kursten, M., Schnitzer, W. A., Murti, K. S., and Srivastava, N. K., 1977. K/Ar dates of two glauconites from Chandarpur series (Chattisgarh/ India): on the stratigraphic status of late Precambrian basins of central India. Geol. Jahrb. Bull. 28, 23–36.

Le Roux, 1992. Determining the channel sinuosity of ancient fluvial systems from paleocurrent data. Journal of Sedimentary Petrology 62, 283–291

Leckie, D. A., Krystinik, L. F., 1889. Is There Evidence for Geostrophic Currents Preserved in the Sedimentary Record of Inner to Middle-Shelf Deposits? Journal of Sedimentary Petrology 59, 862-870.

Leeder, M. R., 1978. A quantitative stratigraphic model for alluvium, with special ref-erence to channel deposit density and interconnectedness. In: Miall, A.D. (Ed.), Fluvial Sedimentology. Canadian Society of Petroleum Geologist, Memoir 5, 587–596.

Leeder M. R., 2011. Tectonic sedimentology: sediment systems deciphering global to local tectonics. Sedimentology 58, 2–56.

Lehmann, B., Storey, C., Mainkar, D., Jeffries, T., 2007. In-situ U–Pb dating of titanite in the Tokapal–Bhejripadar kimberlite system, central India. Journal Geological Society of India 69, 553-556.

Lehmann, B., Burgess, R., Frei, D., Belyatsky, B., d, Mainkar, D., Chalapathi Rao, N.V., Heaman, L.M., 2010. Diamondiferous kimberlites in central India synchronous with Deccan flood basalts.Earth and Planetary Science Letters 290, 142–149.

Leopold, L. B., Wolman, G. M., Miller, J. P., 1964. Fluvial Processes in River Geomorphology. Freeman, San Francisco. 522pp.

Liew, T. C., Hoffmann, A. W., 1988. Precambrian crustal components, plutonic associations, plate environment of the Hercynian Fold Belt of central Europe: Indications from a Nd and Sr isotopic study; Contribution to Mineralogy and Petrology 88, 129–138.

Long, D. G. F., 1978. Proterozoic stream deposits: some problems of recognition and interpretation of ancient sandy fluvial systems. In: Miall, A.D. (Ed.), Fluvial Sedimentology. Canadian Society of Petroleum Geology Memoir 5, 313–341.

Long, D. G. F., 2004. Precambrian rivers. In: Eriksson, P.G., Altermann, W., Nelson, D.R., Mueller, W.U., Catuneanu, O. (Eds.), The Precambrian Earth: Tempos and Events. Elsevier, Amsterdam, pp. 660–663.

Long, D. G. F., 2011. Architecture and depositional style of fluvial systems before land plants: a comparison of Precambrian, Early Palaeozoic, and modern river deposits. In: North, C. (Ed.), From River to Rock Record—The Preservation of Flu-vial Sediments and their Subsequent Interpretation. SEPM Special Publication 97, 37–61.

Lowe, D. R., 1982. Sediment gravity flows II. Depositional models with special reference to the deposits of high-density turbidity currents. Journal of Sedimentary Petrology 52, 279–297.

Lucas-Tooth, H. J., Pyne, C., 1964. Advance X-ray Analysis 7, 523-541.

MacEachern, J., Zaitlin, B. A., Pemberton, S. G., 1999. A sharp-based sandstone of the Viking Formation, Joffre Field, Alberta, Canada: Criteria for recognition of trans-gressively incised shoreface complexes. Journal of Sedimentary Research 69, 876–892.

Macnaughton, R., Dalrymple, R., Narbonne, G., 1997. Early Cambrian braid-delta deposits, Mackenzie Mountains, northwestern Canada. Sedimentology 44, 587–609.

Major, J. J., Iverson, R. M., 1999. Debris flow deposition: effects of pore fluid pressure and friction concentrated at flow margins. Bulletin of Geological Society of America 111, 1424–1434.

Major, J. J., 1997. Depositional processes in large-scale debris flowexperiments. Journal of Geology 105, 345–366.

Mallikharjuna Rao, J., 2004. The Wide Spread 2 Ga Dyke Activity in the Indian Shield-Evidences from Bundelkhand Mafic Dyke Swarm, Central India and Their Tectonic Implications. Gondwana Research (Gondwana Newsletter Section) 7, 1219-1228.

Maniar, P. D., Piccoli, P. M., 1989. Tectonic discrimination of granitoids*Geological Society of America Bulletin* 101, 635-643.

Martel,A. T., Gibling, M. R., 1994.Combined-flowgeneration of sole structures, including recurved groove casts, associated with lower Carboniferous lacustrine storm deposits in Nova Scotia, Canada. Journal of Sedimentary Research A64, 508–517.

Martins-Neto, M. A., Pedrosa-Soares, A. C., Lima, S. A. A., 2001. Tectono-sedimentary evolution of sedimentary basins from Late Paleoproterozoic to Late Neoproterozoic in the São Francisco craton and Araçuaí fold belt, eastern Brazil. Sedimentary Geology 141-142, 343-370.

McKee, E. D., Crosby, E. J., Berryhill Jr., H. L., 1967. Flood deposits, Bijou Creek, Colorado, June 1965. Journal of Sedimentary Petrology 34, 829–851.

Mcpherson, J. G., Shanmugam, G., Moiola, R. J., 1987. Fan deltas and braid-deltas: varieties of coarse-grained deltas. Bulletin GSA 99, 331–340.

Mellere, D., Steel, R., 1995. Variability of lowstand wedges and their distinction from forced regressive wedges in the Mesaverde Group, southesat Wyoming. Geology 23, 803–806.

Melvin, J., 1986. Upper Carboniferous fine grained turbidite sandstone from southwest England: a model for growth in an ancient, delta-fed sub sea fan. Journal of Sedimentary Research 56, 19–34.

Miall, A. D., 1976. Paleocurrent and paleohydrologic analysis of some vertical profiles through a Cretaceous braided stream deposit, Banks Island, Arctic Canada. Sedimentology 23, 459-484.

Miall, A. D., 1977. A review of the braided river depositional environment. Earth Science Review 13, 1–62.

Miall, A. D., 1978. Lithofacies types and vertical profile models in braided river deposits: a summary. In: Miall, A.D. (Ed.), Fluvial Sedimentology, vol. 5. Memoir of Canadian Society of Petroleum Geology, pp. 597–604.

Miall, A. D., 1985. Architectural-element analysis: a new method of facies analysis applied to fluvial deposits. Earth Science Reviews 22, 261–308.

Miall, A. D., 1996. The geology of fluvial deposits. Springer-Verlag, New York, 582 pp.

Mial, A. D., 1983. The Narcs Strait problem: a re-evaluation of the geological evidence in terms of a diffuse, oblique-slip plate boundary between Greenland and the Canadian Arctic Islands. In: M. Friedman and M.N. Toksoz (Editors). Continental Tectonics: Structure. Kinematics and Dvnamics. Tectonophysics. 100, 227-239.

Miall, A. D., 1985. Architectural-element analysis: a new method of facies analysis applied to fluvial deposits. Earth brgaScience Reviews 22, 261–308.

Miall, A. D., 1988a. Architectural elements and bounding surfaces in fluvial deposits: Anatomy of the Kayenta Formation (Lower Jurassic), southwest Colorado. Sedi-mentary Geology 55, 233–262.

Miall, A. D., 1996. The geology of fluvial deposits. Springer-Verlag, New York, 582 pp.

Miall, A. D., 1990. Principles of Sedimentary Basin Analysis (2nd ed.). Springer-Verlag, New York.

Midtgaard, H. H., 1996. Inner shelf to lower shoreface hummocky sandstone bodies with evidence for geostropic influenced combined flow, lower Cretaceous, west Greenland. Journal of Sedimentary Research 66, 343–353.

Moitra, A. K., 1986. Preliminary study of Raipur Formation, M.P. Proc. XI Colloquium on micropaleontology and stratigraphy. Bull. Geol. Surv. Ind. 54, 124–130.

Moitra, A. K., 1995. Depositional environmental history of the Chattisgarh basin, M.P, based on Stomatolites and Microbiota. J. Geol. Soc. Ind. 46, 359–368.

Moitra, A. K., 1984. Microbiota from Raipur Formation, Chhattisgarh Group, M.P., Rec. Geol. Surv. India 116, 163–171.

Moitra, A. K., 1996. Preliminary study of stromatolites of Raipur Formation, M.P., Proc. xi Colloq. On Micropaleont. and Stratigraphy Bulletin 54, 124–130.

Moitra, A.K., Pal, 1984. Microbiota from Raipur Formation, Chhattisgarh Group, M.P., Rec. Geological Survey of India 116, 163–171.

Moitra, A.K., 1990. Chronologic implications of the stromatolites, microbiota and tracefossils of the Chattisgarh Basin, M.P. Geological Survey of India special Publication 28, 384–399.

Moitra, A. K., 1999. Biostratigraphic study of stromatolites and microbiota of Chhattisgarh basin, M.P., India, Palaeontologia Indica, Geol. Surv. India. 51, 95.

Montel, J. M., Foret, S., Veschambre, M., Nicollet, C., Provost, A., 1996. Electron microprobe dating of monazite. Chemical Geology 131, 37-53.

Mueller, W. U., Corcoran, P. L., 1998. Late-orogenic basins in the Archean Superior Province Canada: characteristics and inferences. Sedimentary Geology 120. 177–203.

Mueller, W. U., Corcoran P.L., 2001. Volcano-sedimentary processes operating on a marginal continental arc: the Archean Raquette Lake Formation, Slave Province, Canada. Sedimentary Geology 141-142, 169-196.

Mukherjee, A., Bickford, M. E., Hietpas, J., Schieber, J., Basu. A., 2012. Implications of a Newly Dated Ca. 1000-Ma Rhyolitic Tuff in the Indravati Basin, Bastar Craton, India. The Journal of Geology 120, 477-485.

Mulder, T., Alexander, J., 2001. The physical character of subaqueous sedimentary density flows and their deposits. Sedimentology 48, 269–299.

Mulder, T., Syvitski, J. P. M., 1996. Climatic and morphologic relationships of rivers: Implications of sea level fluctuations on river loads. Journal of Geology 104, 509–523.

Mursky, G., 1987. Flow Chart for Mineral Separation from Granitic Rocks. Journal of Geological Education 35, 256-259.

Murti, K. S., 1987. Stratigraphy and sedimentation in Chattisgarh basin. In: Radhakrishna, B.P. (Ed.), Purana Basins of Peninsular India. Geological Society of India Memoir 6, 239–257.

Myrow, P. M., Southard, J. B., 1991. Combined-Flow Model for Vertical Stratification Sequences in Shallow Marine Storm-Deposited Beds. Journal of Sedimentary Petrology 61, 202-210.

Myrow, P. M., 1992. Bypass zone tempestite facies model and proximality trends from an ancient muddy shoreline and shelf. Journal of Sedimentary Petrology 62, 99–115.

Naqvi, S. M., 2005. Geology and the Evolution of the Indian Plate. Capital, New Delhi.

Nemec, W., Steel, R. J., 1988. What is fan delta and howdowe recognize it? In:Neme W., Steel, R.J. (Eds.), Fan Deltas: Sedimentology and Tectonic Setting. Blackie, Glasgow, pp. 3–13.

Nilsen, T. H., 1982. Alluvial fan deposits. In: Scholle, P.A., Spearing, D. (Eds.), Sandstone Depositional Environments, AAPG Memoir 31, 49–86.

Oelkers, E. H., and Poitrrason, F. 2002. An experimental study of the dissolution stoichiometry and rates of a natural monazite as a function of temperature from 50° to 230°C and pH from 1.5 to 10. Chemical Geology 191, 73–87.

Osterkamp, W. R., Hedman, E. R., 1982. Perennial stream flow characteristics related to channel geometry and sediment in the Missouri River Basin. Professional Paper USGS 1242, 37.

Pal, T., Dutta gupta, T., Chakraborty, P. P., Das Gupta, S. C., 2005. Pyroclastic deposits of Mio-Pliocene age in the Arakan Yoma – Andaman - Java subduction complex, Andaman Islands, Bay of Bengal, India. Geochemical Journal 39, 69–82.

Sarbani Patranabis Deb, S., Chaudhuri, A. K., 2002. Stratigraphic architecture of the Proterozoic succession in the eastern Chattisgarth Basin, India: tectonic implications Sedimentary Geology 147, 105–125.

Patranabis-Deb, S., Chaudhuri, A. K., 2007. A retreating fan delta system in the Neoproterozoic Chattisgarh rift basin, central India: major controls on its evolution. AAPG Bulletin 91, 785–808.

Patranabis-Deb, S., Chaudhuri, A. K., 2008. Sequence evolution in the eastern Chhattisgarh basin: constraints on correlation and stratigraphic analysis. Paleobotanist 57, 15–32.

Patranabis-Deb, S., Bickford, M. E., Hill, B., Chaudhuri, A. K., Basu, A., 2007. SHRIMP ages of Zircon in the uppermost tuff in Chattisgarh Basin in central India require 500-Ma adjustment in Indian Proterozoic Stratigraphy. Journal of Geology 115, 407–415.

Pattison, S. A. J., Walker, R. G., 1992. Deposition and interpretation of long, narrow sandbodies underlain by a basinwide erosion surface; Cardium Formation, Cretaceous Western Interior Seaway, Alberta, Canada. Journal of Sedimentary Petrology 62, 292–309.

Pattison, S. A. J., 2005. Storm-influenced prodelta turbidite complex in the lower Kenilworth member at Hatch Mesa, Book Cliffs, Utah, U.S.A.: implications for shallow marine facies models. Journal of Sedimentary Research 75, 420–439.

Patton, P. C., 1988. Drainage basin morphometry and floods. In: Baker, V.R., Kochel, R.C., Patton, P.C. (Eds.), Flood Geomorphology.Wiley, New York, 51–64.

Paul, S., 2006. Facies, palaeogeography and depositional sequence analyses in parts of Meso- to Neoproterozoic rocks of Chattishgarh Supergroup, India. Unpublished Ph.D. thesis, Indian School of Mines, Dhanbad, p. 153.

Paul, S., Dongree, K.P., Chakraborty, P.P., 2003. Facies and system tract development on a Neoproterozoic lowstand shelf: Raipur Sandstone, Chattisgarh Supergroup, India. In:

Swamy, S.N., Kapoor, P.N., (Eds.), Proc. Association of Petroleum Geologists: Strategic challenges and Paradigm Shift in Hydrocarbon Exploration, pp. 405–416.

Paul, S., Chakraborty, P. P., 2003. Tidal Sand Wave Geometry in Neo Proterozoic Epeiric Sea: examples from two basins of Central India. Gondwana Geolological Magazine Spl. 7, 349–361.

Paul, S., Chakraborty, P. P., 2006. Depositional discontinuity in Neo-Mesoproterozoic rocks of Chandarpur Group, Chhattisgarh Supergroup, central India. Indian Journal of Geology 78, 159–174.

Pearce, J. A.; Harris, N. B. W., Tindle, A. G., 1984. Trace element discrimination diagrams for the tectonic interpretation of granitic rocks. Journal of Petrology 25, 956–983.

Pearce, J.A., 1996. A user's guide to basalt discrimination diagrams in: D.A. Wyman (Ed.), Trace Element Geochemistry of Volcanic rocks: Applications for Massive Sulphide Exploration, Short Course Notes, Geological Association of Canada 12, 79–113

Pierson, T. C., Scott, K. M., 1985. Downstream dilution of a lahar: transition from a debris flow to hyperconcentrated stream flow. Water Resource Research 21, 1511–1524.

Plint, A. G., 1988. Sharp-based shoreface sequences and 'offshore bars' in the Cardium Formation of Alberta: their relationship to relative changes in sea level. In: Wil-gus, C.K., Hastings, B.S., Kendall, C.G.St.C., Posamentier, H.W., Ross, C.A., Van Wagoner, J.C. (Eds.), Sea Level Changes - An Integrated Approach, SEPM Special Publication 42, 357–370.

Posamentier, H. W., Allen, G. P., 1993. Variability of sequence stratigraphic model: effects of local basin factors. Sedimentary Geology 86, 91–109.

Posamentier, H. W., Morris, W. R., 2000. Aspects of the stratal architecture of forced regressive deposits. In: Hunt, D., Gawthorpe, R.L. (Eds.), Sedimentary Responses to Forced Regressions. Geological Society of London Special Publication 72, 19–46.

Posamentier, H. W., Vail, P. R., 1988. Eustatic controls on clastic sedimentation II—Sequence and systems tract models, in Wilgus, C.K., Hastings, B.S., Ross, C.A., Posamentier, H.W., Van Wagoner, J., and Kendall, C.G.St.C., eds., Sea Level Changes: An Integrated Approach: SEPM, Special Publication 42, 125–154.

Posamentier, H. W., Walker, R. G., 2006. Facies Model Revisited, vol. 84. SEPM Special Publication, 527 p.

Posamentier, H. W., Jervey, M. T., Vail, P. R., 1988. Eustatic controls on clastic deposition I-conceptual framework, in Wilgus, C.K., Hastings, B.S., Kendall, C.G.St.C., Posamentier, H.W., Ross, C.A., and Van Wagoner, J.C., eds., Sea Level Changes: An Integrated Approach: SEPM, Special Publication 42, 109–124.

Posamentier, H. W.., Allen, G. P., James, D. P., Tesson, M., 1992. Forced regressions in a sequence stratigraphic framework: concepts, examples, and exploration significance: American Association of Petroleum Geologists, Bulletin 76, 1687–1709.

Potter, P. E., 1959. Facies models conference: Science 129, 1272–1273.

Pradhan, V. R., Meert, J. G., Pandit, M. K., Kamenov, G., Mondal, M. E. A., 2012. Paleomagnetic and geochronological studies of the mafic dyke swarms of Bundelkhand craton, central India: Implications for the tectonic evolution and paleogeographic reconstructions. Precambrian Research 198– 199, 51– 76.

Proust, J. N., Mahieux, G., Tessier, B., 2001. Field and Seismic Images of Sharp-Based Shoreface Deposits: Implications for Sequence Stratigraphic Analysis Journal of Sedimentary Research, Section B: Stratigraphy and Global Studies 71 (6), 944-957.

Radhakrishna, T., Joseph, M., 1996. Proterozoic palaeomagnetism of the mafic dyke swarms in the high-grade region of southern India. Precambrian Research 76, 31-46.

Rainbird, R. H., 1992. Anatomy of a large-scale braid-plain quartz arenite from the Neoproterozoic Shaler Group, Victoria Island, Northwest Territories, Canada. Canadian Journal of Earth Sciences 29, 2537–2550.

Ram, B., Singh, N. P., Murthy, A. S., 2007. A note on the qualitative appraisal of aeromagnetic image of Chhattisgarh basin. Journal of Indian Geophysical Union 11(3), 129-133.

Ramachandra, H. M., Mishra, V. P., Deshmukh, S. S., 1995. Mafic dykes in the Bastar Precambrians: study of the Bhanupratappur-Keshkal mafic dykes swarm. Geological Survey of India Memoir 33, 183-207.

Ramakrishnan, M., 1990. Crustal development in southern Bastar, Central India craton. Geological Survey of India Special Publication 28, 44-66.

Rasmussen, B., Bose, P. K., Sarkar, S., Banerjee, S., Fletcher, I. R., McNaughton, N. J., 2002. 1.6 Ga U–Pb zircon age for the Chorhat Sandstone, lower Vindhyan, India: possible implications for early evolution of animals. Geology 30, 103–106.

Ratre, K., Waele, B. D., Biswal, T. K., Sinha, S., 2010. SHRIMP geochronology for the 1450Ma Lakhna dyke swarm: Its implication for the presence of Eoarchaean crust in the Bastar Craton and 1450–517Ma depositional age for Purana basin (Khariar), Eastern Indian Peninsula. Journal of Asian Earth Sciences 39, 565–577.

Ray, J. S., Martin, M. W., Veizer, J., Bowring, S. A., 2002. U–Pb zircon dating and Sr isotope systematics of the Vindhyan Supergroup, India. Geology 30, 131–134.

Reading, H. G., 1996. Facies. In: Reading, H.G. (Ed.), Sedimentary Environments: Processes, Facies and Stratigraphy, 3rd edition. Blackwell Science Publication, p 688.

Rigsby, C. A., 1994. Deepening-upward sequences in Oligocene and lower Miocene fan-delta deposits, Western Santa Ynez mountains, California. Journal of Sedimentary Research B64, 380-391.

Roe, S.L., Hermansen, M., 1993. Processes and products of large, late Precambrian sandyrivers in northernNorway. Special Publication of International Association of Sedimentology 17, 151–166.

Roy, A., Kagami, H., Yoshida, M., Roy, A., Bandopadhyay, B. K., Chattopadhyay, A., Khan, A. K., Huin, A. K., Pal, T., 2006. Rb–Sr and Sm–Nd dating of differentmetamorphic events from the Sausar mobile belt, central India: Implications for Proterozoic crustal evolution; J. Asian Earth Sci. 26 61–76.

Saha, S., Das, K., Chakraborty, P. P., Das, P., Karmakar, S., Mamtani, M. A., 2013.Tectono-magmatic evolution of the Meosproterozoic Singhora basin, central India: Evidence for compressional tectonics from structural data, AMS study and geochemistry of basic rocks: Precambrian Research 227, 276–294.

Saito, K., Oguchi, T., 2005. Slope of alluvial fans in humid regions of Japan, Taiwan and the Philippines: Geomorphology 70, 147–162.

Shanker, R., Nag, S., Ganguly, A., Absar, A., Rawat, B. P., Singh, G. S., 2001. Are Majhgawan–Hinota pipe rocks truly group-I kimberlite? Procedings of Indian Academy of Science (Earth and Planetary Science) 110, 63-76.

Santosh, M., Zhao, G., 2009. Supercontinent dynamics. Gondwana Research 15, 225–227.

Santosh, M., Yokoyama, K., Acharyya, S. K., 2004. Geochronology and Tectonic Evolution of Karimnagar and Bhopalpatnam Granulite Belts, Central India. Gondwana Research7, 501-518.

Santosh, M., Sajeev, K., Li, J. H., 2006. Extreme crustal metamorphism during Columbia supercontinent assembly: Evidence from North China Craton. Gondwana Research 10 (3–4), 256–266.

Santosh, M., 2010. A synopsis of recent conceptual models on supercontinent tectonics in relation to mantle dynamics, life evolution and surface environment. Journal of Geodynamics 50, 116–133

Sarkar, A., Sarkar, G., Paul, D. K., Mitra, N. D., 1990. Precambrian geochronology of the central Indian shield—a review. Geological Survey of India Special Publication 28, 453-482.

Sarkar, S., Chakraborty, P. P., Bose, P. K., 1996. Proterozoic Lakheri Limestone, central India: facies, paleogeography and physiography. In: Bhattacharya, A. (Ed.), Recent Advances in Vindhyan Geology, vol. 36. Memoir Geological Society of India, pp. 5–26.

Sarkar, S., Samanta, P., Mukhopadhyay, S., Bose, P. K., 2012. Stratigraphic architecture of the Sonia Fluvial interval, India in its Precambrian context; Precamb. Res. 214–215, 210–226.

Saula, E., Mato, E., Puigdefabregas, C., 2002. Catastrophic debrisflow deposits from an inferred landslide-dam failure, the Eocene Berga Formation, eastern Pyrenees, Spain. In: Baker, V., Martini, I.P., Garzon, G. (Eds.), Floods and Megafloods Processes and Deposits. Special publication, vol. 32, International Association of Sedimentologists, Oxford, pp. 195–209.

Schnitzer, W. A., 1977. Distribution of stromatolites and strornatolitic recfs in the Precambrian of India. In: Folril Algae (Ed. by E. Flugel), pp. 107-1 12.

Schnitzer, W. A., 1969. Die jung-algonkischen sedimentation straume Peninsular lndiens. N. 3. Ccol. Poloeont. Abh. 133, 191-198.

Schumm, S. A., 1968. Speculations concerning palaeohydrologic controls of ter-restrial sedimentation. Geological Society of America Bulletin 79, 1573– 1588.

Schumm, S. A., 1993. River response to baselevel change: implications for sequence stratigraphy. Journal of Geology 101, 279–94.

Schwarzacher, W., Fischer, A. G., 1982. Limestone-shale bedding perturbations of the Earth's orbit. In: Einsele, G., Seilacher, A. (Eds.), Cyclic and Event Stratification. Springer-Verlag, pp. 72–95.

Seif, S., Sparks, R. S. J., 1978. Characteristics of widespread pyroclastic deposits formed by the interaction of silicic magma and water. Bulletin of Volcanology 41, 196–212.

Shanmugam, G., Poffenberger, M., Toro Alava, J., 2000. Tide—dominated estuarine facies in the Hollin and Napo ("T" and "U") formations (Cretaceous) Sacha Field, Oriente Basin, Ecuador. AAPG Bulletin 84 (5), 652–682.

Shaw, R. K., Arima, M., Kagami, H., Fanning, C. M., Shiraishi, K., Motoyoshi, Y., 1997. Proterozoic events in the Eastern Ghats Granulite Belt, India: evidence from Rb–Sr, Sm–Nd systematics and SHRIMP dating. The Journal of Geology 105, 645–656.

Singh, R. K., Srivastava, R. K., Hsean, A. R. 1997. Petrology of the Precambrian Mafic Rocks of Katekalyan area, Bastar District, Madhya Pradesh, India. Gondwana Research 1, 129-136.

Sinha, D. K., Jain, S. K., Naganath, K. P., 2011. Tectonic Significance and Age of Doleritic Sill Near Bandhalimal in the Singhora Protobasin of Chhattisgarh Basin, Central India. In: Srivastava R. K. (Eds.) Dyke Swarms: Keys for Geodynamic Interpretation.Springer-Verlag, Chapter-10, 167-187.

Siringan, F. P., Anderson, J. B., 1994. Modern shoreface and inner shelf storm deposits off the east Texas coast, Gulf of Mexico. Journal of Sedimentary Petrology B64, 99–110.

Sohn, Y. K., Rhee, C. W., Kim, B. C., 1999. Debris flowand hyperconcentrated flood-flow deposits in an alluvial fan, northwestern part of the Cretaceous Yongdong Basin, Central Korea. Journal of Geology 107, 111–132.

Srinivas, S., Murthy, A. S. K., Yaday, G. S., Srivastava, K. M. 2004. Basinal and Structural Appraisal of Magnetic Data of Chattisgarh Region, Central India. Journal Geolouical Society of India 63, 323-335

Srivastava, R. K., Verma, R., 1998. Precambrian basic magmatism of the southern Bastar craton, Central India. In: B.S. Paliwal (Ed.), Scientific Publ. (India), Jodhpur, pp.409- 416.

Srivastava, N. K., 1977. Sedimentary petrographical and geochemical studies of the late Precambrian stromatolites of India: *in* Flugel, Eds., Fossil Algae- Recent Results and Developments: Springer-Verlag, Barlin, pp 107-112.

Srivastava, R. K., Hall, R. P., Verma, R., Singh, R. K. 1996. Contrasting Precambrian Mafic Dykes of the Bastar craton, Central India: Petrological and geochemical characteristics. Journal of Geological Society of India 48, 537-546.

Srivastava, R. K., Singh, R. K.,1999. Petrology and geochemistry of the late Archaean siliceous high-magnesian basalts (SHMB) from Kaklur, southern Bastar craton, Central India. J. Geol. Soc. India 53, 693–704.

Srivastava, R. K., Singh, R. K. Verma, R. 2000. Juxtaposition of India and Antarctica during the Precambrian: inferences from geochemistry of mafic dykes. Gondwana Research 3, 227-234.

Srivastava, R. K., Singh, R. K., 2001. Petrology, tectonic setting, and genesis of early Precambrian mafic volcanics from the southern Bastar greenstone belt, central India. AGSO-Geosci. Australia Rec. 37, 196-198.

Srivastava, R.K., Singh, R.K., 2003a. The paleoproterozoic dolerite dyke swarm of the southern Bastar craton, central-East India: a supporting evidence for the Columbia. Supercontinent. Mem. Geological Society of India 52, 163–177.

Srivastava, R. K., Singh, R. K. 2003b. Geochemistry of high- Mg mafic dykes from the Bastar Craton: evidence of Late Archaean boninite-like rocks in an intracratonic setting. Current Science 85, 808-812.

Srivastava, R. K., Singh, R. K., 2003c. Precambrian mafic magmatism in southern Bastar craton, Central India: present status and future perspective. Gondwana Geological Magazine 7, 177-191.

Srivastava, R. K., Singh, R. K. 2004. Trace element geochemistry and genesis of Precambrian sub-alkaline mafic dikes from the central Indian craton: evidence for mantle metasomatism. Journal of Asian Earth Science 23, 373–389.

Srivastava, R. K. 2005b. Implication of high-field strength element geochemistry in altered igneous rocks: a case study from the Precambrian mafic dykes of southern Bastar craton, Central India. Indian Journal Geology 75, 72-88.

Srivastava, R. K. 2005c. Geochemical characteristics of Precambrian high-magnesium mafic rocks in an intracratonic rift-setting, Bastar craton, central India. *In:* S. Rajan and P.C. Pandey (Eds.), Antarctic Geoscience, Ocean-Atmosphere Interaction & Paleoclimatology, NCAOR, Goa, 263- 282.

Srivastava, R. K. 2006a. Geochemistry and Petrogenesis of Neoarchaean High-Mg Low-Ti Mafic Igneous Rocks in an Intracratonic Setting, Central India Craton: Evidence for Boninite Magmatism. Geochemical Journal 40, 15–31.

Srivastava, R. K. 2006b. Precambrian mafic dyke swarms from the Central Indian Bastar craton: temporal evolution of the subcontinental mantle. In: E. Hanski, S. Mertanen, T. Ramo and J. Vuollo (Eds.), Dyke Swarms – time markers of crustal evolution. Taylor & Francis Group, London, 147-159.

Srivastava, R. K. Gautam, G. C. 2007. Geochemistry of Distinct Mafic Intrusive Rocks from Darba-Kukanar and Kerlapal-Sukma-Mokhpal areas, Southern Bastar craton: Further data on the Early Precambrian Mafic Magmatism of Central India. Journal of Geological Society of India 69, 1176-1188.

Srivastava, R. K., Gautam, G. C., 2009. Precambrian Mafic Magmatism in the Bastar Craton, Central India. Journal of Geological Society of India 73, 52-72.

Suzuki, K., Adachi, M. 1991. Precambrian prov- enance and Silurian metamorphism of the Tsubosawaparagneiss in the South Kitakami terrane, northeast Japan, revealed by the chemical Th–U–total Pb iso- chron ages of monazite, zircon and xenotime. Geochemical Journal 25, 357–376.

Suzuki, K., Adachi, M., 1992. Middle Precambrian detrital monazite and zircon from the Hida gneiss on Oki-Dogo island, Japan: their origin and implications for the correlation of basement gneiss of Southwest Japan and Korea. Tec- tonophysics 235:277–292.

Swift, D. J. P., Niedoroda, A. W., 1985. Fluid and sediment dynamics on continental shelves. In: Tilman, R.W., Swift, D.J.P., Walker, R.G. (Eds.), Shelf Sands and Sandstone Reservoirs. Soc. Econ. Paleont. Mineral. Short course 13, Society for Sedimentary Geology, pp. 47–134.

Talling, P. J., 1998. How and where do incised valleys form if sea level remains above the shelf edge? Geology 26, 87–90.

Tamura, T., Nanayama, F., Saito, T., Murakami, F., Nakashima, R., Watanabe, K., 2007. Intra-shoreface erosion in response to rapid sea-level fall: depositional record of a tectonically uplifted strand plain Pacific coast of Japan. Sedimentology 54, 1149–1162.

Taylor, S.R., McLennan, S.M., 1997. The origin and evolution of Earth's continental crust. Journal of Australian Geology and Geophysics 17, 52–62.

Tirsgaard, H., 1993. The architecture of Precambrian High energy Tidal Channel Deposits: an example from the Lyell Lond Group (Eloomore Bay Supergroup), northeast Greenland. Sedimentary Geology 88, 137–152.

Todd, S.P., 1989. Stream-driven, high-density gravelly traction carpets: possible deposits in the Trabeg Conglomerate Formation, SW Ireland, and some theoretical considerations of their origin. Sedimentology 36, 513–530.

Upadhyay, D., Raith, M.M., Mezger, K., Hammerschmidt. K., 2006. Mesoproterozoic rift-related alkaline magmatism at Elchuru, Prakasam Alkaline Province, SE India. Lithos 89, 447–477.

Upadhyay, D., Gerdes, A., Raith, M. M., 2009. Unraveling sedimentary provenance and tectonothermal history of high temperature metapelites using zircon and monazite chemistry: A case study from the Eastern Ghats Belt, Indian Journal of Geology 117, 665–683.

Vail, P. R., 1987. Seismic stratigraphy interpreta- tion using sequence stratigraphy. Part I: Seismic stratigraphy interpretation procedure. In Atlas of Seismic Stratigraphy, ed. AW Bally,pp. 1-10. American Association of Petrolium Geologist. No.27, Vol.1, pp125.

Vallance, J. W., 2000. Lahars. In: Sigurdsson, H., Houghton, B.F., Mcnutt, R.S.,Rymer, H., Stix, J. (Eds.), Encyclopedia of Volcanoes.Academic Press, San Diego, pp. 601–615.

Van der Neut, M., Eriksson, P. G., Callaghan, C. C., 1991. Distal alluvial fan sediments in early Proterozoic red beds of the Wilgerivier Formation, Waterberg Group, South Africa. Journal of African Earth Science 12, 537–547.

Van der Nuet, M., Eriksson, P. G., 1999. Palaeohydrolical parameters of a Protero-zoic braided fluvial system (Wilgerivier Formation, Waterberg, South Africa) compared with a Phanerozoic example. International Association of Sedimen-tologists, Special Publication 28, 381–392.

Van Wagoner, J. C., Posamentier, H. W., Mitchum Jr., R. M., Vail, P. R., Sarg, J. F., Loutit, T. S., Hardenbol, J., 1988. An overview of the fundamentals of Sequence stratig-raphy and key definitions. In: Wilgus, C.K., Hastings, B.S., Kendall, C.G.St.C.,

Van Wagoner, J. C., Mitchum, Jr., R. M., Campion, K.M., Rahmanian, V.D., 1990. Siliciclastic sequence stratigraphy in well logs, core, and outcrops: concepts for high-resolution correlation of time and facies. American Association of Petroleum Geologists Methods in Exploration Series 7, 55 pp.

Van Wagoner, J. C., 1995. Overview of sequence Stratigraphy of foreland basin deposits. In: VanWagoner, J.C., Bertram, G.T. (Eds.), Sequence Stratigraphy of Foreland Basin Deposits, vol. 64. AAPG Memoir, pp. ix–xxi.

Van Weering, T. C. E., Nielsen, T., Kenyon, N. H., Akentieva, K., Kuijpers, A. H., 1998. Large submarine slides on the NE Faeroe continental margin. In: Stoker, M.S., Evans, D., Crampl, A. (Eds.), Geological Processes on Continental Margins: Sedimentation, Mass Wasting and Stability, vol. 129. Geological Society of London Special Publication, pp. 5–17.

Visser, J. N. J., 1972. The Timeball formation of Pretoria- a prograding shoreline deposit. Annals of the Geological Survey South Africa 9, 115–118.

Von der Borch, C.C., Christie-Blick, N. and Grady, A.E., 1988. Depositional sequence analysis applied to Late Proterozoic Wilpena Group, Adelaide Geosyncline, South Australia. Australian Jounal of Earth Science 35, 59-71

Walker, R. G., Eyles, C. H., 1988. Geometry and facies of stacked shallow marine sandier upward sequences dissected by an erosion surface, Cardium Formation, Willesden Green, Alberta. AAPG Bulletin 72, 1469–1494.

Walker, R. G., Plint, A. G., 1992. Wave and storm-dominated shallow marine systems. In: Walker, R.G., James, N.P. (Eds.), Facies Models: Response to Sea-Level Change. Geological Association of Canada, St. John's, Newfoundland, pp. 219–238.

Walker, R. G., Wiseman, T. R., 1995. Lowstand shorefaces, transgressive incised shorefaces, and forced regressions: Examples from the Viking Formation, Joarcam area, Alberta. Journal of Sedimentary Research B65, 132–141.

Walker, R.G., 1979. Facies and facies models, general introduction. In: R.G. Walker (Editor), Facies models. Geoscience Canada, Reprint Ser. 1, 1-7.

Walker, R. G., 1984. Shelf and shallow marine sands. In: Walker, R.G. (Ed.), Facies Models. Geological Society of Canada, pp. 141e170. Reprint Series 1, Toronto.

Whalen, J.B., Currie, K.L., Chappell, B.W., 1987. A-type granites: geochemical char- acteristics, discrimination and petrogenesis. Contributions to Mineral Petrology 95, 407–419.

Williams , G. P., 1978. Bank-full discharge of rivers. Water Resources Research 14 (6), 1141–1154.

Williams, G. P., 1984. Palaeohydrologic equations for rivers. In: Costa, J.E., Flcisher, P.J. (Eds.), Development and Application of Geomorphology. Springer-Verlag, Berlin, pp. 343–367.

Williams, G. E., Schmidt, P.W., 1996. Origin and palaeomagnetism of the Mesoproterozoic Gangau tilloid (basal Vindhyan Supergroup), central India. Precambrian Research 79, 307–325.

Winchester, J. A., Floyd, P. A., 1977. Geochemical discrimination of different magma series and their differentiation products using immobile elements. Chemical Geology 20, 325–343.

Windley, B., 1995. The Evolving Continents, 3rd edn. Wiley, Chi- chester, 526 pp.

Yakubchuk, A., 2010. Restoring the supercontinent Columbia and tracing its fragments after its breakup: a new configuration and a Super-Horde hypothesis. Journal of Geodynamics 50, 166–175.

Zhao, D., Tian, Y., Lei, J., Liu, L., Zheng, S., 2009. Seismic image and origin of the Changbai intraplate volcano in East Asia: role of big mantle wedge above the stagnant Pacific slab. Physics of the Earth and Planetary Interiors, 173, 197–206.

LIST OF PUBLICATIONS

主論文

Title of Doctoral Thesis

Facies model, Geochronology and Sequence analysis of the Singhora Group of rocks: implications to age and basinal forcings in early history of the Chhattisgarh basin, central India（Singhora 層群の堆積相モデル、地質年代およびシーケンス解析、特に、中央インド Chhattisgarh 堆積盆形成初期における年代論と堆積盆強制力について）

公表論文

1. Alluvial fan to storm-dominated shelf transition in the Mesoproterozoic Singhora Group, Chattisgarh Supergroup, Central India. Partha Pratim Chakraborty, Ashish Sarkar, Kaushik Das, Priyabrata Das. 2009. Precambrian Research, 170 (1-2) (2009) 88-106.

2. 1420 Ma diabasic intrusives from the Mesoproterozoic Singhora Group, Chhattisgarh Supergroup, India: Implications towards non-plume intrusive activity. Priyabrata Das, Kaushik Das, Partha Pratim Chakraborty, S. Balakrishnan. Journal of Earth System Sciences, 120 (2) (2011) 223-236.

3. Regressive depositional architecture on a Mesoproterozoic siliciclastic ramp: sequence stratigraphic and Nd isotopic evidences from Bhalukona Formation, Singhora Group, Chhattisgarh Supergroup, central India. Partha Pratim Chakraborty, Priyabrata Das, Kaushik Das, Subhojit Saha, S. Balakrishnan. Precambrian Research. 200-203 (2012) 129-149.

4. Microbial mat related structures (MRS) from Mesoproterozoic Chhattisgarh and Khariar basins, Central India and their bearing on shallow marine sedimentation. Partha Pratim Chakraborty, Priyabrata Das, Subhojit Saha, Kaushik Das, Shruti Ranjan Mishra and Pritam Paul. Episodes, 35 (4) (2012) 513-523.

5. Geology of Mesoproterozoic Chhattisgarh basin, central India: current status and future goals. Precambrian Basins of India: Stratigraphic and Tectonic Context. Partha Pratim Chakraborty, Subhojit Saha, and Priyabrata Das. 2014. Journal of Geological Society of London. Manuscript Accepted dt. 24.01.14.

参考論文

1. Tectono-magmatic evolution of Meosproterozoic Singhora basin, central India: Evidences for compressional tectonics from structural data, AMS study and geochemistry of basic rocks. Subhojit Saha, Kaushik Das, Partha Pratim Chakraborty, Priyabrata Das, Subroto Karmakar, Manish A. Mamtani. Precambrian Reseach, 227 (2013) 276-294 .

2. Reply to the discussion of Deb (2013) on the paper of Saha et al.(2013) entitled 'Tectono-magmatic evolution of the Mesoproterozoic Singhora basin, central India: Evidence for compressional tectonics from structural data, AMS study and geochemistry of basic rocks. Partha Pratim Chakraborty, Kaushik Das, Subhojit Saha, Priyabrata Das, Subrata Karmakar, Manish A. Mamtani. Precambrian Research, 236 (2013) 297-302.